Institute for Molecular Science

annual review

2008

Published by
Institute for Molecular Science
National Institutes of Natural Sciences
Myodaiji, Okazaki 444-8585, Japan
Phone: +81-564-55-7418 (Secretary Room)
Fax: +81-564-54-2254 (Secretary Room)
URL: http://www.ims.ac.jp/

Editorial Committee 2008

The style of IMS Annual Review was largely modified from the last issue, and we believe that this new style is much more attractive and informative.

The re-structuring of IMS into four Departments and seven Research Centers has been functioning nicely and stimulated new collaborations.

In addition to the four special programs going on, two new ones supported by the MEXT have started this fiscal year: (i) "Networked Laboratories for the Frontiers of Photon Science and Technology" in collaboration with the Advanced Photon Research Center of Japan Atomic Energy Research Institute, Osaka University and Kyoto University, and (ii) "Quantum Beam Development Program" in collaboration with Kyoto University and Nagoya University.

The network system for efficient mutual use of experimental equipments covering 72 universities has been upgraded so that users can utilize the system with high usability and security. We really hope that this system will be strongly financially supported so that the basic research activities in Japan can be kept and further promoted.

In this 2008 fiscal year four new faculty members have joined us: Professor Masahiro HIRAMOTO, Professor Koichi KATO, Professor Masahiro EHARA, and Associate Professor Mizuki TADA (from October). Two more new members are expected in the latter half of this fiscal year. Although the severe financial circumstances are still continuing because of the tight financial condition of the government, we always have to strive to carry out excellent researches at IMS as a Center of Excellence.

This volume of Annual Review is a summary of research activities performed at IMS in the period of September 2007–August 2008. As usual a lot of activities are going on and we are proud of that. Any constructive comments and/or questions are welcome. It is also a great pleasure to announce that many colleagues received various prizes as explained in this volume.

September, 2008

H. Nakamura

NAKAMURA, Hiroki
Director-General, Institute for Molecular Science

ORGANIZATION

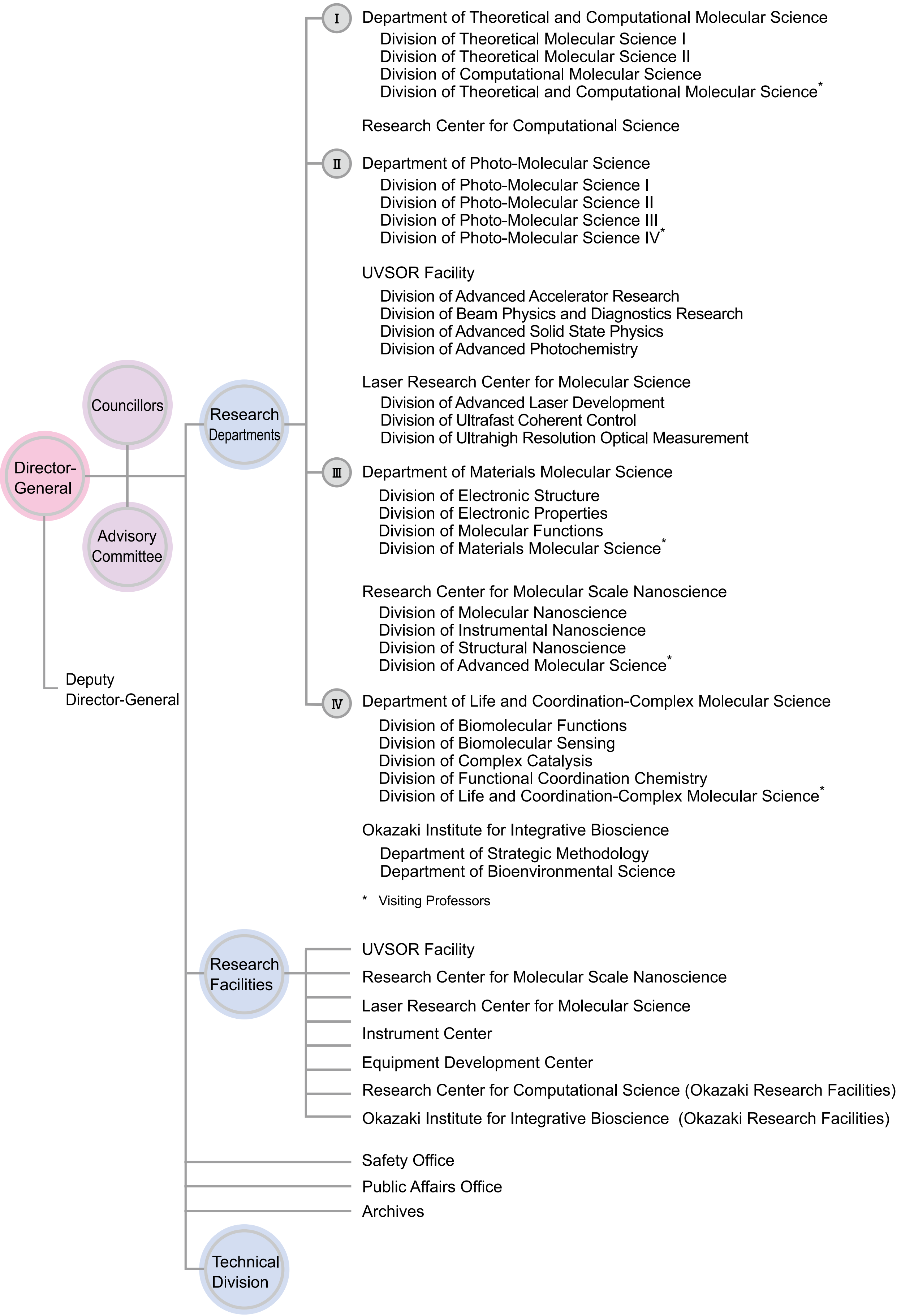

- Director-General
  - Councillors
  - Advisory Committee
  - Deputy Director-General
  - Research Departments
    - Ⅰ Department of Theoretical and Computational Molecular Science
      - Division of Theoretical Molecular Science I
      - Division of Theoretical Molecular Science II
      - Division of Computational Molecular Science
      - Division of Theoretical and Computational Molecular Science*
    - Research Center for Computational Science
    - Ⅱ Department of Photo-Molecular Science
      - Division of Photo-Molecular Science I
      - Division of Photo-Molecular Science II
      - Division of Photo-Molecular Science III
      - Division of Photo-Molecular Science IV*
    - UVSOR Facility
      - Division of Advanced Accelerator Research
      - Division of Beam Physics and Diagnostics Research
      - Division of Advanced Solid State Physics
      - Division of Advanced Photochemistry
    - Laser Research Center for Molecular Science
      - Division of Advanced Laser Development
      - Division of Ultrafast Coherent Control
      - Division of Ultrahigh Resolution Optical Measurement
    - Ⅲ Department of Materials Molecular Science
      - Division of Electronic Structure
      - Division of Electronic Properties
      - Division of Molecular Functions
      - Division of Materials Molecular Science*
    - Research Center for Molecular Scale Nanoscience
      - Division of Molecular Nanoscience
      - Division of Instrumental Nanoscience
      - Division of Structural Nanoscience
      - Division of Advanced Molecular Science*
    - Ⅳ Department of Life and Coordination-Complex Molecular Science
      - Division of Biomolecular Functions
      - Division of Biomolecular Sensing
      - Division of Complex Catalysis
      - Division of Functional Coordination Chemistry
      - Division of Life and Coordination-Complex Molecular Science*
    - Okazaki Institute for Integrative Bioscience
      - Department of Strategic Methodology
      - Department of Bioenvironmental Science
  - Research Facilities
    - UVSOR Facility
    - Research Center for Molecular Scale Nanoscience
    - Laser Research Center for Molecular Science
    - Instrument Center
    - Equipment Development Center
    - Research Center for Computational Science (Okazaki Research Facilities)
    - Okazaki Institute for Integrative Bioscience (Okazaki Research Facilities)
  - Safety Office
  - Public Affairs Office
  - Archives
  - Technical Division

* Visiting Professors

COUNCIL

NAKAMURA, Hiroki **Director-General**

Councillors

KATO, Shinichi	Chief Executive Officer, Toyota Central Research & Development Laboratories, Inc.
TSUCHIYA, Soji	Professor Emeritus, Tokyo University; Visiting Professor, National Chiao Tung University
TOKITOH, Norihiro	Director, Institute for Chemical Research, Kyoto University
TANAKA, Hiroaki	Culture News Editor, The Chunichi Shinbun Press
MILLER, William H.*	Professor, University of California, Barkeley
LAUBEREAU, Alfred*	Professor, Technische Universität München

The Council is the advisory board for the Director-General.
* Two of the councillors are selected among distinguished foreign scientists.

Distinguished Consultants

NAGAKURA, Saburo	Professor Emeritus, Institute for Molecular Science, The Graduate University for Advanced Studies, and The University of Tokyo
INOKUCHI, Hiroo	Advisor, Japan Aerospace Exploration Agency
ITO, Mitsuo	Professor Emeritus, Institute for Molecular Science, The Graduate University for Advanced Studies, and Tohoku University
KAYA, Koji	Director, Advanced Computational Science Department, RIKEN Advanced Science Institute

Research Consultants

HIROTA, Noboru	Professor Emeritus, Kyoto University
KONDOW, Tamotsu	Visiting Professor, Toyota Technological Institute
IRIE, Masahiro	Professor, Rikkyo University

Advisory Committee

EBATA, Takayuki	Professor, Hiroshima University
ENOKI, Toshiaki	Professor, Tokyo Institute of Technology
FUKE, Kiyokazu	Professor, Kobe University (Vice chair)
KATO, Masako	Professor, Hokkaido University
NAKAJIMA, Atsushi	Professor, Keio University
SEKIYA, Hiroshi	Professor, Kyushu University
SHINOHARA, Hisanori	Professor, Nagoya University
WATANABE, Yoshihito	Professor, Nagoya University
YAMASHITA, Kouichi	Professor, The University of Tokyo
YAMASHITA, Masahiro	Professor, Tohoku University
HIRATA, Fumio	Professor, Institute for Molecular Science
KOSUGI, Nobuhiro	Professor, Institute for Molecular Science
NAGASE, Shigeru	Professor, Institute for Molecular Science
NISHI, Nobuyuki	Professor, Institute for Molecular Science
OKAMOTO, Hiromi	Professor, Institute for Molecular Science
OHMORI, Kenji	Professor, Institute for Molecular Science
TANAKA, Koji	Professor, Institute for Molecular Science
URISU, Tsuneo	Professor, Institute for Molecular Science (Chair)
YAKUSHI, Kyuya	Professor, Institute for Molecular Science
YOKOYAMA, Toshihiko	Professor, Institute for Molecular Science

Administration Bureau

KURATA, Yutaka	Director, Okazaki Administration Office Director, General Affairs Department
MURANO, Hiroaki	Director, Financial Affairs Department
HARADA, Eiichiro	Head, General Affairs Division
ISHIKAWA, Shinji	Head, International Relations and Research Cooperation Division
SUEMURA, Shinichiro	Head, Financial Affairs Division
SAKAMOTO, Kazuhiro	Head, Procurement Division
SHINOHARA, Kenji	Head, Facilities Division

Emeritus Professors

NAGAKURA, Saburo	Professor Emeritus, The Graduate University for Advanced Studies and The University of Tokyo
HIROTA, Eizi	Professor Emeritus, The Graduate University for Advanced Studies
KIMURA, Katsumi	IMS, Professor Emeritus, Japan Advanced Institute of Science and Technology
MOROKUMA, Keiji	Research Leader, Fukui Institute for Fundamental Chemistry, Kyoto University
INOKUCHI, Hiroo	Advisor, Japan Aerospace Exploration Agency
MARUYAMA, Yusei	Professor, Hosei University
YOSHIHARA, Keitaro	Fellow, Toyota Physical and Chemical Research Institute
HANAZAKI, Ichiro	Professor Emeritus, The Graduate University for Advanced Studies
IWAMURA, Hiizu	Professor, Nihon University
SAITO, Shuji	Professor Emeritus, The Graduate University for Advanced Studies
IWATA, Suehiro	Fellow, Toyota Physical and Chemical Research Institute
ITO, Mitsuo	Professor Emeritus, The Graduate University for Advanced Studies and Tohoku University
KAYA, Koji	Director, Advanced Computational Science Department, RIKEN Advanced Science Institute
KITAGAWA, Teizo	Fellow, Toyota Physical and Chemical Research Institute
KOABAYASHI, Hayao	Visiting Professor, Nihon University

ACTIVITIES IN EDUCATION AND COLLABORATION

Graduate Programs

IMS promotes pioneering and outstanding research by young scientists as a core academic organization in Japan. IMS trains graduate students in the Departments of Structural Molecular Science and Functional Molecular Science, Graduate School of Physical Sciences, the Graduate University for Advanced Studies (SOKENDAI). By virtue of open seminars in each research division, Colloquiums and the Molecular Science Forum to which speakers are invited from within Japan and all over the world, as well as other conferences held within IMS, graduate students have regular opportunities to be exposed to valuable information related to their own fields of research as well as other scientific fields. Graduate students can benefit from these liberal and academic circumstances, all of which are aimed at extending the frontiers of fundamental molecular science and to facilitate their potential to deliver outstanding scientific contributions.

For more details on the Departments of Structural Molecular Science and Functional Molecular Science, young scientists are encouraged to visit IMS through many opportunities such as the IMS Open Campus in May, Graduate-School Experience Program (Taiken Nyugaku) in August, Open Lectures in summer and winter, *etc*.

International Collaboration and International Exchange

IMS has accepted many foreign scientists and hosted numerous international conferences (*e.g*. Okazaki Conference) since its establishment and is now universally recognized as an institute that is open to foreign countries. In 2004, IMS initiated a new program to further promote international collaborations. As a part of this new program, IMS faculty members can (1) nominate senior foreign scientists for short-term visits, (2) invite young scientists for long-term stays, and (3) undertake visits overseas to conduct international collaborations. In 2006, IMS started a new program, JSPS Asian CORE Program on “Frontiers of material, photo- and theoretical molecular sciences” (2006–2011). This new program aims to develop a new frontier in the molecular sciences and to foster the next generation of leading researchers through the collaboration and exchange among IMS and core Asian institutions: ICCAS (China), KAIST (Korea), and IAMS (Taiwan). See the details in pages 116–117.

Joint Study Programs

As one of the important functions of an inter-university research institute, IMS facilitates joint study programs for which funds are available to cover the costs of research expenses as well as the travel and accommodation expenses of individuals. Proposals from domestic scientists are reviewed and selected by an interuniversity committee. See the details in pages 112–115.

The programs are conducted under one of the following categories:

(1) Joint Studies on Special Projects (a special project of significant relevance to the advancement of molecular science can be carried out by a team of several groups of scientists).

(2) Research Symposia (a symposium on timely topics organized as a collaborative effort between outside and IMS scientists).

(3) Cooperative Research (a research program conducted by outside scientists with collaboration from an IMS scientist).

(4) Use of Facilities (a research program conducted by outside scientists using the research facilities of IMS, except the UVSOR facility).

(5) Joint Studies Programs using beam lines of UVSOR Facility.

(6) Use of Facility Program of the Computer Center (research programs conducted by outside scientists at research facilities in the Research Center for Computational Science).

RESEARCH ACTIVITIES

Theoretical and Computational Molecular Science

It is our goal to develop theoretical and computational methodologies that include quantum mechanics, statistical mechanics, and molecular simulation in order to understand correctly the structures, reactivities, and functions of molecules in gas, solution, and condensed phases as well as in nano- and bio-systems.

Theoretical Study and Design of Functional Molecules: New Bonding, Structures, and Reactions

Department of Theoretical and Computational Molecular Science
Division of Theoretical Molecular Science I

NAGASE, Shigeru	Professor
CHOI, Cheol Ho	Visiting Associate Professor*
JANG, Joonkyung	Visiting Associate Professor
OHTSUKA, Yuki	Assistant Professor
ISHIMURA, Kazuya	Technical Associate[†]
KATOUDA, Michio	Post-Doctoral Fellow
GAO, Xingfa	Post-Doctoral Fellow
GUO, Jing-Doing	Post-Doctoral Fellow
MIZOROGI, Naomi	Post-Doctoral Fellow[‡]
WANG, Lu	Post-Doctoral Fellow
SUTCLIFFE, Brian	Visiting Scientist[§]
KIM, Tae-Rae	Graduate Student[||]
YAMADA, Mariko	Secretary
KONDOU, Naoko	Secretary

In theoretical and computational chemistry, it is an important goal to develop functional molecules prior to or in cooperation with experiment. Thus, new bonds and structures provided by heavier atoms are investigated together with the reactivities. In addition, chemical modification and properties of large molecules are investigated to develop functional nanomolecular systems. Efficient computational methods are also developed to perform reliable quantum chemistry calculations for small and large molecular systems.

1. Projector Monte Carlo Method Based on Configuration State Functions. Test Applications to the H_4 System and Dissociation of LiH¹⁾

The diffusion Monte Carlo (DMC) method, also called the projector Monte Carlo (PMC) method, has attracted a lot of attention because of its high accuracy and high parallel efficiency. The parallel DMC programs have been developed and applied to various systems. However, the DMC method has an important fermion sign problem because electrons are treated as particles, and the accuracy depends strongly on the nodes of trial wave functions because the fixed-node approximation is generally used to avoid the fermion sign problem. In addition, the accuracy is not always improved systematically even if the nodes of trial functions are generated at high levels of theory. It has been shown that the trial nodes are improved using variational Monte Carlo techniques. However, it is also important to develop a quantum Monte Carlo method that does not require the nodes of trial wave functions.

Thus, we have developed a new PMC method by using configuration state functions (CSFs), spin-adapted linear combinations of Slater determinants, as walkers, to avoid the fermion sign problem (the name “PMC” is used instead of “DMC” because the diffusion equation is not used apparently in the PMC-CSF method). In the PMC-CSF method, new theory and effective calculation algorithm are developed and tested by making a simple program that can treat up to 4 electrons. The accuracy of the PMC-CSF method depends on the basis sets constructing CSFs, but is systematically improved, regardless of trial functions, by increasing the number of walkers. As verified by test applications to the H_4 and LiH systems, full-CI (configuration interaction) energies are obtainable as a limit for a given basis set (Figure 1).

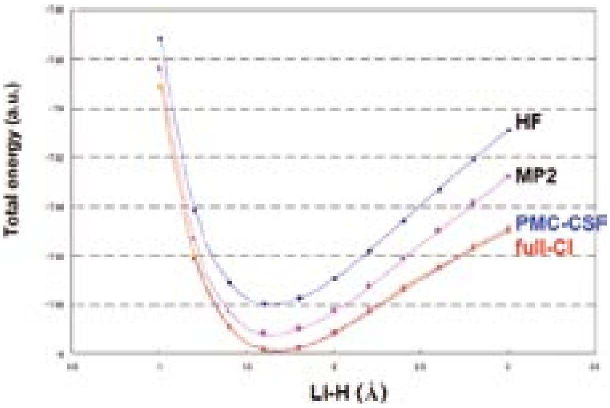

Figure 1. The dissociation of the LiH moilecule.

Obviously, the PMC-CSF method becomes highly accurate by enhancing the quality of basis sets. Unlike conventional CI calculations, no diagonalization of matrices is necessary and important CSFs are effectively selected for the PMC-CSF method. In addition, the PMC-CSF method shows good parallel efficiency, as shown in Table 1.

Table 1. Elapse time (in second) and speedup of the PMC-CSF parallel calculations of the H_4 system.

CPU	1	2	4	8
Time	3999	2010	1008	511
Speedup	1.00	1.99	3.97	7.82

We are now developing a general program suitable high parallel calculations and applicable to large molecules.

2. Chemical Modification of Endohedral Metallofullerenes$^{2–5)}$

The reactivities and chemical modification of endohedral metallofullerenes are of considerable interest in developing functional nanomolecules. Addition of adamantylidene to $La_2@C_{78}$ takes place at the [5,6] and [6,6] positions around the pole and equator of $La_2@C_{78}$. The Addition to $M_2@C_{80}$ (M = La and Ce) makes the two metal atoms collinear with the spiro carbon of the 6,6-oen adduct. Bissilylation of $Ce_2@C_{78}$ affords regioselectively the 1,4-adduct in which the two Ce atoms stand still by facing toward the hexagonal rings at the equator. Addition of adamantylidene to $La_2@C_{72}$ (that does not satisfy the isolated pentagon rule) mainly takes place at the fused pentagons because of the high surface curvature.

3. Nanographenes and BN Analougues: Ground Electronic States and Energy Gap Engineeering$^{6)}$

Graphene has attracted great interest as the new generation of carbon electronics. The lack of an energy gap prevents using graphene in carbon nanoelectronics. It is very important to engineer the band gap by patterning and cutting the graphene sheet into rectangular shapes. Thus, carbon nanographenes (CNGs) were theoretically investigated together with boron nitride nanographenes (BNNGs). As the size of CNGs increases, the HOMO–LUMO energy gaps decrease with a direct inverse dependence on the length of zigzag edges, CNGs with long zigzag edges having open-shell singlet ground states. In contrast, the energy gaps of BNNGs have a weak size-dependence; all BNNGs have closed-shell singlet ground states and those with long zigzag edges have slightly larger energy gaps. CNGs with long zigzag edges are less favorable energetically than their structural isomers with long armchair edges, while BNNGs have the opposite preference. Chemical modifications that change the long zigzag edge into armchair type can efficiently stabilize the kinetically unstable CNGs (with open-shell singlet ground states) and modify their energy gaps.

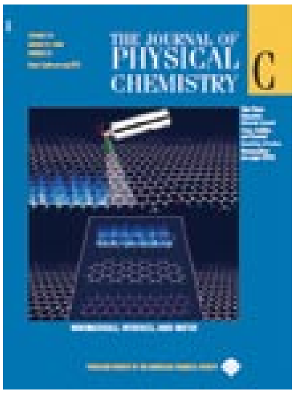

References

1) Y. Ohtsuka and S. Nagase, *Chem. Phys. Lett.* **463**, 431–434 (2008).
2) B. Gao, H. Nikawa, T. Nakahodo, T. Tsuchiya, Y. Maeda, T. Akasak, H. Sawa, Z. Slanina, N. Mizorogi and S. Nagase, *J. Am. Chem. Soc.* **130**, 983–989 (2008).
3) M. Yamada, C. Someya, T. Wakahara, T. Tsuchiya, Y. Maeda, T. Akasak, K. Yoza, E. Horn, M. T. H. Liu, N. Mizorogi and S. Nagase, *J. Am. Chem. Soc.* **130**, 1171–1176 (2008).
4) M. Yamada, T. Wakahara, T. Tsuchiya, Y. Maeda, M. Kako, T. Akasaka, K. Ypza, E. Horn. N. Mizorogi and S. Nagase, *Chem. Commun.* 558–560 (2008).
5) X. Lu, H. Nikawa, T. Nakahodo, T. Tsuchiya, M. O. Ishitsuka, Y. Maeda, T. Akasaka, M. Toki, H. Sawa, Z. Slanina, N. Mizorogi and S. Nagase, *J. Am. Chem. Soc.* **130**, 9129–9136 (2008).
6) X. Gao, Z. Zhou, Y. Zhao, S. Nagase, S. B. Zhang and Z. Chen, *J. Phys. Chem. C* **112**, 12677–12682 (2008).

* Present Address; Department of Chemistry, Kyungpook National University, Taegu 702-701, Korea

† Present Address; Toyota Central R&D Labs., Inc, Nagakute, Aichi 480-1192

‡ Present Address; Center for Tsukuba Advanced Research Alliance, University of Tsukuba, Tsukuba, Ibaraki 305-8577

§ Present Address: School of Chemistry, Seoul National University, Seoul 151-747, Korea

|| Present Address; Faculte des Sciences, Universite Libre de Bruxelles, Bruxelles 1050, Belgium

Electronic Structure and Electron-Nuclear Dynamics of Molecules in Contact with an Electron Reservoir

Department of Theoretical and Computational Molecular Science
Division of Theoretical Molecular Science I

NOBUSADA, Katsuyuki	Associate Professor
YASUIKE, Tomokazu	Assistant Professor
KUBOTA, Yoji	Post-Doctoral Fellow
NODA, Masashi	Post-Doctoral Fellow
SHIRATORI, Kazuya	Graduate Student
IWASA, Takeshi	Graduate Student
YAMADA, Mariko	Secretary

Electronic structures and electron dynamics of molecules or nanostructured materials in contact with an electron reservoir play important roles in heterogeneous catalysis, surface photochemistry, and also electrochemistry. We have developed theoretical methods to calculate electronic structures of adsorbate-surface and electrochemical systems. We have also investigated exciton transfer dynamics in an array of quantum dot.

1. Open-Boundary Cluster Model for Calculation of Adsorbate-Surface Electronic States[1)]

We have developed a simple embedded-cluster model approach to investigate adsorbate-surface systems. In our approach, the physically-relevant subsystem is described as an open-quantum system by considering a model cluster subject to an outgoing-wave boundary condition at the edge. This open-boundary cluster model (OCM) is free from artificial waves reflected at the cluster edge, and thus the adsorbate properties computed with the OCM are almost independent of the model cluster size. The exact continuous density of states (DOS) of a 1D periodic potential model is shown to be precisely reproduced with the OCM. The accurate DOS leads to an appropriate description of adsorbate-surface chemical bonding. Moreover, the open-boundary treatment of the OCM allows us to evaluate the electron-transfer rate from the adsorbate to the surface, whereas the conventional cluster model does not give any information about such a dynamical process.

2. Quasi-Diabatic Decoupling of Born-Oppenheimer Potential Energy Curves for Adsorbate-Metal Surface Systems[2)]

We have applied the open-system treatment, recently developed by the authors, to a simple adsorbate-metal surface model potential. The open-system treatment is found to give a quasi-diabatic representation where the adsorbate electronic states cross the metal ones in the manifold consisting of the Born-Oppenheimer potential energy curves of the whole system. On the obtained quasi-diabatic curves, one can effectively follow time propagation of a nuclear wave packet. The computed propagation has revealed that the formation of a metastable adsorbate leads to the coherent vibrational motion of the neutral adsorbate as well as the desorption induced by electronic transitions.

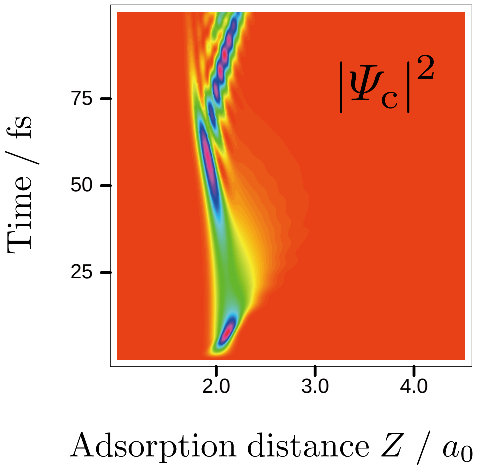

Figure 1. Nuclear wave-packet motion of the neutral adsorbate.

3. Exciton Transfer in Quantum Dot Arrays: Comparison of Eigenbasis and Site Basis Representations[3)]

We discuss differences between eigenbasis and site basis representations for models of exciton transfers in an array of quantum dots. The exciton relaxation processes are well described by the master equation in the eigenbasis representation. The site-basis evolution equation up to the second order of the interdot interaction is straightforwardly derived from the eigenbasis equation by using perturbation theory when the interaction is sufficiently small compared with the energy difference between the exciton states in each quantum dot. Although the higher order site basis equations can be derived similarly, the resultant equations are too complicated to use in the actual calculations. The master equation in the eigenbasis representation has several advantages over the site basis one: (i) the system described in terms of the eigenbasis representation can evolve into thermal equilibrium because the equation satisfies the detailed balance, (ii) the site basis equation does not reasonably describe the exciton state trapped in a local energy minimum at very low temperature, and (iii) it is computationally less demanding to carry out the eigenbasis evolution equation.

4. Development of Finite-Temperature Density Functional Approach to Electrochemical Reactions[4)]

We present a computational method to calculate the electronic states of a molecule in an electrochemical environment. The method is based on our recently developed finite-temperature density functional theory approach to calculate the electronic structures at a constant chemical potential. A solvent effect is treated at the level of the extended self-consistent reaction field model, which allows considering a nonequilibrium solvation effect. An exchange-correlation functional with a long-range correction is employed in this calculation, because the functional is adjusted so that the derivative discontinuity of energy with respect to a number of electrons could be satisfied. It has been found that the derivative discontinuity condition plays a crucial role in an electrochemical system. The computational results are presented for a reaction of $NO^+ + e^- \rightleftarrows NO$ in chemical equilibrium. Owing to the improvement in the solvation effect and the exchange-correlation functional, the calculated activation free energy is in good agreement with experimental results.

5. Oligomeric Gold Clusters with Vertex-Sharing Bi- and Triicosahedral Structures[5)]

We present density functional studies of geometric and electronic structures of a gold cluster compound $[Au_{25}(PH_3)_{10}(SCH_3)_5Cl_2]^{2+}$ (**1**). The cluster has a unique geometric structure consisting of two icosahedral Au_{13} clusters bridged by methanethiolates sharing a vertex gold atom and terminated by chlorine atoms. This structure is very close to the biicosahedral gold cluster $[Au_{25}(PPh_3)_{10}(SC_2H_5)_5Cl_2]^{2+}$ reported in the recent experiment. We further demonstrate that a vertex-sharing triicosahedral gold cluster $[Au_{37}(PH_3)_{10}(SCH_3)_{10}Cl_2]^+$ is also achieved through bridging with the methanethiolates. A comparison between the absorption spectra of the bi- and triicosahedral clusters shows that the new electronic levels due to each oligomeric structure appear sequentially, whereas other electronic properties remain almost unchanged compared to the individual icosahedral Au_{13} cluster

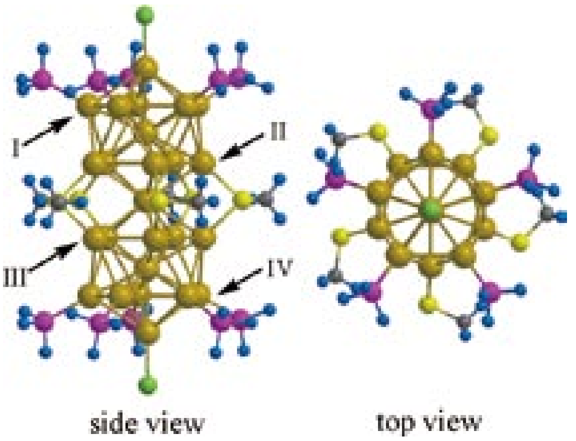

Figure 2. Side and top views of the optimized structure of **1**. The colored balls represent constituent atoms: Au (gold), S (yellow), C (gray), H (blue), P (magenta), Cl (green).

References

1) T. Yasuike and K. Nobusada, *Phys. Rev. B* **76**, 235401 (12 pages) (2007).
2) T. Yasuike and K. Nobusada, *Chem. Phys. Lett.* **457**, 241–245 (2008).
3) Y. Kubota and K. Nobusada, *J. Chem. Phys.* **129**, 094704 (7 pages) (2008).
4) K. Shiratori and K. Nobusada, *J. Phys. Chem. A* **112**, 10681–10688 (2008).
5) K. Nobusada and T. Iwasa, *J. Phys. Chem. C* **111**, 14279–14282 (2007).

Advanced Electronic Structure Theory in Quantum Chemistry

Department of Theoretical and Computational Molecular Science
Division of Theoretical Molecular Science I

YANAI, Takeshi	Associate Professor
KURASHIGE, Yuki	Assistant Professor
MIZUKAMI, Wataru	Graduate Student
YAMADA, Mariko	Secretary

Aiming at predictive computational modelings of molecular electronic structures with *ab initio* quantum chemistry calculations, our scientific exploration is to establish a cutting-edge theoretical methodology that allows one to compute accurately and efficiently the complex electronic structures where the substantial multireference character in the wave functions has to be handled for the qualitative and quantitative descriptions. Our resultant works to be reported here are (1) to develop a new type of the multireference correlation model named Canonical Transformation (CT) theory, which can efficiently describe short-range dynamic correlation on top of the multi-configurational staring wave function, and (2) to construct the extensive complete active space self-consistent field (CASSCF) method combined with *ab initio* density matrix renormalization group (DMRG) method for making unprecedentedly larger active spaces available for the CASSCF calculations. These two pivotal developments are tailored to eventually be incorporated for solving large-scale multireference electronic structure problems.

1. Large-Scale Complete Active Space Self-Consistent Field (CASSCF) with *ab initio* Density Matrix Renormalization Group (DMRG): "DMRG-CASSCF"1)

To perform the large-scale multireference calculations with CT or other multireference methods, the extensively active-spaced reference wave functions where a large number of active electrons are highly (or fully) correlated within the selected active orbitals must be found. The CASSCF method provides the most desirable, optimal reference wave functions, in which the static correlations are effectively captured with the relaxed active orbitals that are optimized self-consistently by energy minimization at a high computational cost. We have developed the large-scale CASSCF method by implementing orbital optimization in the extant DMRG implementation to further allow the self-consistent improvement of the active orbitals, as is done in the standard CASSCF calculations. By virtue of the compact nature of the DMRG wavefunction, this now enables us to handle unprecedentedly larger active space than are possible with the traditional CASSCF. The further feasibility comes concomitantly with a new development of the parallelized orbital optimization allowing for high-quality basis representations of the orbitals. We have named the resulting method DMRG-CASSCF (Figure 1).

Figure 1. Schematic sketch of DMRG-CASSCF implementation. CI and MO coefficients are determined with the alternating two-step algorithm. The new development has realized the efficient computation of 1-, 2-RDMs of DMRG wavefunction, taking advantage of the compact structure of DMRG ansatz.

As applications, we have used our DMRG-CASSCF method to study the low-lying excitations of polyenes from C_8H_{10} to $C_{24}H_{26}$ (11 conjugated bonds) as well as light-harvesting pigment, β-carotene (10 conjugated bonds) with up to a CAS (24e,24o) of full π valences (Figure 2–3). The

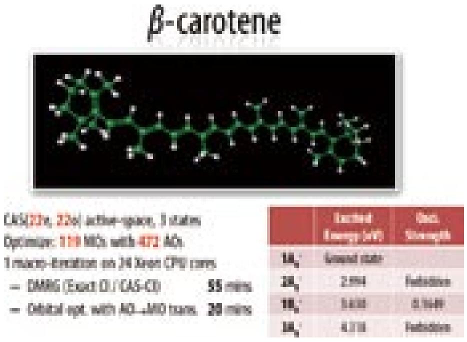

Figure 2. Details of the DMRG-CASSCF calculation for β-carotene along with excitation energies of its three dark states.

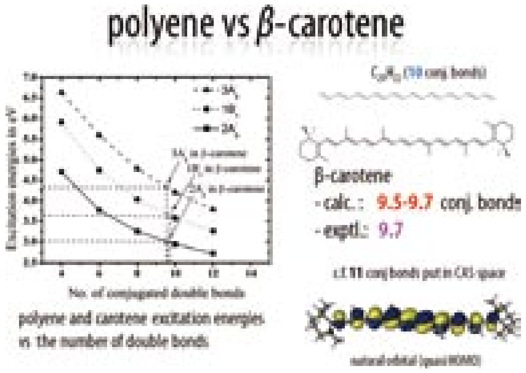

Figure 3. Carotene excitation energies of three states are fitted to polyene excitation energies. We estimated an effective conjugation length of beta-carotene to be 9.5–9.7. These numbers are in good agreement with the experimental estimation 9.7.

conjugated π-system in polyenes and substituted species such as β-carotene give rise to an unusual excitation spectrum, with "dark" electronic states lying beneath the optically allowed HOMO-LUMO transition. The electronic structure of these low-lying states lies at the heart of energy transport in system ranging from the conjugated organic semiconductors to the biological centers of light-harvesting and vision. While the relevant active space on these systems clearly consists of the conjugated π-valence orbitals, to the best of our knowledge, previous calculations have used "incomplete" π-valence space which is limited up to CAS (10e,10o) (*i.e.* 5 nominal conjugated bonds).

2. Robust Implementation of *ab initio* DMRG for Transition Metal Molecular Complexes

Our group has started an alternative implementation of *ab initio* DMRG with algorithmic improvements in which we have some new tricks in constructing operators in renormalization and subspacing Hamiltonian. The development is ongoing with a new scheme of computer parallelism for flop- and memory-distributions of DMRG operators. The development is tailored to computationally affordable applications to accurate, robust electronic structure calculations of complex transition-metal complexes, for which the conventional theoretical treatments get in trouble with entangled electronic states inherent to *d* electrons/orbitals. Figure 4 shows the recent achievement in the performances of our DMRG implementation for calculating isomerization energies of $Cu_2O_2^{2+}$ core. Our method recovers a substantial portion of the full correlation energies efficiently from correlating valence *d* electrons of two Cu atoms with other valences of Cu and O atoms on equal footing

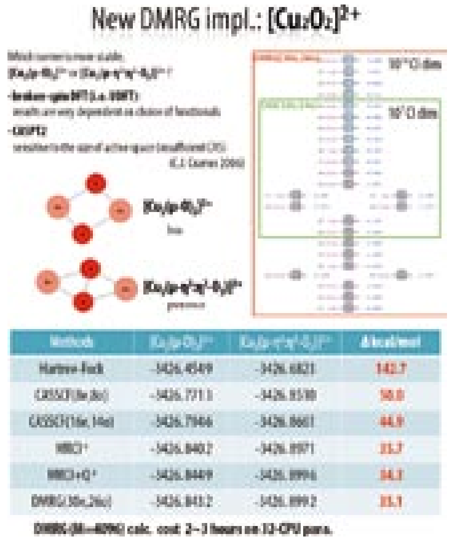

Figure 4. Isomerization energies of $Cu_2O_2^{2+}$ core between bis and peroxo structures by various methods including our new implementation of DMRG. The new, efficient implementation carried out the fully correlated electronic structure calculations.

3. Canonical Transformation (CT) Theory for Efficient Multireference Method(2)

We have been developing a many-body technique based on canonical transformation (CT) for realizing large-scale multireference calculations for the purpose of attaining the chemical accuracy, for which dynamical correlations are described by using cluster expansion on top of muticonfigurational setting (*e.g.* DMRG-CASSCF). We are working on extending the implementation to the wider applications in terms of tractable size of molecules of target. The ongoing reimplementation fixes some of problems in the extant implementation that relies on infinite computer memory. Figure 5 presents the recent application of CT to the description of an energy curve along the isomerization coordinate between bis and peroxo cores of $Cu_2O_2^{2+}$.

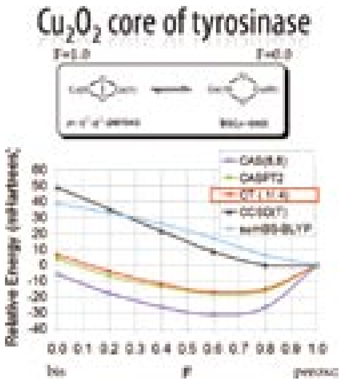

Figure 5. Relative energy curves along the isomerization coordinate between bis and peroxo cores. The difficulty in describing electronic structure of this isomerization arises in maintaining the balanced description of rapidly changing dynamic and static correlation effects and a varying degree of biradical character along the coordinate.

References

1) D. Ghosh, J. Hachmann, T. Yanai and G. K-L. Chan, *J. Chem. Phys.* **128**, 144117 (2008).
2) T. Yanai and G. K-L. Chan, *J. Chem. Phys.* **127**, 104107 (2007).
3) H. Sekino, Y. Maeda, T. Yanai and R. J. Harrison, *J. Chem. Phys.* **129**, 034111 (6 pages) (2008).

Developing the Statistical Mechanics Theory of Liquids in Chemistry and Biophysics

Department of Theoretical and Computational Molecular Science
Division of Theoretical Molecular Science II

HIRATA, Fumio	Professor
CHONG, Song-ho	Assistant Professor
YOSHIDA, Norio	Assistant Professor
MARUYAMA, Yutaka	Post-Doctoral Fellow
MIYATA, Tatsuhiko	Post-Doctoral Fellow
ISHIZUKA, Ryosuke	Post-Doctoral Fellow
PHONGPHANPHANEE, Saree	Graduate Student
KIYOTA, Yasuomi	Graduate Student
YAMAZAKI, Yumi	Secretary
KATAYAMA, Naoko	Secretary
KONDO, Naoko	Secretary
YAMADA, Mariko	Secretary

We have been exploring the chemical and biological processes in solutions, based on the statistical mechanics of liquids, especially, on the integral equation theory of molecular liquids or the "RISM" and "3D-RISM" theories.[1–3] Such exploration can be realized by combining the statistical mechanics theories with the other theoretical methods in the molecular science, which describes the different aspects of the physics such as the quantum processes and the liquid dynamics.

Our recent attention is focused on the "molecular recognition" and "fluctuation" of bio-molecules, which are the two key-processes in the living system. For examples, for an enzymatic reaction to take place, substrate molecules should be accommodated by the enzyme. The process is nothing but the molecular recognition which is regulated by the solvation free energy of the enzyme-substrate (ES) complex, and by the structural fluctuation of the protein.

1. A Water Molecules Identified as a Substrate of Enzymatic Hydrolysis of Cellulose: A Statistical-Mechanics Study[4)]

Among the technologies to utilize the solar energy, the cellulose decomposition due to the enzymatic hydrolysis is getting the highest expectation, because the available resource on the earth is essentially inexhaustible, and the reaction proceeds in natural conditions without using precious metals as a catalyst. However, there is a high barrier to be cleared for the technology to be established as the ultimate substitute for the fossil fuel, that is, how to improve the efficiency of the enzyme. In order to improve the efficiency, one has to clarify the mechanism of the enzymatic hydrolysis reaction. We have started to investigate the problem last year based on the 3D-RISM theory, taking a cellulase-cellohexaose complex as an example.

There are two models proposed by experimentalists for the mechanism of the enzymatic hydrolysis reaction of cellulose, the inverting and retention processes, which can be distinguished by the distance between the two catalytic residues, and by the position of a water molecule as the substrate of the reaction. In our particular example of the Cel44A-cellohexaose complex, the distance is ~5.5 Å for the retention process, whereas that for the inverting process is ~10.0 Å. The water molecule in the inverting process can make hydrogen bonds only with one of the catalytic residues due to the large separation between the residues, while the molecule can make hydrogen-bonds with the both catalytic residues in the retention process (Figure 1).

Shown in Figure 2 is our result for the distribution of water molecules (yellow and green spots) around the active site of the ES-complex. We have identified the water molecule (colored green) as the substrate of the reaction, since the peak of which is distinctly high among other spots. The water molecule is apparently making hydrogen-bonds with the two catalytic residues, Glu186 and Glu359. This is a clear support to the retention mechanism explained above.

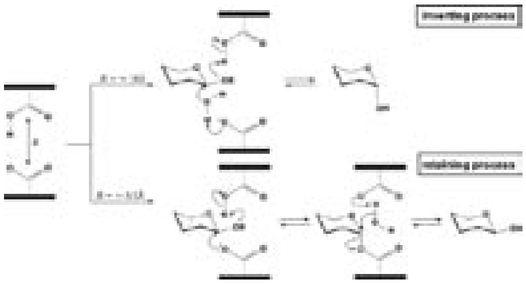

Figure 1. Schematic description of enzymatic hydrolysis of cellulose.

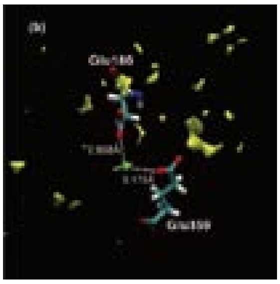

Figure 2. Distribution of water around the active site of the ES-complex.

2. RISM-SCF Study of Temperature and Solvent Dependence of the Free-Energy Surface of the Intramolecular Electron-Transfer[5)]

The free energy surfaces along the intramolecular electron transfer reaction of 1,3-dinitrobenzene radical anion in acetonitrile and methanol are investigated with the reference interaction site model self-consistent field theory. The scheme of the intramolecular electron transfer reaction of 1,3-dinitrobenzene radical anion is shown in figure 3. Although acetonitrile and methanol have similar values of the dielectric constant, the free energy profiles are quite different. In the methanol solution, the charge is strongly localized on one of the nitrile substituents due to a strong hydrogen bond between 1,3-dinitrobenzene and the solvent, while the polarization is not so large in the case of acetonitrile. The temperature dependence of the reorganization energy, the coupling strength and the activation barrier are evaluated in both acetonitrile and methanol. The reorganization energy and the activation barrier decrease with increasing temperature for both cases. The electronic coupling strength also shows similar tendency in the temperature dependence: it increases with increasing temperature in the both solvents, but with different rates. The behavior is explained in terms of the strong polarization induced by the hydrogen bond between solute and solvent in the methanol solution.

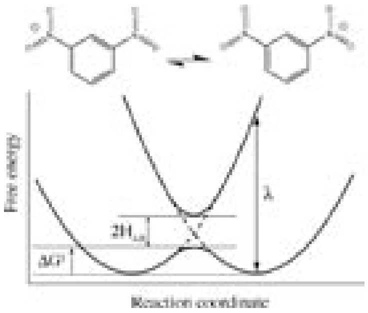

Figure 3. The scheme of the intramolecular electron transfer reaction of 1,3-dinitrobenzene radical anion.

3. On the Proton Exclusion of Aquaporins: A Statistical Mechanics Study[6,7)]

The proton exclusion from aquaporins (AQPs) is one of the most important questions to be solved in the fields of biochemistry, medicine and pharmacology. Although the channels are extremely permeable for water, approximately a billion molecules per second pass through the channel, protons are strictly excluded from the permeation. The mechanism should be readily examined if one can calculate the distribution of the hydronium ion in the channel. The information of the hydronium-ion distribution in the channel may also be useful for examining the possibility of the proton-jump mechanism, because a proton should be existing most likely in the form of the hydronium ion except for the moment of barrier crossing. In this study, we apply the 3D-RISM theory to AQP1 and GlpF for elucidating the proton exclusion from those channels.

In Figure 4, the contour map of the electrostatic potential due to the channel atoms, the 3D-distribution of the water and of hydronium ions, and the one-dimensional profile of the distribution of the solution components are depicted along the channel axis. In both channels, water distributes continuously throughout the channel, while the distribution of hydronium ions is intermitted by gaps due to the electrostatic repulsion originated from the positive charges in the channels. The gap is very large in the case of AQP1, extending from R197 to the NPA region. From the results, we can readily conclude in the case of AQP1 that protons are excluded from permeation primarily due to the electrostatic repulsion inside channel. On the other hand, in the case of GlpF, the results leave slight possibility for proton to permeate through the gap around R206 by the proton jump mechanism. However, the mechanism does not work entirely through out the channel due to the formation of the bipolar orientation at the NPA region. So, a proton has small but discernable conductivity in GlpF through the combined mechanism of the proton jump and the diffusion of hydronium ions in accord with the experiment.

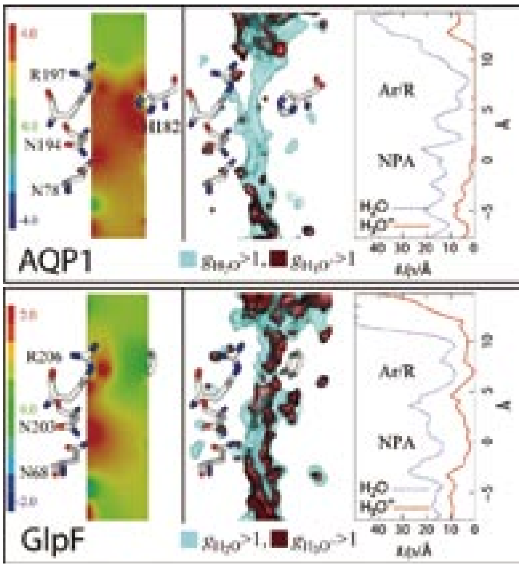

Figure 4. The distribution functions of water and hydronium ion in aquaporin channels. The contour colors show the electrostatic potential of protein in esu unit.

References

1) F. Hirata, *Molecular Theory of Solvation*, Kluwer; Dordrecht, Netherlands (2003).
2) A. Kovalenko and F. Hirata, *J. Chem. Phys.* **110**, 10095–10112 (1999).
3) T. Imai, R. Hiraoka, A. Kovalenko and F. Hirata, *J. Am. Chem. Soc. (Communication)* **127**, 15334–15335 (2005).
4) Y. Ikuta, S. Karita, Y. Kitago, N. Watanabe and F. Hirata, *Chem. Phys. Lett.* **465**, 279–284 (2008).
5) N. Yoshida, T. Ishida and F. Hirata, *J. Phys. Chem. B* **112**, 433–440 (2008).
6) S. Phongphanphanee, N. Yoshida and F. Hirata, *J. Am. Chem. Soc. (Communication)* **130**, 1540–1541 (2008).
7) S. Phongphanphanee, N. Yoshida and F. Hirata, *J.Mol. Liq.* in press.

Nonequilibrium Theory of Conductors

Department of Theoretical and Computational Molecular Science
Division of Theoretical Molecular Science II

YONEMITSU, Kenji	Associate Professor
YAMASHITA, Yasufumi	Assistant Professor
MAESHIMA, Nobuya	Post-Doctoral Fellow*
MIYASHITA, Satoshi	Post-Doctoral Fellow
TANAKA, Yasuhiro	Post-Doctoral Fellow
KATAYAMA, Naoko	Secretary

When low-dimensional correlated electron systems such as organic conductors are placed in nonequilibrium environments, they sometimes show novel phenomena that never appeared in conventional conductors based on rigid bands. One example is found in the current-voltage characteristics and the field-effect characteristics caused by metal-Mott-insulator interfaces. Another example is found in photoinduced phase-transition dynamics, where the induced transient state is not reached by simply changing temperature or pressure. It is possible because the energy of a photon is much higher than thermal energies. Our theoretical researches are focused on the mechanisms of such nonlinear phenomena.

1. Suppression of Rectification at Metal–Mott-Insulator Interfaces$^{1)}$

Charge transport through metal–Mott-insulator interfaces is studied and compared with that through metal-band-insulator interfaces. For band insulators, rectification has been known to occur owing to a Schottky barrier, which is produced by the work-function difference.

For Mott insulators, however, qualitative different current-voltage characteristics are obtained. Theoretically, we use the one-dimensional Hubbard model for a Mott insulator and attach to it the tight-binding model for metallic electrodes. A Schottky barrier is introduced by a solution to the Poisson equation. The current density is calculated by solving the time-dependent Schrödinger equation. We mainly use the time-dependent Hartree-Fock approximation and also use exact many-electron wave functions on small systems for comparison. Rectification is found to be strongly suppressed even for large work-function differences.

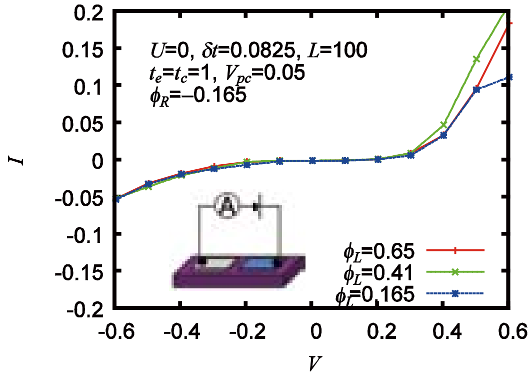

Figure 1. Current-voltage characteristics for a band insulator. Rectification is clearly seen.

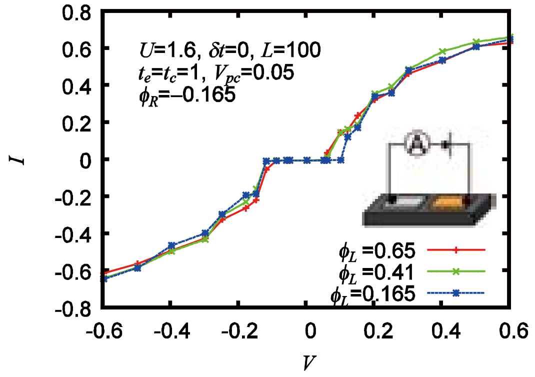

Figure 2. Current-voltage characteristics for a Mott insulator. Rectification is suppressed.

Its close relationship is shown with the fact that field-effect injections into one-dimensional Mott insulators are ambipolar. Experimentally, we fabricated asymmetric contacts on top of single crystals of quasi-one-dimensional organic Mott and band insulators. Rectification is strongly suppressed at an interface between metallic magnesium and Mott-insulating (BEDT-TTF)(F_2TCNQ).

2. Charge Order with Structural Distortion in Organic Conductors: Comparison between θ-$(ET)_2X$ and α-$(ET)_2X$ Salts$^{2)}$

Charge ordering with structural distortion in quasi-two-dimensional organic conductors θ-(BEDT-TTF)$_2$RbZn(SCN)$_4$ and α-(BEDT-TTF)$_2$I$_3$ is investigated theoretically. We use the Hartree-Fock approximation, strong-coupling perturbation theory, and exact diagonalization of a 3/4-flled extended Hubbard model for an anisotropic triangular lattice. The model includes on-site and inter-site Coulomb interactions together with Peierls-type electron-lattice couplings. We examine the effect of lattice degrees of freedom on charge order. It is found that the experimentally observed, horizontal charge order is stabilized by lattice distortion in both compounds. In particular, the lattice effect is crucial to the realization of the charge order in θ-(BEDT-TTF)$_2$RbZn(SCN)$_4$, while the peculiar band structure of α-(BEDT-TTF)$_2$I$_3$ whose symmetry is lower than that of θ-(BEDT-TTF)$_2$RbZn(SCN)$_4$ is also an important factor in α-(BEDT-TTF)$_2$I$_3$ together with the lattice distortion. For α-(BEDT-TTF)$_2$I$_3$, we obtain a transition from the metallic phase with charge disproportion to the horizontal charge order with lattice modulations, which is consistent with the latest X-ray experimental result.

3. Photoinduced Change in the Charge Ordering Pattern in (EDO-TTF)$_2$PF$_6$ with Strong Electron-Phonon Interaction[3)]

The quasi-stable state in the photoinduced phase transition for the quasi-one-dimensional quarter-filled organic conductor (EDO-TTF)$_2$PF$_6$ has been examined by ultrafast reflective measurements and time-dependent model calculations incorporating both electron-electron and electron-phonon interactions. The transient optical conductivity spectrum over a wide probe photon energy range revealed that photo- excitation induced a new type of charge-disproportionate state. Additionally, coherent and incoherent oscillations dependent on probe photon energies were found, as predicted by the calculation.

The photoinduced state has a (1010) charge separation owing to competing long-range e–e and e–anion interactions.

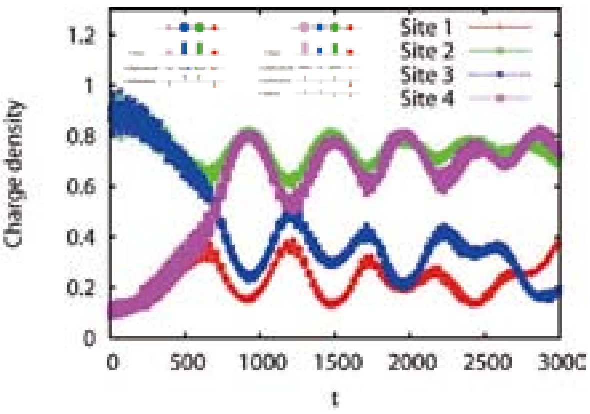

Figure 3. Time dependence of charge densities after the (0110)-charge-order ground state is photoexcited to a {0200} state.

On the low-energy side of the photoinduced peak, the transient spectrum shows irregular time dependences. It is because delocalized electrons are observed there, which are scattered by phonons on different molecules and times. Thus, the coherence is easily lost.

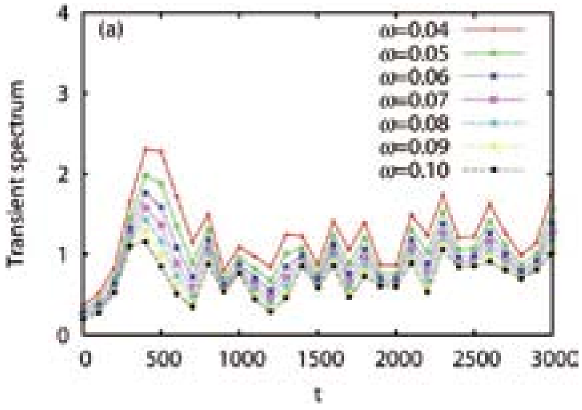

Figure 4. Time dependence of transient spectra on the low-energy side of a main peak, after photoexcitation from (0110) to {0200}.

On the high-energy side of the photoinduced peak, the transient spectrum shows coherent oscillations. It is because localized charge-transfer processes are observed there, which are governed by the instantaneous distribution of charge and displacements. The coherence is rather robust.

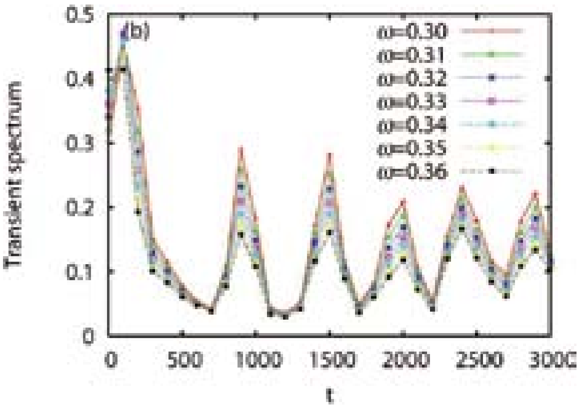

Figure 5. Time dependence of transient spectra on the high-energy side of a main peak, after photoexcitation from (0110) to {0200}.

References

1) K. Yonemitsu, N. Maeshima and T. Hasegawa, *Phys. Rev. B* **76**, 235118 (6 pages) (2007).

2) Y. Tanaka and K. Yonemitsu, *J. Phys. Soc. Jpn.* **77**, 034708 (9 pages) (2008).

3) K. Onda, S. Ogihara, K. Yonemitsu, N. Maeshima, T. Ishikawa, Y. Okimoto, X. -F. Shao, Y. Nakano, H. Yamochi, G. Saito and S. Koshihara, *Phys. Rev. Lett.* **101**, 067403 (4 pages) (2008).

---

* Present Address: Institute of Materials Science, University of Tsukuba, Tsukuba, Ibaraki 305-8573

Molecular Dynamics Study of Classical Complex Systems and Quantum Systems in Condensed Phase

Department of Theoretical and Computational Molecular Science
Division of Computational Molecular Science

OKAZAKI, Susumu	Professor*
YAMADA, Atsushi	Assistant Professor
MIKAMI, Taiji	Post-Doctoral Fellow
ANDOH, Yoshimichi	Post-Doctoral Fellow
FUJIMOTO, Kazushi	Graduate Student

1. Electrostatic Potential Gap at the Interface between Triethylamine and Water Phases Studied by Molecular Dynamics Simulation[1)]

Molecular dynamics calculations were carried out in order to investigate the interfacial properties of the two-phase coexistence state of the triethylamine (TEA) and water mixture, which is known to have a lower critical soluble temperature. Two kinds of initial configuration were adopted. One was a two-phase coexistence state and the other was a random mixed state of TEA and water molecules. After an equilibration calculation of several nanoseconds, the density profiles converged to the same equilibrated two-phase coexistenc state. In the equilibrated state, anisotropic orientations were observed for both molecules, which makes an electrostatic potential gap between these phases.

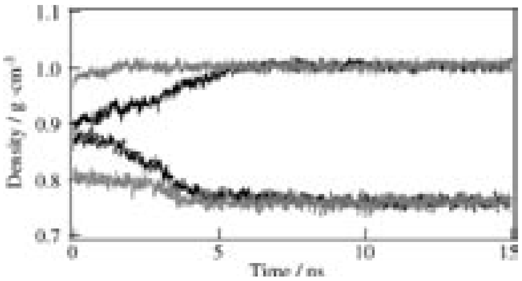

Figure 1. Time evolution of the density of the water phase (solid line) and TEA phase (dotted line) obtained from the MD calculation started from the two-phase state (gray) and from the mixed state (black).

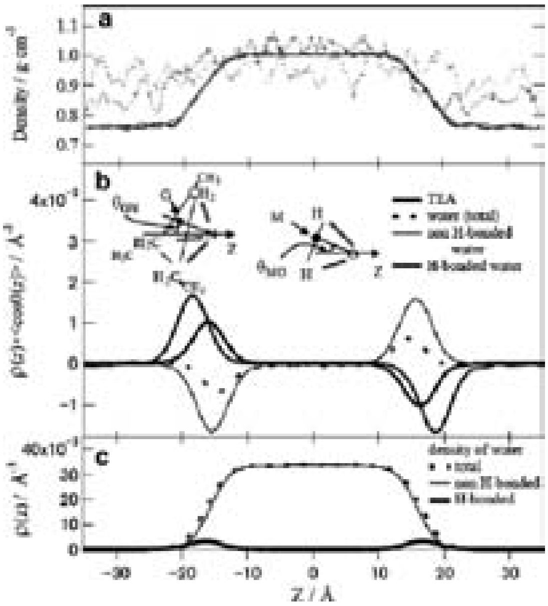

Figure 2. (a) Equilibrated density (solid line) profile calculated from the twophase state (black) and from the mixed state (gray). The corresponding density profile of the initial states is also shown with dotted lines. (b) q(*z*) A Acosha for TEA molecule (gray) and for water (black) as a function of the *z*-coordinate. Those with respect to the water molecule, hydrogen bonded (dotted) and non-hydrogen bonded molecules (thin line) to the nitrogen atom of TEA molecule are shown. Definition of hGN and hMO are also shown schematically (see text). (c) Density profile for water molecules.

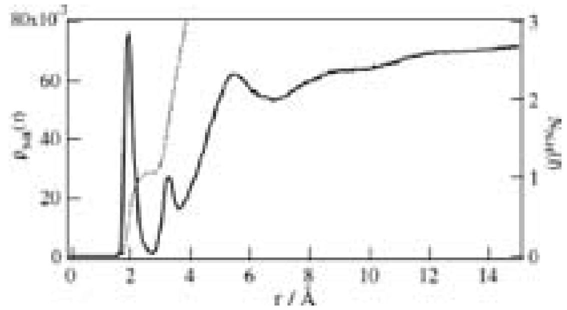

Figure 3. Pair distribution function $\rho_{N\text{–}H}(r)$ (solid line) and its running coordination number, $N_{N\text{–}H}(r)$ (dotted line), at the vicinity of the interface with a width of 10 Å.

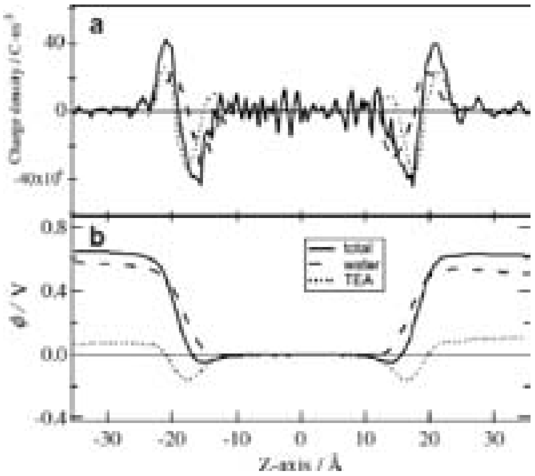

Figure 4. Charge density (a) and electrostatic potential profile (b) as a function of the *z*-coordinate. Solid line; the total system, dotted line; TEA molecule contribution and broken line: Water molecule contribution.

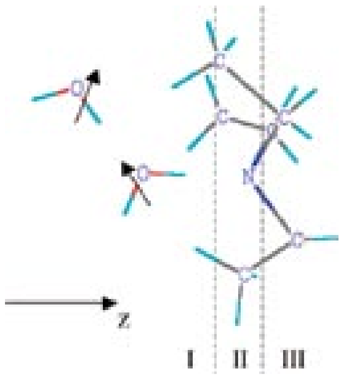

Figure 5. Schematic image of water and TEA molecules at the interface.

We have performed molecular dynamics calculations for the two-phase coexistence state of the TEA and water mixture. At the interface between the two phases, both molecules have unique orientations, which results from hydrogen bonding between TEA and water molecules. These anisotropic orientations lead to a large potential gap of 0.65 V between two phases. Additionally, resulting from the orientation of the TEA molecules, the electric potential has the minimum value in the vicinity of the interface

2. A molecular Dynamics Study of Structure and Dynamics of Surfactant Molecules in SDS Spherical Micelle$^{2)}$

An analysis of structure and dynamics of surfactant molecules in SDS micelle is presented based on molecular dynamics calculations. Two-dimensional surface correlation function for the hydrophilic sulfur atoms as well as the bond analysis between the hydrophobic alkyl chains shows that the surfactant molecules are packed sparsely in the micelle such that they form a soccer ball-like structure characterized by the coordination number of three. The hydrophobic bond between the surfactant molecules is produced and annihilated repeatedly in a time scale of about 100 ps but disappears by their diffusion in a time scale of about 1 ns.

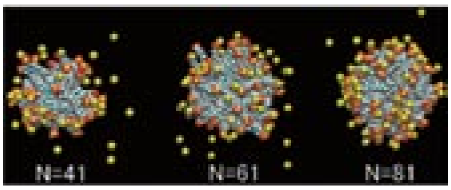

Figure 6. Snapshots of the simulated SDS spherical micelles formed in water. In the figure, water molecules are not drawn just for clarification.

References

1) S. Kajimoto, N. Yoshii, J. Hobley, H. Fukumura and S. Okazaki, *Chem. Phys. Lett.* **448**, 70–74 (2007).
2) N. Yoshii and S. Okazaki, *Cond. Matt. Phys.* **10**, 573–578 (2007).

---

* Present Address; Nagoya University

Theoretical Studies on Condensed Phase Dynamics

Department of Theoretical and Computational Molecular Science
Division of Computational Molecular Science

SAITO, Shinji	Professor
KIM, Kang	Assistant Professor
KOBAYASHI, Chigusa	Post-Doctoral Fellow
YAGASAKI, Takuma	Post-Doctoral Fellow
UENO, Harumi	Secretary

Liquids and biological systems show complicated dynamics because of their structural flexibility and dynamical hierarchy. Understanding these complicated dynamics is indispensable to elucidate chemical reactions and relaxation in solutions and functions of proteins. We have been investigating liquid dynamics and chemical reactions in biological systems using molecular dynamics simulation and electronic structure calculation. In addition, we have been analyzing complicated liquid dynamics using multi-dimensional spectroscopy.

1. Slow Dynamics in Random Media: Crossover from Glass to Localization Transition

The transport phenomena of fluids confined in random media is of great important in physics, chemistry, biology, and engineering, *e.g.* water in micelles or living cells. Spatial restrictions in random media can cause unusual slow dynamical properties. Recent experiments suggest that the glass transition temperature in spatially confined systems, *e.g.* a thin film or a porous media, is largely different from that in bulk, though little is understood about these phenomena.

Recently, the glass transition of hard-spheres confined in random media has intensively investigated based on the mode-coupling theory (MCT) and two notable results were predicted. First, the memory kernel in the MCT equation consists of the linear and nonlinear terms. Coupling coefficients in the memory kernel representing fluid-fluid and fluid-matrix interactions are controlled by varying fluid and matrix densities. Thus, the glass transition dynamics is characterized by two kinds of dynamics which are called the two-step type B dynamics at high fluid densities and the single-step type A dynamics at small fluid densities, respectively. Second prediction is the existence of the reentrant transition in low fluid density regime at a certain high matrix density, where delocalization of fluid particles occurs and the dynamics become faster in spite of the increase in the fluid density with a fixed matrix density.

In the present study, we carry out molecular dynamics simulations of soft sphere supercooled liquids and hard sphere liquids in random media to obtain quantitative information about dynamics over a broad range of fluid and matrix densities and the physical interpretation of the above theoretical predictions. Dynamical phase diagram of the liquid-glass transition at various fluid and matrix densities has been determined from simulations, which is well correlated with MCT's predictions. Two types of dynamics, type A and B, have been found in density correlation function, mean square displacement, non-ergodic parameter, and four-point correlation function. Furthermore, it is found that in the low fluid density at a certain high matrix density the reentrant transition exists as MCT predicts, where the delocalization of particles occur due to kick-out mechanics resulting from hopping motions of fluid particles surrounded by the random media.

2. Conformational Changes and Fluctuations of Ras

Ras superfamily is a signal transduction protein. Ras is cycled between two states of bound guanine nucleotide, the GTP- and GDP-bound states, by hydrolysis. Ras binds to effectors for regulation of cell proliferation in the GTP-bound state, whereas it is inactivated in the GDP-bound state. X-ray crystallography studies revealed conformational changes of two regions around a nucleotide binding site, switch I and switch II, in the two states. The conformational changes result from the difference of the coordinations of γ-phosphate, Gly60 and Thr35 in the two states. In addition to the conformational change between the GTP- and GDP-bound states, two states with different conformations are experimentally found in the GTP-bound state. The two states are called state 1 and state 2. The results of ^{31}P NMR show that the interconversion between states 1 and 2 is governed by the coordination between Thr35 and Mg^{2+} and that state 2 is a predominant form of H-Ras and interacts with effectors. We investigated the conformational changes and fluctuations in the two states, states 1 and 2, in the GTP-bound state and the GDP-bound state by using molecular dynamics calculations.

We found the large difference of the secondary structure of switch I in states 1 and 2 and the GDP-bound state. The differences arise from the change in coordinations; Thr35 binds to Mg^{2+} in state 2, whereas the coordination is broken in state 1 and the GDP-bound state. The absence of the coordinations results in not only the distortions but also the large fluctuation of switch I in state 1. The present result suggests that the distortion caused by the breaking of the coordinations in switch I weakens affinities with effectors in state I.

In switch II, we found no significant difference between the secondary structure in states 1 and 2 because the coordinations in the region are conserved in these states. In contrast, structural change between the GTP- and GDP-bound states, arising from the breaking of the HB between γ-phosphate and Gly60, is found and Gly60 and its neighbor residues adopt an extended form in the GDP-bound state. Large fluctuations are experimentally found in switch II in GTP-bound state. As experimental results, large fluctuations in the α2 helix, the transitions among 3_{10}-helix, α-helix, and a partially unwound helix are found in states 1 and 2, on the other hand, any significant fluctuation in α2 helix is not seen in the GDP-bound state. We found that the fluctuations are correlated with the rearrangement of transient HBs involving the polar side-chains in switch II in the states 1 and 2. The present result implies that conformations in fluctuation are stabilized by transient HBs, so that interconversions among multiple states take place in GTP-bound state.

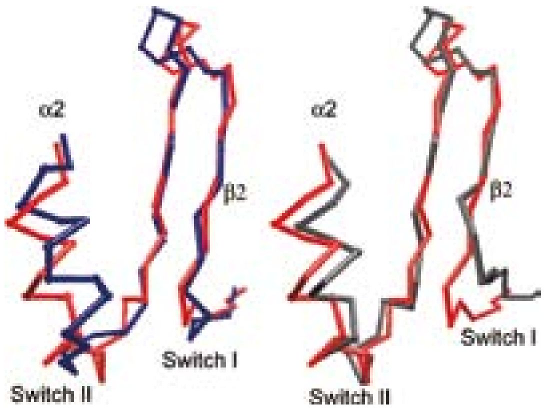

Figure 1. Superposition of the average Cα traces in switches I and II, and the neighbor region in state 1 (gray), state 2 (red), and GDP-bound state (blue), respectively.

3. Ultrafast Intermolecular Dynamics of Liquid Water: Theoretical Study of Two-Dimensional Infrared Spectroscopy

Physical and chemical properties of liquid water are dominated by hydrogen bond structure and dynamics. Recent studies of nonlinear vibrational spectroscopy of intramolecular motion provide new insight into ultrafast hydrogen bond dynamics. However, our understanding of intermolecular dynamics of water is still limited. In this study, we theoretically investigated intermolecular dynamics of liquid water in terms of two-dimensional infrared (2D IR) spectroscopy. We calculated the 2D IR spectrum by explicitly estimating the three-time correlation function of the total dipole moment, and thus obtained novel information about the time dependent mode couplings that cannot be available from the one-dimensional spectroscopy (Figure 2).

We found that the frequency correlation, *i.e.* the initial inhomogeneity, of the libration motion is lost with the time scale of ~110 fs. The energy of the libration motion relaxes to the low frequency motion with the time scale of ~80 fs. The energy relaxation to the low frequency motion is followed by the slow relaxation due to the hydrogen bond structural change induced by incident electric field pulses. We analyzed the effect of the hindered translation motion on these ultrafast dynamics. It was shown that both the frequency modulation of libration motion and the energy relaxation from the libration to the low frequency motion significantly slow down in the absence of the hindered translation motion. The present result revealed that the anharmonic coupling between the hindered translation and libration motions is essential for the ultrafast relaxation dynamics in liquid water.

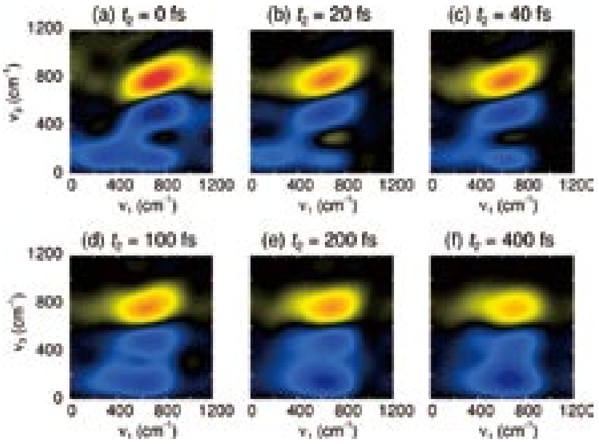

Figure 2. 2D IR correlation spectra of intermolecular motion of liquid water at several waiting times. The positive peak at (ν_1,ν_3) = (~700 cm^{-1},~800 cm^{-1}) is due to the stimulated emission and the bleaching of the libration motion and the negative peak at (~700 cm^{-1},~500 cm^{-1}) is due to the excited state absorption.

Reference

1) T. Yagasaki and S. Saito, J. *Chem. Phys.* **128**, 154521 (7 pages) (2008).

Theoretical Study on Molecular Excited States and Chemical Reactions

Department of Theoretical and Computational Molecular Science
Division of Computational Molecular Science

EHARA, Masahiro	Professor
KAWAGUCHI, Ritsuko	Secretary

Molecules in the excited states show characteristic photophysical properties and reactivity. We investigate the molecular excited states and chemical reactions which are relevant in chemistry, physics, and chemical biology with developing the highly accurate electronic structure theory. We are also interested in the excited-state dynamics and energy relaxation so that we also develop the methodology of large-scale quantum dynamics. In this report, we report our recent studies on the inner-shell spectroscopy[1,2] and catalytic reaction.[3]

1. Theoretical Study of the Vibration-Induced Suppression of Valence-Rydberg Mixing[1]

The vibrational wave function of a molecule is spatially more spread out when the molecule has one or more quanta of vibrational excitation. Thus spectroscopic studies of vibrationally excited molecules can be used to probe different regions of the potential surfaces of electronically excited states. In this work, we examine that vibrational excitation of the electronic ground state significantly affects the amount of valence character observed in the Rydberg series in the x-ray absorption spectrum of N_2O. In the O1s x-ray absorption spectrum of ground state N_2O, the ns σ Rydberg series appears with significant intensity due to a mixing of σ* valence character in the Rydberg states. But, the excitation of the Rydberg states is significantly suppressed for ground state molecules in excited bending-mode vibrational states.

Figure 1 compares the initial-state specific ARIY (Angle-Resolved Ion Yield) spectra in the vicinity of the O 1s ionization threshold. The absorption spectra were observed at 300/700 K and the vibrationally excited absorption spectrum was extracted assuming the Boltzmann distribution. A key finding is that the intensity of the *ns* σ Rydberg series and *A*' state are significantly suppressed and increased for excitation from vibrationally excited states, respectively, whereas the intensity of the *ns* σ Rydberg series is unchanged. These observations suggest that the decrease in the bond angle causes a decrease in the mixing in of valence character that enhances the transition probability to the Rydberg states. In order to understand these phenomena, we executed the SAC-CI calculations of the energies and the second moment $<r^2>$ of the O1s excited states varying the bond angle.

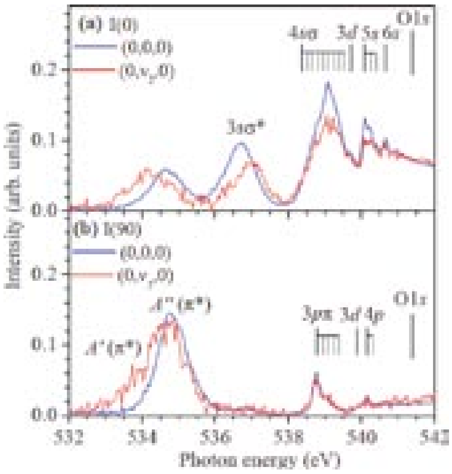

Figure 1. ARIY spectra in the N_2O O1s π* and Rydberg excitation region. (a) Initial state specific 0°ARIY spectra for the vibrationally ground state (blue) and vibrationally excited states (red). (b) Initial state specific 90°ARIY spectra.

Figure 2 shows cuts of the calculated potential energy surfaces of the O 1s excited states of *A*' symmetry. The 1*A*' state is correlated to the π* state and stabilizes along the bending coordinate. All other states are stable in the linear structure. A characteristic curve crossing occurs between the σ and π Rydberg states along the bending coordinate. These potential curves explain the red shift of the π* state and the blue shift of 3sσ and 4sσ states. In order to analyze the mixing of the valence character in the Rydberg states, we examined the electronic part of the second moment $<r^2>$, which is anticorrelated to the amount of valence character (Figure 3). The second moments of the 3*s*σ, 4*s*σ, and 5*s*σ states become large as the molecule becomes bent. This indicates that the mixing of the valence character in these states becomes less as the bond angle decreases. Consequently, the absorption oscillator strength to the *ns* σ Rydberg states becomes small. These results confirm the interpretation of the intensity changes observed for excitation from vibrationally excited molecules.

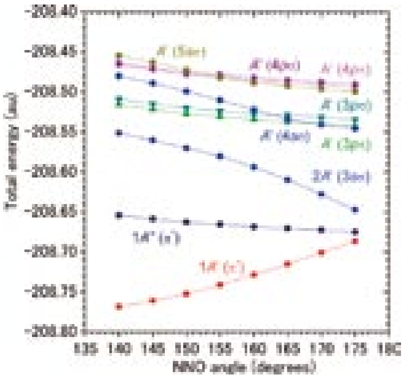

Figure 2. Potential energy curves of the low-lying O1s excited states of N_2O at R_{NN} = 1.127 Å and R_{NO} = 1.185 Å.

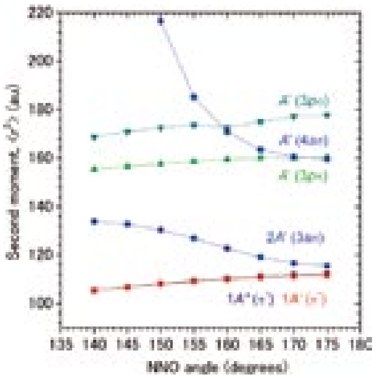

Figure 3. Second moments $<r^2>$ of the low-lying O1s excited states of N_2O at R_{NN} = 1.127 Å and R_{NO} = 1.185 Å.

As seen in Figure 2, the 1*A*'(π*) state stabilizes along the bending coordinate whereas the 2*A*'(3*s*) state destabilizes more than the 1*A*''(π*) state. This anticorrelation indicates that the 1*A*'(π*) and 3*sA*' states are strongly coupled. We believe that this coupling opens a flow of the valence character from the 3*sA*', 4*sA*', and 5*sA*' Rydberg states to the 1*A*'(π*) state. Analyzing the MOs which contribute to the excitations, we concluded that the counterpart of the decrease in the mixing of the valence character in the 3*s*, 4*s*, and 5*s* states is an increase in the *s*σ -type character of the *a*'(π*) orbital.

Thus, using an *ab initio* analysis of the electronic part of the second moment $<r^2>$, the suppression is interpreted as being due to a decrease in the mixing of the valence character in the *ns* σ Rydberg states with decreasing bond angle.

2. Theoretical Study of the Palladium-Catalyzed Regioselective Silaboration of Allene3)

Transition-metal catalyzed additions of silicon-containing σ-bonds to unsaturated bonds of organic molecules have been a major strategy for the synthesis of organosilicon compounds. While Si–Si bond addition has been extensively studied, addition reactions involving silicon–heteroatom bonds such as B, Sn and Ge have become important topics in recent years. Many reactions of these interelement σ-bonds proceed regioselectively, leading to the effective syntheses of regiodefined organosilicon compounds. Recently, effective silaboration reactions of allenes using silylborane have been developed. These reactions proceed in a regio- and stereoselective fashion in the presence of the palladium catalyst, producing synthetically useful β-borylallylsilanes in high yields.

We theoretically investigated this catalytic reaction, the silaboration of allene catalyzed by the Pd complex, to clarify the reaction mechanism and the origin of the regioselectivity (Figure 4). We examined the overall reaction scheme in particular to determine the mechanism of the regioselectivity. The present catalytic reaction is exothermic and the rate-determining step is the insertion of allene into the Pd–B bond of the Pd complex. σ-Allylic and π-allylic complexes exist as intermediates and play an important role in the regioselectivity. Selective insertion of the unsubstituted C=C bond into the Pd–B bond produces the most stable σ-allylic complex, which converts to the π-allylic complex while maintaining the Pd–O coordination. The selective formation of the specific σ-allylic complex and the large activation barrier between two isomeric π-allylic complexes dominantly determines the regioselectivity of the present reaction. The major-product complex is less stable than the minor-product complex, and therefore kinetic control is predominant in the present reaction.

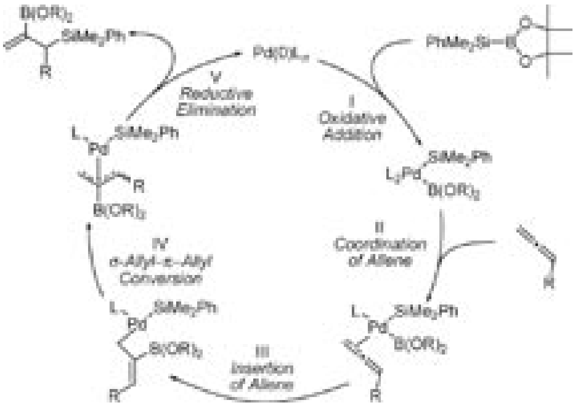

Figure 4. Reaction mechanism of the palladium-catalyzed regioselective silaboration of allene.

References

1) T. Tanaka, M. Hoshino, H. Kato, M. Ehara, N. Yamada, R. Fukuda, H. Nakatsuji, Y. Tamenori, J. R. Harries, G. Prümper, H. Tanaka and K. Ueda, *Phys. Rev. A* **77**, 012709 (4 pages) (2008).

2) M. Ehara and H. Nakatsuji, *Collect. Czech. Chem. Commun.* **73**, 771–785 (2008).

3) Y. Abe, K. Kuramoto, M. Ehara, H. Nakatsuji, M. Suginome, M. Murakami and Y. Ito, *Organometallics* **27**, 1736–1742 (2008).

Theory and Computation of Liquids and Liquid Interfaces

Department of Theoretical and Computational Molecular Science
Division of Computational Molecular Science

MORITA, Akihiro	Professor*
ISHIDA, Tateki	Assistant Professor
KAWAGUCHI, Ritsuko	Secretary

The following projects 1 and 2 focus on the development of theory and computational analysis methods for interfacial sum frequency generation (SFG) spectroscopy and its application to aqueous interfaces. The visible-infrared sum frequency generation spectroscopy is a powerful method to obtain interface-specific vibrational spectra. While this experimental technique is now widely used as an interface probe in a molecular level, reliable interpretation of the observed spectra is often lacking which significantly hinders the progress of this surface characterization method. The following project 1 summarized the theoretical methods of SFG analysis that we have developed. Project 2 is a collaborative work with experimental groups of Drs. Miyamae at AIST and Dr. Ouchi at Nagoya. Collaboration of SFG experiments and the theoretical analysis will be a powerful way to study liquid interfaces. Project 3 summarizes theoretical study of mass transfer dynamics and kinetics at liquid-water interfaces.

Projects 4, 5, and 6 are mainly conducted by Dr. Ishida and his collaborators.

1. Theory of Sum Frequency Generation Spectroscopy[1)]

Gas-liquid interfacial structures of NaCl and NaI aqueous soluThis article summarizes computational analysis of the vibrational Sum Frequency Generation (SFG) spectroscopy with molecular dynamics simulation. The analysis allows direct comparison of experimental SFG spectra and microscopic interface structure obtained by molecular simulation, and thereby obviates empirical fitting procedures of observed spectra. In the theoretical formulation, the frequency-dependent nonlinear susceptibility of an interface is calculated in two ways, based on the energy representation and time-dependent representation. The application to aqueous interfaces revealed a number of new insight into the local structure of electrolyte interfaces and interpretation of the SFG spectroscopy.

2. Sulfuric Acid Aqueous Solution Surfaces Studied by a Combination of Sum Frequency Generation and Molecular Simulation[2)]

This project is a collaborative work with experiment of SFG spectroscopy. The vibrational sum frequency generation spectra of the air-liquid interface of H_2SO_4-H_2O solutions over the wide range of concentration are measured in the SO stretch region (1000–1300 cm^{-1}). This is the first measurement of sulphur species at the surface region with distinguishing their ionization state. The analogy of the concentration dependence of Raman and SFG is indicative of a nearly identical behavior of the first acid dissociation at the air-liquid interface as in the bulk.

3. Theoretical Investigation of Aqueous Surface Structure and Mass Transfer Dynamics[3)]

The mass transfer mechanism across gas/water interface is studied with molecular dynamics (MD) simulation. The MD results provide a robust and qualitatively consistent picture to previous studies about microscopic aspects of mass transfer, including interface structure, free energy profiles for the uptake, scattering dynamics and energy relaxation of impinging molecules. These MD results are quantitatively compared with experimental uptake measurements, and we find that the apparent inconsistency between MD and experiment could be partly resolved by precise decomposition of the observed kinetics into elemental steps. Remaining issues and future perspectives toward constructing a comprehensive multi-scale description of interfacial mass transfer are summarized.

4. Theoretical Study of Temperature and Solvent Dependence of the Free-Energy Surface of the Intramolecular Electron-Transfer Based on the RISM-SCF Theory4)

The free-energy surfaces along the intramolecular electron-transfer reaction path of the 1,3-dinitrobenzene radical anion in acetonitrile and methanol are investigated with the reference interaction site model self-consistent field theory. Although acetonitrile and methanol have similar values of the dielectric constant, the free-energy profiles are quite different. In the methanol solution, the charge is strongly localized on one of the nitrile substituents due to a strong hydrogen bond between 1,3-dinitrobenzene and the solvent, while the polarization is not so large in the case of acetonitrile. The temperature dependence of the reorganization energy, the coupling strength, and the activation barrier decrease with increasing temperature for both cases. The electronic coupling strength also shows a similar tendency in the temperature dependence; it increases with increasing temperature in both solvents but with different rates. The behavior is explained in terms of the strong polarization induced by the hydrogen bond between the solute and solvent in the methanol solution.

5. Optimal Charge and Charge Response Determination through Conformational Space: Global Fitting Scheme for Representative Charge and Charge Response Kernel5)

We propose global fitting scheme derived in least-square sense to estimate optimal partial charge and charge response kernel (CRK), $\partial Q_a/\partial V_b$, with the data collected from conformational space sampling. We applied the global fitting method to 1-butanol system and the performance and accuracy of our global fitting procedure are shown. In addition, we choose 1-pentanol as the test system with the electronic structure change via conformational change and applied the global fitting method to it. From our study, it is indicated that intramolecular polarization can be influenced by intramolecular hydrogen bonding, and it is shown that our global fitting method can correspond to such situation. Also, the global fitting procedure is tested in a large molecular system, 1-dodecanol. We show the results of the availability of our fitting method for the system needed to sample large sets of data over large conformational space. It is indicated that the nonlocality in intramolecular polarization in alkyl chain sequence can be observed and that the large fluctuation of CRKs via nonbonded interaction such as intramolecular hydrogen bonding, as seen in the 1-pentanol case, can appear in common. The global fitting scheme we proposed is available for building molecular modeling considering polarization effect explicitly even in the case that target systems include a lot of conformers.

6. Theoretical Study of Strong Coupling between Solvation and Electronic Structure in the Excited State of a Betaine Dye6)

The electronic ground and excited state structures of the betaine dye molecule pyridinium-N-phenoxide [4-(1-pyridinio) phenolate] are investigated both in the gas phase and in aqueous solution, using the reference interaction site model self-consistent-field (RISM-SCF) procedure within a CASSCF framework. We obtain the total free energy profiles in both the ground and excited states with respect to variation in the torsion angle between the phenoxide and pyridinium rings. We analyze the effect of solvent on the variation of the solute dipole moment and on the charge transfer character in the excited state. In the gas phase, it is shown that the potential energy profile in the excited state decreases monotonically toward a perpendicular ring orientation and the dipole moment decreases along with decreasing charge localization. In water, the free energy surface for twisting is better characterized as nearly flat along the same coordinate for sterically accessible angles. These results are analyzed in terms of contributions of the solvation free energy, the solute electronic energy, and their coupling. Correspondingly, the dependence of the charge transfer character on solute geometry and solvation are analyzed, and the important roles in the excitation and subsequent relaxation processes for the betaine dye are discussed. It is found that there is considerable solute electronic reorganization associated with the evolution of solvation in the excited state, and it is suggested that this reorganization may contribute significantly to the early time evolution of transient spectra following photoexcitation.

References

1) A. Morita and T. Ishiyama, *Phys. Chem. Chem. Phys.* in press (2008).
2) T. Miyamae, A. Morita and Y. Ouchi, *Phys. Chem. Chem. Phys.* **10**, 2010–2013 (2008).
3) A. Morita and B. J. Garett, *Flu. Dyn. Res.* **40**, 459–473 (2008).
4) N. Yoshida, T. Ishida and F. Hirata, *J. Phys. Chem. B* **112**, 433–440 (2008).
5) T. Ishida, *J. Phys. Chem. A* **112**, 7035–7046 (2008).
6) T. Ishida and P. J. Rossky, *J. Phys. Chem. B* **112**, 11353–11360 (2008).

---

* Present Address; Department of Chemistry, Graduate School of Science, Tohoku University, Aoba-ku, Sendai 980-85788

Visiting Professors

Visiting Professor

AIDA, Misako *(from Hiroshima University)*

Topological Analysis of Water Clusters

A water cluster is relevant to a digraph and can be classified to an H-bond pattern. The NVT ensembles of water clusters are created and divided into the configurational subsets, which correspond to the topology-distinct H-bond patterns, and the relative molar Helmholtz energies of the H-bond patterns are evaluated. The method is based on the combination of the standard Monte Carlo techniques with defined H-bond patterns. The structure distributions of water clusters at different temperatures are presented based on the H-bond patterns instead of the 'inherent structures.' The thermodynamically favored structures of water clusters, which are energetically favored and readily feasible (entropy-favored for cluster formation), are presented. The aim of the present work is to demonstrate that the classification to the H-bond pattern corresponds to the division of the configurational space of water cluster structures, where the H-bond patterns can be used to distinguish water cluster structures at finite temperatures created by a simulation technique.

Visiting Associate Professor

NISHINO, Masamichi *(from National Institute for Materials Science)*

Elucidation of the Mechanism of Photoinduced Phase Transitions in Molecular Solids

The discovery of LIESST (light-induced excited spin state trapping) phenomena has accelerated studies of functional spin-crossover (SC) molecular solids. SC compounds have been studied intensively not only because of their potential applicability to novel optical devices, *e.g.*, optical data storage and optical sensors, *etc.*, but also because of the fundamental scientific interest in the mechanism of the phase transition and the accompanied nonlinear relaxation processes. Focusing on such novel phenomena, through the development of theoretical and computational methods, I am studying the properties of cooperative effects which are the key to understand the mechanism of the photoinduced phase transition.

Visiting Associate Professor

KITAO, Akio *(from The University of Tokyo)*

Theoretical Study on Dynamics and Function of Biopolymer and Biological Supramolecule

Recently, rapid progress in computational power and algorithms enable us to carry out massive molecular simulations of biomolecular systems in longer time scale than before. Proteins are essential molecules that manage various chemical reactions in biological systems. Our main targets are proteins, other biopolymers and biological supramolecules, which act as essential functional units in living organisms. We have been studying assembly process, properties and functional mechanisms of biomolecules using theoretical and computational approaches. In order to achieve this, we create new computational methodologies and programs to simulate biomolecular systems more realistically and accurately and use them to investigate atomic mechanisms of supramolecules to fold, assemble and function. We also develop methodology to extract useful information from experimental data and analyze molecular mechanisms to function. In addition, we analyze accumulated information on protein structure and function and store it as databases.

RESEARCH ACTIVITIES

Photo-Molecular Science

Molecules respond to photon irradiation in a variety of ways, including photo-induced transitions and photochemical reactions. We have employed various light sources and experimental schemes to elucidate molecular structures and properties, and to control chemical reactions and molecular functions. We have also developed novel and advanced light sources for molecular science. Two of research facilities, the Laser Research Center for Molecular Science and the UVSOR Facility, conduct collaborative researches having intimate contacts with the Department of Photo-Molecular Science.

The main topics pursued in the Department include: Development of novel laser spectroscopic methods to reveal fundamental properties of molecules, development of high-resolution optical microscopic methods and application to nanomaterials, coherent control of molecules with ultrafast techniques, spectroscopy of inner-shell excited molecules and fundamental vacuum-UV photochemistry, investigation of the functionality of solid-state materials, developments of novel laser and synchrotron-orbit radiation sources, and so on.

Development of Advanced Near-Field Spectroscopy and Application to Nanometric Systems

Department of Photo-Molecular Science
Division of Photo-Molecular Science I

OKAMOTO, Hiromi	Professor
IMURA, Kohei	Assistant Professor
NARUSHIMA, Tetsuya	Assistant Professor
JIANG, Yuqiang	Post-Doctoral Fellow
HARADA, Yosuke	Post-Doctoral Fellow
WU, Huijun	Graduate Student
KIM, Su Il	Graduate Student*
NOMURA, Emiko	Secretary

There is much demand for the study of local optical properties of molecular assemblies and materials, to understand mesoscopic phenomena and/or to construct optoelectronic devices in the nanometric scale. Scanning near-field optical microscopy (SNOM), which enables spatial resolution beyond the diffraction limit of light, has been remarkably progressed in technology in the past decade. Combination of this advanced optical technology with various nonlinear and ultrafast laser spectroscopic methods may offer a direct probe of molecular dynamical processes in mesoscopic materials systems. It may provide essential and basic knowledge for analyzing origins of characteristic features and functionalities of the mesoscopic systems. We have constructed apparatuses for near-field dynamic spectroscopy with the femtosecond time resolution and the nanometer spatial resolution. They are capable of measuring conventional near-field transmission, emission, and Raman-scattering, and unique near-field two-photon induced emission and ultrafast transient transmission as well. Based on these methods, we are observing the characteristic spatio-temporal behavior of various metal nanoparticle systems and molecular assemblies, for the purpose of understanding nano-optical characteristics, spatial coherence of excitations, dynamics, *etc*. We also investigate the basic characteristics of near-field microscopic measurements.

1. Visualization of Plasmon Wavefunctions Induced in Various Metal Nanoparticles

We recently reported that wavefunctions of localized plasmon resonances of metal nanoparticles can be visualized by near-field transmission or two-photon excitation measurements.[1] The plasmons we visualized include the longitudinal modes of chemically synthesized gold and silver nanorods and in-plane modes of chemically synthesized gold triangular nanoplates. Figure 1 shows typical examples of near-field transmission images for longitudinal plasmon modes on a nanorod (the images correspond to the square moduli of the wavefunctions). We reported that the images show excellent agreement with calculated images of local density of electromagnetic states (LDOS) which correspond to the square moduli of the resonant plasmon wavefunctions.

We are extending the study to the metal nanostructures manufactured by the electron-beam lithography technique, in collaboration with researchers of other institution. We have obtained preliminary results for some metal nanostructures and have found characteristic plasmon waves. Such a study is essential as a basis to design unique optical properties and functions of metal nanostructures.

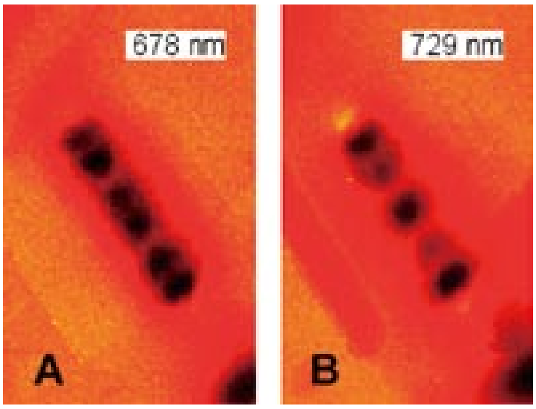

Figure 1. Near-field transmission images of a gold nanorod (diameter 20 nm, length 510 nm), observed at 678 nm (A) and 729 nm (B).

2. Ultrafast Transient Images of Gold Nanoparticles

We previously reported ultrafast near-field transient transmission (space/time resolution was *ca.* 50 nm/100 fs) of single gold nanorods to reveal dynamic behavior of the material.[2)] We used a near-infrared pulse to excite longitudinal plasmon resonance of the rod and detect transient transmission change after that. Figure 2A shows the transient image of a nanorod at *ca.* 600 fs. Although the rod consists of uniform crystalline gold, the signal is strongly dependent on the position: bleached absorption is observed in the central part, while induced absorption is found in both ends.

To understand the observed features, we simulated in the present study position-dependent transient transmission change based on electromagnetic LDOS calculation.[3)] Figure 2B shows a simulated image. The image reproduces well the observed features of the transient image in Figure 2A. From this analysis, it has been revealed that the LDOS change arises from variation in plasmon mode wavefunctions due to the photoinduced transient electronic temperature elevation in the nanorod. The present result suggests a potential for transient optical control of plasmon modes by photoexcitation of metal nanostructures.

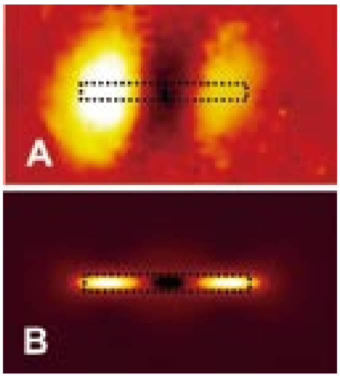

Figure 2. (A) Transient transmission image of a single gold nanorod (diameter 30 nm, length 300 nm) observed at a delay time of 600 fs. A dotted square indicates an approximate shape of the nanorod estimated from the topography measurement. Bright and dark parts indicate regions giving induced absorption and bleached absorption, respectively. (B) Simulated transient transmission (LDOS) change image for the nanorod. Bright and dark parts indicate regions giving enhanced and reduced LDOS, respectively.

3. Near-Field Imaging of Locally Enhanced Optical Fields in Metal Nanoparticle Assemblies

It is of fundamental importance to reveal spatial distribution of localized optical field in metal nanostructures. In aggregated noble metal nanoparticles, for example, strong electric field is expected in the interstitial gaps between the nanoparticles, according to the electromagnetic calculations. Such an enhanced optical field is considered as the major origin of the huge Raman enhancement in single-molecule level surface-enhanced Raman scattering (SERS). Recently, we visualized highly localized optical fields at interstitial sites in gold-nanoparticle dimers, by two-photon excitation imaging using SNOM.[4)] For larger nanostructures, however, the correlation between the geometrical structure and the optical field distribution has been less understood.

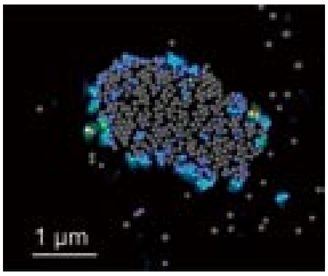

Figure 3. Two-photon excitation SNOM image of monolayer assembly of gold nanoparticles. The image is superimposed on the SEM image (displayed in black-white).

In this study, we analyzed the correlation between the near-field optical properties and the particle configuration in monolayer assemblies of gold nanoparticles by a combination of SNOM and SEM images (Figure 3).[5)] Two-photon excitation SNOM measurements show enhanced optical fields distributed over the whole area of assembly, and especially intensified at the rim of the assembly. The difference between the inner part and the rim may be related to delocalization of surface plasmon excitation in two-dimensional nanostructures. The non-uniform nature of the enhanced electric field in the assembly found here gives a new guideline for designing highly sensitive SERS substrate.

4. Near-Field Imaging of Organic Molecular Assemblies

We are studying mesoscopic structures and optical properties of organic molecular assemblies such as porphyrin wires, carbon nanotubes embedded in sugar molecule chains, Lagmuir-Blodgett films of functional conjugated molecules, mainly as collaborations with other research groups.

References

1) H. Okamoto and K. Imura, *Jpn. J. Appl. Phys.* **47**, 6055–6062 (2008).
2) K. Imura, T. Nagahara and H. Okamoto, *J. Phys. Chem. B* **108**, 16344–16347 (2004).
3) K. Imura and H. Okamoto, *Phys. Rev. B* **77**, 041401(R) (4 pages) (2008).
4) K. Imura, H. Okamoto, M. K. Hossain and M. Kitajima, *Nano Lett.* **6**, 2173–2176 (2006).
5) T. Shimada, K. Imura, M. K. Hossain, H. Okamoto and M. Kitajima, *J. Phys. Chem. C* **112**, 4033–4035 (2008).

---

* from KAIST, Korea

Quantum-State Manupulation of Molecular Motions

Department of Photo-Molecular Science
Division of Photo-Molecular Science I

OHSHIMA, Yasuhiro	Professor
HASEGAWA, Hirokazu	Assistant Professor
BAEK, Dae Yul	IMS Fellow
SUMA, Kosuke	JSPS Post-Doctoral Fellow*
PAVLOV, Lubomir	Visiting Scientist†
KITANO, Kenta	Graduate Student
MIYAKE, Shinichiro	Graduate Student
INAGAKI, Itsuko	Secretary

Molecules in gas phase undergo translational, rotational and vibrational motions in a random manner, and the total molecular system is a statistical ensemble that contains a number of molecules in many different states of motions. This research group aims to establish methods to manipulate the quantum-state distribution pertinent to molecular motions, by utilizing the coherent interaction with laser lights. Here lasers with ultimate resolution in time and energy domains are employed complementally and cooperatively for manipulation of molecular motions.

1. Nonadiabatic Rotational Excitation of Benzene by Nonresonant Intense Femtosecond Laser Fields[1)]

When a gaseous molecular sample is irradiated by an intense nonresonant ultrafast laser pulse, the laser field exerts a torque that aligns the molecular axis along the laser polarization vector, due to the interaction with the molecular anisotropic polarizability. The process has now been termed commonly as "nonadiabatic molecular alignment," and has been attracting much attention because of interesting physics involved and possible broader applications.[2)] Here the field–molecule interaction only remains in much shorter duration than the characteristic time for molecular rotation, and thus the nonadiabatic alignment is inherently accomplished by nonadiabatic rotational excitation (NAREX), where rotation of the molecules is coherently excited to create a rotational quantum wave packet (WP), a non-stationary superposition of rotational eigenstates.

We have recently developed a method for exploring the NAREX process in a quantum-state resolved manner by using resonance-enhanced multiphoton ionization (REMPI), and reported state distribution of NO molecules after the impulsive excitation with a fundamental output of a femtosecond titanium-sapphire laser.[3)] It has been shown that the state distribution is a useful experimental source for verifying the excitation process, since population for each rotational level is proportional to the square of the probability amplitude of the corresponding eigenstate in the rotational WP thus created.

The method has been further applied to the oblate symmetric-top molecule, benzene. Rotational excitation up to J = 10 was observed for the irradiation of a molecular ensemble, initially cooled to 0.5 K in an adiabatic expansion, by the femtosecond laser pulse with the intensity of 2.2 TW/cm^2 (Figure 1). The observed excitation was analyzed by the aid of quantum mechanical calculations. These calculations show the systematic change in the excitation pathways for different K, which is characteristic of NARAX in symmetric-top molecules.

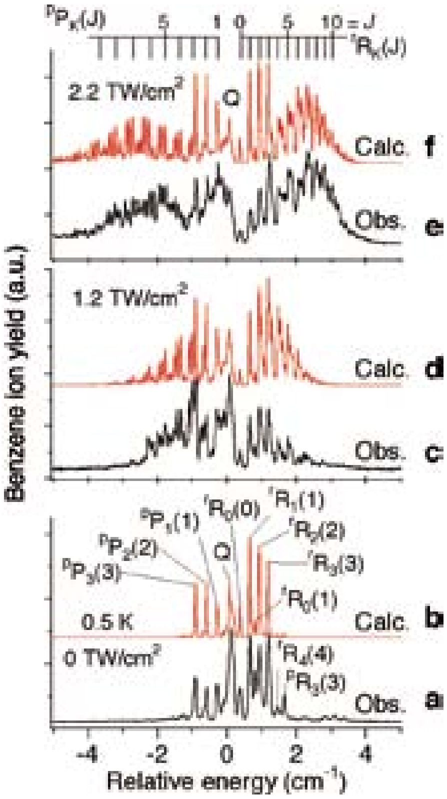

Figure 1. REMPI excitation spectra of the S_1–S_0 6_0^1 band of benzene. Observed (a) without pump pulses, (c) with the pump pulse of 1.25 mJ and (e) 2.40 mJ with 700 fs duration. Calculated with the laser intensities of (b) 0 TW/cm^2, (d) 1.2 TW/cm^2, and (f) 2.2 TW/cm^2.

2. Quantum State Reconstruction of a Rotational Wave Packet Created by a Nonresonant Intense Femtosecond Laser Field[4)]

We further succeeded in experimentally reconstructing a rotational WP created in the NAREX process by utilizing a nonresonant intense femtosecond laser field. Specifically, a rotational WP in an adiabatically cooled benzene molecule was determined. In this WP reconstruction, the initial WP was further interfered by a replica of the first laser pulse, and a REMPI probe was conducted to observe the resultant modulation in population. The time dependent population was fitted to determine the phases as well as the amplitudes of the WP, as shown in Figure 2. Though several states with different nuclear-spin modifications were populated in the initial condition, a single wave packet created from one of them (with $J = 0$) is specifically reconstructed owing to the state-selective probing. From the experimentally determined phases and amplitudes, the angular probability distribution can be evaluated, as shown in Figure 3.

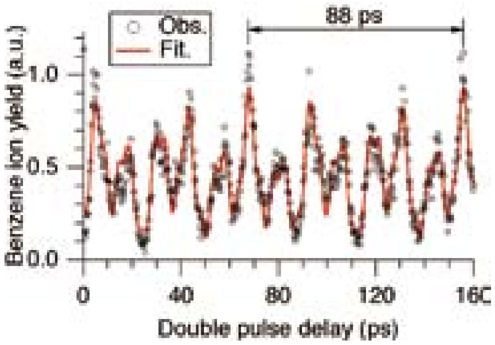

Figure 2. Population of the $J_{|K|} = 0_0$, state in benzene molecules after double-pulse excitation, plotted against the delay between the two pulses. Open circles represent the observed value, and the red line is the results from a least-squares fitting.

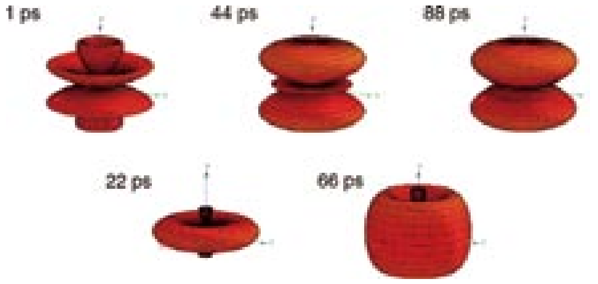

Figure 3. Angular probability distribution of the molecular symmetry axis of benzene at some delay times, evaluated from the experimentally determined amplitude and phase.

3. Realization of Nonadiabatic Vibrational Excitation by Nonresonant Intense Femtosecond Laser Fields

Nonadiabatic interaction with a nonresonant intense ultrafast laser field can also coherently excite the vibration of molecules. Realization of such a nonadiabatic vibrational excitation (NAVEX) and the resultant creation of a vibrational WP is definitely the next step to be proceeded. We have extended the research into this direction, and just recently succeeded in modifying the vibrational-state distribution by utilizing nonresonant intense femtosecond laser pulse(s).

4. Construction of Coherent ns Pulsed Light Sources for Adiabatic Population Transfer

Highly efficient population transfer between quantum states can be accomplished with adiabatic interactions with ns coherent laser pulses, such as stimulated Raman adiabatic passage.[5)] For realizing such an adiabatic quantum-state manipulation, we are constructing two independent laser systems, both of which will deliver pulsed outputs with almost Fourier-transform (FT) limited resolution. The first system, already in operation, is based on the pulsed amplification of the output from a cw ring titanium-sapphire laser.

The second laser system is based on the optical parametric oscillation (OPO) injection-seeded by an extra-cavity cw diode laser. We have succeeded in single-mode operation of the OPO system with the following characteristics: the laser bandwidth of 160 MHz (FWHM), the pulse duration of ~4 ns, and the output power of 7 mJ/pulse (at ~530 nm as the signal wave). Measurements of high-resolution excitation spectra of aromatic molecules are now underway by utilizing the single-mode OPO system.

References

1) H. Hasegawa and Y. Ohshima, *Chem. Phys. Lett.* **454**, 148–152 (2008).
2) H. Stapelfeldt and T. Seideman, *Rev. Mod. Phys.* **75**, 543–557 (2003).
3) H. Hasegawa and Y. Ohshima, *Phys. Rev. A* **74**, 061401 (4 pages) (2006).
4) H. Hasegawa and Y. Ohshima, *Phys. Rev. Lett.* **101**, 053002 (4 pages) (2008).
5) N. V. Vitanov, T. Halfmann, B. W. Shore and .K. Bergmann, *Annu. Rev. Phys. Chem.* **52**, 763–809 (2001).

---

* Present address: The University of Tokyo, Graduate School of Engineering, Department of Chemical System Engineering, Tokyo113-8656

† from Bulgarian Academy of Science

Development of High-Precision Coherent Control and Its Applications

Department of Photo-Molecular Science
Division of Photo-Molecular Science II

OHMORI, Kenji	Professor
KATSUKI, Hiroyuki	Assistant Professor
HOSAKA, Kouichi	IMS Fellow*
DELAGNES, Jean-Christophe	Post-Doctoral Fellow†
SHIMADA, Hiroyuki	Post-Doctoral Fellow
GOTO, Haruka	Graduate Student
INAGAKI, Itsuko	Secretary

Coherent control is based on manipulation of quantum phases of wave functions. It is a basic scheme of controlling a variety of quantum systems from simple atoms to nanostructures with possible applications to novel quantum technologies such as bond-selective chemistry and quantum computation. Coherent control is thus currently one of the principal subjects of various fields of science and technology such as atomic and molecular physics, solid-state physics, quantum electronics, and information science and technology. One promising strategy to carry out coherent control is to use coherent light to modulate a matter wave with its optical phase. We have so far developed a high-precision wave-packet interferometry by stabilizing the relative quantum phase of the two molecular wave packets generated by a pair of femtosecond laser pulses on the attosecond time scale. We will apply our high-precision quantum interferometry to gas, liquid, solid, and surface systems to explore and control various quantum phenomena.

1. Actively Tailored Spatiotemporal Images of Quantum Interference on the Picometer and Femtosecond Scales[1)]

Interference fringes of quantum waves weave highly regular space-time images, which could be seen in various wave systems such as wave packets in atoms and molecules, Bose Einstein condensates, and Fermions in a box potential. We have experimentally designed and visualized spatiotemporal images of dynamical quantum interferences of two counter-propagating nuclear wave packets in the iodine molecule; the wave packets are generated with a pair of femtosecond laser pulses whose relative phase is locked within the attosecond time scale. The design of the image has picometer and femtosecond resolutions, and changes drastically as we change the relative phase of the laser pulses, providing a direct spatio-temporal control of quantum interferences.

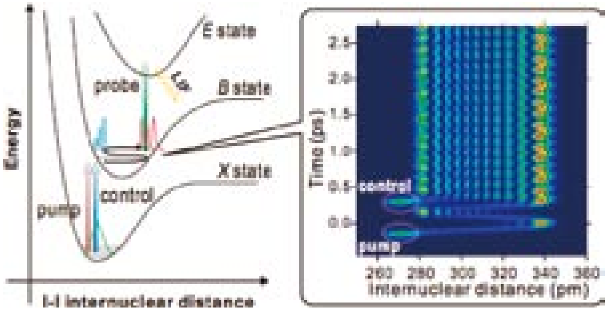

Figure 1. Pump-control-probe scheme for tailoring and visualizing the quantum carpet in the iodine molecule. (Left) Three femtosecond laser pulses are employed. Two of them are phase-locked and used as the pump and control pulses, and the other one is not phase-locked and is used as the probe pulse. The fluorescence signal induced by the probe pulse is measured with a photomultiplier tube attached to a monochromator. (Right) The model simulation of the quantum interference of two wave packets created on the *B*-state potential curve of the iodine molecule by the pump and control pulses. The interference shows a highly regular space-time image that looks like a carpet.

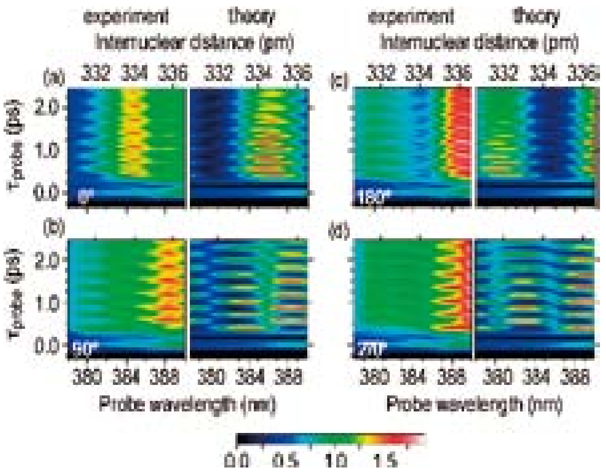

Figure 2. Comparisons of the quantum carpets measured (left) and simulated (right) at the pump-control relative phases θ_{pc} = (a) 0°, (b) 90°, (c) 180°, and (d) 270°. The color scaling is common within each set of measured or simulated carpets; the maxima of those two sets have the same color. The origin $\tau_{peobe} = 0$ of the simulated carpet denotes a position of the top of the first oscillation around the outer turning point. The simulations include the interactions with the pump, control, and probe pulses. The parameter $\tau_{control}$, used for the simulation of $\theta_{pc} = 0°$, was 468.920 fs.

Reference

1) H. Katsuki, H. Chiba, C. Meier, B. Girard and K. Ohmori, *Phys. Rev. Lett.* submitted.

---

* Present Affiliation; Postdoctral Fellow, Japan Atomic Energy Agency

† Present Affiliation; Senior Lecturer, The University of Bordeaux, France

Molecular Inner-Shell Spectroscopy: Electronic Structure and Intermolecular Interaction

Department of Photo-Molecular Science
Division of Photo-Molecular Science III

KOSUGI, Nobuhiro	Professor
YAMANE, Hiroyuki	Assistant Professor
NAGASAKA, Masanari	Assistant Professor
KIMBERG, Victor	Post-Doctoral Fellow
NAKANE, Junko	Secretary

In order to reveal electronic structure and intermolecular interaction of molecular solids, liquids, and clusters, we are developing and improving soft X-ray spectrometers for resonant Auger spectroscopy (RAS) and inelastic soft X-ray emission spectroscopy (XES). We are also developing and improving an original *ab initio* quantum chemical program package GSCF, which is optimized to calculation of molecular inner-shell processes.

1. Charge-Transfer- to-Solvent States of Aqueous Chloride Ions Revealed by Cl^- 2p Resonant Auger Spectroscopy1)

Charge transfer-to-solvent (CTTS) excited states of 2 mol/l NaCl and 3 mol/l LiCl aqueous solutions are revealed through soft X-ray electron spectroscopy. The excitation of the Cl 2p core electrons to the CTTS states is hardly visible in soft X-ray absorption spectroscopy. In this work it is clearly shown that the CTTS states can be detected by measuring RAS following the Cl 2p excitation to the CTTS state. During the resonance Auger decay emitting an Auger electron the CTTS electron behaves like a spectator; in the Auger final state with valence double holes, the CTTS electron gets strongly bound by a singly charged state and definitely observable.

The observed results are satisfactorily reproduced by *ab initio* calculations of four different cluster models to simulate about 2 mol/l NaCl and LiCl aqueous solutions, that is, 1 alkali halide and about 30 water molecules in a volume of $(10\ \text{Å})^3$. The initial guess of these geometries was chosen from a stable cluster of 30 H_2O molecules composed of five- and four-member water rings, where the center water molecule of this cluster was exchanged to either Cl or Na/Li. We chose two local minima for $LiCl+29\cdot H_2O$ and a local minimum for $NaCl+29\cdot H_2O$ and for $NaCl+31\cdot H_2O$. In these clusters Cl^- is stabilized by five or six nearest-neighbor H_2O molecules. The theoretical method for the Cl 2p ionized states (to describe photoionization) and Cl 3p doubly ionized states (to describe Auger decay) is also an all-electron ab initio approach taking into account Cl 2p and Cl 3p holes explicitly, using the GSCF3 code. The energy levels corresponding to CTTS electrons bound by single and double hole states, which are optimized within the static exchange (STEX) method, simulate the experimental results quite well.

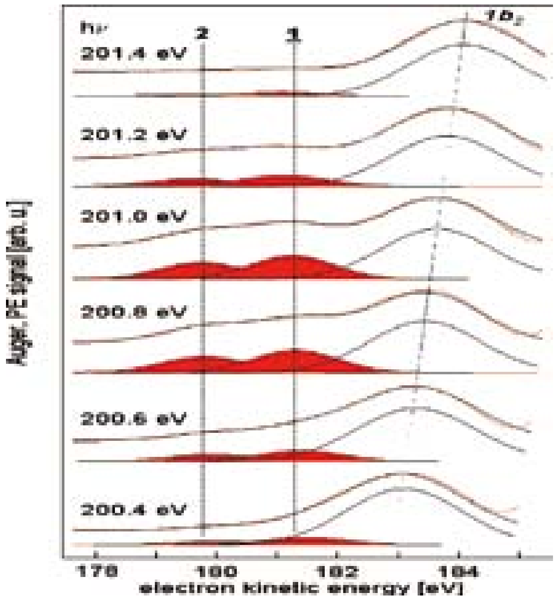

Figure 1. Photon energy dependence of electron kinetic energy spectra of resonant Auger electrons from the Cl 2p CTTS states in aqueous Cl^- ions and non-resonant photoelectrons from the liquid water $1b_2$ level.

As shown in Figure 1, we also have observed the small negative photon-energy dependence of the lowest spectator Auger electron, which indicates localized character of the lowest CTTS electron. Similar negative photon-energy dependence of the resonant Auger electron energy has been observed in molecular solid2) and DNA,3) and discussed in terms of localization and delocalization of the excitonic features.

The present liquid-jet experiments and *ab initio* calculations highlight the potential of combination of resonant inner-shell excitations with liquid photoelectron spectroscopy to explicitly characterize CTTS electron dynamics in aqueous solutions.

2. Exchange Interaction of Rydberg Electrons bound by Singly and Doubly Charged States in Small Kr Clusters[4)]

Similarly to the CTTS electron in aqueous solutions, the Rydberg electron in atomic van der Waals clusters is characterized by means of soft X-ray inner-shell spectroscopy. The Rydberg electron from neutral species is more strongly bound and more clearly observed than the CTTS electron from Cl^-.

Singly charged ion cores created by photoionization of atomic clusters are stabilized by the induced polarization (PL) interaction of the surrounding atoms, showing characteristic redshifts of the ionization energy. On the other hand, the photoexcitation creates Rydberg electrons bound by singly charged ion cores, as schematically shown in Figure 2(a). The photoexcitation energy sometimes shows blueshifts due to larger exchange (EX) interaction of a Rydberg electron with electrons of the surrounding atoms. Following the photoexcitation, the resonant Auger decay creates doubly charged ion cores with the Rydberg electron as a spectator. The doubly charged state can have four times larger PL interaction than the singly charged state. On the other hand, the EX interaction of Rydberg electrons is dependent on overlap of the wavefunctions, indicating that shrink of the Rydberg orbital in the doubly charged state increases more or less EX interaction.

Furthermore, small Kr clusters show surface site (‘corner,’ ‘edge,’ and ‘face’) dependent redshifts in ionization energy in X-ray photoelectron spectroscopy (XPS)[5)] and surface site dependent blueshifts and redshifts in excitation energy in x-ray absorption spectroscopy (XAS).[6)] In the present work, surface site dependent EX and PL interactions of small Kr clusters with an average size of Kr_{15} are investigated in doubly charged ion cores by resonant Auger spectroscopy (RAS), and compared by those in singly ionized core obtained by XAS.

Figure 2(b) shows XAS of Kr clusters at the Kr $3d_{5/2}$ edge. Several surface sites show different energy shifts at the 5p and 6p Rydberg states. The 5p electron has the largest EX interaction of the Rydberg states, because the radius of the 5p Rydberg orbital is close to the inter-atomic distance in Kr clusters and the higher Rydberg electron is more diluted in the cluster with decreasing overlap with the surroundings. It is also noted that the EX interaction is almost proportional to the nearest coordination number at the surface site.

Figure 2(c) shows RAS of Kr clusters in the $4s^{-1}4p^{-1}5p$ and $4p^{-2}6p$ regions after the ‘edge’ site excitation of the $3d_{5/2}{}^{-1}5p$ transition (91.37 eV). The EX interaction of the Rydberg electron in doubly charged ion core can be evaluated from the energy shift of RAS assuming the PL effect of the doubly charged ion is four times larger than that of the singly charged ion. Thus, we have found that the EX interaction of the Rydberg electron is greatly enhanced in the doubly charged ion core due to sudden shrink of the Rydberg orbital; the EX interaction of the 6p Rydberg electron with the doubly charged ion core is almost the same as EX of the 5p Rydberg with the singly charged ion core.

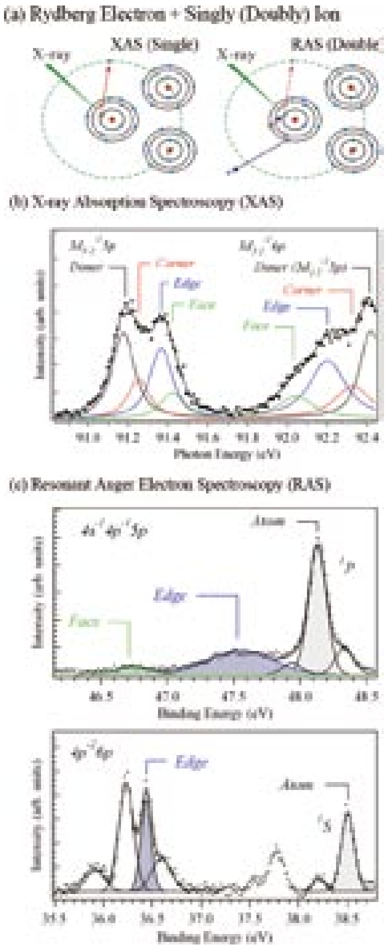

Figure 2. (a) Singly charged ion core and Rydberg electron as revealed by XAS. Doubly charged ion core and Rydberg electron as revealed by RAS. (b) Kr $3d_{5/2}$ XAS spectra of small Kr clusters in the $3d_{5/2}{}^{-1}5p$ and $3d_{5/2}{}^{-1}6p$ region. (c) RAS spectra of small Kr clusters in the $4s^{-1}4p^{-1}5p$ and $4p^{-2}6p$ region after the ‘edge’ site excitation of the $3d_{5/2}{}^{-1}5p$ transition (91.37 eV).

References

1) B. Winter, E. F. Aziz, N. Ottosson, M. Faubel, N. Kosugi and I. V. Hertel, *J. Am. Chem. Soc.* **130**, 7130 (2008).
2) Y. Takata, T. Hatsui and N. Kosugi, *J. Electron Spectrosc.* **88-91**, 235 (1998).
3) H. S. Kato, M. Furukawa, M. Kawai, M. Taniguchi, T. Kawai, T. Hatsui and N. Kosugi, *Phys. Rev. Lett.* **93**, 086403 (2004).
4) M. Nagasaka, T. Hatsui and N. Kosugi, *J. Electron Spectrosc.* **166-167**, 16 (2008).
5) T. Hatsui, H. Setoyama, N. Kosugi, B. Wassermann, I. L. Bradeanu and E. Rühl, *J. Chem. Phys.* **123**, 154304 (2005).
6) A. Knop, B. Wassermann and E. Rühl, *Phys. Rev. Lett.* **80**, 2302 (1998).

Extreme UV Photoionization Studies of Fullerenes by Using Synchrotron Radiation and High-Temperature Mass Spectrometer

Department of Photo-Molecular Science
Division of Photo-Molecular Science III

MITSUKE, Koichiro	Associate Professor
KATAYANAGI, Hideki	Assistant Professor
HUANG, Chaoqun	IMS Fellow
YAGI, Hajime	Post-Doctoral Fellow
KAFLE, Bhim Prasad	Graduate Student (–March ’08) Post-Doctoral Fellow (April ’08–)
NAKAJIMA, Koichi	Visiting Scientist*
PRODHAN, Md. Serajul Islam	Graduate Student

Interactions of C_{60}, C_{70}, C_{84} … with photons have attracted considerable attention, since fullerene family provide unique molecular systems characterized by exceptionally stable electronic structures associated with dense and highly degenerated molecular orbitals and by extremely large vibrational degrees of freedom. In UVSOR we succeeded in determining the total photoabsorption cross section curves of $C_{60(70)}$ at $h\nu = 1.3$ to 42 eV by using photon attenuation method. Moreover, the yield curves of singly- and multiply-charged photoions from fullerenes were measured at $h\nu = 25$ to 200 eV. We have studied the mechanisms and kinetics of sequential C_2-release reactions from the yield curves for $C_{60(70)-2n}^{z+}$ as a function of the internal energy of the parent $C_{60(70)}^{z+}$ ions. To gain more insight into the dissociation mechanisms we have constructed a velocity map imaging spectrometer for achieving the 3D velocity distributions of the fragments $C_{60(70)-2n}^{z+}$.

1. Photoabsorption Cross Section of C_{60} Thin Films from the Visible to Vacuum Ultraviolet[1)]

Absolute photoabsorption cross sections of C_{60} thin films are determined in the $h\nu$ range from 1.3 to 42 eV by using photon attenuation method. The spectrum shows a prominent peak of 1180 Mb at 22.1 eV with several fine structures due to single-electron excitation similarly to the case of C_{60} in the gas phase. The complex refractive index and complex dielectric function are calculated up to 42 eV through the Kramers-Kronig analyses. From the present data of C_{60} thin films the cross section curve of a molecular C_{60} is calculated with an assumption that the polarization effect of surrounding C_{60} molecules can be expressed by the standard Clausius-Mossotti relation. The spectrum thus obtained shows an excellent agreement with that of C_{60} in the gas phase measured independently.

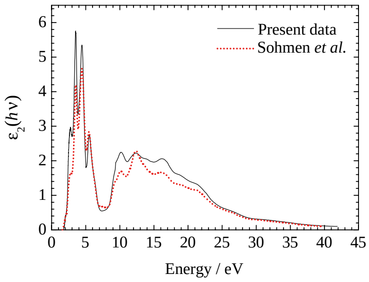

Figure 1. Dependences on $h\nu$ of $\varepsilon_2(\nu)$ of the complex dielectric function $\varepsilon(\nu) = \varepsilon_1(\nu) + i\varepsilon_2(\nu)$ of the C_{60} film.

2. Photoabsorption Cross Section of C_{70} Thin Films from the Visible to Vacuum Ultraviolet

Absolute photoabsorption cross sections of C_{70} thin films are determined in the $h\nu$ range from 1.3 to 42 eV by using photon attenuation method. The spectrum shows a prominent peak of 1320 Mb at 21.4 eV with several fine structures probably due to single-electron excitation. The complex refractive index and complex dielectric function are calculated up to 42 eV through the Kramers-Kronig analyses. From the present data of C_{70} thin films the cross section curve of a molecular C_{70} is calculated using the standard Clausius-Mossotti relation dealing with the correction of the local electromagnetic field, with a plausible assumption that the molecular rotation at room temperature could smear out the effect of the anisotropic molecular structure of C_{70}.

3. Performance Test of a New Velocity Map Imaging (VMI) Spectrometer[2)]

We have constructed a photoion imaging spectrometer to measure the velocity distributions of fragments produced by dissociative photoionization of fullerenes with synchrotron radiation. The performance of this spectrometer has been tested using rare gas samples at room temperature. We have compared the images experimentally obtained with those generated by a simulation program based on a field free expansion of photoions. The experimental and simulated images agree well with each other, if we assume the Maxwell-Boltzmann velocity distribution and the Gaussian distribution for the defocusing of the images with a standard deviation σ of 2 mm.

4. VMI of C_{60} Molecular Beams[3]

The speed and angular distributions of C_{60} molecular beams have been determined by using a VMI technique for photoions produced by irradiation of synchrotron radiation. The C_{60} powder in the sample cell was heated and the beam was generated in an effusive condition. The two-dimensional projection of the velocity distribution was recorded (Figure 2) as an image on the position sensitive detector (PSD), and was converted to the speed and angular distributions. The speed distribution was expressed by the Maxwell-Boltzmann distribution at the temperature of the sample cell, while the angular distribution was determined by the geometry of the fullerene beam source. The speed distribution of helium in thermal motion was used to calibrate the velocity scale.

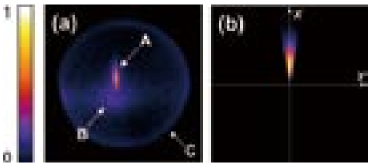

Figure 2. (a) Ion image of the fullerene beam at *h*ν = 70 eV. Pattern A is assigned to the signal of the C_{60} beam. (b) Ion image of the fullerene beam by computer simulation.

5. VMI Spectroscopy of Photofragments from C_{60} Beams

Simulations have been performed to calculate the scattering distributions of C_{56}^+ fragment ions produced by two different mechanisms of dissociative photoionization of C_{60}: (1) sequential ejection of C_2 units and (2) fission into C_{56}^+ + C_4. The simulated images for the two mechanisms can be distinguished clearly at $T = 0$ K, whereas their differences appear to be less obvious for bulk C_{60} at room temperature. Nevertheless, our VMI spectrometer is found to have an enough resolution under the beam condition to reveal such differences in the velocity distribution, because the transverse velocity of the beam is estimated to be less than 20 m s^{-1} even at $T = 785$ K.

6. Revision of our VMI Spectrometer[4]

We have improved our earlier version of VMI spectrometer to be applied for measuring the momentum distributions of the fragments from fullerenes. The revised spectrometer is equipped with four electrostatic lens elements, a drift tube, a mass gate and a PSD. Application of an additional element to the conventional three-element lens system provides better focusing of an extended interaction region. Moreover, the electric field in the ionization region is kept cylindrically symmetric in spite of the field penetration from the oven and surface thickness monitor. The optimum arrangement and dimensions of the elements are determined from the calculations of ion trajectories of C_{56}^+, C_{58}^+ and C_{60}^+.

7. Measurements of Incident Photon-to-Current Efficiency (IPCE) and Photoabsorbance of Dye-Sensitized Solar Cells

We have fabricated dye-sensitized solar cells (DSC) comprised of Ru535 dye and PN50 electrolyte and measured their short current and the intensity of the transmitted light to estimate the wavelength dependence of the incidence photon-to-current efficiency (IPCE) and photoabsorbance (ABS) in the range of 300 to 1000 nm. In addition, we evaluated the quantum yield (EIQY) of DSCs for the electron injection from the excited orbital of Ru535 dye to the conduction band of TiO_2 nano particles. Our final goal is to develop DSCs with high performance and long lifetime by improving mainly ABS and EIQY in the near infrared region.

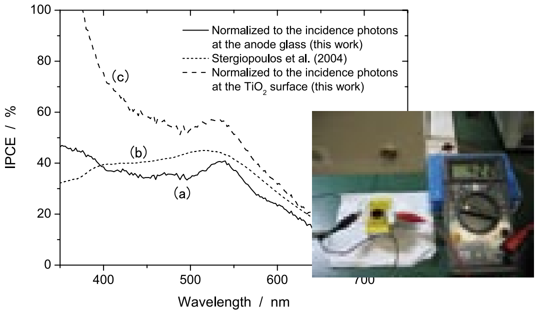

Figure 3. IPCE curves of dye-sensitized solar cells comprised of Ru535 dye and PN50 electrolyte. Normalization is made to the incidence light either (a) at the anode FTO glass or (c) at the TiO_2 surface. (b) Reported by Stergiopoulos *et al.* in 2004.

References

1) H. Yagi, K. Nakajima, K. R. Koswattage, K. Nakagawa, C. Huang, Md. S. I. Prodhan, B. P. Kafle, H. Katayanagi and K. Mitsuke, *Carbon* in press.
2) Md. S. I. Prodhan, H. Katayanagi, C. Huang, H. Yagi, B. P. Kafle and K. Mitsuke, *Chem. Phys. Lett.* in press.
3) H. Katayanagi, C. Huang, H. Yagi, B. P. Kafle, Md. S. I. Prodhan, K. Nakajima and K. Mitsuke, *Rev. Sci. Instrum.* submitted.
4) B. P. Kafle, H. Katayanagi, C. Huang, Md. S. I. Prodhan, H. Yagi and K. Mitsuke, *Nucl. Instrum. Methods Phys. Res., Sect. A* to be submitted.

---

* from Hosei University

Atoms & Molecules in Few-Cycle Intense Laser Fields

Department of Photo-Molecular Science
Division of Photo-Molecular Science III

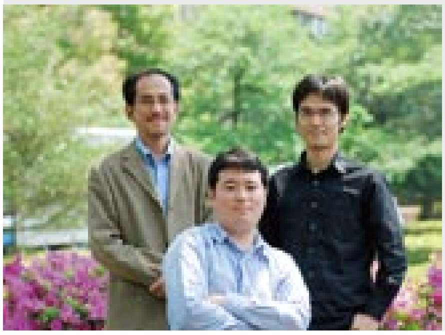

HISHIKAWA, Akiyoshi	Associate Professor
FUSHITANI, Mizuho	Assistant Professor
MATSUDA, Akitaka	IMS Fellow*
NAKANE, Junko	Secretary

Intense laser fields, comparable in magnitude with the Coulomb field within atoms and molecules, can be generated by focussing high-energy and ultrashort laser pulses. When exposed to such an intense laser field, molecules exhibit various exotic features that cannot be observed in weak laser fields. We are seeking a deeper understanding of the behavior of molecules in intense laser fields, to elucidate how molecules interact with light, as well as to apply the new features they exhibit to the real-time visualization of ultrafast chemical reactions and their control. In particular, we focus on the following research themes:

(1) Understanding of atomic and molecular dynamics in intense laser fields
(2) Ultrafast reaction imaging by laser Coulomb explosion imaging
(3) Generation and application of ultrashort soft-X-ray pulses by laser high-order harmonics.

1. Visualizing Recurrently Migrating Hydrogen in Acetylene Dication by Ultrashort Intense Laser Pulses[1,2)]

Highly charged molecular ions formed in ultrashort intense laser fields subsequently explode into fragments due to the strong electrostatic repulsion among the positive charges. The structure of the molecules at the instance of the laser irradiation can be studied by measuring precisely the momenta of the fragments. This can be compared to fireworks exploded in the night sky, which reflect how the "stars" containing sparklers are embedded in the shells. We studied the location of hydrogen atoms in deuterated acetylene dication, by igniting the "molecular fireworks" at different times after the creation of dication. We demonstrate the visualization of ultrafast hydrogen migration in deuterated acetylene dication ($C_2D_2^{2+}$) by employing the pump-probe Coulomb explosion imaging with sub-10-fs intense laser pulses (9 fs, 0.13 PW/cm^2, 800 nm). It is shown, from the temporal evolution of the momenta of the fragment ions produced by the three-body explosion, $C_2D_2^{3+} \rightarrow D^+ + C^+ + CD^+$, that the migration proceeds in a recurrent manner: The deuterium atom first shifts from one carbon site to the other in a short time scale (~90 fs) and then migrates back to the original carbon site by 280 fs, in competition with the molecular dissociation. Hydrogen migration plays important roles in various chemical reactions such as the synthesis of vitamin D in skin. The direct visualization demonstrated here will provide a deeper understanding of such chemical reactions as well as new prospects for their control.

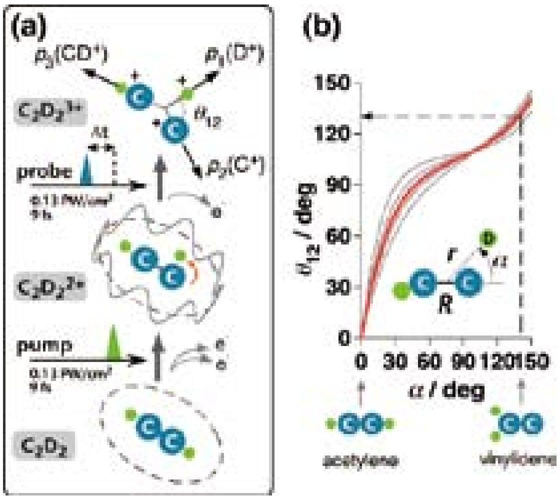

Figure 1. (a) Pump-probe Coulomb explosion imaging employed in the present study. The pump pulse creates $C_2D_2^{2+}$ and triggers the hydrogen migration. The instantaneous location of migrating deuterium atoms is determined from the momenta of fragment ions, D$^+$, C$^+$, CD$^+$, ejected in the Coulomb explosion of $C_2D_2^{3+}$ induced by the probe pulse. (b) Momentum angle θ_{12} as a function of the polar angle α obtained by classical simulation of the three-body Coulomb explosion.

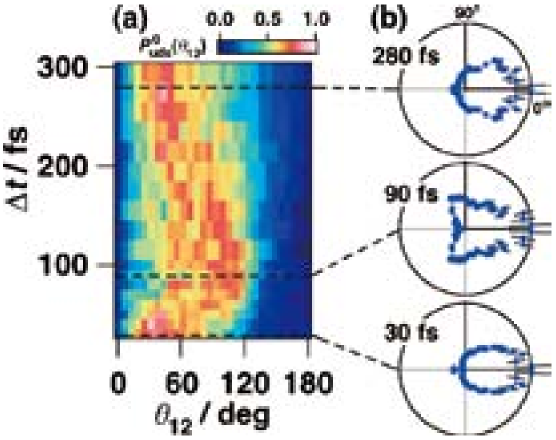

Figure 2. (a) Evolution of the momentum angle (θ_{12}) distribution and (b) the polar plot, showing the recurrent hydrogen migration in $C_2D_2^{2+}$.

2. Acetylene-Vinylidene Isomerization in Ultrashort Intense Laser Fields Studied by Triple-Ion Coincidence Momentum Imaging[3)]

Polyatomic molecules exposed to intense laser fields exhibit a variety of characteristic features associated with their many degrees of vibrational freedom. Due to the strong interaction with the laser fields, the geometrical structure can be strongly deformed by bond stretching or bending, and by isomerization through the rearrangement of chemical bonds. Hydrogen migration is one such processes, in which hydrogen atoms shift from one site to another within a molecule. Because of their large mobility, hydrogen atoms can explore the potential energy surfaces over long distances within the ultrashort laser pulse, leading to the formation of molecular hydrogen ion and the emission of energetic protons. In the present study, the isomerization of acetylene via hydrogen migration in intense laser fields (8×10^{14} W/cm^2) has been investigated by coincidence momentum imaging of the three-body Coulomb explosion process, $C_2H_2^{3+} \rightarrow H^+ + C^+ + CH^+$.

When ultrashort (9 fs) laser pulse are used, the angle between the momenta of C^+ and H^+ fragments exhibits a sharp distribution peaked at a small angle (~20°), showing that the hydrogen atom remains near the original carbon site in the acetylene configuration. On the other hand, a significantly broad distribution extending to larger momentum angles (~120°) is observed when the pulse duration is increased to 35 fs, showing that the ultrafast isomerization to vinylidene is induced in the longer laser pulse.

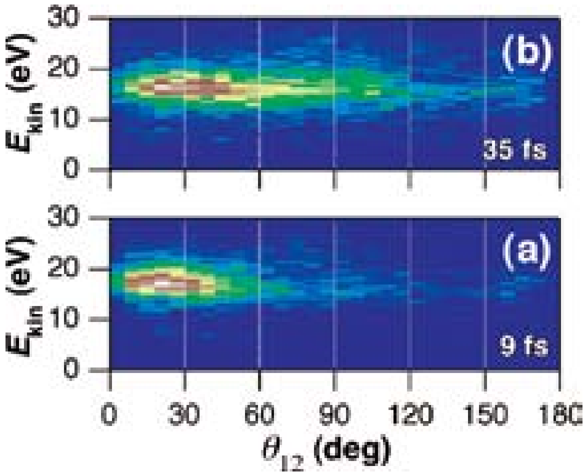

Figure 3. Two-dimensional maps of the momentum angle 12 between $\boldsymbol{p}_1(H^+)$ and $\boldsymbol{p}_2(C^+)$ and the total kinetic energy release for the asymmetric three-body Coulomb explosion process, $C_2H_2^{3+} \rightarrow H^+ + C^+ + CH^+$, observed for the (a) 9 fs and (b) 35 fs intense laser fields 8×10^{14} W/cm^2.

References

1) A. Hishikawa. A. Matsuda, M. Fushitani and E. J. Takahashi, *Phys. Rev. Lett.* **97**, 258302 (2007).
2) A. Hishikawa. A. Matsuda, M. Fushitani and E. J. Takahashi, *J. Phys.: Conf. Series* **88**, 012056 (2007).
3) A. Hishikawa, A. Matsuda, E. J. Takahashi and M. Fushitani, *J. Chem. Phys.* **128**, 084302 (2008).

---

* Present Address; Department of Physics, Stockholm University, Stockholm, Sweden

Light Source Developments by Using Relativistic Electron Beams

UVSOR Facility
Division of Advanced Accelerator Research

KATOH, Masahiro	Professor
ADACHI, Masahiro	Assistant Professor
SHIMADA, Miho	IMS Fellow*
TANIKAWA, Takanori	Graduate Student
KOIKE, Masashi	Graduate Student[†]
SUZUKI, Yasuhiro	Graduate Student[†]
YOSHIDA, Mitsuhiro	Graduate Student[†]
NAGATANI, Atsumune	Graduate Student[†]
FURUI, Yuta	Graduate Student[†]

This project involves researches and developments on synchrotron light source, free electron laser, beam physics and related technologies. Most of these works are performed at the UVSOR-II electron storage ring and its injector.

1. Developments on UVSOR-II Accelerators

Even after the major upgrade in 2003,1) the UVSOR-II electron storage ring and its injector have been continuously improved. In these years, the ring has been operated with a small emittance of 27 nm-rad, that enables four undulators to produce highly brilliant synchrotron radiation in the VUV region. This small emittance, on the other hand, makes the beam lifetime short through the intrabeam scattering, so called Touschek effect. To solve this lifetime problem eternally, we are preparing for top-up injection scheme. In this scheme, the electron beam is re-filled with a short interval, typically one minute, to keep the beam current almost constant.

To realize the top up injection, the maximum operating energy of the injector and the beam transport line was increased from 600 MeV to 750 MeV, by reinforcing the magnet power supplies. Since July, 2007, we have been operating the ring with full energy injection in the user runs. Generally, during injections, the beam loss rate becomes higher. An interlock system for the radiation safety is being developed, which limits the number of injected electrons. Test operation of the top-up scheme will be started in September, 2008.

2. Storage Ring Free Electron Laser

The low emittance and the high peak current of UVSOR-II enable the free electron laser to oscillate in the deep UV region with high output power exceeding 1W.2) In 2007, the shortest wavelength has reached 199 nm. Lasing around 190 nm will be tried soon.

Several users' experiments using this high power and tunable laser beam in the deep UV are in progress. However, during the high power operation of the free electron laser, a rapid change of the output power was observed, which was presumably due to the thermal deformation of the mirrors of the optical cavity. A feedback system is being developed to stabilize the output power.

Table 1. Parameters of UVSOR-II Free Electron Laser.

Electron Energy	600–750 MeV
Wave Length	800–199 nm
Spectral Band Width	$\sim 10^{-4}$
Polarization	Linear/Circular
Repetition Rate	11.26 MHz
Average Output Power	~1 W

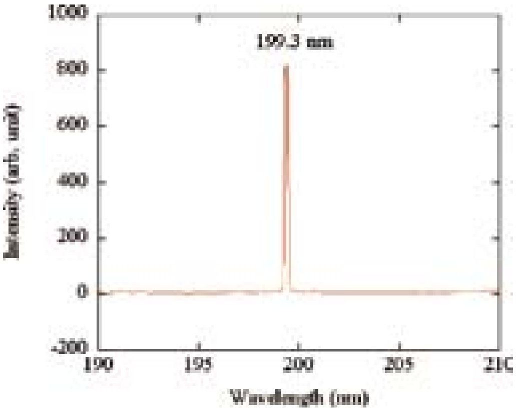

Figure 1. Successful lasing at 199.3 nm of UVSOR-II Free Electron Laser.

3. Terahertz Coherent Synchrotron Radiation by Laser-Electron Interaction

When an electron bunch has a micro-structure on its longitudinal density distribution whose typical scale is close to the radiation wavelength, the synchrotron radiation fields

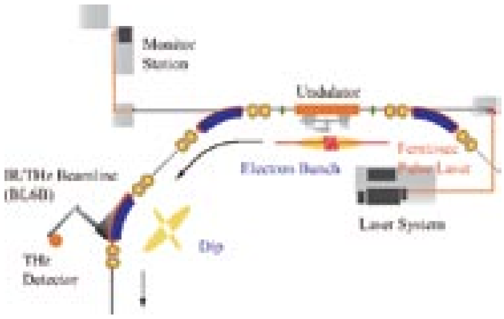

Figure 2. Laser Modulation System at UVSOR-II.

emitted by each electron are linearly accumulated and the total radiation power is proportional to the square of the number of the electrons. This is called coherent synchrotron radiation (CSR).

We have developed a system to create micro-density structure on electron bunches circulating in the storage ring, as shown in Figure 2.[3)] Laser pulses are injected to the ring and interact with the electron beam in an undulator. The electrons lose or gain its energy depending on the phase to the laser field. As the result, energy modulation is created on the electron bunch. As the bunch is proceeding in the ring, the energy modulation is converted to a density modulation. By controlling the laser pulse shape, we can create various density structures. When we use a sub-picosecond laser pulse, we can produce a short dip structure. When we use a amplitude modulated laser pulse, we can produce periodic density structure. In the former case, broadband coherent terahertz radiation was produced.[3)] In the latter case, quasi-monochromatic coherent terahertz radiation was produced, as shown Figure 3.[4)] This was the first experiment in which monochromatic synchrotron radiation was produced in a uniform magnetic field.

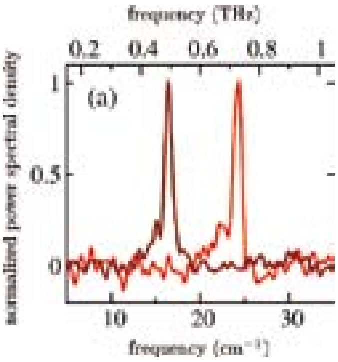

Figure 3. Quasi-monochromatic synchrotron radiation emitted in a uniform magnetic field.

4. Coherent Harmonic Generation

Coherent harmonic generation is a method to produce coherent harmonics of laser light by using relativistic electron beam. The laser-electron interaction in an undulator produces density modulation of a period of laser wavelength. When the energy modulation is sufficiently larger than the natural energy spread, the density modulation contains higher harmonic component of the laser wavelength. Such an electron bunch emits coherent harmonics of the injected laser. We have successfully observed the coherent third harmonics of Ti:Sa laser.[5)] Optical properties of the coherent harmonic radiation were experimentally investigated.

References

1) M. Katoh, M. Hosaka, A. Mochihashi, J. Yamazaki, K. Hayashi, Y. Hori, T. Honda, K. Haga, Y. Takashima, T. Koseki, S. Koda, H. Kitamura, T. Hara and T. Tanaka, *AIP Conf. Proc.* **705**, 49–52 (2004).
2) M. Hosaka, M. Katoh, A. Mochihashi, M. Shimada, T. Hara and Y. Takashima, *Proc. 28th Internat. Free Electron Laser Conf. (Berlin)* 368–370 (2006).
3) M. Shimada, M. Katoh, S. Kimura, A. Mochihashi, M. Hosaka, Y. Takashima, T. Hara and T. Takahashi, *Jpn. J. Appl. Phys.* **46**, 7939–7944 (2007).
4) S. Bielawski, C. Evain, T. Hara, M. Hosaka, M. Katoh, S. Kimura, A. Mochihashi, M. Shimada, C. Szwaj, T. Takahashi and Y. Takashima (in alphabetic order), *Nat. Phys.* **4**, 390–393 (2008).
5) M. Labat, M. Hosaka, A. Mochihashi, M. Shimada, M. Katoh, G. Lambert, T. Hara, Y. Takashima and M. E. Couprie, *Eur. Phys. J. D* **44**, 187–200 (2007) (Highlighted Paper).

---

* Present Address; High Energy Accelerator Research Organization (KEK), Tsukuba, 305-0801

† carrying out graduate research on Cooperative Education Program of IMS with Nagoya University

Synchrotron Radiation Spectroscopy on Strongly Correlated Electron Systems

UVSOR Facility
Division of Advanced Solid State Physics

KIMURA, Shin-ichi	Associate Professor
ITO, Takahiro	Assistant Professor
TERASHIMA, Kensei	JSPS Post-Doctoral Fellow
IM, Hojun	Post-Doctoral Fellow*
TSUNEKAWA, Masanori	Post-Doctoral Fellow†
MIZUNO, Takafumi	Graduate Student
IIZUKA, Takuya	Graduate Student
MIYAZAKI, Hidetoshi	Graduate Student‡
MATSUI, Takafumi	Graduate Student‡

Solids with strong electron–electron interaction, so-called strongly correlated electron systems (SCES), have a various physical properties, such as non-BCS superconducting, colossal magneto-resistance, heavy fermion and so on, which cannot be predicted by a first-principle band structure calculation. Thanks to the physical properties, the materials are the candidates of the next generation functional materials. We are investigating the mechanism of the physical properties of SCES, especially rare-earth compounds, organic superconductors and transition-metal compounds, by infrared/THz spectroscopy and angle-resolved photoemission spectroscopy using synchrotron radiation. Since experimental techniques using synchrotron radiation are evolved rapidly, the development of the synchrotron radiation instruments is also one of our research subjects.

1. Direct Observation of Dispersive Kondo Resonance Peaks in a Heavy-Fermion System[1)]

In heavy-fermion Ce compounds, it is widely accepted that a localized Ce 4f electron due to the strong correlation forms a sharp Kondo resonance (KR) peak just above the Fermi level through the hybridization with an itinerant conduction electron. As a function of this hybridization, the ground state varies from a magnetic to nonmagnetic heavy-fermion separated by a quantum critical point, revealing two characteristic energy scales: the Kondo temperature (T_K) and coherent temperature (T^*). However, an accurate electronic structure for the Ce 4f state has remained a long debated issue since the discovery of the heavy-fermion system in 1970’s. Then we carried out the Ce 4d-4f resonant angle-resolved photoemission spectroscopy to study the electronic structure of strongly correlated Ce 4f electrons in a quasi-two-dimensional nonmagnetic heavy-fermion system $CeCoGe_{1.2}Si_{0.8}$. For the first time, dispersive coherent KR peaks of an f state crossing the Fermi level are directly observed together with the hybridized conduction band. Moreover, the experimental band dispersion is quantitatively in good agreement with a simple hybridization-band picture based on the periodic Anderson model. The obtained physical quantities, *i.e.*, T^*, T_K, and mass enhancement, are comparable to the results of thermodynamic measurements. These results manifest an itinerant nature of Ce 4f electrons in heavy-fermion systems and clarify their microscopic hybridization mechanism.

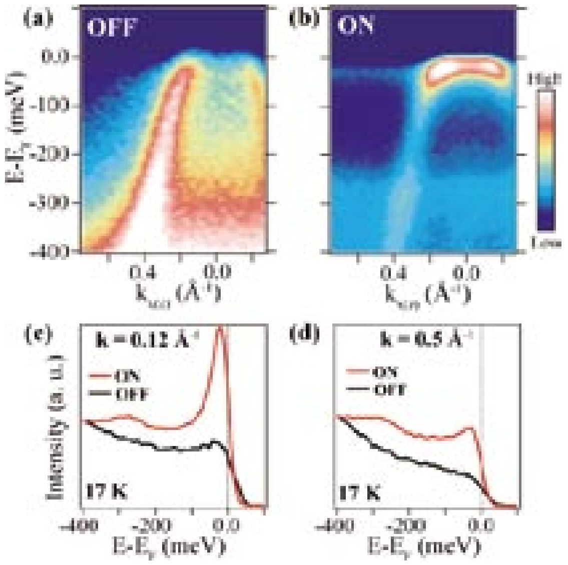

Figure 1. (a), (b) Intensity plots of off- and on-resonant ARPES spectra of $CeCoGe_{1.2}Si_{0.8}$ represent the band dispersion of conduction and f electrons, respectively, along the RT line. (c), (d) EDCs of on- and off-resonant ARPES spectra at the momentum k = 0.12 and 0.5 Å^{-1}, respectively.

2. Excitonic Instability in the Transition from the Black Phase to the Golden Phase of SmS under Pressure Investigated by Infrared Spectroscopy[2,3)]

In the translocation process from the local to itinerant character of carriers in strongly correlated electron systems, the physical properties drastically change due to the complex relation of the transport to magnetic properties. A strongly correlated insulator, samarium monosulfide (SmS), is a semiconductor with an energy gap size of ~1000 K (~90 meV) and its color is black (namely, the "black phase") at ambient pressure.[2] Above the critical pressure (P_c) of 0.65 GPa, the sample color changes to golden-yellow (the "golden phase") and the electrical resistivity then suddenly drops to one-tenth that in the black phase. To investigate the origin of the pressure-induced phase transition from the black phase to the golden phase, we measured the pressure-dependent optical reflectivity spectra of SmS in the far- and middle-infrared regions. The energy gap becomes narrow with increasing pressure in the black phase. A valence transition from Sm^{2+} in the black phase to mainly Sm^{3+} in the golden phase accompanied by spectral change from insulator to metal were observed at the transition pressure of 0.65 GPa. The black-to-golden phase transition occurs when the energy gap size of black SmS becomes the same as the binding energy of the exciton at the indirect energy gap before the gap closes. This result indicates that the valence transition originates from an excitonic instability.

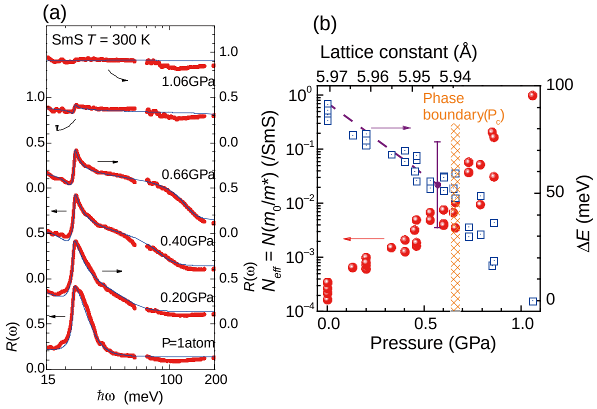

Figure 2. (a) Pressure dependence of the reflectivity spectrum [$R(\omega)$] of black SmS (thick lines) in the energy region of $\hbar\omega$ = 15–200 meV at 300 K. The fitting curve of the combination of Drude and Lorentz functions (thin lines) are also plotted. Successive curves are offset by 0.5 for clarity. (b) Pressure dependences of the effective carrier density (N_{eff}, solid circles) evaluated from the Drude and Lorentz fitting in the left figure and energy gap size (ΔE, open squares) evaluated from N_{eff} and ΔE at 1 atm. The lattice constant that is proportional to the pressure is also denoted in the figure for reference. The energy shift of the exciton peak of the direct transition at the X point at around 0.5 eV (dashed line) normalized at the energy gap size at ambient pressure are plotted as well.

3. Valence Electronic Structure of Cross-Linked C_{60} Polymer: In situ High-Resolution Photoelectron Spectroscopic and Density-Functional Studies[4]

When a C_{60} film is irradiated with a 3 keV electron beam, a cross-linked C_{60} polymer is formed and exhibits metallic electron-transport (I-V) properties in air at room temperature. To elucidate the origin of the metallic I-V characteristics of the cross-linked polymer, we examined the valence photoelectron spectra of the polymer using in situ high-resolution ultraviolet photoelectron spectroscopy (UPS) and found that the spectrum for the cross-linked C_{60} polymer came across the Fermi level (E_F). To understand the UPS results for the C_{60} polymer, we performed first-principles calculations of the band structure for three kinds of optimized three-dimensional unit cells of one-dimensional (1D) cross-linked C_{60} polymers with a cross-linkage consisting of both six- and seven-membered rings and of five- and eight-membered rings (P58). It was found that one quasi-1D P58 cross-linked C_{60} polymer shows semimetallic properties, which provides one possible explanation of both previous (metallic I-V characteristics) and present (valence photoelectron spectra) experimental results.

References

1) H. J. Im, T. Ito, H. -D. Kim, S. Kimura, K. E. Lee, J. B. Hong, Y. S. Kwon, A. Yasui and H. Yamagami, *Phys. Rev. Lett.* **100**, 176402 (2008).
2) S. Kimura, T. Mizuno, K. Matsubayashi, K. Imura, H. S. Suzuki and N. K. Sato, *Physica B* **403**, 805–807 (2008).
3) T. Mizuno, T. Iizuka, S. Kimura, K. Matsubayashi, K. Imura, H. S. Suzuki and N. K. Sato, *J. Phys. Soc. Jpn.* **77**, 113704 (2008).
4) J. Onoe, T. Ito, S. Kimura, K. Ohno, Y. Noguchi and S. Ueda, *Phys. Rev. B* **75**, 233410 (2007).

Awards

KIMURA, Shin-ichi; The Prize for Science and Technology in Research Category, the Commendation for Science and Technology by the Minister of Education, Culture, Sports, Science and Technology.
MIYAZAKI, Hidetoshi; Best Presentation Award, JSR 08.
MIYAZAKI, Hidetoshi; Best Presentation Award, Annual meeting of Tokai Branch of Japan Institute of Metals.

---

* from Sungkyunkwan University, Korea
† from Nagoya University
‡ carrying out graduate research on Cooperative Education Program of IMS with Nagoya University

Electronic Structure and Decay Dynamics in Atoms and Molecules Following Core Hole Creation

UVSOR Facility
Division of Advanced Photochemistry

SHIGEMASA, Eiji Associate Professor
HIKOSAKA, Yasumasa Assistant Professor

The dynamics of the inner-shell photoexcitation, photoionization, and subsequent decay processes is much more complex, in comparison to outer-shell photo-processes. For instance, the inner-shell photoionization is concomitant with the excitation and ionization of valence electrons, which reveal themselves as shake-up and shake-off satellite structures in the corresponding photoelectron spectrum. The one-photon multi-electron processes, which are entirely due to the electron correlation in the system, are known to happen not only in the primary inner-shell hole creation processes, but also in their relaxation processes. Our research project is focused on elucidating the electronic structures and decay dynamics in core-excited atoms and molecules, by utilizing various spectroscopic techniques together with monochromatized synchrotron radiation in the soft x-ray region.

1. Dissociation Dynamics in Polyatomic Molecules Following Core Hole Creation

Auger decay is the main relaxation process following core ionization in molecules composed of light atoms. In the decay process, a valence electron fills the core-hole while another valence electron is ejected. Doubly charged molecular ions with two holes in the valence shell, thus formed, often break up into ion fragments, due to the Coulomb repulsion between the nuclear charges. The coincidence detection between the energy-selected Auger electrons and fragment ions is one of the most powerful methods to gain a close insight into the dissociation mechanism of the Auger final states. To realize efficient coincidences among these charged particles, we have developed an Auger electron-ion coincidence spectrometer which consists of a double toroidal electron analyzer and a three-dimensional ion momentum spectrometer.

The Auger electron emission from the S $2p^{-1}$ core-hole states of OCS and subsequent dissociation processes of the doubly charged states have been investigated. The measurement has provided direct correlation between the doubly charged ion states and the dissociation pathways. The lowest-lying $(3\pi)^{-2}$ states located at about 32 eV binding energy produce the metastable OCS^{2+} and their lifetimes are expected to be much longer than 3.5 μs. The $(9\sigma)^{-1}(3\pi)^{-1}$, $(8\sigma)^{-1}(3\pi)^{-1}$ and $(2\pi)^{-1}(3\pi)^{-1}$ states around 36 eV are associated with both the formation of metastable OCS^{2+} and the dissociation into CO^{+} + S^{+}. The three-body dissociation into O + C^{+} + S^{+} originates only from the high-lying states above 42 eV, whose main configurations are $(9\sigma)^{-2}$ and $(8\sigma)^{-1}(9\sigma)^{-1}$.

In order to investigate the influence of the localized core-hole creation to the formation of the valence two-hole states, and to elucidate their characters, the Auger decays following the C 1s and O 1s ionization in OCS have also been studied by using the same experimental setup. It was found that the lowest-lying $(3\pi)^{-2}$ states related to the production of the metastable OCS^{2+} are formed mainly via the Auger decay from the S $2p^{-1}$ core-hole states, which is explained by the localized nature of the 3π molecular orbital at the S atom.

2. One-Photon Multi-Electron Emission Processes Studied by Multi-Eelectron Coincidence Spectroscopy

When an inner-shell electron in atoms and molecules is removed, the core-hole state decays via the Auger electron transition. The kinetic energy of the Auger electron is element specific and therefore Auger electron spectroscopy is widely used as a powerful analytical tool in many different fields of research or even application. However, the detailed interpretation of the measured Auger spectra is difficult, even for atoms and small molecules. This is because inner-shell ionization of atoms and molecules is concomitant with the excitation and ionization of valence electrons, and all these core-hole states contribute to the conventional Auger electron spectra. Recently, we have successfully applied a magnetic bottle electron spectrometer to multi-electron coincidence spectroscopy for different systems.[1–4] We describe here the results for the photoelectron-Auger-electron coincidence study in N_2 molecules, where the Auger decays from the individual inner-shell satellite states have been revealed.[1]

Figure 1(a) displays a two-dimensional (2D) map showing coincidences between 1s photoelectrons and Auger electrons. The conventional photoelectron and Auger electron spectra are plotted in Figures 1(b) and 1(c), respectively. Here the photoelectron spectrum is plotted in a binding energy scale relative to the $1s^{-1}$ state (409.94 eV). Inner-shell satellite structures (S_1–S_4) as well as the 1s mainline are clearly observed in the photoelectron spectrum. The 2D map shows horizontal structures at the 1s main line and the satellite states, which correspond to the Auger decays of these states. The decay mechanisms of the individual satellite states have been examined by extracting the coincidence Auger spectra from the 2D map. The decay features of the satellite states can be interpreted as spectator and participator behavior of the excited electrons.

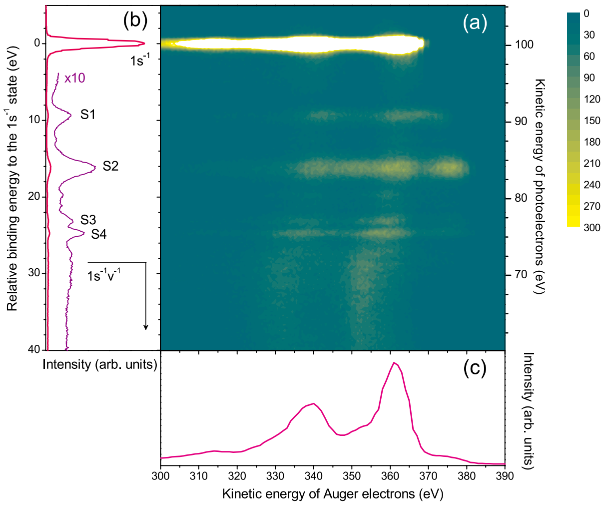

Figure 1. (a) Two-dimensional map of electron-electron coincidences, represented as a function of kinetic energies of photoelectrons and Auger electrons. (b) Conventional N 1s photoelectron spectrum. (c) Conventional Auger electron spectrum.

3. X-Ray Absorption Spectroscopy Measured in Resonant Auger Scattering Mode

The element specific information obtained by x-ray absorption spectroscopy (XAS) has a long history of application in various fields of research. A well-known bottleneck for XAS is the rather poor spectral resolution caused by the lifetime broadening of the core-excited states. Thanks to the rapid technological development related to synchrotron radiation, the possibilities of super-high resolution beyond the inherent lifetime widths have attracted considerable interest. The simple idea behind XAS with super-high resolution is to measure x-ray absorption in resonant x-ray Raman scattering (RXRS) or resonant Auger scattering (RAS) modes. Thus, an immediate advantage can be taken from the fact that the spectral resolution of RXRS and RAS is independent of the lifetime broadening of the core-excited states. The width of the XAS resonance in resonant scattering mode is then determined by the spectral function width of the incident x-ray radiation. Sharpening of the x-ray absorption resonances was indeed experimentally evidenced by scanning over the incident photon energy of these scattering processes within fixed narrow scattered-energy windows.

Recently it has been demonstrated that the super-narrow x-ray absorption profiles obtained in the RAS mode for the CO molecules give wrong resonance positions, owing to the lifetime vibrational interference between coherently populated core-excited levels.[5] Figure 2 denotes the 2D map of the resonant Auger scattering yields, as a function of photon energy and electron kinetic energy, measured around the O1s → 2π resonance. The slight deviations of the positions of the hilltops from the vibrational progression of the core excited state can be seen in Figure 2.

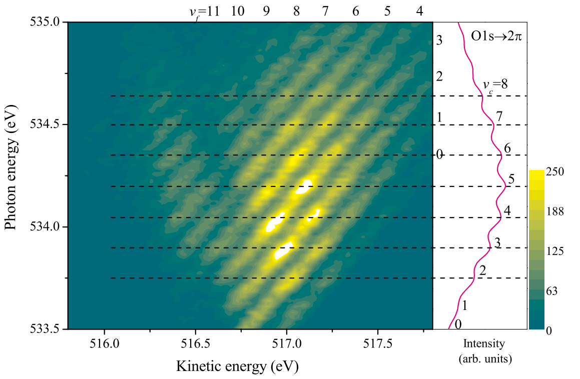

Figure 2. Two-dimensional map of the resonant Auger scattering yields from CO as a function of photon energy and electron kinetic energy, measured around the O1s → 2π resonance.

References

1) T. Kaneyasu, Y. Hikosaka, E. Shigemasa, F. Penent, P. Lablanquie, T. Aoto and K. Ito, *J. Phys. B* **40**, 4047–4060 (2007).

2) Y. Hikosaka, P. Lablanquie, F. Penent, T. Kaneyasu, E. Shigemasa, J. H. D. Eland, T. Aoto and K. Ito, *Phys. Rev. A* **76**, 032708 (6 pages) (2007).

3) T. Kaneyasu, Y. Hikosaka, E. Shigemasa, F. Penent, P. Lablanquie, T. Aoto and K. Ito, *Phys. Rev. A* **76**, 012717 (7 pages) (2007).

4) T. Kaneyasu, Y. Hikosaka, E. Shigemasa, P. Lablanquie, F. Penent and K. Ito, *J. Phys. B* **41**, 135101 (6 pages) (2008).

5) Y. Hikosaka, Y. Velkov, E. Shigemasa, T. Kaneyasu, Y. Tamenori, J. Liu and F. Gel'mukhanov, *Phys. Rev. Lett.* **101**, 073001 (4pages) (2008).

Micro Solid-State Photonics

Laser Research Center for Molecular Science
Division of Advanced Laser Development

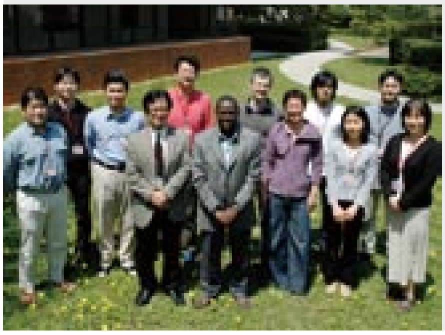

TAIRA, Takunori	Associate Professor
ISHIZUKI, Hideki	Assistant Professor
AKIYAMA, Jun	IMS Fellow
TSUNEKANE, Masaki	Post-Doctoral Fellow*
SATO, Yoichi	Post-Doctoral Fellow
SAIKAWA, Jiro	Post-Doctoral Fellow†
OISHI, Yu	Post-Doctoral Fellow‡
ONO, Yoko	Secretary
INAGAKI, Yayoi	Secretary
SUZUKI, Yukie	Secretary (for ASSP 2008 conference)

The artistic optical devices should be compact, reliable, efficient and high power light sources. With the approaches of domain structures and boundaries engineering, it is possible to bring the new interaction in their coherent radiation. The high-brightness nature of Yb or Nd doped single crystal or ceramic microchip lasers can realize efficient nonlinear wavelength conversion. In addition, designed nonlinear polarization under coherent length level allows us new function, such as the quasi phase matching (QPM). The development of "***Micro Solid-State Photonics***," which is based on the micro domain structure and boundary controlled materials, opens new horizon in the laser science.

1. High Peak Power, Passively Q-Switched Cr:YAG/Nd:YAG Micro-Laser for Ignition of Engines

The diode longitudinally pumped, passively Q-switched Nd:YAG/Cr:YAG micro-laser was researched and developed for ignition of automobile's engines. The length of the micro-laser module is 61 mm, comparable to that of a spark plug. The maximum output pulse energy of 2.7 mJ and totally 11 mJ was obtained at the pump duration of 500 µs (70 mJ) of QCW LDs. The pulse width was measured 0.6 ns. The M^2 value was 1.2 and longitudinal mode of the laser was single. The brightness of the micro-laser was calculated 0.3 PW/sr-cm^2. It was understood that the cross-section area of the flame kernel generated by the laser is 3-times larger than a spark plug as shown in Figure 1. The accelerated development of flame kernel due to the absence of quenching effects by electrodes shortens ignition delay and combustion time, and will improve the efficiency of real engines.

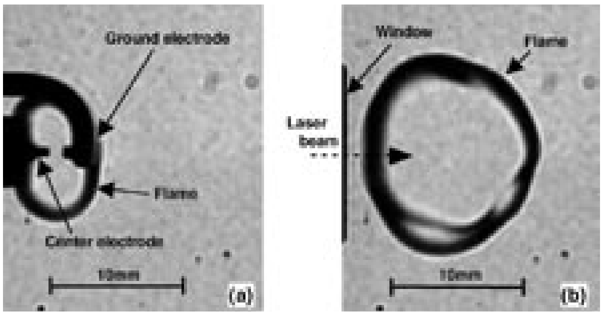

Figure 1. Schlieren photographs of the flame kernel ignited by a spark plug (a) and the micro-laser (b) in a constant volume combustion chamber at 6 ms after ignition trigger.

2. High-Energy, Broadly Tunable, Narrow-Bandwidth Mid-Infrared Optical Parametric System Pumped by Quasi-Phase-Matched Devices

We have developed a tunable, narrow-bandwidth (< 2 cm^{-1}) mid-infrared (MIR) optical parametric system with a large-aperture periodically poled Mg-doped $LiNbO_3$ (LA-PPMgLN)-based high-energy pump source. The system has a continuously tunable tuning range from 4.6 to 11.2 µm and produces a maximum output energy of 2.0 mJ at 5.1 µm as shown in Figure 2. Practical use of the MIR source is demonstrated by MIR-UV double-resonance spectroscopy of jet-cooled acetanilide.

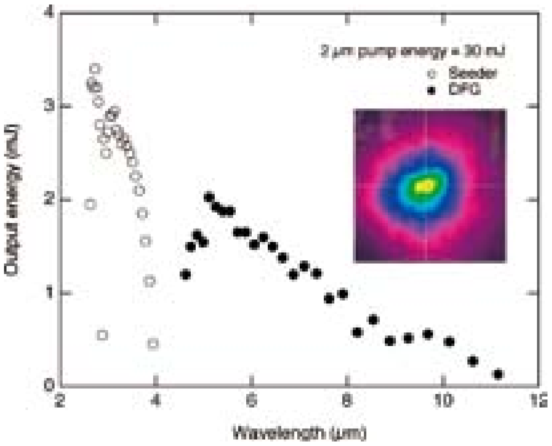

Figure 2. Tuning characteristics of the ZGP-DFG system (closed circle) and the LN-DFG system (open circle). Inset shows the intensity distribution of the ZGP-DFG system at 5.3 µm.

3. Mg-Doped Congruent $LiTaO_3$ Crystal for Large-Aperture Quasi-Phase Matching Device

We have characterized the crystal properties of Mg-doped congruent $LiTaO_3$ (MgLT), and demonstrated the first optical parametric oscillation experiment using periodically poled MgLT (PPMgLT) device. The MgLT could be a candidate for the material of high power quasi phase matching device because of the improved cut off wavelength and the decreased coercive field. The characteristics in the field poling of MgLT is similar to that of MgLN, and the coercive field of MgLT is enough low to realize a large-aperture PPMgLT device for high power applications as shown in Figure 3. We can expect the realization of several-mm-aperture PPMgLT device in near future.

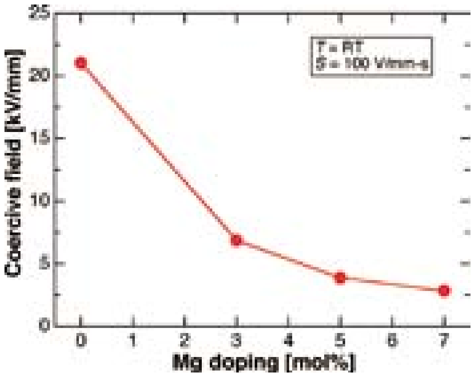

Figure 3. Coercive field of MgLT on Mg-doping (crystal temperature: T = RT, electric-field ramping rate : S = 100 V/mm-s).

4. Dependence of Rare-Earth Doped $Y_3Al_5O_{12}$ Ceramics on Doping Concentration: Electronic Structures of Host and Dopant

We have confirmed experimentally that there is severe dependence of spectral profiles of fluorescence emitted from neodymium doped $Y_3Al_5O_{12}$ (Nd:YAG) ceramics. Figure 4 shows the dependence of fluorescent spectral profile emitted from Nd:YAG on Nd^{3+}-doping concentration. It was found that there was a maximum line-shift of 2 cm^{-1} in fluorescence peaks from 1.0 at.% to 8.9 at.% Nd^{3+}-concentration (C_{Nd}). Maximum line broadening of 1.85 times was also detected due to heavily Nd^{3+}-doping. It directly indicates that heavily Nd^{3+}-doping makes the peaks of stimulated emission cross section.

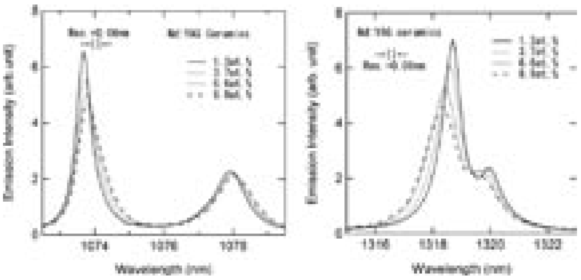

Figure 4. The dependence of fluorescent spectral profile emitted from Nd:YAG on Nd^{3+}-doping concentration. Heavily doping concentration causes both line shift and spectral-broadening.

References

1) M. Tsunekane, T. Inohara, A. Ando, K. Kanehara and T. Taira, *Tech. Digest of Advanced Solid State Photonics (ASSP2008)*, MB4 (2008).
2) J. Saikawa, M. Miyazaki, M. Fujii, H. Ishizuki and T. Taira, *Opt. Lett.* **33**, 1699–1701 (2008).
3) H. Ishizuki and T. Taira, *Tech. Digest of Conf. on Lasers and Electro-Optics (CLEO2008)*, CWG1 (2008).
4) Y. Sato, J. Akiyama, T. Taira and A. Ikesue, *Tech. Digest of The 15th International Conference on Luminescence and Optical Spectroscopy of Condensed Matter (ICL'08)* Tu-P-62 (2008).

---

* from JST Innovation Plaza Tokai
† from Tokyo Institute of Technology
‡ from RIKEN

Photo-Induced Dynamics and Reactions at Solid Surfaces

Laser Research Center for Molecular Science
Division of Ultrahigh Resolution Optical Measurement

MATSUMOTO, Yoshiyasu Professor*
WATANABE, Kazuya Assistant Professor*

Solid surfaces provide an interesting environment where two completely different electronic systems meet to each other: Localized electronic system, *i.e.*, atoms and molecules and delocalized one, *i.e.*, solid bulk surfaces. Charge transfer at surfaces is fundamental to adsorbate-metal interactions and reactions. Moreover, dynamic processes including chemical reactions on surfaces, particularly metal surfaces, are associated with continuous nonadiabatic transitions. This research program aims for understanding electron and nuclear dynamics at surfaces. Photo-induced processes including photochemistry at surfaces are the major focus in this program. Photons are used for not only exciting electronic states of adsorbate and substrate, but also for probing those states with various types of nonlinear optical spectroscopy.

1. Ultrafast Dynamics at Well-Defined Surfaces[1)]

To understand the mechanism of surface photochemistry, it is vital to know how photoinduced electronic excitation induces adsorbate nuclear motions that ultimately lead to chemical reactions. We have demonstrated the real-time observations of surface phonons and adsorbate-substrate vibrational modes by fs time-resolved second harmonics generation (TRSHG). If an excitation light pulse has a duration sufficiently shorter than a period of a vibrational mode or a phonon mode, it can excite the mode with a high degree of temporal and spatial coherence. This coherent nuclear motion modulates the second-order susceptibility $\chi^{(2)}$. Thus, by monitoring the intensity modulation of the second harmonics (SH) generation of a probe pulse, we can observe the evolution of the coherent nuclear motion subsequent to the electronic excitation at the surfaces. We have focused on the excitation mechanism of coherent surface phonons at Na-covered Cu(111) surfaces.

Changing the photon energy of the pump pulse (25 fs) from 2.0 to 2.5 eV, the oscillation amplitude derived from the Na–Cu stretching motion is enhanced. As shown in Figure 1, the careful measurements of photon-energy dependence indicates that the excitation efficiency mimics the absorbance of bulk Cu. Holes created in the d-bands by the optical transitions could be filled by electrons in the adsorbate-induced occupied state of the metallic quantum well by an Auger-type transition. Hence, holes can be created in the adsorbate-induced occupied state. Moreover, since this Auger decay can occur significantly faster than the oscillation period of the Na–Cu stretching mode, the substrate excitation may be a possible excitation mechanism for the coherent oscillation.

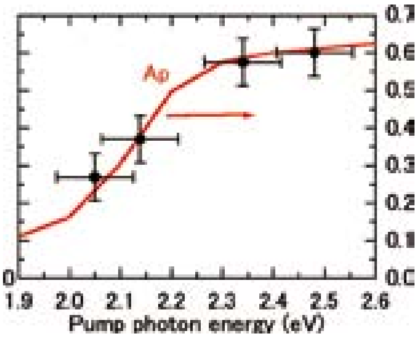

Figure 1. Action spectrum for the initial amplitude of the oscillating component in TRSHG traces due to the coherent Na–Cu stretching mode.

2. Spectroscopy of Molecules at Interfaces in Organic Field Effect Transistors by a Sum Frequency Generation Microscope

Organic field effect transistors have gained substantial attentions recently. In order to understand the efficiency of the device and the mechanism of charge transport, it is important to know carriers at the interface between a gate electrode and an organic semiconductor thin film. Since the interface is buried in the device, there are a few methods to investigate what is really happening at the interface. Sum frequency generation (SFG) is one of promising methods to realize it, since this is sensitive to the molecules at interfaces. SFG is a nonlinear optical process and, in particular, when visible and infrared beams are used, SFG is a powerful means for vibrational spectroscopy. We have developed a SFG microscope and applied it to the interface between pentacene and silicon oxide at the gate electrode. SFG signals generated at the interface are spatially resolved by the SFG microscope. We found that SFG signals are largely enhanced when carriers are injected at the interface.

3. Chemistry of One-Dimensional Nano-Surface Compounds

The fluctuating configurations of low-dimensional structures can be thermodynamically favorable at finite temperatures, because the energy gain overcomes the energy cost that accompanies local structural fluctuation. In particular, one-dimensional (1D) systems have a propensity to be sensitive to these fluctuations as described by one of the maxims of condensed matter physics, *i.e.*, one chain does not make a crystal. Thus, the dynamical formation of active species and sites by these fluctuations is a key factor in establishing a microscopic model for chemical reactions at surfaces and nano-structured compounds. It is well known that the adsorption of O on Ag(110) results in the formation of quasi-1D structures, AgO chains, accompanied by the mass transfer of substrate atoms.

We have studied the structures of continuous and truncated AgO chains on Ag(110) surfaces by using density functional theory (DFT) calculations. In addition, the thermal fluctuations of truncated chains are simulated by using the Monte Carlo method. Although it is known that oxygen elimination by CO from one dimensional AgO chains takes place exclusively at chain ends when the chains keep a linear structure at low temperatures, the structure of chain ends has been unexplored. The DFT calculations reveal that oxygen-terminated chains are more stable than silver-terminated ones and have an enhanced density of states near the Fermi level at the terminal oxygen, which is consistent with scanning-tunneling microscope (STM) observations. The Monte Carlo simulations with pairwise interactions between AgO units reproduce characteristic features observed in STM studies, including the existence of an onset temperature for the chain fluctuations and the oxygen-coverage dependence of average chain length. The onset temperature, on the one hand, is largely controlled by attractive interactions in the direction parallel to chain growth. On the other hand, the spatial distribution of fragmented AgO chains depends strongly on repulsive interactions in the direction perpendicular to chains. In particular, the repulsive interactions ranging ten units of the lattice constant in the direction perpendicular to the AgO chains are essential to mimic STM observations, where fragmented chains almost keep the mutual distance inherent to the (n×1)-O phase even under thermal fluctuations.

Reference

1) M. Fuyuki, K. Watanabe, D. Ino, H. Petek and Y. Matsumoto, *Phys. Rev. B* **76**, 115427 (5 pages) (2007).

---

* Present Address; Kyoto University, Graduate School of Sciences, Department of Chemistry, Kyoto 606-8502

Visiting Professors

Visiting Professor

MIDORIKAWA, Katsumi *(from RIKEN)*

XUV Nonlinear Optics and Attosecond Dynamics in Atoms and Molecules

Nonlinear optical process in the XUV region is of paramount importance not only in the field of quantum electronic but also in ultrafast optics. From the viewpoint of quantum electronics, new features of the interaction between intense XUV photons and matters are expected to be revealed through observation of those nonlinear phenomena. On the other hand, those nonlinear processes in the XUV region is indispensable for progress of attosecond science including attosecond atomic/molecular physics and chemistry, because it is very useful for investigating ultrafast phenomena directly in attosecond time scale. Using high harmonic generation by intense femtosecond lasers, we are pursuing extreme optical science including XUV nonlinear optics and attosecond physics/chemistry.

Visiting Professor

TOMINAGA, Keisuke *(from Kobe University)*

Molecular Dynamics in Condensed Phases Studied by Ultrafast Laser Spectroscopy

Molecules in liquids interact with each other in a complex manner, and this complicated interaction is a source of various aspects of the dynamical behaviors in liquids. Mainly, we employ two ultrafast spectroscopic techniques. One is terahertz time-domain spectroscopy. We have studied collective dynamics of liquid methanol from analysis of THz spectra based on the results by molecular dynamics simulation. The other technique is infrared nonlinear spectroscopy such as three-pulse photon echo. By this method we have made data base of time correlation functions of the frequency fluctuation of vibrational transitions of various solute/solvent systems.

Visiting Associate Professor

OKADA, Kazumasa *(from Hiroshima University)*

Study on the Fragmentation of Molecules and Clusters in the Inner-Valence and Inner-Shell Electron Excitation Regions

The knowledge of the mechanisms involved in the ionization helps us to understand various processes in which there exists interaction of molecules and photons or electrons. The fragmentation dynamics of highly-excited or multiply-ionized molecules and clusters is studied by means of time-of-flight mass spectrometry. Multiple modes of measurement are used to obtain branching ratios of fragment ions or breakdown diagrams. Kinetic energy distribution of fragments provides insight into the nature of the fragmentation process.

Visiting Associate Professor

AMEMIYA, Kenta *(from High Energy Accelerator Research Organization)*

Development of Soft X-Ray Optics and X-Ray Absorption Techniques

The soft X-ray region includes absorption edges of light elements such as carbon, nitrogen and oxygen, which are main components of organic molecules. X-ray absorption spectroscopy (XAS) is a powerful technique to investigate atomic and electronic structures of condensed materials, owing to its element and orbital selectivity. Soft X-rays with high energy resolution is necessary, however, in order to obtain significant information from X-ray absorption spectra. We develop a high-resolution soft X-ray beamline in UVSOR, as well as a novel experimental technique, three-dimensional XAS, which combines soft X-ray microbeam with the depth-resolved XAS technique. By applying this technique, lateral and depth profiles of atomic and electronic structures of organic thin films can be determined with lateral and depth resolution of several micron and sub nanometer, respectively.

RESEARCH ACTIVITIES

Materials Molecular Science

Extensive development of new molecules, molecular systems and their higher-order assemblies is being conducted in the four divisions and in the research center for molecular scale nanoscience. Their electronic, optical and magnetic properties as well as reactivities and catalytic activities are being examined in an attempt to discover new phenomena and useful functions.

Structures and Functions of Metal–Carbon Nano-Systems Produced from Metal-Acetylides

Department of Materials Molecular Science
Division of Electronic Structure

NISHI, Nobuyuki	Professor
JUDAI, Ken	Assistant Professor
NISHIJO, Junichi	Assistant Professor
OISHI, Osamu	Technical Associate
FURUYA, Ari	Post-Doctoral Fellow
NUMAO, Shigenori	Graduate Student
UBAHARA, Wakana	Secretary

Metal acetylides or metal ethynyl conpounds are made of the $M^+–C^−$ ionic bonds. However, the ionic states of the acetylides are essentially metastable resulting in the segregation into metal-carbon or metal-organic polymer nanophases. This segregation still maintains $M^+–C^−$ ionic bonds around the interfaces of the metal wire, particles, and dendroid sponges exhibiting various functions depending on the metal species. Removal of the metals produces two types of carbon materials: One is mesoporous carbon with graphene walls and the other is amorphous carbon containing small amount of metals.

1. A Novel Functional Carbon Material: Mesoporous Carbon Nano-Dendrite with Graphene Walls

We have succeeded to synthesize a new material, Mesoporous Carbon Nano-Dendrites (MCNDs) with graphenen walls. The novel material exhibits good electric conductance due to large particle sizes and excellent ion fluidity. These properties could be attributed to the dendriform branching structure of the main bodies. Silver acetylide (Ag_2C_2) produces dendriform nanostructures under ultrasonic irradiation. The dendrites were quickly warmed to 150 °C emitting a brilliant flash of reddish orange lighting and thunderous sound indicative of the sudden jump of the local temperature to higher than 2000 °C. This sudden heating boils off the silver from the main body, leaving MCNDs. Raman spectra clearly indicate that the bodies consist of mainly single-layer graphene walls. Scanning Electron Microscope (SEM) and Transmission Electron Microscope (TEM) images as well as EELS spectra show that the main bodies with ~50 nm radii ramifies at every 100–150 nm and composed of the cells with graphene walls. Figure 1a shows a SEM image of MCND. The MCNDs showed a BET surface area of 1600~1800 m^2/g. As shown in Figure 1b, cyclic voltammetry of the supercapacitor with MCND electrodes exhibited good rectangular curves, even at a scanning rate of 400 mV/s, suggesting applicability for high current and high-speed charge-discharge capacitors for motor vehicles. By filling metallic layers or cluster islands in the pores, one can utilize the extremely large surface area for the electrodes of lithium ion batteries or fuel cells, respectively.

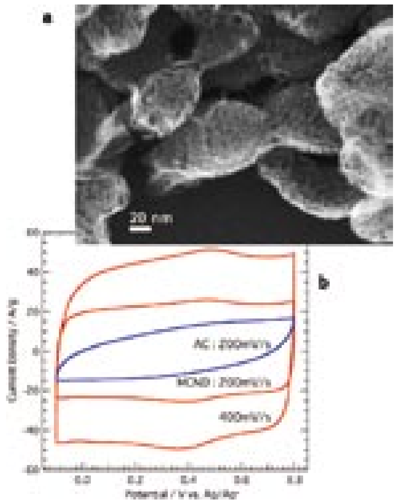

Figure 1. a: a high resolution SEM image of the edge region of MCND. **b**: Cyclic voltammograms of a MCND EDLC with an electrode thickness of 80 µm. Although the commercial activated carbon never shows a rectangular response with changing potentials at a scan rate faster than 50 mV/s, MCND can afford high-speed charge-discharge performance at a rate faster than 400 mV/s and current densities higher than 40 A/g.

2. Amorphous Carbon Material Converted from Self-Assembled Copper Acetylide Nanowires

In the next case, we deal with copper acetylide (Cu_2C_2) nanowires as less explosive nano-materials. Cu_2C_2 has been well-known as explosive substance. However, decreasing the size of material into the nanometer makes it possible to control the explosive segregation reaction. We suggest a new method to produce amorphous carbon material by lower temperature process converted from the less explosive Cu_2C_2 nanowires. Amorphous carbon is normally produced with high temperature process of carbonization. An explosive nature of Cu_2C_2 itself provides segregation reaction into elemental carbon and copper at a temperature below 150 °C. The product by this low temperature process shows unique spectroscopic characters and material properties.

It is very simple to produce Cu_2C_2 nanowires. The fabrication method for Cu_2C_2 nanowire involves bubbling acetylene (C_2H_2) gas into an ammonia solution of copper chloride (CuCl). When the C_2H_2 reacts slowly, Cu_2C_2 molecules can self-assemble into nanowires 5 nm in diameter. Gradual heating of the product up to 150 °C for 1–5 hours in a vacuum transforms Cu_2C_2 nanowire into elemental copper and carbon via a segregation reaction without explosion. Aqueous NH_3 or nitric acid treatment can separate amorphous carbon from Cu element dissolving in solution.

Figure 2 shows Raman spectra of various carbon materials. Graphite displayed sharp peak around 1575 cm^{-1}, which could be assigned to G band of inherent in graphite lattices. For more poorly crystallized graphite, an additional broad band appears at 1350 cm^{-1} (so-called D band. Raman spectra demonstrated difference of crystalline characters between graphite and activated carbon. The amorphous carbon converted from Cu_2C_2 nanowires exhibits no distinct peak in the Raman spectrum. The spectroscopic study tells us that the low temperature process can generate genuine amorphous carbon materials without any trace of crystalline graphite. We attempt this new amorphous carbon evaluated to the application as hydrogen storage and so on right now.

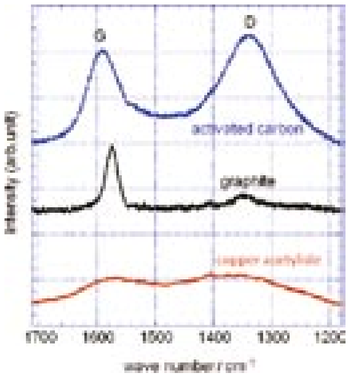

Figure 2. Raman spectra of various carbon materials. Graphite (black line, middle) shows a sharp G band at 1575 cm^{-1}, and active carbon (blue line, top) gives broad G band and also broad D band around 1350 cm^{-1}. Amorphous carbon converted from Cu_2C_2 nanowires shows extremely broad band (red line, bottom).

3. Surface Environment of Ag Nanoparticles Formed by Decomposition of Silver Phenylacetylide

Recently, we developed a facile preparation method of one dimensional Ag nanoparticle arrays via thermal- or photo-decomposition of silver phenylacetylide (Ag–C≡C–Ph). The nanoparticle is stabilized by the surface organic layer which keeps the nanoparticles from aggregation and oxidation. The structure of the surface layer was investigated by surface enhanced Raman spectroscopy and IR spectroscopy.

Figure 3 shows the Raman spectra of as-prepared, thermal- and photo-decomposed Ag–C≡C–Ph. Decomposed samples clearly show broad peaks at around 1970 cm^{-1} regardless of the decomposition process. The peaks are characteristic of the C≡C stretching mode of a surface adsorbed phenylacetylide anion, and indicates that the surface of the Ag nanoparticle is covered with vertically adsorbed phenylacetylene molecules. The peak shows no significant change even after 12 h thermal- or photo- decomposition, indicating the quite strong interaction between Ag nanoparticles and surface adsorbed molecules. Phenylacetylenes except surface adsorbed molecules are rapidly dimerized in decomposition processes to 1,4-diphenylbutadiyne which shows Raman and IR peaks of in- and out-phase =C≡C–C≡C= stretching at 2215 and 2150 cm^{-1}, respectively. In the case of long-time UV irradiated sample, the polymerization continues and results in the graphitic structure as evidenced by the occurrence of D- and G-bands in Raman spectrum at around 1350 and 1580 cm^{-1}, respectively, while the peak of –C≡C–C≡C– in-phase stretching disappears. In contrast, polymerization of 1,4-diphenylbutadiyne is rare in the case of after 12 h heat treatment at 150 °C, where only a small amount of graphitic structure is observed as shown in Figure 3. These results suggest that we can control not only the nanoparticle size of one dimensional Ag arrays but also the conductivity of its intermediate organic matrix from insulating to metallic, in which the Ag nanoparticles are firmly protected by surface adsorbed phenylacetylenes from chemical reactions.

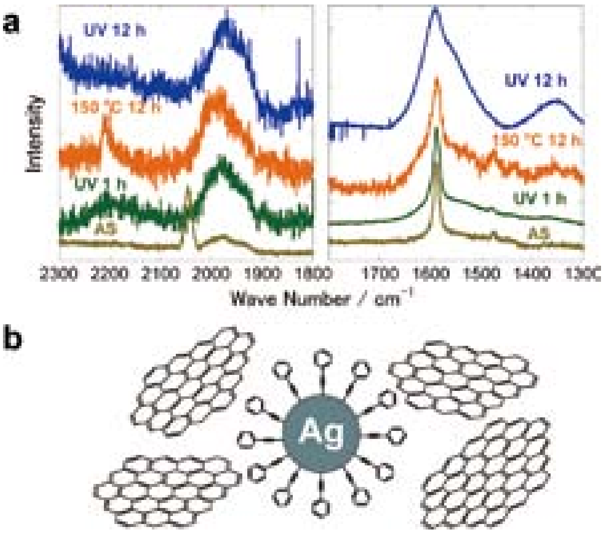

Figure 3. a) Raman spectra of as-prepared and decomposed Ag–C≡C–Ph. b) Schematic drawing of decomposed Ag–C≡C–Ph after 12 h UV irradiation.

Awards

JUDAI, Ken; Young Best presenter Award, 6th Annual Meeting of Society of Nano Science and Technology.
NUMAO, Shigenori; Young Best presenter Award, 6th Annual Meeting of Society of Nano Science and Technology.

Characterization of Magnetic Ultrathin Films by Novel Spectroscopic Methods

Department of Materials Molecular Science
Division of Electronic Structure

YOKOYAMA, Toshihiko	Professor
NAKAGAWA, Takeshi	Assistant Professor
TAKAGI, Yasumasa	Assistant Professor
YAMAMOTO, Isamu	Post-Doctoral Fellow
ISAMI, Kyohei	Graduate Student
NOTO, Madomi	Secretary

Novel properties of magnetic metal ultrathin films have been attractive both from fundamental interest and from technological requirements. We are interested in drastic modification of metal thin films by surface chemical treatment such as adsorption-induced spin transitions and morphological changes. The magnetic properties are characterized by means of several kinds of spectroscopic methods like MOKE (Magneto-Optical Kerr Effect) using lasers and XMCD (X-ray Magnetic Circular Dichroism) using synchrotron radiation. In 2007, we have installed an *in situ* XMCD system with a superconducting magnet (up to 7 T) and a liq. He cryostat (down to 5 K). Some results obtained by the XMCD system are described below.

We are also exploiting new techniques of ultrafast time resolved ultraviolet (UV) magnetic circular dichroism (MCD) photoelectron emission microscopy (PEEM) in order to perform spatiotemporal magnetic imaging. Moreover, we are developing a two-photon photoemission MCD technique including PEEM.

1. First Observation of Ultrafast UV Magnetic Circular Dichroism Photoemission Electron Microscope Images

In 2006, we discovered surprising enhancement of the visible/ultraviolet photoemission MCD from ultrathin Ni films on Cu(001) when the photon energy was tuned to the work function threshold.[1] Based on this discovery, we succeeded in the first observation of UV MCD PEEM images of ultrathin magnetic films.[2] This method allows us to do in-laboratory MCD PEEM measurements instead of the usage of synchrotron radiation XMCD PEEM. Moreover, when ultrashort pulsed lasers are employed, pump-and-probe UV MCD PEEM measurements provide us a time resolving power of ~100 fs rather easily, which is two to three orders of magnitude faster than that of XMCD PEEM.

Since 2007 we have been reconstructing the measurement system by installing an ultrashort-pulsed deep UV laser and new UHV chambers to combine the MOKE, PEEM and photoemission experiments. Although the system is still under construction, we have tentatively observed time-resolved UV MCD PEEM images by using the previous setup. This work is a collaboration with Profs. Kazuya Watanabe and Yoshiyasu Matsumoto in Kyoto University.

Ultrafast UV MCD PEEM images were recorded by means of the pump-and-probe technique, in which the pump and probe lights were respectively the linearly-polarized fundamental (800 nm, ~70 fs) and the circularly-polarized second-order (400 nm, ~200 fs) harmonics of a Ti:sapphire laser. The sample is Cs-coated Ni (12 monolayer) grown epitaxially on Cu(001).

Figure 1 shows the femtosecond time resolved UV MCD PEEM image and the time evolution of the local magnetization observed for the first time. Although the present result is rather tentative, we will measure more beautiful images in near future by using the new apparatus.

Moreover, we have succeeded in the first observation of the two-photon MCD PEEM. By employing a newly installed tunable deep UV laser, the maximum MCD asymmetry was found to be quite large. Especially, at 45° incidence the MCD is maximized, and this is quite useful for two-photon UV MCD PEEM.

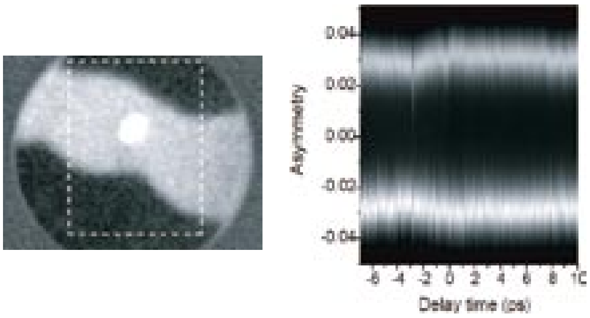

Figure 1. Time resolved UV MCD PEEM image (left, 10µm area) and the time dependence of the local magnetization (right) of Cs-coated Ni(12ML)/Cu(001). Time resolution is ~200 f.

2. X-Ray Magnetic Circular Dichroism under High Magnetic Field and Extremely Low Temperature[3)]

XMCD is a powerful tool for the investigation of magnetism since it provides valuable information on element specific orbital and spin magnetic moments. A XMCD measurement system with a superconducting magnet and a liq. He cryostat is, however, not so popular in the world especially for public usage, although XMCD measurements under high magnetic fields are crucial for the investigation of magnetic anisotropy, because the saturated magnetization along the hard axis can be achieved around several tesla. We have thus constructed an in situ UHV soft X-ray XMCD system.

Figure 2 shows the schematic view and the photo of the present UHV XMCD system, which is usually installed at Beamline 4B of UVSOR-II. The magnetic field applied is ±7 T (typically ±5 T) and the sample temperature is ~5 K using liq. He. Samples are prepared in the preparation chamber and are transferred to the measurement chamber under UHV condition. The polar angle of the sample can be rotated by 360°, allowing us to examine angle dependence of XMCD.

In order to demonstrate the usefulness of the system, we have investigated angle dependent Co *L*-edge XMCD of Co(0.4 ML) on Cu(001). Since the sample shows strong in-plane magnetic anisotropy, the saturation along the perpendicular magnetization direction (hard axis) requires a magnetic field of >3.4 T (5 T was applied). Through the analysis of the angle-dependent XMCD spectra, which can be done with saturated magnetization data even for the hard axis. As a result, the enhancements of the magnetic moments compared to the corresponding bulk values were clearly elucidated: ~15% for the spin magnetic moment, and ~96% and ~53% for the orbital magnetic moments along the surface parallel and normal directions, respectively. The surface magnetization is found to be essentially different from the bulk one.

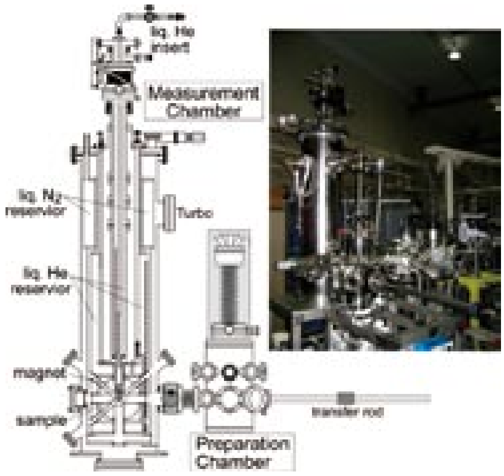

Figure 2. Schematic view and photo of the XMCD system with a superconducting magnet and a liq. He cryostat.

3. Magnetism of Self-Assembled Co Nanorods Grown on Cu(110)-(2x3)N[4)]

Magnetic properties of low dimensional magnets has recently attracted much interest due to their importance for further dense magnetic recording media. In this work, we have investigated magnetic properties of self-assembled Co nanorods grown on Cu(110)-(2×3)N[5)] using the superconducting magnet XMCD system described above. This work was performed in collaboration with Prof. F. M. Leibsle (University of Missouri, Kansas) and Dr. X. -D. Ma and Prof. M. Przybylski (Max-Planck Institut, Halle).

Magnetic properties have been characterized by MOKE and XMCD. Figure 3(a) shows the angular dependence of Co *L*-edge *in situ* XMCD obtained by using the superconducting magnet at 4.9 K. Angle dependent magnetization curves of the Co nanorods recorded by MOKE (not shown) and XMCD [Figure 3(b)] show that the magnetic easy axis is perpendicular to the rod within the substrate plane, irrespective of the Co thickness down to 0.8 ML. From Figure 3(b), one can recognize that a high magnetic field is necessary to magnetize the sample along the magnetic field direction. The analysis of the magnetization curves clarify that the magnetic anisotropy is not dominated by the shape anisotropy but by the magneto-crystalline anisotropy. The XMCD analysis reveals significant enhancement of the orbital magnetic moment along the easy axis compared to the hard axes ([001] > [1$\bar{1}$0] > [110]). The magnetocrystalline anisotropy is found to be directly related to the anisotropy of the orbital magnetic moment.

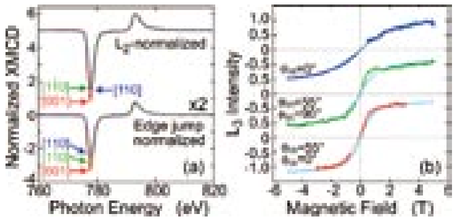

Figure 3. (a) Angle dependent Co *L*-edge XMCD spectra of Co/Cu(110)-(2×3)N (Co 0.8 ML) at T = 4.9 K and H = ±5.0 or ±3.0 T. The lower and upper spectra correspond to those normalized with the edge jumps (×2 magnified) and the L_2 peak top intensity (+5 shifted), respectively. (b) Magnetization curves at T = 4.9 K recorded with the L_3 peak top. The simulated magnetization curves (light blue dotted lines) using a simple magnetic anisotropy model are also shown.

References

1) T. Nakagawa and T. Yokoyama, *Phys. Rev. Lett.* **96**, 237402 (2006).
2) T. Nakagawa, T. Yokoyama, M. Hosaka and M. Katoh, *Rev. Sci. Instrum.* **78**, 023907 (2007).
3) T. Nakagawa, Y. Takagi, Y. Matsumoto and T. Yokoyama, *Jpn. J. Appl. Phys.* **47**, 2132 (2008).
4) X. -D. Ma, T. Nakagawa, Y. Takagi, M. Przybylski, F. M. Leibsle and T. Yokoyama, to be published.
5) S. M. York and F. M. Leibsle, *Phys. Rev. B* **64**, 033411 (2001).

Award

TAKAGI, Yasumasa; Young Researcher Promotion (Wakate-Shourei) Award, The Physical Society of Japan (2007).

Structure and Properties of Metal Clusters Protected by Organic Molecules

Department of Materials Molecular Science
Division of Electronic Structure

TSUKUDA, Tatsuya	Associate Professor[*]
NEGISHI, Yuichi	Assistant Professor[†]
CHAKI, Nirmalya K.	IMS Fellow[‡]
TSUNOYAMA, Hironori	Post-Doctoral Fellow[§]
SHICHIBU, Yukatsu	Post-Doctoral Fellow[‖]
NAKAO, Satoru	Post-Doctoral Fellow
UBAHARA, Wakana	Secretary

1. Origin of Magic Stability of Thiolated Gold Clusters: A Case Study on $Au_{25}(SC_6H_{13})_{18}$[1)]

The present work aims to test the validity of the electronic shell model for $Au_{25}(SC_6H_{13})_{18}$ by monitoring the charge state of the Au:S core and thereby to elucidate the origin of magic stability. Electrospray ionization mass spectrometry revealed that the Schiffrin method yields $[Au_{25}(SC_6H_{13})_{18}]^x$ with a distribution of charge states, which shifts toward negative values with reduction time. The stable ions $[Au_{25}(SC_6H_{13})_{18}]^{1+}$ and $[Au_{25}(SC_6H_{13})_{18}]^{1-}$ can be synthesized by chemical oxidation and reduction of $[Au_{25}(SC_6H_{13})_{18}]^0$, respectively. These findings lead us to conclude that electronic shell closing is not a crucial factor for the high stability of $[Au_{25}(SC_6H_{13})_{18}]^x$ (x = 1–, 0, 1+). We ascribe magic stability to the core-in-cage structure predicted theoretically.

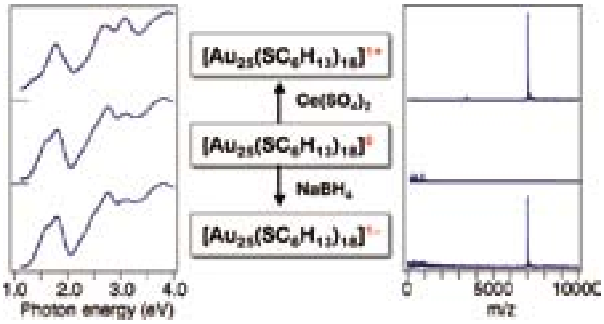

Figure 1. Optical absorption spectra (left) and ESI mass spectra (right) of $[Au_{25}(SC_6H_{18})_{18}]^z$ with different charge states.

2. Ubiquitous 8 and 29 kDa Gold: Alkanethiolate Cluster Compounds: Mass-Spectrometric Determination of Molecular Formulas and Structural Implications[2)]

The molecular formula and charge state distributions of thus-far known, ubiquitous alkanethiolate-protected gold clusters with core-masses of 8 and 29 kDa were assessed using electrospray ionization mass spectrometry (ESI-MS). The 8 and 29 kDa clusters were determined to be composed of single species, $[Au_{38}(SC_n)_{24}]^z$ and $[Au_{144}(SC_n)_{59}]^z$, respectively, with charge states of $z \geq 0$. Possible geometric structures for $Au_{38}(SC_n)_{24}$ and $Au_{144}(SC_n)_{59}$ are discussed based on the structures of relevant systems that have been recently determined experimentally and theoretically; $[Au_{25}(SR)_{18}]^{-1}$ and $Au_{102}(SR)_{44}$, in which the Au cores are protected by monomers [–SR–Au–SR–] and/or dimers [–SR–Au–SR–Au–SR–]. Their preferential formation and chemical robustness are proposed as being associated with high stability due to geometric factors, while the Au-thiolate interface takes on common motifs regardless of the underlying Au core.

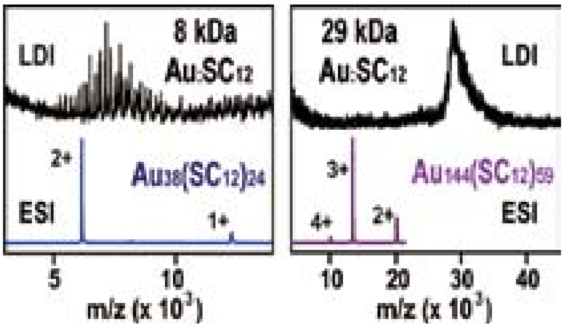

Figure 2. LDI and ESI mass spectra of $[Au_{38}(SC_6H_{18})_{24}]^z$ (left) and $[Au_{144}(SC_6H_{18})_{59}]^z$ (right).

3. Thermosensitive Gold Nanoclusters Stabilized by Well-Defined Vinyl Ester Star Polymers: Reusable and Durable Catalysts for Aerobic Alcohol Oxidation[3)]

Au nanoclusters of less than 4 nm with a narrow size distribution were prepared and supported in thermosensitive vinyl ether star polymers obtained by living cationic polymerization. The thermosensitivity of the star polymers permitted easy separation of the clusters from the reaction mixture without any negative aggregation. Thus, the Au clusters could be recovered for reuse several times to induce alcohol oxidation with similar reactivity in each run.

4. Ligand exchange of $Au_{25}SG_{18}$ Leading to Functionalized Gold Clusters: Spectroscopy, Kinetics, and Luminescence[4)]

Ligand exchange offers an effective way to modify the properties of the recently prepared quantum clusters of gold. To tune optical and photoluminescence properties of one of the most stable quantum clusters of gold, $Au_{25}SG_{18}$ (SG-glutathione thiolate), we functionalized it by the exchange of -SG with functionalized-SG and with an altogether different ligand, namely, 3-mercapto-2-butanol (MB). The products were characterized by various techniques such as optical absorption (UV-vis), Fourier-transform infrared (FTIR), nuclear magnetic resonance (NMR), X-ray photoelectron (XPS), and luminescence spectroscopies, mass spectrometry, and thermogravimetry (TG). Analyses of the TG data helped to establish the molecular composition of the products. Ligand exchange reaction was monitored by NMR spectroscopy, and it was found that the exchange reaction follows a first order kinetics. The XPS study showed that after the exchange reaction there was no change in the chemical nature of the metal core and binding energy values of Au $4f_{7/2}$ and $4f_{5/2}$, which are similar in both the parent and the exchanged products. Photoluminescence studies of these clusters, done in the aerated conditions, showed that the excitation spectrum of the MB-exchanged product is entirely different from the acetyl- and formyl-glutathione exchanged products. The inherent fluorescence and solid-state emission of these clusters were observed. This intense emission allows optical imaging of the material in the solid state. The emission is strongly temperature dependent. The synthesis of a diverse variety of clusters and their chemical stability and intense luminescence offer numerous applications in areas such as energy transfer, sensors, biolabeling, and drug delivery.

5. Electronic Structure of Dendrimer-Au Hybrid Nanoparticle: Hard X-Ray Photoemission Study[5)]

We have carried out the hard X-ray photoemission study of dendrimer-Au hybrid nanoparticles/nanoclusters supported on the HOPG substrates. From the detailed line-shape analysis for Au 4f core-level photoemission spectrum of dendrimer-Au hybrid nanoparticles with mean diameter of 2.6 nm, it is found that Au 4f core-level spectrum consists of three components. We attribute these components to the interior Au atoms, surface Au atoms, and surface Au atoms bonded to dendrimers. Furthermore, we have investigated the valence-band photoemission spectra. From these results, we discuss the electronic structures and interfacial properties of dendrimer-Au hybrid nanoparticles/nanoclusters.

References

1) Y. Negishi, N. K. Chaki, Y. Shichibu, R. L. Whetten and T. Tsukuda, *J. Am. Chem. Soc.* **129**, 11322–11323 (2007).
2) N. K. Chaki, Y. Negishi, H. Tsunoyama, Y. Shichibu and T. Tsukuda, *J. Am. Chem. Soc.* **130**, 8608–8610 (2008).
3) S. Kanaoka, N. Yagi, Y. Fukuyama, S. Aoshima, H. Tsunoyama, T. Tsukuda and H. Sakurai, *J. Am. Chem. Soc.* **129**, 12060–12061 (2007).
4) E. S. Shibu, M. A. Habeeb Muhammed, T. Tuskuda and T. Pradeep, *J. Phys. Chem. C* **112**, 12168–12176 (2008).
5) Y. Murase, T. Kitagawa, M. Imamura, A. Tanaka, H. Yasuda, Y. Negishi, T. Tsukuda, S. Ueda, Y. Yamashita, H. Yoshikawa and K. Kobayashi, *Trans. Mater. Res. Soc. Jpn.* **33**, 169–172 (2008).

Award

NEGISHI, Yuichi; The Chemical Society of Japan Award for Young Chemists.

---

* Present Position; Professor, Catalysis Research Center, Hokkaido University, Sapporo 001-0021

† Present Address; Tokyo University of Sciences, Tokyo 162-8601

‡ Present Address; The Pennsylvania State University, Pennsylvania 16802, U. S. A.

§ Present Address; Catalysis Research Center, Hokkaido University, Sapporo 001-0021

|| Present Address; Hokkaido University, Sapporo 068-0810

Optical Studies of Charge Ordering in Organic Conductors

Department of Materials Molecular Science
Division of Electronic Properties

YAKUSHI, Kyuya	Professor
YAMAMOTO, Kaoru	Assistant Professor
URUICHI, Mikio	Technical Associate
KOWALSKA, Aneta	JSPS Post-Doctoral Fellow
NAKANO, Chikako	Research Fellow
YUE, Yue	Graduate Student
ABE, Hitomi	Secretary

In many organic charge-transfer salts, the electronic state of charge carriers is located at the boundary between localized and delocalized states. Recently the charge ordering (CO) originated from the localization due to Coulomb interaction is widely found in organic conductors, and the electronic phase diagrams of typical organic conductors are re-considered taking CO into account. We are interested in the CO state, first because a CO phase is neighbored on a superconducting phase, wherein a charge-mediated superconductivity is theoretically predicted, second because some compounds in a CO phase shows ferroelectricity, the origin of which is attributable to the electron displacement, third because the narrow-band compounds have an inhomogeneous intermediate state between metallic and CO states, which is not well understood. We employ infrared and Raman spectroscopy to study the CO state.

1. Strong Optical Nonlinearity and Its Ultrafast Response Associated with Electron Ferroelectricity in an Organic Conductor[1)]

We yielded an experimental evidence for spontaneous generation of electric polarization in an organic conductor α-$(ET)_2I_3$ [ET: bis(ethylenedithio)tetrathiafulvalene] by measuring optical second-harmonic generation (SHG), and discussed an electron-associated mechanism of the ferroelectric polarization based on the observation of ultrafast photo-modulation of the SHG.

This compound belongs to a series of radical-cationic complex with strongly correlated electrons. On account of D_2A chemical stoichiometry (D: donor, A: monovalent anion), donor molecules (ET) of the class of compounds receive one-half of positive charge from counterions ($2D + A \rightarrow 2D^{0.5+} + A^-$). It has been manifested however that some complexes including α-$(ET)_2I_3$ lost the mixed valency due to charge disproportionation ($2D^{0.5+} \rightarrow D^+ + D^0$) driven by repulsive Coulomb interactions between charges (Wigner crystallization).

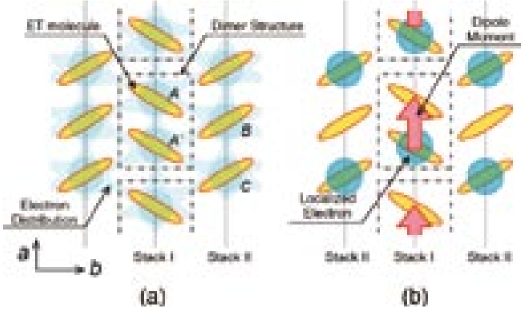

Figure 1. Schematic views of the arrangement of ETs and electrons. (a) In the metallic phase ($T > T_{CO}$), electrons are delocalized, and thus each ET has +0.5e. (b) In the charge ordered insulator phase ($T < T_{CO}$), charges are localized on some ETs. Because of finite alternation in Stack I, dipole moments between *A* and *A'* (solid arrows) survives in the unit cell.

The crystal of α-$(ET)_2I_3$ contains four ETs in the triclinic $P\bar{1}$ unit cell [Figure 1(a)]. There are two crystallographically independent stacks of ETs along the *a* axis; Stack I is a weakly dimerized chain composed of crystallographically equivalent ETs (labeled by *A* and *A'*), and Stack II is a uniform chain composed of *B* and *C*. According to an expected pattern of charge ordering, charges, which are delocalized in the metallic phase [Figure 1(a)], are localized to form such a pattern as illustrated in Figure 1(b) by the charge ordering. Since the equivalence between *A* and *A'* is broken in this pattern, the unit cell should possess a finite electrical dipole moment.

For most materials, electrical fields of those dipoles are cancelled out by the formation of an antiparallel dipole pair. However, we discovered that this complex exhibits SHG signal when it undergoes a metal-to-insulator transition due to charge ordering, manifesting that the transition is ferroelectric one, *i. e.*, local dipole moments are ordered in a polar arrangement to generate macroscopic polarization.

To examine the dynamic properties of the permanent polarization, we performed femtosecond pump-and-probe measurements of SHG; a crystal of the complex in ferroelectric state (T = 100 K) was stimulated by a pumping pulse, then induced variation of SHG was recorded with a probing pulse. Figure 2 shows the evolution of the photoinduced variation of SHG observed. The profile demonstrates the very fast photoresponse of the permanent polarization. The SHG signal instantly loses a large part of its intensity on pumping with the femtosecond pulse. Afterwards, it recovers to its original magnitude in the picosecond regime.

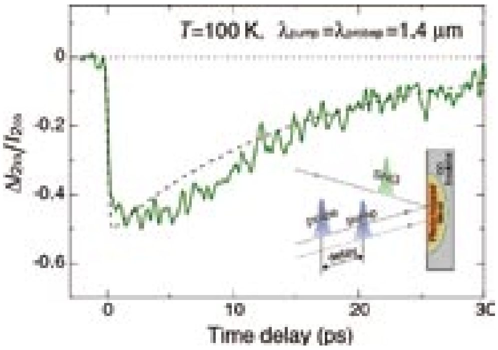

Figure 2. Photoinduced variation of SHG intensity as a function of the delay time between pump ($E||b$, 100 μJ/cm^2) and probe ($E||a$, 5 μJ/cm^2) pulses. The sample temperature was 100 K. The dashed line shows the fitted curve of single exponential decay (τ = 15 ps). The inset illustrates the pulse sequence of the time-resolved measurements.

Polarization in conventional ferroelectrics is attributed to a lattice modulation, such as polar displacement of ions, whereas one can hardly explain such fast photo-response of SHG with such a crystal lattice modulation. The substantially fast response illustrates that the ferroelectric polarization is modulated via a pure electronic process. It would be sure that the polarization is essentially attributed to the displacement of electrons due to the charge ordering.

Such electron-associated ferroelectrics are being recognized as a distinct class of the polar dielectrics. We believe that fast response of the polarization to external perturbations is one important characteristic of the new ferroelectrics, which may help to solve the problem in applying the controllable polarization to optoelectronic devices.

2. Inhomogeneous Site Charges at the Boundary between the Insulating, Superconducting, and Metallic Phases of β”-Type bis-ethylenedithio-tetrathiafulvalene Molecular Charge-Transfer Salts[2)]

β”-type ET salt involves rich superconducting compounds with the absence of strong dimerization. This family is possibly the good candidate for the charge-mediated superconducting transition, which is predicted by Merion and McKenzie. Some compounds in this family exhibits superconducting transition from an insulating ($d\rho/dT < 0$) state. We examined time-averaged charges on ET molecules around the phase boundary between the insulating, superconducting, and metal phases of β”-type ET salts with one hole per two molecules and two holes per three molecules by means of vibrational spectroscopy. We found that around the phase boundary, the site charges are neither those expected for a well-developed charge-ordered sate nor a uniform metallic state. The charge distribution is slightly inhomogeneous just above the insulator-superconductor phase transition temperature. We analyzed the distribution of the site charges from the viewpoint of the alternation of the strongest intersite Coulomb interaction along the stacking direction. The degenerate energy of several charge-ordered configuration generates a uniform state, the closeness in the energy of several charge-ordering configuration mostly contributes to the slight inhomogeneous distribution, and a large difference in their energy levels contributes to the charge ordered state. Our observation indicates that the instability due to the closeness in the energy of several configurations correlates with the insulator-superconductor transition in nondimerized or weakly dimerized molecular conductors.

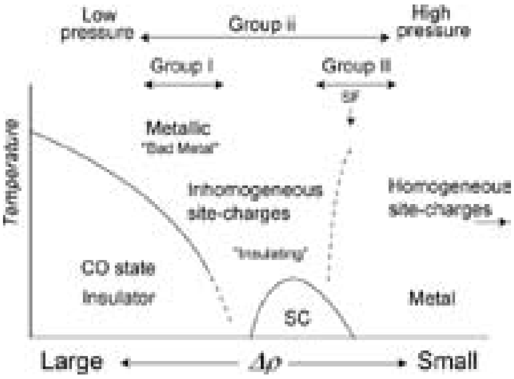

Figure 3. Schematic phase diagram of the β”-type ET salts plotted against the amplitude (Δρ) of charge density wave. “SF” denotes β”-$(ET)_2SF_5CH_2CF_2SO_3$. The superconducting phase appears when $\Delta\rho \neq 0$.

References

1) K. Yamamoto, *et al.*, *J. Phys. Soc. Jpn.* **77**, 074709 (2008).
2) T. Yamamoto, *et al.*, *Phys. Rev. B* **77**, 205120 (2008).

Award

YAMAMOTO, Kaoru; Outstanding Poster Preasentation Prize, 7th International Symposium on Crystalline Organic Metals, Superconductors and Ferromagnets (ISCOM2007).

Magnetic Resonance Studies for Molecular-Based Conductors

Department of Materials Molecular Science
Division of Electronic Properties

NAKAMURA, Toshikazu	Associate Professor
FURUKAWA, Ko	Assistant Professor
IWASE, Fumitatsu	IMS Fellow
SUGIURA, Koichi	Graduate Student
ABE, Hitomi	Secretary

Magnetic resonance measurements are advantageous for studying fundamental electronic properties and for understanding the detailed electronic structures of molecular based compounds. Developing an understanding of the electronic phases and functionality of these materials enables us to perform systematic investigations of low-dimensional, highly-correlated electron systems and functional materials. Competition between the electronic phases in molecular-based conductors has attracted much attention.1) The investigations of such electronic phases by magnetic resonance measurements are important to understanding unsolved fundamental problems in the field of solid state physics, and to explore novel functionalities in the field of material science.

In this study, we performed broad-line NMR and ESR measurements on molecular-based conductors to understand electron spin dynamics and functionality in low-temperature electronic phases.

1. Another Commensurate Antiferromagnetic State in $(\mathrm{TMTTF})_2X$: ^{13}C NMR Investigation of $(\mathrm{TMTTF})_2\mathrm{SbF}_6$

^{13}C nuclear magnetic resonance (NMR) investigations were performed on the one-dimensional organic conductor $(\mathrm{TMTTF})_2\mathrm{SbF}_6$ to clarify its electronic properties in the proximity of the ground states. An abrupt broadening of ^{13}C NMR absorption lines below 8 K (T_N = 8 K), confirmed a long-range antiferromagnetic phase transition. Below T_N, the absorption lines are composed of four distinct broad lines.

The ^{13}C NMR spin-lattice relaxation rates, ^{13}C T_1^{-1}, for the distinct lines show critical enhancement just above T_N, and rapid decease below T_N. These observations indicate that the ground state of $(\mathrm{TMTTF})_2\mathrm{SbF}_6$ is a commensurate antiferromagnetic phase. The amplitude of staggered magnetization, ρ, is comparable to $(\mathrm{TMTTF})_2\mathrm{Br}$, and on the order of 0.1 μ_B, according to the splitting of ^{13}C NMR lines at 3 K. However the angular dependence of the ^{13}C NMR shifts shows slight differences between $(\mathrm{TMTTF})_2\mathrm{SbF}_6$ and $(\mathrm{TMTTF})_2\mathrm{Br}$.

2. ^{13}C NMR Study of the Chemical Pressure Effect in $(\mathrm{TMTTF})_2[(\mathrm{AsF}_6)_x(\mathrm{SbF}_6)_{1-x}]$ (x ~ 0.5), and Physical Pressure Effect for $(\mathrm{TMTTF})_2\mathrm{SbF}_6$

Recently ISSP group discover superconductivity in $(\mathrm{TMTTF})_2\mathrm{SbF}_6$ and $(\mathrm{TMTTF})_2\mathrm{AsF}_6$ salts under ultra high pressures.2,3) If we remind the ground states of SbF_6 and AsF_6 are spin-Peierls (sP) and antiferromagnetic (AF), respectively, the so-called generalized phase diagram should be modified (AFI-sP-AFII). Curiously enough, the one-dimensional sP phase is sandwiched by two AF phases. And it is also an open question whether QCP is likely or unlikely. Hence, We performed ^{13}C NMR measurements for $(\mathrm{TMTTF})_2[(\mathrm{AsF}_6)_x(\mathrm{SbF}_6)_{1-x}]$ (x ~ 0.5) alloy, and $(\mathrm{TMTTF})_2\mathrm{SbF}_6$ under pressure in order to clarify following issues: 1) Does Quantum Critical phenomena exist between the sP and AF Phase boundary? 2) Is the sP phase actually sandwiched by two AF phase? 3) Are AF-I and AF-II of the same origin or not?

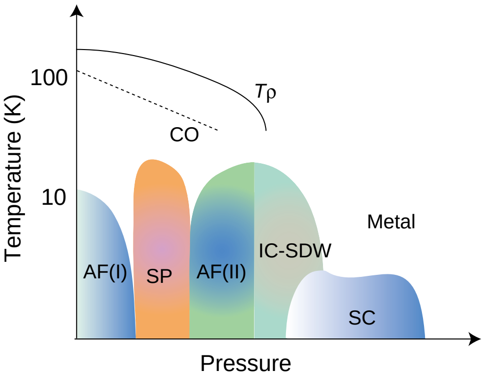

Figure 1. Modified generalized phase diagram for one-dimensional organic conductors, $(\mathrm{TMT}C\mathrm{F})_2X$.

As for $(\mathrm{TMTTF})_2[(\mathrm{AsF}_6)_x(\mathrm{SbF}_6)_{1-x}]$ (x ~ 0.5), the charge-order transition temperature is the intermediate value between the critical temperatures of SbF_6 and AsF_6. At low temperatures, we observed the characteristic behavior toward the spin-Peierls phase transition. However, the temperature dependence of the spin-lattice relaxation rate is weak suggesting that this salt is situated in the vicinity of the phase boundary between the spin-Peierls and antiferromagnetic phases.

In the case of $(TMTTF)_2SbF_6$, we observed clear phase change from AF to sP under 5 kbar. This observation supports the modified generalized phase diagram.

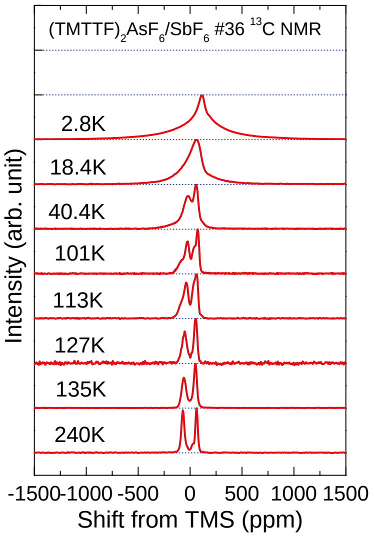

Figure 2. ^{13}C NMR spectra of $(TMTTF)_2[(AsF_6)_x(SbF_6)_{1-x}]$ ($x \sim 0.5$). The shift origin is TMS.

3. ESR Investigation of Novel Low-Dimensional Conductors, $(TMTTF)_2TaF_6$ and $(TMTTF)_3Ta_2F_{11}$

The electronic properties of one-dimensional organic conductor $(TMTTF)_2X$ were extremely investigated by a lot of researchers because of the variety of the electric properties. These electronic properties were drastically changed by external pressures or variety of counter anions (chemical pressure). In fact, the counter anion size is recognized as an important factor to emerge various type phases such as sP (spin-Peierls), SDW (spin density wave), CO (charge-order), AF (antiferromagnetic) and SC (superconductor).

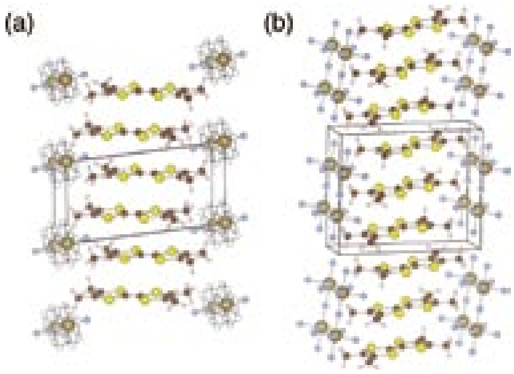

Figure 3. Crystal Structure of novel organic conductors, $(TMTTF)_2TaF_6$ and $(TMTTF)_3Ta_2F_{11}$.

Recently, we obtained novel organic conductors, $(TMTTF)_2TaF_6$ and $(TMTTF)_3Ta_2F_{11}$, by electrochemical oxidation. The lattice parameters of $(TMTTF)_2TaF_6$ are expected to be the largest among $(TMTTF)_2X$ family, and $(TMTTF)_2TaF_6$ is beyond the pristine Jérome phase diagram.1) Hence, the electronic properties of $(TMTTF)_2TaF_6$ are not clarified and attracted much attention. It should be noted that the bandstructure of $(TMTTF)_3Ta_2F_{11}$ is different from those of typical organic conductors, $(TMTTF)_2X$ salts, since $(TMTTF)_3Ta_2F_{11}$ is a 3:1 salt. In this study, we carried out ESR measurements, and discuss the electronic states from the temperature dependence of the spin susceptibility, linewidth and *g*-value.

4. ESR Study of Spin Dynamics for Dye-Sensitized Solar Cell

In dye-sensitized solar cells (DSSC),4) dye molecules are excited from the ground state S to the excited state S* by photo energy. The electron transfer from the excited dye molecules to the electrode plays an important role of the photoelectric transfer characteristic in DSSC. A various type of dye molecules were investigated. Time-resolved ESR measurements give us to detailed information of the photoelectric transfer characteristic. The aim of the present study is to reveal the relationship between the photoelectric transfer characteristic and the spin dynamics of electron in DSSC. The spin dynamics of the various organic dye molecules such as the eosin-Y was investigated by time-resolved ESR spectroscopy with laser photolysis (Nd:YAG 2nd harmonics, 532 nm). We discuss the spin dynamics of the various organic dye molecules with TiO_2.

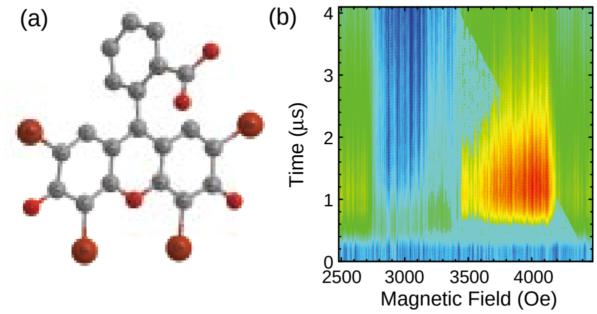

Figure 4. Molecular structure of eosin-Y, and time-resolved ESR spectroscopy of eosin-Y with laser photolysis.

References

1) for example: T. Ishiguro, K. Yamaji and G. Saito, *Organic Superconductors*, 2nd ed., Springer-Verlag; Berlin/Heidelberg (1998).
2) M. Itoi, M. Kano, N. Kurita, M. Hedo, Y. Uwatoko and T. Nakamura, *J. Phys. Soc. Jpn.* **76**, 053703 (5 pages) (2007).
3) M. Itoi, C. Araki, M. Hedo, Y. Uwatoko and T. Nakamura, *J. Phys. Soc. Jpn.* **77**, 023701 (4 pages) (2008).
4) B. O'regan and M. Gratzel, *Nature* **353**, 737 (1991).

Topological Design of Sheet-Shaped Macromolecules and Organic Frameworks

Department of Materials Molecular Science
Division of Molecular Functions

JIANG, Donglin	Associate Professor
ISHIZUKA, Tomoya	Assistant Professor
HE, Zheng	IMS Fellow
GUO, Jia	JSPS Post-Doctral Fellow
WAN, Shun	Graduate Student
CHEN, Long	Graduate Student
ODA, Masafumi	Graduate Student
YUSA, Masaaki	Graduate Student
ISONO, Yukiko	Technical Fellow
SUZUKI, Hiroko	Secretary

Covalent organic frameworks (COFs) are porous and crystalline macromolecules with a well-defined and predictable network of building blocks. Compared with inorganic porous materials, COFs are unique in that they are made from light elements, tunable in skeleton and robust against air and organic solvents. From synthetic point of view, COFs are attractive motifs since they allow, upon topological design, a total control over structure parameters including composition and porosity. Most studies up to date have focused on the development of synthetic methodologies with an aim to optimize pore size and surface area. By contrast, the functions of COFs except for gas storage have not yet been well explored. This motivated us to explore the possibility for constructing functional COFs with novel properties by utilizing highly ordered π-conjugation systems. We succeeded in the molecular design and synthesis of a series of novel COFs with unique semiconductive and photoconductive functionalities.

1. A Belt-Shaped, Blue Luminescent and Semiconductive Covalent Organic Framework

Herein, we report the first example of a luminescent and semiconductive COF, which adopts belt shape and consists of pyrene and triphenylene functionalities linked alternatively in a mesoporous hexagonal skeleton (Figure 1, TP-COF).

TP-COF was topologically designed by employing a D_{3h} symmetric monomer as corner and a D_{2h} symmetric monomer as edge for pore hexagons and synthesized by a condensation reaction of 2,3,6,7,10,11-hexahydroxytriphenylene (HHTP) and pyrene-2,7-diboronic acid (PDBA). FE SEM images of TP-COF reveal that the condensation polymerization of PDBA and HHTP afford belts with length extended to micrometers and width of about 300 nm and thickness of 100 nm. The belt morphology is quite uniform with a similar width and thickness to one another, and no other morphologies are observable. In high resolution TEM, clear aligned patterns were observed along the (110) facet. From the aligned layer structure, the distance between sheets is estimated to be 3.40 Å, which is reasonable for π-π stacking. Such a belt texture with a uniform morphology and the direct visualization of a stacked sheet structure are unprecedented for COFs. To our surprise, along the (001) facet, hexagonal mesostructure can be observed and enables the estimation of center-to-center distance between the neighboring pores to be about 3.3 nm. Powder x-ray diffraction (PXRD) exhibits a main diffraction peak due to 100 at 2.70°, along with diffractions owing to 110, 200, 210, 300, 310, and

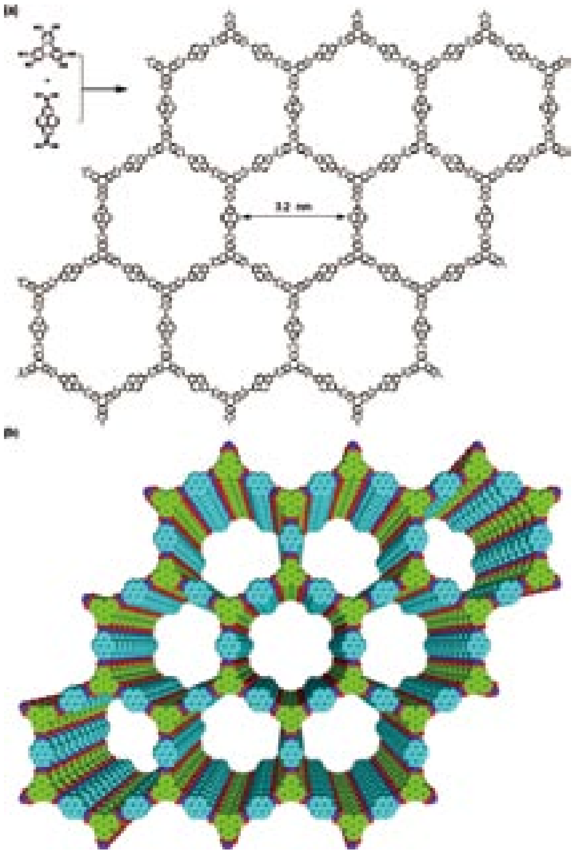

Figure 1. (a) Synthesis of TP-COF. (b) Schematic representation of TP-COF (Structure is based on quantum calculation and crystal lattice parameters; Purple: B, Red: O, Green: Triphenylene, Blue: Pyrene; H atoms are omitted for clarity).

001 at 4.74°, 5.46°, 7.26°, 8.24°, 9.54° and 26.32°, respectively. Simulation using the space group of *P*6/mmm (No. 191) with $a = b = 37.5412$ Å and $c = 3.3784$ Å gives a PXRD pattern in good agreement with the experimentally observed one. All the diffraction peaks can be reasonably assigned. Therefore, the 2-D sheets crystallize in an eclipsed fashion to give a perfect superimposition of the triphenylene and pyrene units on themselves. Such a crystalline structure would provide open and aligned mesopores of 3.26 nm in diameter. In fact, TP-COF exhibits a typical type IV nitrogen sorption curve, indicative of a mesoporous character (Figure 2). BET calculation gives specific surface area and pore volume of 868 m^2 g^{-1} and 0.7907 cm^3 g^{-1}, respectively. Estimation of pore size with the DFT model shows a diameter of 3.14 nm, which is close to the theoretical one. Pore distribution profile shows that the specific surface area in TP-COF originates predominately from the persistent mesopores, whereas contributions of other pores formed between belts or from defects are small. All the above results indicate that TP-COF is a crystalline material with a uniformly sized mesopore formed via the eclipsed packing of the polymeric sheets.

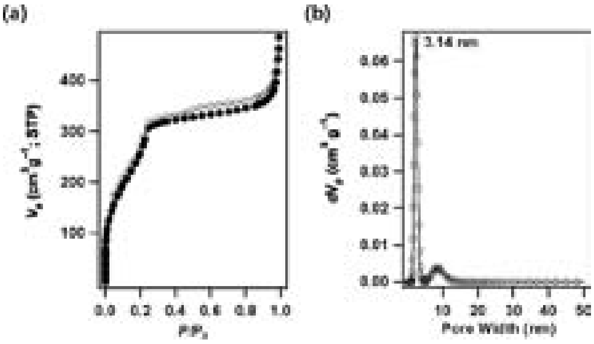

Figure 2. (a) Nitrogen adsorption (●) and desorption (○) isotherm profiles of TP-COF at 77 K. (b) Pore size distribution of TP-COF by DFT modeling on the N_2 adsorption isotherms.

Fluorescence microscopy exhibits that the belts of TP-COF are highly blue luminescent. Fluorescence spectroscopy shows that TP-COF emitted a luminescence at 474 nm, upon excitation of the pyrene units at 376 or 417 nm. Excitation of the triphenylene units in TP-COF at 340 nm resulted in negligibly weak emission at 402 nm from the triphenylene units but a strong emission from the pyrene moieties at 474 nm, where the fluorescence intensity ratio $I_{474\ \mathrm{nm}}/I_{402\ \mathrm{nm}}$ was as high as 16. In sharp contrast, when a 2:3 mixture of HHTP and PDBA was excited at 340 nm, it emitted predominately at 402 nm to furnish a low $I_{474\ \mathrm{nm}}/I_{402\ \mathrm{nm}}$ ratio (0.6). Therefore, the strong pyrene fluorescence, observed for TP-COF upon 340 nm excitation, is obviously due to an intramolecular singlet energy from the triphenylene units to pyrene units. Comparison of the excitation spectrum with diffuse reflectance UV-Vis spectrum, the quantum yield of energy transfer was estimated to be 60%. Therefore, by virtue of the triphenylene units, TP-COF can harvest photons of a wide wavelength range covering from ultraviolet to visible regions and converts them to blue emission. We further investigated the fluorescence anisotropy of TP-COF upon excitation with a polarized light. The 2:3 mixture of HHTP and PDBA shows a p value of 0.058. In sharp contrast, TP-COF under identical conditions exhibited a significantly depolarized fluorescence with an extremely low p value of 0.017. This observation reveals that TP-COF not only mediates energy transfer between components but facilitates energy migration over the crystalline belt as well.

Single crystals of pyrene and triphenylene have been reported to function as semiconductors. Due to the ultimate π-stacking of these large π-conjugated components, TP-COF may have a high probability of becoming electrically semiconductive. We investigated this possibility by measuring the electric conductivity with a 10-μm width Pt gap using a two-probe method. TP-COF in air at 25 °C shows an almost linear I-V profile, while the gap itself is silent irrespective of voltage bias. For example, at 2-V bais voltage, the electric current is 4.3 nA. In contrast, a 2:3 mixture of HHTP and PDBA shows a low current (79 pA) under otherwise identical conditions. Moreover, the electric current can be on/off switched repeatedly for many times without significant deterioration. The relatively high electric current observed for TP-COF is likely related to the highly order structure that enables the formation of a conductive path. Upon doping with iodine, the electric current was increased, suggesting a *p*-type semiconductor character of TP-COF.

Exploration of functional COFs is a subject with a high probability to the development of new materials. We have succeeded in the synthesis of a new COF based on the condensation reaction of triphenylene and pyrene monomers. TP-COF is highly luminescent, harvests a wide wavelength range of photons and allows energy transfer and migration. Furthermore, TP-COF is electrically conductive and capable of repetitive on-off current switching at room temperature. These characters are unique and clearly originate from the highly ordered structure of TP-COF. By filling the mesopores with photoactive molecules such as electron acceptor, we expect the fabrication of COF-based optoelectronic device, which is one of the targets under investigation.

Reference

1) S. Wan, J. Guo, J. Kim, H. Ihee and D. Jiang, *Angew. Chem., Int. Ed.* **47**, 8826–8830 (2008) (VIP, Selected as a frontispiece of ACIE).
2) Jyllian N. Kemsley, *C&EN* **86**, 29 (2008) (Highlight).

Award

CHEN, Long; Student Lecture Award of Chemical Society of Japan (2008).

Methodology Developments of Solid State NMR Spectroscopy for Structural Biology and Material Science

Department of Materials Molecular Science
Division of Molecular Functions

NISHIMURA, Katsuyuki — Associate Professor
IIJIMA, Takahiro — Assistant Professor
UEKAMA, Naoko — IMS Fellow

Solid state NMR is one of the useful tools to characterize dynamics and structures of molecules on amorphous condition without specific limitations. We are focusing on methodology developments of solid state NMR especially for structural biology and material science. We are also attempting to elucidate functions and dynamic structure of peripheral membrane protein bound to lipid bilayer surface based on solid state NMR. In the following, we show the newly developed techniques to enhance spectral resolution and sensitivity in solid state NMR spectroscopy, and a study of structural change depending on weak interaction between peripheral membrane protein and lipid bilayer surface.

1. Spectral Resolution Enhancements Based on Doubly Magnified Evolution of Internal Interaction in Solid State NMR[1)]

In order to enhance the spectral resolution of 2D correlation experiments in solid state NMR spectroscopy, general scheme enabling doubly magnified evolution of specific internal interaction was developed. The efficacy of this approach was verified by applying it to several conventional techniques. As first example, doubly magnified heteronuclear 2D J-spectroscopy under magic angle spinning (MAS) in solid was developed to enhance separation of multiplet signals due to heteronuclear J-coupling. J-couplings are very useful parameters in solution NMR for assignments of peaks and establishment of through bond connectivities. In solid-state NMR, however, J-couplings are less frequently observed because of their small amplitudes respect to the other interactions.

In conventional constant evolution time heteronuclear J-spectroscopy, heteronuclear J-coupling evolution takes place by replacement of heteronuclear decoupling sequence with multiple-pulse (MP) sequence removing ^{1}H homonuclear dipolar interaction under MAS. In contrast to the conventional technique, MP is applied to whole constant evolution time in newly developed one. Then, MPs are replaced by the ones exhibiting the same form of average Hamiltonian (AH) for heteronuclear J-coupling with opposite sign. As a result, the effective evolution becomes double and it gives doubled multiplets due to J-couplings in Hz unit without change of line width. Thus the spectral resolution can be improved by twice. Figure 1 (b) and (c) show the J-resolved spectra obtained from

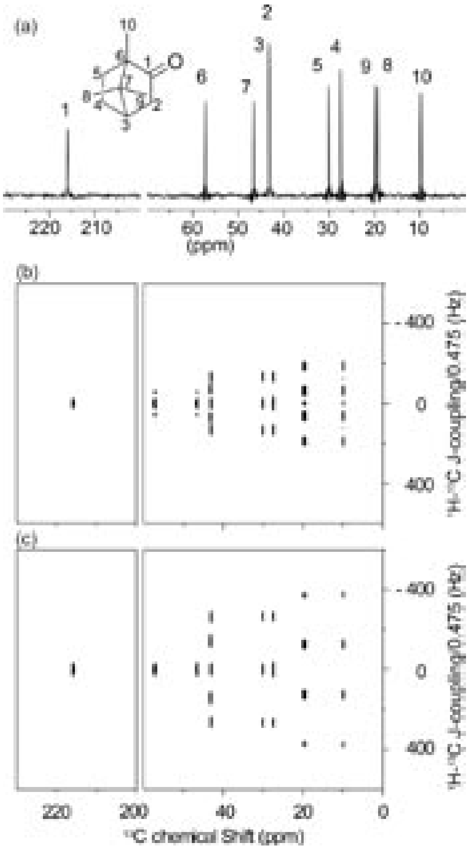

Figure 1. (a) 1D-CPMAS spectrum of Camphor. 2D J-resolved spectra of solid Camphor obtained from (b) conventional and (c) doubly magnified techniques under MAS, respectively. J-coupling axes are corrected by scaling factor of MP.

conventional and newly developed ones, respectively. It is important to note that no specific limitation over conventional technique exists to perform new experiment.

Similar idea can be applied for the measurements of heteronuclear dipolar interaction. That technique is effective especially to observe motionally averaged dipolar interaction in oriented sample.[2)]

2. QCPMG NMR of Spin-1 Nuclei in the Presence of Shift Interaction[3)]

Quadrupole Curr-Purcell-Meiboom-Gill (QCPMG) sequence is an efficient method to enhance NMR signals of quadrupole nuclei with acquisition of successive echo signals generated by refocusing pulses. QCPMG sequence that can be combined with other solid-state NMR techniques such as magic angle spinning, multiple quantum/magic angle spinning and double frequency sweep has been widely utilized for structural investigation of materials possessing quadrupole nuclei. However, it has been recently reported that QCPMG is inefficient in the presence of a shift interaction for spin-1 nuclei including ^{2}H and ^{14}N, and application of QCPMG of such nuclei for structural study has been limited.

In this work, we developed improved QCPMG technique for spin-1 nuclei that can obtain an in-phase spectrum under the influence both of the quadrupole and shift interactions. Essences of the present method are (i) addition of radio-frequency (RF) pulses that only affect the refocusing of the shift interaction and (ii) an irradiation of a strong RF field to prevent a signal arising from unwanted coherence pathways.

Figure 2 shows comparison of ^{2}H NMR spectra for a model compound of $CoSiF_6{\cdot}6H_2O$ obtained from conventional and improved QCPMG methods. It is known that a paramagnetic shift interaction between ^{2}H nuclei and electron spins in Co^{2+} ion in addition to the quadrupole interaction contributes to the ^{2}H NMR spectrum of this sample. Since the former interaction is considerably large (> 30 kHz), application of conventional QCPMG pulse sequence results in a phase distorted spectrum as shown in Figure 2 (a). Figure 2 (b) is the QCPMG spectrum obtained from improved QCPMG pulse sequence with the RF field of 210 kHz. As expected, the spectrum is free from distortion. Thus, NMR parameters can be obtained by comparison with simulated one as shown in Figure 2 (c).

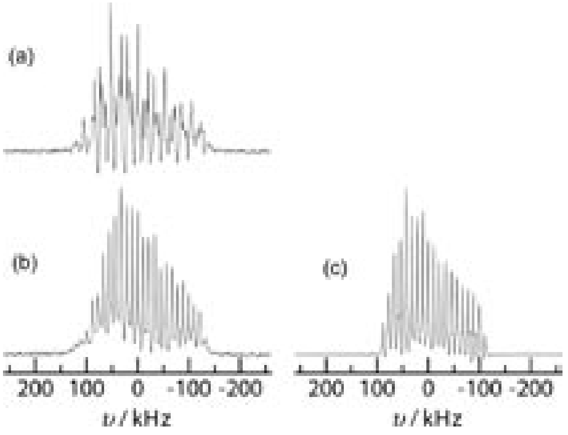

Figure 2. ^{2}H (I = 1) QCPMG NMR spectrum of $CoSiF_6{\cdot}6H_2O$ at 61.385 MHz. (a) and (b) show the spectra obtained by the conventional and improved QCPMG methods, respectively. (c) The simulated spectrum for improved QCPMG.

3. Influence of Membrane Curvature on the Structure of the Membrane-Associated Pleckstrin Homology Domain of Phospholipase C-δ1[4)]

Phospholipase C-δ1 (PLC-δ1) hydrolyzes phosphatidylinositol 4, 5-bisphosphate (PIP_2) in the plasma membrane to produce the second messengers on the membrane surface. The PH domain in the N-terminus of PLC-δ1 selectively forms high affinity complex with PIP_2 in the plasma membrane and IP_3 in the cytoplasm. Consequently those complex formations regulate membrane localization of PLC-δ1. From the previous studies, it is known that α2-helix is responsible for auxiliary membrane binding site in addition to the PIP_2 specific membrane binding site and the terminous of β5/β6 loop plays a role of hinge connecting the β-sandwich core of the PH domain.

In this study, conformational changes of the PLC-δ1 PH domain bound to the surfaces of multilamellar vesicles (MLVs), small unilamellar vesicles (SUVs), and micelles were investigated to evaluate the effects of membrane curvatures on the membrane-associated protein based on solid-state NMR spectroscopy. The conformational changes of PLC-δ1 PH domain bound to those surfaces were evaluated from the analyses of conformational dependent ^{13}C isotropic chemical shifts of isotope enriched [3-^{13}C] Ala sites in PH domain. As results, ^{13}C NMR signals of Ala88 in the α2-helix and Ala112 spatially close to the terminus of the β5/β6 loop containing the α2-helix exhibited conformational changes due to the reorientation of the α2-helix on the surface of MLV and SUV membrane. In contrast, no conformational change of those regions was observed on the surfaces of the DPC and DM micelles with diameter of 33–40 Å. According to those results, we found out that the terminus of β5/β6 loop is susceptible to the alteration of the curvature of lipid bilayer surface, and the mutual orientation of two membrane binding sites of the PH domain on the curved membrane.

It is known that the membranes in the cell undergo dynamic alterations of their structures and their chemical composition during the physiological processes. Those induce time dependence of local curvature of membrane. Thus the conformational changes of the membrane binding domain such as found in this study for the PLC-δ1 PH domain may affect the membrane binding mechanism of peripheral membrane proteins.

References

1) K. Nishimura, submitted.
2) K. Nishimura, to be submitted.
3) T. Iijima and K. Nishimura, to be submitted.
4) N. Uekama, T. Aoki, T. Maruoka, S. Kurisu, A. Hatakeyama, M. Okada, H. Yagisawa, K. Nishimura and S. Tuzi, submitted.

Organic Solar Cells

Research Center for Molecular Scale Nanoscience
Division of Molecular Nanoscience

HIRAMOTO, Masahiro	Professor
IKETAKI, Kai	IMS Fellow
NAKAO, Satoru	Post-Doctoral Fellow
KITADA, Keitaro	Graduate Student*
PFÜTZNER, Steffen	Graduate Student†
SUZUKI, Hiroko	Secretary

Organic EL television was commercialized last year. Next target of organic electronics is organic solar cell. Our group accomplished the world record conversion efficiency of 5.3% based on the fundamental research on the organic semiconductors such as ultra-high purification, nanostructure design. Moreover, 1000 h (42 days) operation of organic solar cell without degradation was accomplished.

1. Efficient Organic *p-i-n* Solar Cells Having 1 µm-Thick Codeposited *i*-Layer Incorporating Seven-Nine (7N) Purified Fullerene[1)]

In 1991, we proposed *p-i-n* organic solar cells in which the *i*-interlayer is a codeposited film composed of *p*- and *n*-type organic semiconductors.[2,3)] Since *i*-interlayer acts as an efficient photocarrier generation layer, if this codeposited *i*-interlayer could be thick enough to be able to absorb entire irradiated solar light, organic *p-i-n* cells would show the magnitude of photocurrent density comparable to inorganic solar cells.

Unfortunately, *i*-interlayer has been inevitably very thin. For example, we have reported *p-i-n* organic solar cells in which the *i*-interlayer is nanostructure-optimized codepostied film composed of fullerene and metal-free phthalocyanine (C_{60}:H_2Pc).[4)] At that time, thickness of C_{60}:H_2Pc *i*-interlayer was limited below 180 nm since the fill factor (FF) was seriously decreased for thicker *i*-interlayer due to the increase of internal resistance of *i*-layer.

On the analogy of the case of Si which is usually purified to eleven-nine (11N), we convinced that the purity of organic semiconductors should be reached to ppm level at least in order to draw out their essential nature.

In this study, we performed the single-crystal formed sublimation under N_2 gas of 1 atm (Figure 1). Due to the gas convection, in the case of C_{60}, single crystals of the maximum size of 2 mm × 2 mm were obtained (Figure 2). C_{60} purity was determined by the secondary ion mass spectroscopy (SIMS), which has been used for the analysis of dopants in Si wafer. Purity of C_{60} crystals purified three times was more than 0.1 ppm, *i.e.*, seven-nine (7N). On the other hand, purity of H_2Pc sample purified four times was five-nine (5N).

Figure 1. Photograph of single-crystal formed sublimation apparatus.

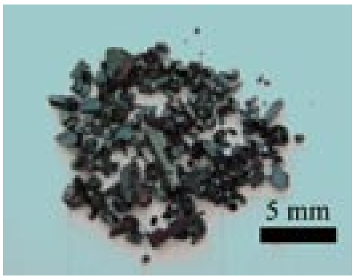

Figure 2. Photograph of C_{60} single crystals. Crystal size reached 2 mm × 2 mm.

p-i-n cell structure is shown in Figure 4. *p*-type layer of H_2Pc, codeposited *i*-interlayer composed of C_{60} and H_2Pc, and *n*-type layer of NTCDA, which also acts as a transparent protection layer, were successively deposited by vacuum evaporation on ITO glass substrate. Codeposited films were fabricated by the coevaporation from two separately controlled sources on the substrate heated at +80 °C.

Figure 3(a) shows the dependence of fill factor (FF) on *i*-interlayer thicknesses (*X*). Surprisingly, FF hardly decreased

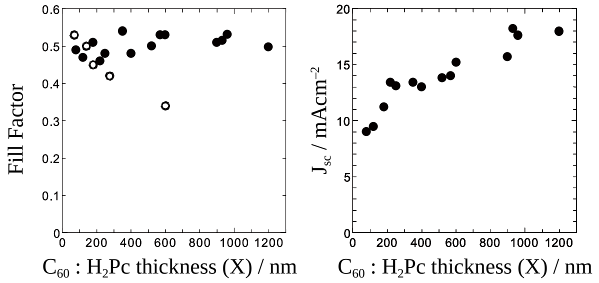

Figure 3. Dependence of fill factor (FF) and short-circuit photocurrent (J_{sc}) on *i*-interlayer thickness (*X*) for organic *p*-*i*-*n* cells.

even for very thick *i*-layer reaching 1.2 µm (closed dots). Accordingly, short-circuit photocurrent density (J_{sc}) increased with *X* and reached maximum value of 19.1 mAcm^{-2} at *X* = 1 µm (Figure 3(b)). When we used C_{60} of low-purity by the conventional sublimation under vacuum, FF monotonically decreased with *X* and, as a result, thick *i*-layer could not be fabricated (Figure 3(a), open dots).

Figure 4 shows the current-voltage (J-V) characteristics for *p*-*i*-*n* cell having 1 µm-thick *i*-interlayer. J_{sc} of 18.3 mAcm^{-2}, open-circuit photovoltage (V_{oc}) of 0.402 V, FF of 0.532, and conversion efficiency 5.3% were observed.

Since the present cell (*X* = 1 µm) absorbs whole visible light, cell color is black (Figure 5(a)). On the contrary, cell having thin *i*-layer (*X* = 180 nm), cell color is transparent green (Figure 5(b)), namely, large portion of irradiated light can not be utilized. Utilization of entire visible light of solar spectrum without decreasing FF by incorporating very thick C_{60}:H_2Pc *i*-interlayer is essential to obtain large J_{sc} value close to 20 mAcm^{-2} and efficiency of 5.3%.

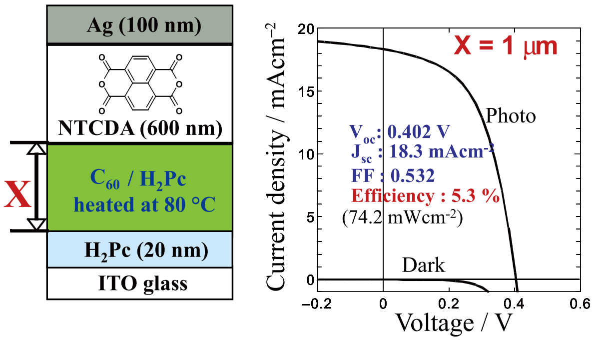

Figure 4. Cell structure and current-voltage (J-V) characteristics for *p*-*i*-*n* cell having 1 µm-thick *i*-layer.

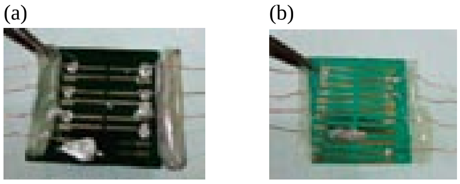
(a) (b)

Figure 5. Photographs of cells. (a) *X* = 1 µm. (b) *X* = 180 nm.

2. Long-Term Operation for 42 Days

The conversion efficiency of organic solar cells is expected to exceed the practical level (10%) within few years. However, few studies have been made on their durability.$^{5)}$

In this study, we performed the long-term operation tests reaching 1000 h in high vacuum (10^{-7} Torr). White light (100 mWcm^{-2}) was continuously irradiated under the short-circuit condition. Gradual degradation within 100 h was observed for *p*-*i*-*n* cells having the structure of Figure 4. Detailed investigation revealed that the photodegradation of NTCDA, which acts as the transparent *n*-type layer, occurred.

Therefore, we replaced NTCDA with Al-doped ZnO (AZO) fabricated by electron beam evaporation on organic film (Figure 6). Fabricated AZO was transparent and showed the conductivity of 10^3 Scm^{-1}, which is comparable to ITO. Little decrease of J_{sc} and efficiency after 1000 h operation was confirmed (Figure 6). This is good news for the practical application of organic solar cells.

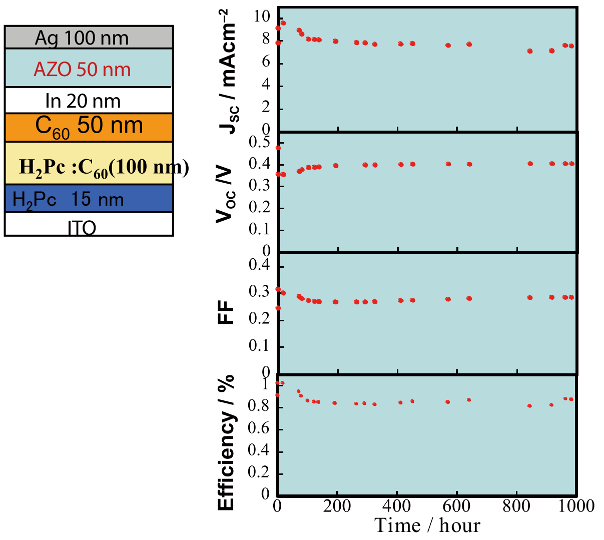

Figure 6. Cell parameters *vs.* operating time for a cell incorporating transparent AZO layer.

References

1) M. Hiramoto, *Proc. SPIE Vol. 7052, Organic photovoltaics IX* pp. 70520H-1–6, San Diego, CA, 12-14 Aug. (2008).

2) M. Hiramoto, H. Fujiwara and M. Yokoyama, *J. Appl. Phys.* **72**, 3781 (1992).

3) M. Hiramoto, H. Fujiwara and M. Yokoyama, *Appl. Phys. Lett.* **58**, 1062 (1991).

4) K. Suemori, T. Miyata, M. Yokoyama and M. Hiramoto, *Appl. Phys. Lett.* **86**, 063509 (2005).

5) H. Shiokawa, M. Yokoyama and M. Hiramoto, *Surf. Rev. Lett.* **14**, 539–542 (2007).

---

* carrying out graduate research on Cooperative Education Program of IMS with Osaka University

† from Technische Universität Dresden

Development of Organic Semiconductors for Molecular Thin-Film Devices

Research Center for Molecular Scale Nanoscience
Division of Molecular Nanoscience

SUZUKI, Toshiyasu	Associate Professor
SAKAMOTO, Youichi	Assistant Professor
OKUBO, Kimitaka	Graduate Student
WATANABE, Yoko	Secretary

Organic light-emitting diodes (OLEDs) and organic field-effect transistors (OFETs) based on π-conjugated oligomers have been extensively studied as molecular thin-film devices. Organic semiconductors with low injection barriers and high mobilities are required for highly efficient OLEDs and OFETs. Radical cations or anions of an organic semiconductor have to be generated easily at the interface with an electrode (or a dielectric), and holes or electrons must move fast in the semiconducting layer. Compared with organic p-type semiconductors, organic n-type semiconductors for practical use are few and rather difficult to develop. Recently, we found that perfluorinated aromatic compounds are efficient n-type semiconductors for OLEDs and OFETs.

1. Synthesis, Structure, and Transport Property of Perfluorinated Oligofluorenes[1)]

We report the synthesis, structure, and properties of perfluorinated oligo(9,9-dimethylfluorene)s (**PF-*n*F**s). The cyclic voltammetry of **PF-3F** and **PF-4F** showed two reversible couples in THF. The reduction potentials are much more positive than those of conventional electron transport materials. **PF-3F** and **PF-4F** exhibited high glass transition temperatures (T_g = 133 and 163 °C, respectively), indicating that they are highly stable amorphous solids. The X-ray crystallography of **PF-2F** showed that a single crystal contained a 1:1 mixture of *cis* and *trans* conformers. The electron mobilities were measured by the time-of-flight technique. **PF-3F** and **PF-4F** displayed weak field dependence and high electron mobilities as amorphous n-type semiconductors (2.1×10^{-4} and 2.0×10^{-4} cm^2 V^{-1} s^{-1} at 6×10^5 V cm^{-1}, respectively).

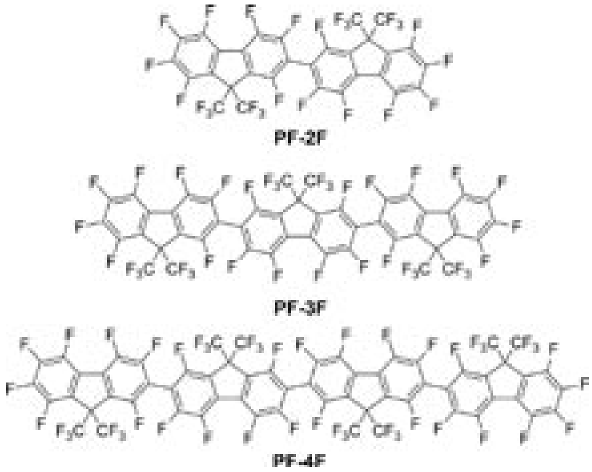

Figure 1. Structures of perfluorinated oligo(9,9-dimethylfluorene)s.

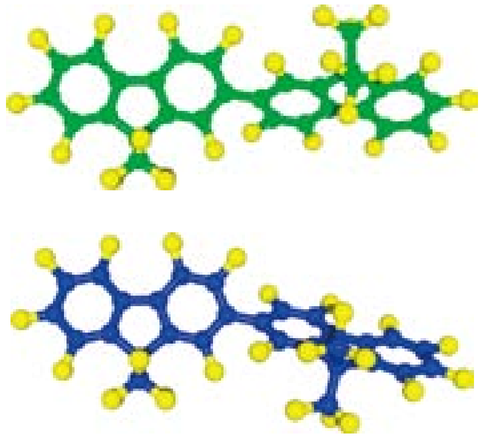

Figure 2. X-ray structures of *trans*-**PF-2F** (top) and *cis*-**PF-2F** (bottom).

2. Optical Properties of Pentacene and Perfluoropentacene Thin Films[2]

The optical properties of pentacene (PEN) and perfluoropentacene (PFP) thin films on various SiO_2 substrates were studied using variable angle spectroscopic ellipsometry. Structural characterization was performed using x-ray reflectivity and atomic force microscopy. A uniaxial model with the optic axis normal to the sample surface was used to analyze the ellipsometry data. A strong optical anisotropy was observed, and enabled the direction of the transition dipole of the absorption bands to be determined. Furthermore, comparison of the optical constants of PEN and PFP thin films with the absorption spectra of the monomers in solution shows significant changes due to the crystalline environment. Relative to the monomer spectrum, the highest occupied molecular orbital to lowest unoccupied molecular orbital transition observed in PEN (PFP) thin film is reduced by 210 meV (280 meV). A second absorption band in the PFP thin film shows a slight blueshift (40 meV) compared to the spectrum of the monomer with its transition dipole perpendicular to that of the first absorption band.

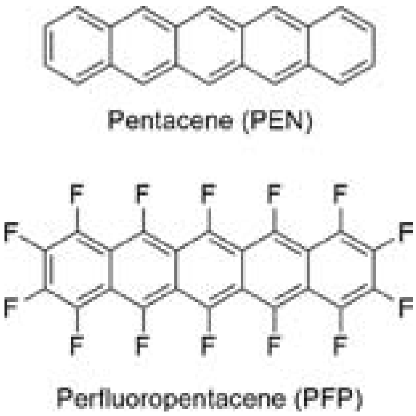

Figure 3. Structures of pentacene (PEN) and perfluoropentacene (PFP).

3. Adsorption-Induced Intramolecular Dipole: Correlating Molecular Conformation and Interface Electronic Structure[3]

The interfaces formed between pentacene (PEN) and perfluoropentacene (PFP) molecules and Cu(111) were studied using photoelectron spectroscopy, X-ray standing wave (XSW), and scanning tunneling microscopy measurements, in conjunction with theoretical modeling. The average carbon bonding distances for PEN and PFP differ strongly, that is, 2.34 Å for PEN versus 2.98 Å for PFP. An adsorption-induced nonplanar conformation of PFP is suggested by XSW (F atoms 0.1 Å above the carbon plane), which causes an intramolecular dipole of ~0.5 D. These observations explain why the hole injection barriers at both molecule/metal interfaces are comparable (1.10 eV for PEN and 1.35 eV for PFP) whereas the molecular ionization energies differ significantly (5.00 eV for PEN and 5.85 eV for PFP). Our results show that the hypothesis of charge injection barrier tuning at organic/metal interfaces by adjusting the ionization energy of molecules is not always readily applicable.

4. TStructural Order in Perfluoropentacene Thin Films and Heterostructures with Pentacene[4]

Synchrotron X-ray diffraction reciprocal space mapping was performed on perfluoropentacene (PFP) thin films on SiO_2 in order to determine the crystal structure of a novel, substrate-induced thin film phase to be monoclinic with unit cell parameters of $a = 15.76 \pm 0.02$ Å, $b = 4.51 \pm 0.02$ Å, $c = 11.48 \pm 0.02$ Å, and $\beta = 90.4 \pm 0.1°$. Moreover, layered and co-deposited heterostructures of PFP and pentacene (PEN) were investigated by specular and grazing-incidence X-ray diffraction, atomic force microscopy, and Fourier-transform infrared spectroscopy. For a ca. three-monolayers-thick PFP film grown on a PEN underlayer, slightly increased lattice spacing was found. In contrast, co-deposited PEN/PFP films form a new mixed-crystal structure with no detectable degree of phase separation. These results highlight the structural complexity of these technically relevant molecular heterojunctions for use in organic electronics.

References

1) K. Ohkubo, Y. Sakamoto, T. Suzuki, T. Tsuzuki, D. Kumaki and S. Tokito, *Chem. Eur. J.* **14**, 4472–4474 (2008).

2) A. Hinderhofer, U. Heinemeyer, A. Gerlach, S. Kowarik, R. M. J. Jacobs, Y. Sakamoto, T. Suzuki and F. Schreiber, *J. Chem. Phys.* **127**, 194705 (6 pages) (2007).

3) N. Koch, A. Gerlach, S. Duhm, H. Glowatzki, G. Heimel, A. Vollmer, Y. Sakamoto, T. Suzuki, J. Zegenhagen, J. P. Rabe and F. Schreiber, *J. Am. Chem. Soc.* **130**, 7300–7304 (2008).

4) I. Salzmann, S. Duhm, G. Heimel, J. P. Rabe, N. Koch, M. Oehzelt, Y. Sakamoto and T. Suzuki, *Langmuir* **24**, 7294–7298 (2008).

Building Photosynthesis by Artificial Molecules

Research Center for Molecular Scale Nanoscience
Division of Molecular Nanoscience

NAGATA, Toshi	Associate Professor
NAGASAWA, Takayuki	Assistant Professor*
KON, Hiroki	IMS Fellow
ALLAKHVERDIEV, Suleyman I.	Visiting Scientist; JSPS Invited Fellow†
KAWAO, Masahiro	JSPS Post-Doctoral Fellow
TANEMURA, Hiroyo	Technical Fellow
WANATABE, Yoko	Secretary

The purpose of this project is to build nanomolecular machinery for photosynthesis by use of artificial molecules. The world's most successful molecular machinery for photosynthesis is that of green plants—the two photosystems and related protein complexes. These are composed almost exclusively from organic molecules, plus a small amount of metal elements playing important roles. Inspired by these natural systems, we are trying to build up multimolecular systems that are capable of light-to-chemical energy conversion. At present, our interest is mainly focused on constructing necessary molecular parts.

1. Synthesis of Porphyrin-Cyclopentadienylcobalt(III) Linked Molecules

The light reactions of oxygenic photosynthesis produce dioxygen and NADPH by the aid of photon energy. Although the actual mechanism is very complicated, the net reaction can be conceptually outlined into three unit reactions; the initial photoinduced electron transfer, and the oxidizing and reducing reactions at the both ends of the charge separated state. In this context, the combination of photoinduced electron transfer and a redox reaction mediated by metal complexes is an interesting subject. One interesting target is the redox chemistry of cyclopentadienylcobalt(III) (CpCo) complexes,1) which are known to catalyze various redox reactions, including production of hydrogen. However, photoinduced electron transfer from organic pigments like porphyrins to CpCo complexes is not so easy to achieve.

In this work, we report the synthesis of new dyad molecules, **1** and **2**, which contain porphyrin and cyclopentadienyl cobalt(III) (CpCo) moieties within one molecule. The fluorescence emission spectra showed that the singlet excited state of the porphyrin was quenched via intramolecular electron transfer to the CpCo moiety.

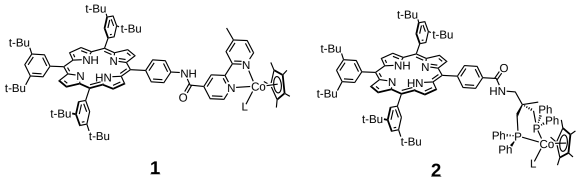

Figure 1. The porphyrin-CpCo linked compounds.

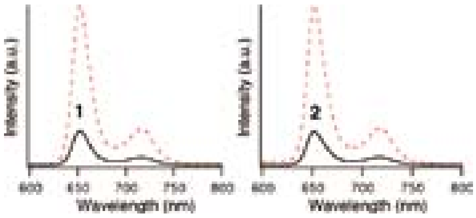

Figure 2. The steady-state emission spectra of compounds **1** and **2** in CH_2Cl_2. The red dotted lines indicate the emission spectra of the reference compound without the CpCo moiety.

2. An Approach towards Artificial Quinone Pools: Alcohols as the Terminal Reductant2)

Quinones are one of the most important cofactors in biological photosynthesis. In the "Type-II" photosynthetic reaction centers, quinones are the terminal electron acceptors, which receive electrons from the photoexcited chlorophylls and are converted into quinols. The quinols are released from the reaction center into the quinone pool, and are eventually reoxidized with concurrent translocation of protons through the membrane. Such a characteristic of natural quinone pools is worth mimicking in artificial systems, because it will provide a key to realize the "Z-scheme" in artificial photosynthesis.

The ultimate goal in mimicking the quinone pools is to convert quinones to quinols with concurrent oxidation of water. However, this is a difficult objective, so we are looking for other oxidation reactions that can be easily realized and can be combined with conversion of quinones to quinols.

In this work, we study the combination of a photoinduced electron tranfer from the porphyrin to the quinone and a TEMPO-catalyzed oxidation of alcohols triggered by one electron oxidation (eq. 1). The dependence of initial rates on the oxidation potentials of the porphyrin showed a characteristic bell shape, which is caused by two competitive factors, the efficiency of photoinduced electron transfer and the equilibrium of electron exchange between the porphyrin cation radical and TEMPO.

$$RCH_2OH + Q \xrightarrow[\text{[porphyrin]}]{h\nu} RCHO + QH_2 \qquad (1)$$

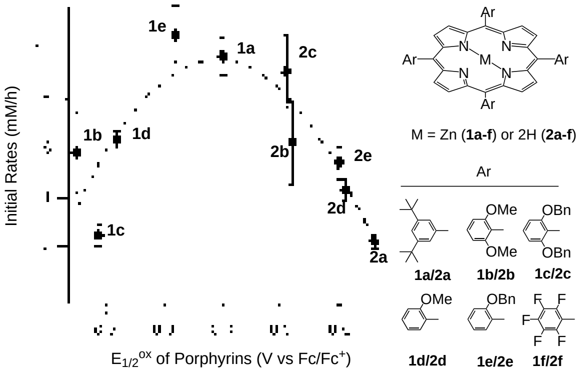

Figure 3. The initial rates of formation of PhCHO plotted versus the oxidation potentials of the porphyrins.

3. Reconstitution of the Water-Oxidizing Complex in Photosystem II Using Synthetic Mn Complexes: A Fluorine-19 NMR Study³⁾

Oxygen evolution is one of the most important processes in plant photosynthesis. The function is performed at the oxygen-evolving complex (OEC), which resides at the oxidizing terminal of Photosystem II (PS2) and contains manganese ions as essential cofactors. One interesting approach research on photosynthetic oxygen evolution is the reconstitution of the Mn-depleted PS2 with synthetic Mn complexes. In some cases the reconstituted PS2 shows similar activity as the native one, and in other cases the reconstituted PS2 performs different reaction from the native one.4) However, owing to the large size and extreme complexity of the PS2 protein, it is not easy to elucidate the reconstitution process at the molecular level. Specifically, the fate of the synthetic ligands during the reconstitution process remained unclear.

In this work, we developed a new tricarboxylate ligand **1** containing fluorine (Figure 4). The ligand is designed suitably to bind to a trinuclear $Mn_3(\mu_3\text{-}O)$ core, which is an important structural motif in the OEC. When the Mn-depleted PS2 particles were treated with the trinuclear Mn complex **2**, all the photosynthetic activities (including oxygen evolution) were restored. It was particularly notable that the reconstitution was completed at much lower concentration than the simple salts like $MnCl_2$, which suggests the positive role of the ligand in the reconstitution process.

The ^{19}F NMR of the reconstituted PS2 was examined. In spite of the very low concentration of the Mn complex, the signal was clearly observed after 30000 scans (Figure 5). This signal was assigned to the free ligand **1**, which indicates that the ligand was released from the complex **2** during the reconstitution. On the other hand, in the absence of the PS2 particles the decomposition of the complex **2** was slow. We propose that the primary step in the reconstitution process is the prebinding of the Mn complex to the hydrophobic part of the PS2 particle. This proposal is also consistent with our previous results on the reconstitution of OEC with synthetic Mn complexes.

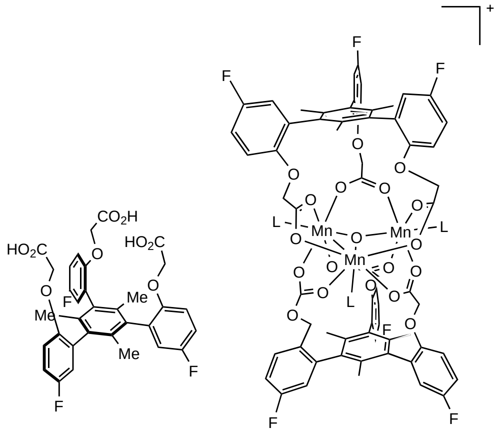

1

2 (L = pyridine-d_5)

Figure 4. The tricarboxylate ligand **1** and the Mn_3 complex **2**.

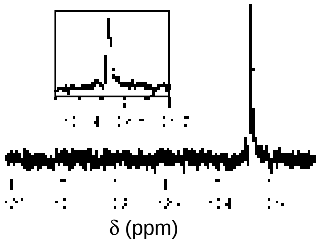

Figure 5. ^{19}F NMR spectra of the mixture of the Mn-depleted PSII particles (Chl 100 mg ml^{-1}) and **2** (10 µM) in the MES/D_2O buffer.

References

1) T. Nagasawa and T. Nagata, *Biochim. Biophys. Acta* **1767**, 666–670 (2007).
2) T. Nagasawa, S. I. Allakhverdiev, Y. Kimura and T. Nagata, *Photochem. Photobiol. Sci.* in press. (DOI: 10.1039/b815101f)
3) T. Nagata, S. K. Zharmukhamedov, A. A. Khorobrykh, V. V. Klimov and S. I. Allakhverdiev, *Photosynth. Res.* in press. (DOI: 10.1007/s11120-008-9319-9)
4) T. Nagata, T. Nagasawa, S. K. Zharmukhamedov, V. V. Klimov and S. I. Allakhverdiev, *Photosynth. Res.* **93**, 133–138 (2007).

* Present Address: Shin-Etsu Chemical Co., Ltd., 28-1 Nishifukushima, Kubiki-ku, Joetsu 942-8601

† Present Address: Institute of Basic Biological Problems, Russian Academy of Sciences, Pushchino, Moscow Region 142290, Russia

Chemistry of Bowl-Shaped Aromatic Compounds and Metal Nanocluster Catalysts

Research Center for Molecular Scale Nanoscience
Division of Molecular Nanoscience

SAKURAI, Hidehiro	Associate Professor
HIGASHIBAYASHI, Shuhei	Assistant Professor
KAMIYA, Ikuyo	IMS Fellow
YARASI, Soujanya	Visiting Scientist
REZA, A. F. G. Masud	Graduate Student
KITAHARA, Hiroaki	Graduate Student
ONOGI, Satoru	Graduate Student
NAKANO, Sachiko	Technical Fellow
KAI, Noriko	Technical Fellow
SASAKI, Tokiyo	Secretary

Bowl-shaped π-conjugated compounds including partial structures of the fullerenes, which are called "buckybowls," are of importance not only as model compounds of fullerenes but also as their own chemical and physical properties. Heteroatom-containing buckybowls (heterobuckybowls) have also been expected to exhibit unique physical characters. For example, in solution they show the characteristic dynamic behavior such as bowl-to-bowl inversion. On the other hand, they sometimes favor stacking structure in a concave-convex fashion in the solid state, giving excellent electron conductivity. Furthermore, some buckybowls are conceivable to possess the bowl-chirality if the racemization process, as equal as bowl-to-bowl inversion, is slow enough to be isolated. However, very few buckybowls/heterobuckybowls has been achieved for preparation mainly due to their strained structure, and no report on the preparation of chiralbowls has appeared. In the present project, we develop the rational route to the various kinds of buckybowls/heterobuckybowls with perfect chirality control using the organic synthesis approach.

We also investigate to develop novel catalytic properties of metal nanoclusters. We focus on the following projects: Preparation of size-selective gold nanoclusters supported by hydrophilic polymers and its application to aerobic oxidation catalysts: Synthetic application using metal nanocluster catalyst: Development of designer metal nanocluster catalyst using the highly- functionalized protective polymers: Catalytic activity of metal nanoclusters under the laser-irradiated conditions.

1. Asymmetric Synthesis of a Chiral Buckybowl, Trimethylsumanene[1)]

Many buckybowls possess "bowl chirality" derived from their three-dimensional geometry, similar to chiral fullerenes and carbon nanotubes. Methods to control the bowl chirality can potentially be applied to the related chiral fullerenes and carbon nanotubes as well. In addition, chiral aromatic compounds are expected to contribute to a variety of applications such as asymmetric molecular recognition, homochiral crystal organic materials, and chiral ligands for organometallic catalysis. Asymmetric synthesis of chiral buckybowls is challenging since synthetic strategies have not yet been established. We developed the first rational asymmetric synthesis of a C_3 symmetric chiral buckybowl, (*C*)-8,13,18-trimethylsumanene (**1**).

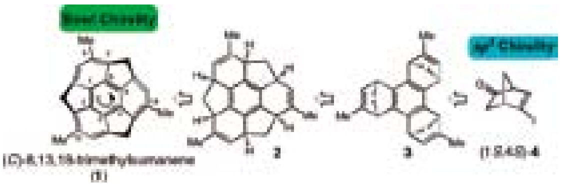

Scheme 1. Strategy for the asymmetric synthesis of (*C*)-**1**.

Figure 1. Racemization of **1** through a bowl-to-bowl inversion.

The bowl-to-bowl inversion energy barrier must be taken into account at this step, because this inversion corresponds to a racemization process for a chiral buckybowl (Figure 1). The bowl-to-bowl inversion energy barrier of **1** is estimated to be ca. 21 kcal/mol. Since the energy barrier corresponds to ca. 2 h half-life time of racemization at 0 °C, the aromatization step must be carried out at a low temperature. The bowl-shaped structure of **2** could be constructed from a benzonorbornene derivative **3** utilizing a tandem ring-opening/closing olefin metathesis approach. The benzonorbornene derivative **3** could be obtained by cyclotrimerization of a chiral halonorbornene derivative (1*S*,4*S*)-**4**. By adopting this approach, the bowl chirality of **1** is controlled by the sp^3 chirality of the starting norbornene derivative. Synthetic route to (*C*)-**1** is listed in Scheme 2.

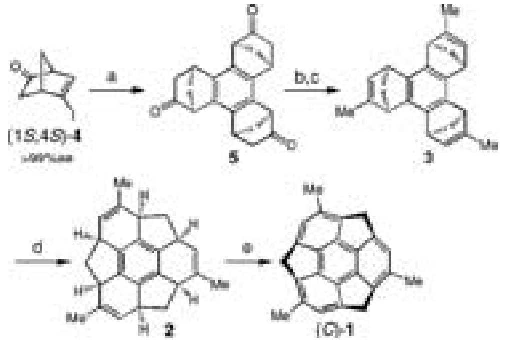

(a) $Pd(OAc)_2$ 5 mol%, PPh_3 10 mol%, Bu_4NOAc 1000 mol%, Na_2CO_3, MS 4 Å, 1,4-dioxane, 100 °C, 2 h, 55%; (b) $NaN(SiMe_3)_2$ 350 mol%, (2,6-diMePhO)$_2$P(O)Cl 350 mol%, $P(O)(NMe_2)_3$ 350 mol%, THF, –80 °C, 75%; (c) $Pd(OAc)_2$ 5 mol%, PCy_3•HBF_4 10 mol%, MeMgI 400 mol%, THF, 40 °C, 2 h, 72%; (d) Grubbs 1st generation catalyst 50 mol%, CH_2Cl_2, under ethylene, 40 °C, 6 h, then Grubbs 2nd generation catalyst 50 mol%, CH_2Cl_2, 40 °C, 12 h, 24%; (e) DDQ 600 mol%, CH_2Cl_2, 0 °C, 1 min 68%.

Scheme 2. Synthesis of (*C*)-8,13,18-trimethylsumanene (**1**).

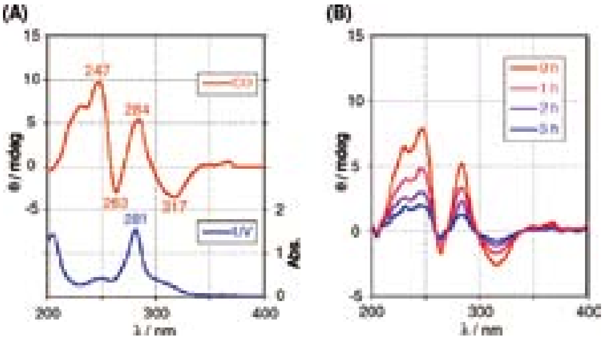

Figure 2. (A) CD spectra of (*C*)-**1** in CH_3CN at –40 °C (red line) and UV spectra of (±)-**1** in CH_3CN at rt (blue line); (B) decay of CD spectra of (*C*)-**1** in CH_3CN at 10 °C for 3 h.

The chirality of thus-obtained (*C*)-**1** was confirmed by measurement of the circular dichroism (CD) spectra. The intensity of the CD spectra at –40 °C scarcely changed but gradually decreased at 10 °C (Figure 2). The bowl-to-bowl inversion energy barrier of **1** in CH_3CN was determined to be 21.6 kcal/mol by tracing the decay of the CD spectra at 247 and 282 nm at 10 °C (Supporting Information). This value is in good accordance with the estimated one.

To determine the enantiomeric excess of synthetic **1**, we needed to derivatize **1** while avoiding racemization through a bowl-to-bowl inversion. Selective introduction of trimethylsilyl groups at the *exo* positions of the dibenzylic positions induces new sp^3 chirality which prevents the enantiomers from racemizing (Scheme 3). However, we were unable to separate the enantiomers of **6** using chiral HPLC. Instead, (*S*)-Ph(CF_3)(OMe)CCO groups were introduced to create diastereomers. Finally the enantiomeric excess of **1** was determined as 90% ee based on the ^{1}H NMR analysis of the diastereomeric ratio of **7**.

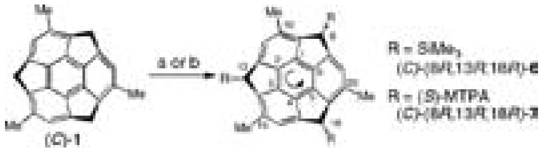

(a) (±)-**1**, LDA 1000 mol%, THF, 0 °C then Me_3SiCl 1000 mol%, (±)-**6** 45%; (b) (*C*)-**1**, LDA 600 mol%, THF, –40 °C, then (*R*)-Ph(CF_3)(MeO)CCOCl = (*R*)-MTPACl 1000 mol% 17%.

Scheme 3. Determination of the enantiomeric excess of **1**.

2. Thermosensitive Gold Nanoclusters Stabilized by Well-Defined Vinyl Ether Star Polymers: Reusable and Durable Catalysts for Aerobic Alcohol Oxidation[2)]

Au nanoclusters of less than 4 nm with a narrow size distribution were prepared and supported in thermosensitive vinyl ether star polymers (Au@star poly(EOEOVE)$_{200}$) obtained by living cationic polymerization. The thermosensitivity of the star polymers permitted easy separation of the clusters from the reaction mixture without any negative aggregation. Thus, the Au clusters could be recovered for reuse several times to induce alcohol oxidation with similar reactivity in each run.

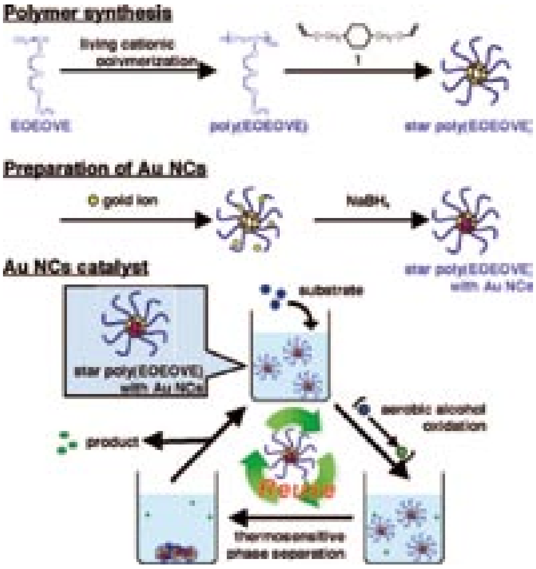

Scheme 4. Preparation and Catalytic Use of Au NCs.

References

1) S. Higashibayashi and H. Sakurai, *J. Am. Chem. Soc.* **130**, 8592–8593 (2008).

2) S. Kanaoka, N. Yagi, Y. Fukuyama, S. Aoshima, H. Tsunoyama, T. Tsukuda, and H. Sakurai, *J. Am. Chem. Soc.* **129**, 12060–12061 (2007).

Multifunction Integrated Macromolecules for Molecular-Scale Electronics

Research Center for Molecular Scale Nanoscience
Division of Molecular Nanoscience

TANAKA, Shoji Assistant Professor

To date there have been demonstrations of molecular-scale diode, switches, transistors, logic circuits, and memory cells, however, the fabrication of complete molecular-scale electronic circuits remains challenging because of the difficulty of connecting molecular device elements to one another. To overcome this problem, we have been developing step-wise synthetic protocols for integrating the molecular functional units required for advanced information processing within a single macromolecule. Our strategy is based on modular architecture using a library of versatile molecular building blocks. The flexible functionality of these blocks is derived from the 3,4-diaminothiophene component, which can be easily modified to tune the structural and electronic properties of the main π-conjugated chain.

1. Thiophene Oligomers for Single-Molecule Charge-transport Measurements

One of the current issues in molecular-scale electronics is to understand and control the charge transport characteristics of single-molecular wires bonded between metal electrodes. To this end, we have synthesized a series of precisely defined oligothiophenes (**1**) ranging in length from 1 to 30 nanometers. These molecular wires have thiocyanate (-**SCN**) anchors that can lead to spontaneous assembly of the wires on Au-based nano-gap electrode systems without activation agents. The systematic nano-scale charge transport measurements using STM break junctions or planar nano-gap electrode systems are now in progress.

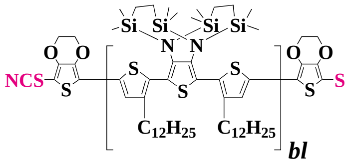

1

***bl* = 1, 2, 3, 4, 5, 6, 7, 8, 10,16, 24**

(*l* = 1 ~ 30 nm)

Figure 1. Structures of oligomers (**1**).

2. Electrical Conductance of Oligothiophene Molecular Wires[1)]

A break junction method using a scanning tunneling microscope has been applied to electrical conductance measurement of newly designed oligothiophene molecules terminated with a thiocyanate group. The tunneling conduction was evident from an exponential decay of the conductance as a function of the molecular length up to ca. 6 nm. The tunneling decay constant was estimated to be 0.1 angstrom^{-1}. The pre-exponential factor was 1.3 × 10^{-6} S, which was smaller than that observed for alkanedithiols.

3. Direct Conformational Analysis of a 10nm Long Oligothiophene Wire[2)]

Conformational variations of a 10 nm long oligothiophene wire (**2**) on Au(111) have been directly visualized by scanning tunneling microscopy (STM). The local bending angles within the wire are well characterized as s-cis/s-trans configurations of individual thiophene rings. We find that the partial stabilization of the metastable s-cis conformation results in the wire bending, which should be influenced by solvent and substituents.

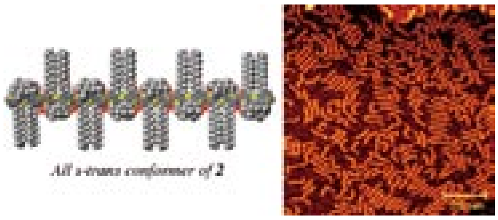

Figure 2. Structure of oligomer (**2**) and Large-area STM image.

References

1) R. Yamada, H. Kumazawa, T. Noutoshi, S. Tanaka and H. Tada, *Nano Lett.* **8**, 1237–1240 (2008).

2) F. Nishiyama, K. Ogawa, S. Tanaka and T. Yokoyama, *J. Phys. Chem. B* **112**, 5272–5275 (2008).

Development of Novel Heterocyclic Compounds and Their Molecular Assemblies for Advanced Materials

Safety Office

TOMURA, Masaaki Assistant Professor

Heterocycles containing sulfur and/or nitrogen atoms are useful as components of functional organic materials since heteroatoms in their rings are helpful to stabilize ions or ion-radical species. In addition, intermolecular interactions caused by heteroatom contacts can be expected to form unique molecular assemblies. In this project, novel functional organic materials based on various heterocycles were synthesized and their physical and structural properties were investigated.

1. Construction of Molecular Networks Using Chloranilic Acid[1)]

In the crystal structure of 4-cyanopyridinium hydrogen chloranilate, the centrosymmetric dimmers with O–H···O hydrogen bonds are linked by intermolecular N–H···O and N···Cl interactions to construct a two-dimensional large square grid molecular network (Figure 1).

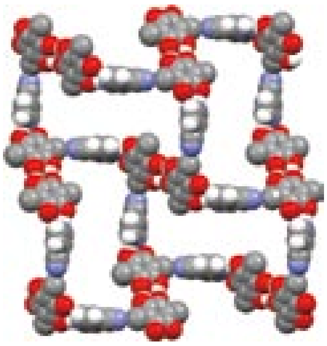

Figure 1. A two-dimensional large square grid molecular network.

2. Photooxidation and Reproduction of Pentacene Derivatives Substituted by Aromatic Groups[2)]

Pentacene derivatives substituted by aromatic groups at the 6,13-positions were prepared and investigated for their electronic properties and the photooxidation–deoxygenation.

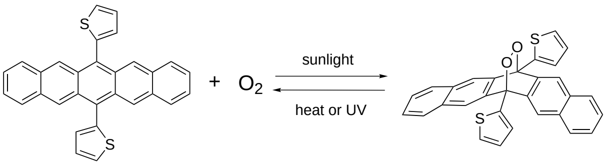

3. X-Ray Crystallographic Analyses of Heterocyclic and Aromatic Compounds[3–9)]

The X-ray crystallographic analyses of seven heterocyclic and aromatic compounds have revealed their interesting structural natures and unique molecular aggregations.

References

1) M. Tomura and Y. Yamashita, *Anal. Sci.* **24**, x31–x32 (2008).
2) K. Ono, H. Totani, T. Hiei, A. Yoshino, K. Saito, K. Eguchi, M. Tomura, J. Nishida and Y. Yamashita, *Tetrahedron* **63**, 9699–9704 (2007).
3) M. Tomura, K. Ono, M. Kaiden, K. Tsukamoto and K. Saito, *Acta Crystallogr., Sect. E* **63**, o4568–o4569 (2007).
4) K. Ono, M. Tomura and K. Saito, *Acta Crystallogr., Sect. E* **63**, o4612–o4612 (2007).
5) M. Tomura, *Acta Crystallogr., Sect. E* **64**, o170–o171 (2008).
6) M. Tomura, H. Yamaguchi, K. Ono, M. Kaiden and K. Saito, *Acta Crystallogr., Sect. E* **64**, o172–o173 (2008).
7) K. Ono, M. Tomura and K. Saito, *Acta Crystallogr., Sect. E* **64**, o468–o468 (2008).
8) M. Tomura and Y. Yamashita, *Acta Crystallogr., Sect. E* **64**, o545–o545 (2008).
9) K. Ono, K. Tsukamoto, M. Tomura and K. Saito, *Acta Crystallogr., Sect. E* **64**, o1069–o1069 (2008).

Visiting Professors

Visiting Professor

BABA, Yoshinobu *(from Nagoya University)*

Biomolecular Imaging by Quantum Dot

We developed the nanofluidic technology for real-time monitoring of interaction between a quantum dot (Qdot)-labeled single DNA molecule and a protein molecule during enzymatic reaction. A Qdot-labeled single DNA molecule is flowing at ca. 20 μm s^{-1} wherein the microchannel without enzyme patterning, but at the enzyme patterning region, we found a DNA molecule is stopped for several seconds to react with enzyme. We measured over 200 DNA molecules and found that a DNA molecule needs 2 second to search a cleavage sequence of DNA and 3 seconds to induced fit and cut a DNA molecule. The kinetic constant evaluated based on the single molecular measurement is consistent with the value evaluated by the conventional measurements.

Visiting Professor

AWAGA, Kunio *(from Nagoya University)*

Research on Organic Radical Materials

Organic radicals are key materials in both solid-state and solution redox processes. Organic radical solids always exhibit semiconductive behavior, due to electrostatic repulsion between unpaired electrons and/or electron-lattice interactions. This strongly suggests a potential application of organic radicals to organic electronics. We are performing fundamental research on electrical and magnetic properties of organic radical solids and application research on photo- and current-induced phenomena. We are also working on solid-state electrochemistry of insoluble self-assembled organic thin-films and transition metal complex clusters, targeting rechargeable batteries, functional electrodes, and electrochromic devices.

Visiting Associate Professor

HIGUCHI, Masayoshi *(from National Institute for Materials Science)*

Organic-Metallic Hybrid Polymers with Multi-Color Electrochromic Functions

Organic-metallic hybrid polymers are expected to have unique electrochemical, photochemical, magnetic, or catalytic properties based on strong interaction between organic modules and metal ions. Novel hybrid polymers are formed by complexation of metal ions such as Fe(II), Co(II), and Ru(II) with bis(terpyridyl)benzenes as an organic module. The polymers have specific colors based on the metal-to-ligand charge transfer and the color disappears by electrochemical oxidation of the polymer. The electrochromic properties are caused by electrochemical redox of metal ions in the polymers. We found that a film of the hybrid polymer including two different kinds of metal ions in the polymer chain shows multi-color electrochromic change at redox potentials of the metal ions. The hybrid polymers with excellent electrochromic functions will be applied to “multi-color electronic papers,” one of next generation displays.

RESEARCH ACTIVITIES

Life and Coordination-Complex Molecular Science

Department of Life and Coordination-Complex Molecular Science is composed of four divisions of Biomolecular science, two divisions of Coordination molecular science and two adjunct divisions. Biomolecular science divisions cover the studies on the elucidation of functions and mechanisms for various types of sensor proteins, protein folding, molecular chaperone, and metal proteins. Coordination complex divisions aim to develop molecular catalysts for the transformation of organic molecules, activation small inorganic molecules, and reversible conversion between chemical and electrical energies. Interdisciplinary alliances in the Department aim to create new basic concepts for the molecular and energy conversion through the fundamental science conducted at each division.

Bioinorganic Chemistry of Novel Hemeproteins

Department of Life and Coordination-Complex Molecular Science
Division of Biomolecular Functions

AONO, Shigetoshi	Professor
YOSHIOKA, Shiro	Assistant Professor
SAWAI, Hitomi	JSPS Post-Doctoral Fellow
NISHIMURA, Muneto	Graduate Student
TANIZAWA, Misako	Secretary

Heme-based sensor proteins show a novel function of the heme prosthetic group, in which the heme acts as the active site for sensing the external signal such as diatomic gas molecules and redox change. Aldoxime dehydratase is another novel hemeprotein, in which the heme prosthetic group tethers the substrate for its dehydration reaction. Our research interests are focused on the elucidation of the structure-function relationships of these novel hemeproteins.

1. Hydrogen Bonding Interaction on the Heme-Bound Ligand in the Heme-Based O_2 Sensor Protein[1)]

HemAT is a signal transducer protein that is a member of methyl accepting chemotaxis proteins (MCPs), which is responsible for aerotaxis control of some bacteria and archaea. HemAT consists of two domains, the N-terminal sensor domain containing a heme and the C-terminal signaling domain that interacts with CheA, a component of CheA/CheY two-component system regulating the rotational direction of a flagellar motor in response to an input signal into MCPs. The heme in the sensor domain of HemAT acts as the active site for sensing its physiological effector, O_2. When O_2 binds to the heme in the sensor domain, it is thought that a specific conformational change will occur, and then signal transduction will proceed from the sensor domain to the signaling domain. As a result, the self-kinase activity of CheA is regulated by a change in the interaction between HemAT and CheA via the specific conformational change of HemAT.

HemAT should discriminate O_2 from other gas molecules such as NO and CO, for which the heme environmental structure plays a crucial role. To elucidate the mechanism of selective O_2 sensing by HemAT, structural, mutagenesis, and spectroscopic studies were carried out for HemAT from *Bacillus subtilis* (HemAT-Bs). The interaction between the heme-bound ligand and the surrounding amino acid residue(s) plays a crucial role for selective sensing of O_2 and signal transduction by HemAT. In this work, we elucidated by resonance Raman spectroscopy how O_2 and CO interact with HemAT-Hs and HemAT-Rr, HemAT from *Halobacterium salinarum* and *Rhodospirillum rubrum*, respectively. HemAT-Hs and HemAT-Rr showed three conformers in the O_2-bound form, as is the case of HemAT-Bs, HemAT from *Bacillus subtilis*. Though the hydrogen bonding patterns observed in the three conformers were same among HemAT-Bs, HemAT-Hs, and HemAT-Rr, the involved residues for the hydrogen bonding interaction were different from one another.

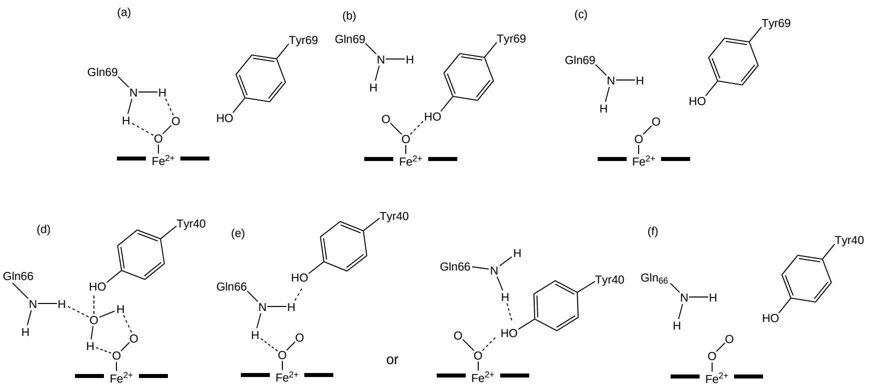

Figure 1. Hydrogen bonding network of the oxygen-bound form of HemAT-Hs (a-c) and HemAT-Rr (d-f).

2. Metal-Containing Sensor Proteins Sensing Diatomic Gas Molecules[2)]

All of the living organisms have a variety of regulatory systems to confront the change in the environmental conditions, which should be essential for maintaining the homeostasis in the cells, organs, and whole bodies. The chemical or physical stimuli act as signals for them to sense the change in the environmental conditions. These regulatory systems are responsible for the control of cell motility, gene expression, and/or enzymatic activity in response to the external stimuli. Sensing the external stimuli is the first step for these regulatory systems to work. Sensor (receptor) proteins should be required to sense these signals in biological systems, which sense the cognate signals in a specific manner.

Recently, it becomes apparent that diatomic gas molecules such as O_2, CO, and NO can act as signaling molecules for many biological processes. The functional role as external signals is a new one of these gas molecules in biological systems while it is well known that gas molecules are involved in biological systems as substrates and/or reaction products of many enzymatic reactions.

The gas sensor proteins usually use some prosthetic group to sense diatomic gas molecules. Heme, iron-sulfur cluster, and non-heme iron are known as the active center for these gas sensor proteins. When the gas sensor proteins sense their effector gas molecules, intramolecular and intermolecular signal transductions take place to regulate many physiological functions including gene expression, aerotaxis, and change in metabolic pathways, *etc*. The metal-containing prosthetic groups in these sensor proteins play a crucial role for selective sensing of their effectors.

In this perspective, I will discuss the structure and function of some O_2-, CO-, and NO-sensor proteins, especially focus on the structural, biochemical and biophysical properties of the active centers of these sensor proteins.

3. Protein Conformation Changes of HemAT-Bs upon Ligand Binding Probed by Ultraviolet Resonance Raman Spectroscopy[3)]

HemAT from *Bacillus subtilis* (HemAT-*Bs*) is a heme-based O_2 sensor protein that acts as a signal transducer responsible for aerotaxis. HemAT-*Bs* discriminates its physiological effector (O_2) from other gas molecules (CO and NO), although all of them bind to a heme. To monitor the conformational changes in the protein moiety upon binding of different ligands, we have investigated ultraviolet resonance Raman (UVRR) spectra of the ligand-free and O_2-, CO-, and NO-bound forms of full-length HemAT-*Bs* and several mutants (Y70F, H86A, T95A, and Y133F) and found that Tyr^{70} in the heme distal side and Tyr^{133} and Trp^{132} from the G-helix in the heme proximal side undergo environmental changes upon ligand binding. In addition, the UVRR results confirmed our previous model, which suggested that Thr^{95} forms a hydrogen bond with heme-bound O_2, but Tyr^{70} does not. It is deduced from this study that hydrogen bonds between Thr^{95} and heme-bound O_2 and between His^{86} and heme 6-propionate communicate the heme structural changes to the protein moiety upon O_2 binding but not upon CO and NO binding. Accordingly, the present UVRR results suggest that O_2 binding to heme causes displacement of the G-helix, which would be important for transduction of the conformational changes from the sensor domain to the signaling domain.

References

1) M. Nishimura, H. Yoshimura, K. Ozawa, S. Yoshioka, M. Kubo, T. Kitagawa and S. Aono, *J. Porpyrins Phthalocyanines* **12**, 142–148 (2008).
2) S. Aono, *Dalton Trans.* 3137–3146 (2008).
3) S. F. El-Mashtoly, Y. Gu, H. Yoshimura, S. Yoshioka, S. Aono and T. Kitagawa, *J. Biol. Chem.* **283**, 6942–6949 (2008).

Award

SAWAI, Hitomi; The best poster prize in 4th International Conference on Metals and Genetics (Paris, France, July 21–24, 2008).

Elucidation of the Molecular Mechanisms of Protein Folding

Department of Life and Coordination-Complex Molecular Science
Division of Biomolecular Functions

KUWAJIMA, Kunihiro	Professor
CHAUDHURI, Tapan K.	Visiting Associate Professor
MAKABE, Koki	Assistant Professor
MUKAIYAMA, Atsushi	IMS Fellow
VOLETY, Srinivas	Visiting Scientist; JSPS Invited Fellow
NAKAMURA, Takashi	Post-Doctoral Fellow
TAKAHASHI, Kazunobu	Graduate Student*
MIZUKI, Hiroko	Technical Fellow
ISOGAI, Miho	Secretary

Kuwajima group is studying mechanisms of *in vitro* protein folding and mechanisms of molecular chaperone function. Our goals are to elucidate the physical principles by which a protein organizes its specific native structure from the amino acid sequence. In this year, we studied the structure of the GroEL-GroES complex under physiological conditions by small-angle X-ray scattering, which is a powerful technique to directly observe the structure of the protein complex in solution.

1. Asymmetry of the GroEL-GroES Complex under Physiological Conditions as Revealed by Small-Angle X-Ray Scattering1)

In spite of the well-known functional importance of GroEL-GroES complex formation during the chaperonin cycle, the stoichiometry of the complex has not been clarified. The complex can occur either as an asymmetric 1:1 GroEL-GroES complex or as a symmetric 1:2 GroEL-GroES complex, although it remains uncertain which type is predominant under physiological conditions. To resolve this question, we studied the structure of the GroEL-GroES complex under physiological conditions by small-angle X-ray scattering, which is a powerful technique to directly observe the structure of the protein complex in solution. We evaluated molecular structural parameters, the radius of gyration and the maximum dimension of the complex, from the X-ray scattering patterns under various nucleotide conditions (3 mM ADP, 3 mM ATPγS and 3 mM ATP in 10 mM MgCl$_2$ and 100 mM KCl) at three different temperatures (10 °C, 25 °C, and 37 °C). We then compared the experimentally observed scattering patterns with those calculated from the known X-ray crystallographic structures of the GroEL-GroES complex. The results clearly demonstrated that the asymmetric complex must be the major species stably present in solution under physiological conditions. On the other hand, in the presence of ATP (3 mM) and beryllium fluoride (10 mM NaF and 300 μM BeCl$_2$), we observed the formation of a stable symmetric complex, suggesting the existence of a transiently formed symmetric complex during the chaperonin cycle.

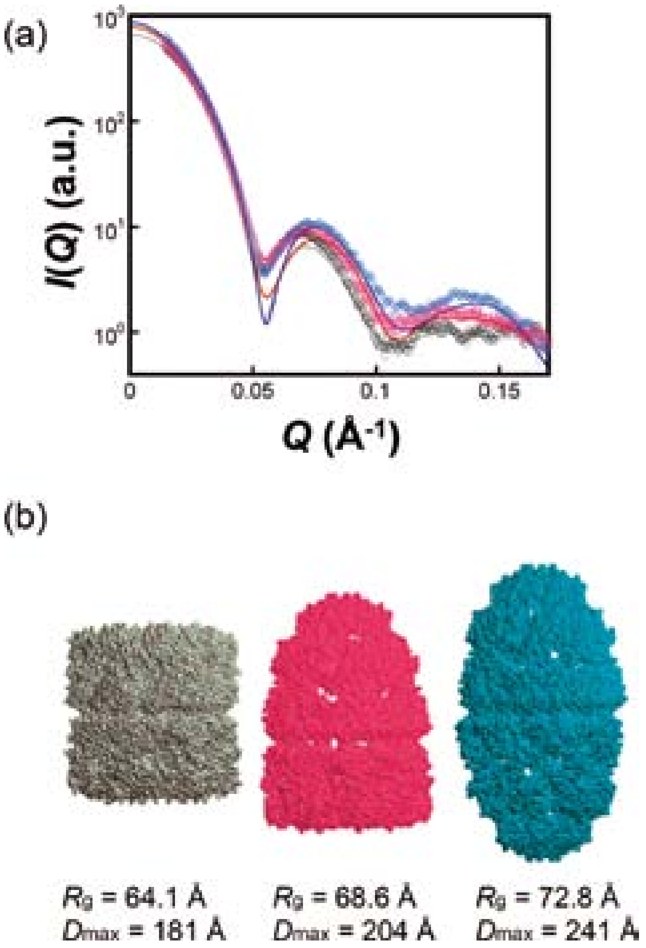

Figure 1. (a) Small-angle X-ray scattering patterns of molecular chaperones, GroEL and the GroEL-GroES complexes. (b) The three-dimensional structures of GroEL (gray), the bullet-type GroEL-GroES complex (magenda), and the football-type GroEL-GroES complex (cyan) (Inobe *et al*., *Biophys. J*. **94**, 1392–1402 (2008)).

Reference

1) T. Inobe, K. Takahashi, K. Maki, S. Enoki, K. Kamagata, A. Kadooka, M. Arai and K. Kuwajima, *Biophys. J.* **94**, 1392–1402 (2008).

---

* carrying out graduate research on Cooperative Education Program of IMS with the University of Tokyo

NMR Analyses of Structures, Dynamics, and Interactions of Biological Macromolecules

Department of Life and Coordination-Complex Molecular Science
Division of Biomolecular Functions

KATO, Koichi	Professor
SASAKAWA, Hiroaki	Assistant Professor*
YAMAGUCHI, Takumi	Assistant Professor
KAMIYA, Yukiko	IMS Fellow
SUGIHARA, Takahiro	Research Fellow
SUZUKI, Mariko	Research Fellow
UTSUMI, Maho	Graduate Student†
YOSHIKAWA, Sumi	Graduate Student†
NISHIO, Miho	Graduate Student†
TANAKA, Kei	Secretary

Our biomolecular studies are based on detailed analyses of structures and dynamics of various biological macromolecules and their complexes at atomic level, primarily using nuclear magnetic resonance (NMR) spectroscopy. In particular, we conducted studies aimed at elucidating dynamic structures of glycoconjugates and proteins for integrative understanding of the mechanisms underlying their biological functions. For this purpose, we use multidisciplinary approaches integrating the methodologies of molecular and cellular biology and nanoscience along with molecular spectroscopy. Here we report NMR studies of Fbs1, α-synuclein, group II chaperonin and prefoldin.

1. Molecular Recognition by Fbs1, an Intracellular Lectin Contributing to Quality Control of Glycoproteins1)

Fbs1 is a cytosolic lectin putatively operating as a chaperone as well as a substrate-recognition subunit of the $\mathrm{SCF^{Fbs1}}$ ubiquitin ligase complex. To provide structural and functional basis of preferential binding of Fbs1 to unfolded glycoproteins, we herein characterize the interaction of Fbs1 with a heptapeptide carrying $\mathrm{Man_3GlcNAc_2}$ by NMR spectroscopy and other biochemical methods. Inspection of the NMR data obtained by use of the isotopically labeled glycopeptide indicated that Fbs1 interacts with sugar-peptide junctions (Figure 1), which are shielded in native glycoprotein, in many cases, but become accessible to Fbs1 in unfolded glycoproteins. Furthermore, Fbs1 was shown to inhibit deglycosylation of denatured ribonuclease B by a cytosolic peptide:*N*-glycanase (PNGase). On the basis of these data, we suggest that Fbs1 captures malfolded glycoproteins, protecting them from the attack of PNGase, during the chaperoning or ubiquitinating operation in the cytosol.

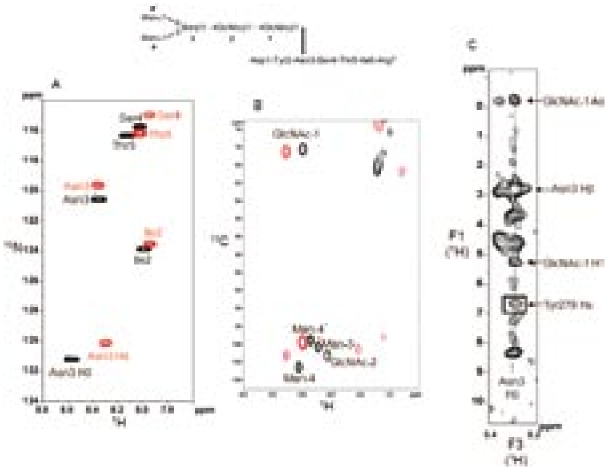

Figure 1. NMR spectra of the isotopically labeled heptapeptide carrying $\mathrm{Man_3GlcNAc_2}$. (A) The anomeric region of ^{1}H-^{13}C HSQC spectrum of the glycopeptides labeled with [u-$^{13}C_6$]glucose and (B) amide region of ^{1}H-^{15}N HSQC spectrum of the ^{15}N-labeled glycopeptide in the presence (red) or absence (black) of equimolar amount of Fbs1-SBD. (C) Part of ^{15}N-edited NOESY spectrum of the ^{15}N-labeled glycopeptides bound to Fbs1-SBD (F2(^{15}N) = 129.6 ppm). The intermolecular NOE peak between Tyr279 Hε (Fbs1-SBD) and Asn3 Hδ (glycopeptide) is boxed.

2. Antibody Binding and Site-Specific Phosphorylation of α-Synuclein, an Intrinsically Disordered Protein2)

Although biological importance of intrinsically disordered proteins is becoming recognized, NMR analyses of this class of proteins remain as tasks with more challenge because of poor chemical shift dispersion. It is expected that ultra-high field NMR spectroscopy offers improved resolution to cope with this difficulty. α-synuclein, an intrinsically disordered protein, is identified as the major component of the Lewy bodies. Epitope mapping of an anti-α-synuclein monoclonal antibody and characterization of conformational effects of phosphorylation at Ser129 of α-synuclein were conducted based on NMR spectral data collected at a 920 MHz proton frequency (Figure 2). These studies demonstrated that the employment of ultra-high field spectrometers is obviously advantageous for obtaining detailed information on conformations, modifications, and interactions of intrinsically disordered proteins in solution.

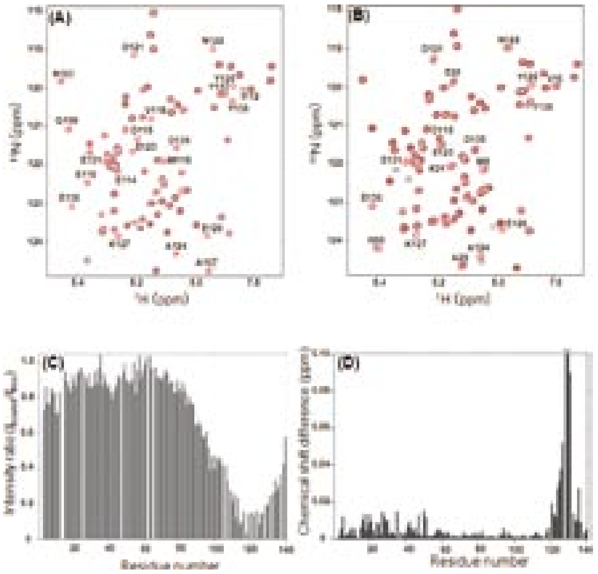

Figure 2. NMR analyses of antibody binding and phosphorylation of α-synuclein ^{1}H-^{15}N HSQC spectra of (A) [^{15}N]α-synuclein in the presence (black) and absence (red) of LB509 and (B) phosphorylated (black) and non-phosphorylated (red) [^{15}N]α-synuclein recorded at a proton frequency of 920 MHz. (C) Plot of the relative peak intensities, $I_{\mathrm{bound}}/I_{\mathrm{free}}$, of the HSQC cross peaks in the α-synuclein/LB509 complex and free α-synuclein versus the amino acid sequence of α-synuclein. (D) Profiles of chemical shift changes $[(\delta_N/5)^2 + \delta_H{}^2]^{1/2}$ upon phosphorylation at Ser129. Asterisks indicate the chemical shift differences are larger than 0.1 ppm for Ser129 (0.48 ppm) and E130 (0.20 ppm).

3. Dynamics of Group II Chaperonin and Prefoldin Probed by ^{13}C NMR Spectroscopy[3)]

Group II chaperonin (CPN) cooperates with prefoldin (PFD), which forms a jellyfish-shaped heterohexameric complex with a molecular mass of 87 kDa. PFD captures an unfolded protein with the tentacles and transfers it to the cavity of CPN. Although X-ray crystal structures of CPN and PFD have been reported, no structural information has been so far available for the terminal regions of the PFD tentacles nor for the C-terminal segments of CPNs, which were regarded to be functionally significant in the previous studies. We conducted ^{13}C NMR analyses on archaeal PFD, CPN and their complex, focusing on those structurally uncharacterized regions. The PFD and CPN complexes selectively labeled with ^{13}C at methionyl carbonyl carbons were separately and jointly subjected to NMR measurements. ^{13}C NMR spectral data demonstrated that the N-terminal segment of the α and β subunits of PFD as well as the C-terminal segments of the CPN hexadecamer retain significant degrees of freedom in internal motion even in the complex with a molecular mass of 1.1 MDa (Figure 3).

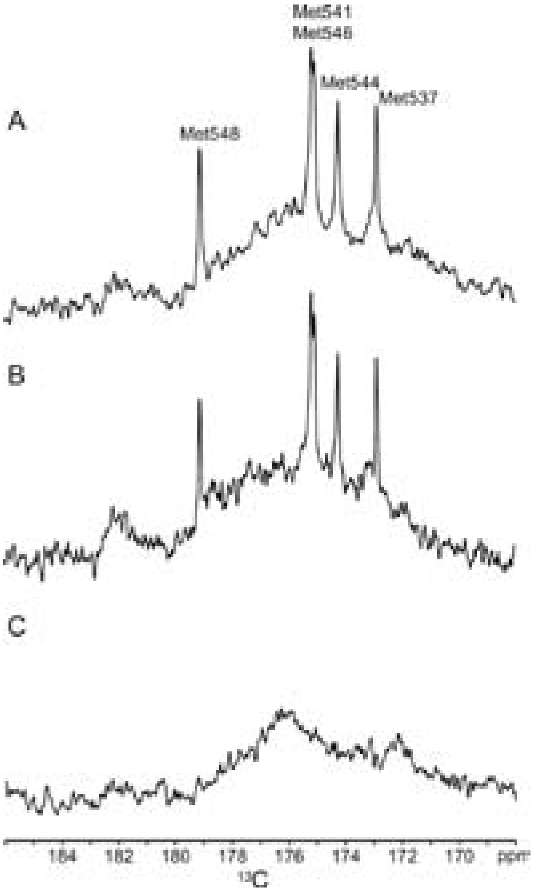

Figure 3. Hundred mega hertz ^{13}C NMR spectra of wild-type *Thermococcus* sp. strain KS-1 CPN (TKSαCPN) (A and B) and the truncated mutant of TKSαCPN that lacks the C-terminal 17 amino acid residues (C) labeled with [1-^{13}C]methionine in the absence (A and C) or presence (B) of 2 molar equivalent PFD. The proteins were dissolved in 50 mM Tris-HCl buffer, pH 8.0, containing 150 mM NaCl, 25 mM $MgCl_2$, 0.02% NaN_3, and 10% $^{2}H_2O$. The probe temperature was 45 °C.

References

1) Y. Yamaguchi, T. Hirao, E. Sakata, Y. Kamiya, E. Kurimoto, Y. Yoshida, T. Suzuki, K. Tanaka and K. Kato, *Biochem. Biophys. Res. Commun.* **362**, 712–716 (2007).
2) H. Sasakawa, E. Sakata, Y. Yamaguchi, M. Masuda, T. Mori, E. Kurimoto, T. Iguchi, S. Hisanaga, T. Iwatsubo, M. Hasegawa and K. Kato, *Biochem. Biophys. Res. Commun.* **363**, 795–799 (2007).
3) E. Kurimoto, Y. Nishi, Y. Yamaguchi, T. Zako, R. Iizuka, N. Ide, M. Yohda and K. Kato, *Proteins: Struct., Funct., Bioinf.* **70**, 1257–1263 (2008).

---

* Present Address; JEOL Ltd. NMR/ESR team, Application & Research Group, Analytical Instrument Division, Akishima, Tokyo 196-8558

† carrying out graduate research on Cooperative Education Program of IMS with Nagoya City University

Structure-Function Relationship of Metalloproteins

Department of Life and Coordination-Complex Molecular Science
Division of Biomolecular Functions

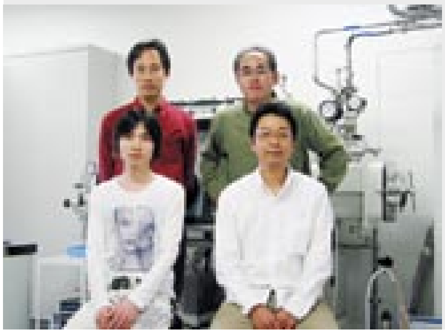

FUJII, Hiroshi	Associate Professor
KURAHASHI, Takuya	Assistant Professor
NONAKA, Daisuke	IMS Fellow
TAKAHASHI, Akihiro	Graduate Student
TANIZAWA, Misako	Secretary

Metalloproteins are a class of biologically important macromolecules, which have various functions such as oxygen transport, electron transfer, oxidation, and oxygenation. These diverse functions of metalloproteins have been thought to depend on the ligands from amino acid, coordination structures, and protein structures in immediate vicinity of metal ions. In this project, we are studying the relationship between the electronic structures of the metal active sites and reactivity of metalloproteins.

1. Effect of a Tridentate Ligand on the Structure, Electronic Structure, and Reactivity of the Copper(I) Nitrite Complex: Role of the Conserved Three-Histidine Ligand Environment of the Type-2 Copper Site in Copper-Containing Nitrite Reductases[1)]

It is postulated that the copper(I) nitrite complex is a key reaction intermediate of copper containing nitrite reductases (Cu-NiRs), which catalyze the reduction of nitrite to nitric oxide (NO) gas in bacterial denitrification. To investigate the structure-function relationship of Cu-NiR, we prepared five new copper(I) nitrite complexes with sterically hindered tris(4-imidazolyl)carbinols [Et-TIC: tris(1-methyl-2-ethyl-4-imidazolyl)carbinol and *i*Pr-TIC: tris(1-methyl-2-isopropyl-4-imidazolyl)carbinol] or tris(1-pyrazolyl)methanes [Me-TPM: tris(3,5-dimethyl-1-pyrazolyl)methane, Et-TPM: tris(3,5-diethyl-1-pyrazolyl)methane, and *i*Pr-TPM: tris(3,5-diisopropyl-1-pyrazolyl)methane]. The X-ray crystal structures of all of these copper(I) nitrite complexes were mononuclear η^1-N-bound nitrite complexes with a distorted tetrahedral geometry. The electronic structures of the complexes were investigated by absorption, MCD, NMR and vibrational spectroscopy. All of these complexes are good functional models of Cu-NiR that form NO and copper(II) acetate complexes well from reactions with acetic acid under anaerobic conditions. A comparison of the reactivity of these complexes, including previously reported (*i*Pr-TACN)Cu(NO_2), *i*Pr-TACN: 1,4,7-triisopropyl-1,4,7-triazacyclononane, clearly shows the drastic effects of the tridentate ligand on Cu-NiR activity. The copper(I) nitrite complex with the Et-TIC ligand, which is similar to the highly conserved three-histidine ((His)$_3$) ligand environment in the catalytic site of Cu-NiR, had the highest Cu-NiR activity. This result suggests that the (His)$_3$ ligand environment is essential for acceleration of the Cu-NiR reaction. The highest Cu-NiR activity for the Et-TIC complex can be explained by the structural and spectroscopic characterizations and the molecular orbital calculations presented in this paper. Based on these results, the functional role of the (His)$_3$ ligand environment in Cu-NiR is discussed.

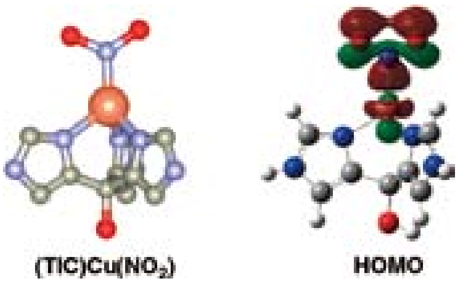

Figure 1. Structure of Active Site Model Complex of Copper Nitrite Reductase (left) and its Electron Density of the HOMO (right).

2. Transient Intermediates from Mn(salen) with Sterically-Hindered Mesityl Groups: Interconversion between Mn^{IV}-Phenolate and Mn^{III}-Phenoxyl Radical as an Origin for Unique Reactivity[2]

In order to reveal structure-reactivity relationships for the high catalytic activity of the epoxidation catalyst Mn(salen), transient intermediates are investigated. Steric hindrance incorporated to the salen ligand enables highly selective generation of three related intermediates, $O{=}Mn^{IV}$(salen), $HO{-}Mn^{IV}$(salen) and $H_2O{-}Mn^{III}(salen^{+\bullet})$, each of which is thoroughly characterized using various spectroscopic techniques including UV-vis, EPR, resonance Raman, ESI-MS, ^{2}H-NMR and X-ray absorption spectroscopy. These intermediates are all one-electron oxidized from the starting Mn^{III} (salen) precursor, but differ only in the degree of protonation. However, structural and electronic features are strikingly different: The Mn–O bond length of $HO{-}Mn^{IV}$(salen) (1.83 Å) is considerably longer than that of $O{=}Mn^{IV}$(salen) (1.58 Å); the electronic configuration of $H_2O{-}Mn^{III}(salen^{+\bullet})$ is Mn^{III}-phenoxyl radical, while those of $O{=}Mn^{IV}$(salen) and $HO{-}Mn^{IV}$(salen) are Mn^{IV}-phenolate. Among $O{=}Mn^{IV}$(salen), $HO{-}Mn^{IV}$(salen) and $H_2O{-}Mn^{III}(salen^{+\bullet})$, only the $O{=}Mn^{IV}$ (salen) can transfer oxygen to phosphine and sulfide substrates, as well as abstract hydrogen from weak C–H bonds, although the oxidizing power is not enough to epoxidize olefins. The high activity of Mn(salen) is a direct consequence of the favored formation of the reactive $O{=}Mn^{IV}$(salen) state.

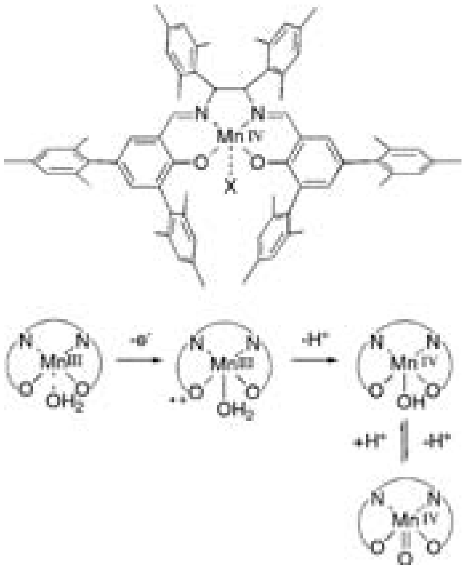

Figure 2. Structure of Manganese(IV) Salen Complex synthesized in this study (upper) and protonation and deprotonation of Mn(IV)=O(Salen) complex (bottom).

3. Chiral Distortion in a $Mn^{IV}(salen)(N_3)_2$ Derived from Jacobsen's Catalyst as a Possible Conformation Model for its Enantioselective Reactions[3]

The $Mn^{IV}(salen)(N_3)_2$ complex (**3**) from Jacobsen's catalyst is synthesized, and the X-ray crystal structures of **3** as well as the starting $Mn^{III}(salen)(N_3)(CH_3OH)$ complex (**2**) are determined in order to investigate the conformation of the high-valent Mn^{IV}(salen) molecule in comparison with that of Mn^{III}(salen). The asymmetric unit of the crystal of **3** contains four complexes, all of which adopt a nonplanar stepped conformation effectively distorted by the chirality of the diimine bridge. The asymmetric unit of **2** also contains four complexes. Two of them show a stepped conformation of a lesser degree, but the other two adopt a bowl-shaped conformation. Comparison of the structural parameters shows that the Mn center in **3** is coordinated from both sides by two external axial N_3 ligands with significantly shorter bond length, which could induce greater preference for the stepped conformation in **3**. The CH_3CN solution of **3** shows circular dichroism with a significantly strong band at 275 nm as compared to **2**, suggesting that **3** may adopt a more chirally-distorted conformation also in solution. The circular dichroism spectrum of **3** is slightly altered with isodichroic points from 298 to 253 K, and shows no further change at temperatures lower than 253 K, suggesting that the solution of **3** contains equilibrium between two conformers, where a low-energy conformer with more chiral distortion is predominantly favored even at room temperature. **2** and **3** are thoroughly characterized using various techniques including cyclic voltammetry, magnetic susceptibility, UV-vis, electron paramagnetic resonance, ^{1}H NMR, infrared spectroscopy and electrospray ionization mass spectrometry.

Figure 3. Equilibrium between stepped and bowl-shaped conformations of Mn(salen), which is directed by the position of the Mn center from the basal N_2O_2 ligand plane.

References

1) M. Kujime, C. Izumi, T. Tomura, M. Hada and H. Fujii, *J. Am. Chem. Soc.* **130**, 6088–6098 (2008).
2) T. Kurahashi, A. Kikuchi, T. Tosha, Y. Shiro, T. Kitagawa and H. Fujii, *Inorg. Chem.* **47**, 1674–1686 (2008).
3) T. Kurahashi and H. Fujii, *Inorg. Chem.* **47**, 7556–7567 (2008).

Fabrication of Silicon-Based Planar Ion-Channel Biosensors and Integration of Functional Cell Membrane Model Systems on Solid Substrates

Department of Life and Coordination-Complex Molecular Science
Division of Biomolecular Sensing

URISU, Tsuneo	Professor
TERO, Ryugo	Assistant Professor
MAO, Yangli	IMS Fellow
KIM, Yong-Hoon	Research Fellow
CHIANG, Tsung-Yi	Research Fellow
ZHANG, Zhen-Long	Graduate Student
UNO, Hidetaka	Graduate Student
SAYED, Abu	Graduate Student
NAKAI, Naohito	Graduate Student
ASANO, Toshifumi	Graduate Student
SHANG, Zhi-Guo	Graduate Student
FUJIWARA, Kuniyo	Graduate Student
SHIMIZU, Atsuko	Secretary

We are interested in the investigation of cell membrane surface reactions and the pathogen mechanism of the neurodegenerative diseases, based on the molecular science. We are advancing two subjects, aiming the creation and development of new molecular science field, “medical molecular science.” One is the development of ion channel biosensor and its application to the neural network analyzer device. The other is the fundamental understanding of bilayer membrane properties using the artificial lipid bilayers on solid substrates, which is called supported bilayers, by means of atomic force microscope and fluorescence microscope-based techniques.

1. The Morphology of $GM1_x/SM_{0.6-x}/Chol_{0.4}$ Planar Bilayers Supported on SiO_2 Surfaces[1)]

Ganglioside GM1 (GM1), sphingomyelin (SM) and cholesterol (Chol) are dominant lipid components of rafts in plasma membranes. The morphology of supported planar bilayers composed of GM1, SM and Chol (Figure 1) on SiO_2 surfaces has been studied by atomic force microscopy and fluorescence microscopy. The component ratio of the SPB ($GM1_x/SM_{0.6-x}/Chol_{0.4}$) was varied in the range of $x = 0$–0.25. The unique changes in morphology depending on the GM1 concentrations (Figure 2) are qualitatively explained by hydrogen bonding and the hydrophobic interactions between SM and Chol, and by hydrogen bonding and the steric effects between bulky GM1 headgroups under Ca^{2+} existing conditions and the electrostatic repulsion between the negative charges of GM1 headgroups under Ca^{2+} nonexisting conditions.

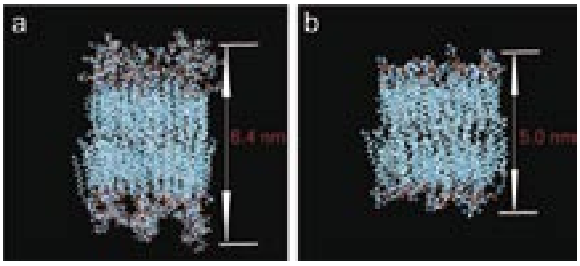

Figure 1. Membrane structure of (a) GM1/SM/Chol (1:2:2 molar ratio) and (b) SM/Chol (1:1 molar ratio) obtained by MD simulation.

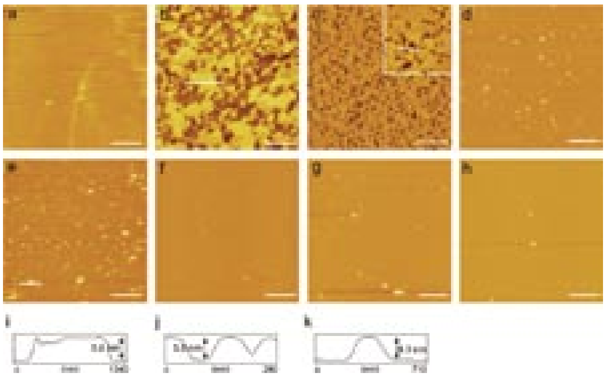

Figure 2. AFM images and line profiles of $GM1_x/SM_{0.6-x}/Chol_{0.4}$ SPBs formed on SiO_2 surface in a buffer solution containing Ca^{2+} with different GM1 content (molar ratio): (a) $x = 0$, (b) $x = 0.05$, (c) $x = 0.1$ (insert is magnified image (1.0×1.0 μm^2)), (d) $x = 0.15$, (e) $x = 0.2$, and (f) $x = 0.25$. Also, AFM images of $GM1_x/SM_{0.6-x}/Chol_{0.4}$ SPBs formed without Ca^{2+}: (g) $x = 0.1$ and (h) $x = 0.2$. (i), (j), and (k) correspond to line profiles along white lines of (b), (c), and (e). Scale bar is 1.0 μm.

2. Lipid Bilayer Membrane with Atomic Step Structure: Supported Bilayer on Step-and-Terrace $TiO_2(100)$ Surface[2)]

Formation of a supported planar lipid bilayer (SPLB) and its morphology on step-and-terrace rutile-$TiO_2(100)$ surfaces were investigated by fluorescence microscopy and atomic force microscopy. The $TiO_2(100)$ surfaces consisting of atomic steps and flat terraces were formed on a rutile-TiO_2 single crystal wafer by a wet-treatment and annealing under oxygen flow. Intact vesicular layer formed on the $TiO_2(100)$ surface when the surface was incubated in a sonicated vesicle suspension in the condition that a full-coverage SPLB forms on SiO_2, as reported in previous studies. However a full-coverage, continuous and fluid SPLB was obtained on the step-and-terrace $TiO_2(100)$ depending on the lipid concentration, incubation time and vesicle size. The SPLB on the $TiO_2(100)$ also has the step-and-terrace morphology following the substrate structure precisely even though the SPLB is in the fluid phase and ~1 nm thick water layer exists between the SPLB and the substrate. This membrane distortion on the atomic scale affects the phase separation structure of a binary bilayer in micrometer order (Figure 3). The interaction energy calculated including DLVO and non-DLVO factors shows that a lipid membrane on the $TiO_2(100)$ gains 20 times larger energy than on SiO_2. This specifically strong attraction on TiO_2 makes the fluid SPLB precisely follow the substrate structure of angstrom order.

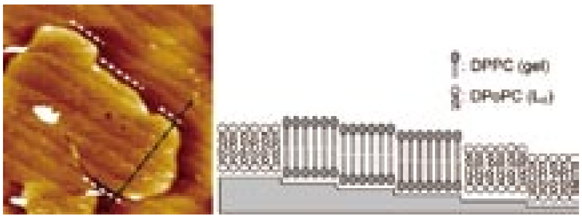

Figure 3. AFM topograph (2.0×2.0 μm^2) of the DPPC+DPoPC binary SPLB. The gel-phase domain edges running along the substrate steps are indicated by white dashed lines. The schematic illustration shows the cross-sectional view perpendicular to the substrate steps, like the black dashed-dotted line in the AFM image.

3. New Infrared Reflection Absorption Spectroscopy System for in-situ Observation of Adsorbed Biomaterials on Solid Surfaces under Water

In situ under water infrared reflection absorption spectroscopy (IRRAS) is an attractive vibration spectroscopy for biomaterials adsorbed on the IR non-transparent materials such as gold substrates, which are important in many biosensors and biochips such as DNA chips and surface plasmon resonance (SPR). We have constructed a new IRRAS system in which the sample solution is confined in the narrow space between CaF_2 prism surface and the substrate surface, and the IR beam is directed onto the substrate surface passing through the prism. The sample holders are designed to keep the thickness highly constant between the prism surface and the substrate surface during the measurements. It is essentially important, in the present system, to make sure of the condition that sample proteins are adsorbed on the substrate surface but not on the prism surface. The quite different condition in this point between fibronectin (FN) and immunoglobulin G (IgG) was well explained by the charge of the amino acid residue and the salt effects. Clear amide I bands were successfully observed under water for FN adsorbed on the SiO_2 surface (Figure 4a) and IgG on the gold surface (Figure 4b).

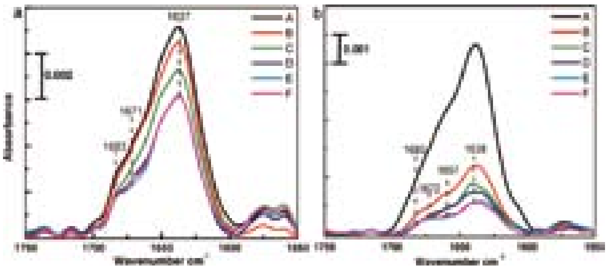

Figure 4. Amide I bands of adsorbed proteins on the substrate surfaces observed by in-situ IRRAS under D_2O solution. a) Spectra of FN using pure D_2O as the solvent; A, B, C, D, E and F. b) Spectra of IgG using NaCl (140 mM) added D_2O based PBS solution; A, B, C, D, E and F. A) Spectra for protein injection and waiting 3 h (FN) and 1h (IgG) for adsorption on solid surface. Spectra were taken every after 0.5 ml D_2O solution flushes; B) 0.50 ml C) 1.0 ml D) 1.5ml E) 2.0 ml F) 2.5 ml.

4. Development of Cell Culture Type Planar Ion Channel Biosensor for Nerve Cell Signaling Analysis[3)]

We have developed a new planar ion channel biosensor with cell culture function using SOI (Silicon On Insulator) substrate. This sensor enables not only the miniaturization of the sensor size and the high throughput screening application, but also is capable of the long time and the time lapse measurements that are difficult in the conventional any planar and pipette patch-clamp methods. The surface of SOI substrate was coated by patterned extracellular matrix (ECM), such as fibronectin and poly-L-lysine, to promote the cell adhesion and control the growth area at the preliminary designed position. TRPV1 (Transient receptor potential vanilloid type 1) channel-expressing single HEK293 cell was positioned on the micropore of the SOI substrate. Whole-cell arrangement was formed by the perforated patch using nystatin. The ion channel current was successfully measured by capsaicin stimulations. Experiments using mouse cerebral cortex cell is now under way.

References

1) Y. Mao, R. Tero, Y. Imai, T. Hoshino and T. Urisu, *Chem. Phys. Lett.* **460**, 289–294 (2008).
2) R. Tero, T. Ujihara and T. Urisu, *Langmuir* **24**, 11567–11576 (2008).
3) Z. L. Zhang, T. Asano, H. Uno, R. Tero, M. Suzui, S. Nakao, T. Kaito, K. Shibasaki, M. Tominaga, Y. Utsumi, Y. L. Gao and T. Urisu, *Thin Solid Films* **516**, 2813–2815 (2008).

Development of Fluorescent and Bioluminescent Proteins for Imaging Biomolecules

Department of Life and Coordination-Complex Molecular Science
Division of Biomolecular Sensing

OZAWA, Takeaki	Associate Professor*
TAKEUCHI, Masaki	Assistant Professor
HIDA, Naoki	IMS Fellow
MUHAMMAD, Awais	Post-Doctoral Fellow

Current focus on biological research is to quantify and visualize biomolecules in living cells and animals. To probe biomolecular functions and dynamics, we are exploring a new way for developing fluorescent and bioluminescent reporter proteins based on protein splicing and complementation techniques. The reporter proteins can be utilized to development of analytical methods for detecting protein–protein interactions, intracellular localization of proteins and their dynamics, enzyme activities, gene expression and production of small biomolecules.

1. Development of Multicolor Bioluminescent Probes for Protein–Protein Interactions in Living Subjects

Bimolecular complementation using luminescent proteins has a potential to perform reversible and multiplex detection of protein–protein interactions in opaque or auto-fluorescent living subjects. We constructed multicolor luciferase fragments, of which sensitivity and signal-to-background ratio were considerably improved by using an engineered carboxy-terminal fragment of a click beetle luciferase and amino-terminal fragments of luciferases with different spectral characteristics. We investigated complementation of split luciferases from firefly (PpyLuc), click beetle in green (ELuc) and click beetle in red (CBRLuc). The N- and C-terminal fragments were fused to FK506-binding protein (FKBP) and FKBP-binding domain (FRB). A pair of the fusion proteins was co-expressed in mammalian cells and the luminescence intensities were examined by a luminometer. Amino- and carboxy-fragments of individual luciferase were found complement enough to recover the bioluminescence upon interaction between FKBP and FRB in the presence of rapamycin. But, no cross complementation was detected when combination of different luciferase fragments was used. To make cross complementation possible, a new C-terminal fragment that has an ability to complement multiple N-terminal fragments was developed by the random mutagenesis. A mutant of the C-terminal fragment including three point mutations (mcLuc1) showed most remarkable properties, which enabled complement to all the N-terminal fragments of PpyLuc, CBR and ELuc. The signal-to-background ratio upon using McLuc1 was improved higher than that of the native one. The competitive inhibitor FK506 prevented rapamycin-induced luciferase activity generated by McLuc1 and N-terminal PpyLuc, confirming that their complementation is reversible. Thus, McLuc1 allowed new complementation partners of all the N-terminal luciferases, which can be widely used for monitoring protein-protein interactions in living cells.

2. Bioluminescence Imaging of Kinase-Induced Interactions Among Bad, 14-3-3, and Bcl-2 in Living Mice

To demonstrate the applicability of the complementation of multicolor split luciferases in mammals, we used three proteins of Bad, 14-3-3 and Bcl-2, which are known to regulate cell survival. In the presence of growth factors, Bad is phosphorylated, thereby interacting with the 14-3-3 protein. Upon deprivation of growth factors, Bad is dephosphorylated and consequently, binds to Bcl-2. The Bad protein was fused to McLuc1, while the 14-3-3 and Bcl-2 proteins were fused to N-terminal fragments of ELuc and PpyLuc, respectively. The fusion constructs were co-transfected into COS-7 cells and photon counts were evaluated. A strong intensity of bioluminescence was obtained from the cells including Bad and 14-3-3 proteins, indicating that Bad interacts 14-3-3 endogenously. To confirm that the increase in the luminescence signal was indeed triggered by the interaction of Bad and 14-3-3, we constructed Bad mutants in which several serine residues were replaced by alanine. These serine residues are necessary for interaction of Bad with 14-3-3. The luminescence signals were significantly reduced upon expression of 14-3-3 with these Bad mutants in the cells. We next used the same construct of Bad-McLuc1 for the analysis of interaction with Bcl-2. Strong bioluminescence was obtained upon overexpression of Bad-McLuc1 and Bcl-2 connected with N-terminal PpyLuc in COS-7 cells. Addition of Bcl-2 inhibitors resulted in reducing the luminescence, demonstrating that three fragments of McLuc1, N-terminal ELuc and PpyLuc can be used for detecting interactions of a protein associated with multiple distinct protein partners.

3. Bioluminescence Imaging of Kinase-Induced Interaction of pSmad1-Smad4 in *Xenopus laevis* Embryo

To evaluate usefulness of the reversible and high-sensitive complementation analysis with McLuc1, we used a heteromeric complex between Smad1 and Smad4 involved in cytoplasmic signaling of the bone morphogenetic protein (BMP) in a *Xenopus laevis* embryo. The embryo has a large amount of fluorescent yolk, which often hampers fluorescence imaging. We constructed a set of probes consisting of Smad1 connected with N-terminal PpyLuc and Smad4 connected with McLuc1. The probes were expressed in COS-7 cells containing either constitutive active form of transmembrane receptor (ALK3), or its dominant negative form (DL). The cells expressing ALK3 resulted in a strong luminescence in comparison to the cells expressing DL receptor or mock-transfected cells. A Smad1 mutant lacking phosphorylation sites showed negligible luminescence, indicating that the phosphorylated Smad1 interacted with Smad4, thereby resulting in complement of the luciferase fragments in living cells. Next, we synthesized mRNA from each cDNA construct of the probes and microinjected into the cell embryo. The embryonic development was monitored under the fluorescence microscope equipped with a CCD camera. From an early stage, a weak but significant signal of luminescence started to be detected in the trunk region of neural tube, and thereafter the signal became intense along the entire neural tube from head to tail. The signal was sustained up for a while, but changed faint gradually, indicating dissociation between Smad1 and Smad4. These results demonstrate that bioluminescence complementation imaging using the McLuc1 and N-terminal PpyLuc enabled spatial and temporal imaging of protein-protein interactions acting on the endogenous cellular signaling in living *Xenopus* embryos.

4. A Genetically Encoded Luminescent Indicator for Detecting Intracellular Cyclic GMP in Living Cells and Plants

In order to quantify and image cellular signaling processes in living cells and subjects, we developed a new analytical method using a luciferase. The principle is based on intramolecular complementation of the split fragments of luciferase. The split fragments of luciferase are fused to a cGMP-binding domain of phosphodiesterase (PDE). When concentration of cGMP increases in cytosol, interaction of cGMP with its binding domain of PDE causes a conformational change in the domain structure. The amino- and carboxyl-terminal fragments of luciferase are brought to come together, and full-length luciferase is reconstituted thereafter. After this luminescent indicator for cGMP was transiently expressed in HEK293 cells, a membrane permeable cGMP analog or a chemical (sodium nitroprusside) was added to the cell lysates or the living cells in the presence of luciferin. We found that luminescence intensities increased with increasing concentrations of the chemicals, which were detected by a luminometer or luminescent microscope. When the indicator was transiently expressed in *Arabidopsis* cells, chemicals that induce salt or osmotic stress were added to the cell lysates or the living cells. We also detected increases in the luminescence intensities upon stimulating stress-inducing chemicals. Thus, we demonstrated quantitative detection and imaging of ligand-induced increases of cGMP in living cells and plants.

References

1) T. Ozawa and Y. Umezawa, *Methods Mol. Biol.* **390**, 269–280 (2007).
2) T. Ozawa and Y. Umezawa, *Methods Mol. Biol.* **390**, 119–130 (2007).
3) C. Wei, M. Yamoto, W. Wei, Z. Zhao, K. Tsumoto, T. Yoshimura, T. Ozawa and Y. J. Chen, *Med. Clin. North Am.* **91**, 889–898 (2007).

---

* Present Position; Professor, The University of Tokyo

Heterogeneous Catalytic Systems for Organic Chemical Transformations in Water

Department of Life and Coordination-Complex Molecular Science
Division of Complex Catalysis

UOZUMI, Yasuhiro	Professor
YAMADA, Yoichi M. A.	Assistant Professor*
OSAKO, Takao	Assistant Professor
OE, Yohei	IMS Fellow†
HAMASAKA, Go	IMS Fellow
MATSUURA, Yutaka	Post-Doctoral Fellow
TAKENAKA, Hiroe	Research Fellow
HIRAI, Yoshinori	Research Fellow
BEPPU, Tomohiko	Graduate Student
WATANABE, Toshihiro	Graduate Student
KOBAYASHI, Noboru	Graduate Student
TORII, Kaoru	Technical Fellow
SASAKI, Tokiyo	Secretary
TANIWAKE, Mayuko	Secretary

Various organic molecular transformations catalyzed by transition metals were achieved under heterogeneous aqueous conditions by use of amphiphilic resin-supported metal complexes or convoluted polymeric metal catalysts which were designed and prepared by this research group. In particular, highly stereoselective asymmetric π-allylic substitution and oxidative cyclization, both of which were performed in water under heterogeneous conditions with high recyclability of the polymeric catalysts, are highlights among the achievements of the 2007–2008 period to approach what may be considered ideal chemical processes of next generation. Representative results are summarized hereunder.

1. Development of Tightly Convoluted Polymeric Phosphotungstate Catalysts and Their Application to Oxidative Cyclization of Alkenols and Alkenoic Acids[1)]

Tightly convoluted polymeric phosphotungstate catalysts were prepared via ionic-assembly of $H_3PW_{12}O_{40}$ and poly(alkylpyridinium)s. An oxidative cyclization of various alkenols and alkenoic acids was efficiently promoted by the polymeric phosphotungstate catalyst in *aq*. H_2O_2 in the absence of organic solvents to afford the corresponding cyclic ethers and lactones in high yield. The catalyst was reused four times without loss of catalytic activity. The polymeric phosphotungstate was unambiguously characterized by spectro- and microscopic studies (MAS $^{31}P\{^1H\}$ NMR, IR spectroscopy, elemental analysis, TEM, SEM, and EDS).

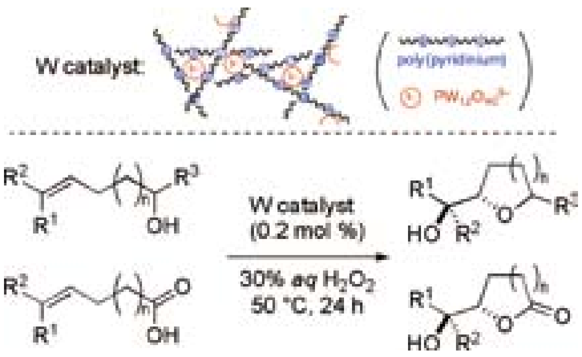

Scheme 1. Oxidative Cyclization of Alkenyl Alcohols and Alkenoic Acids with a Convoluted Polymeric Phosphotungstate.

2. Allylic Substitution of *meso*-1,4-Diacetoxycycloalkenes in Water with an Amphiphilic Resin-Supported Chiral Palladium Complex[3)]

Asymmetric π-allylic substitution of *meso*-1,4-diacetoxycyclopentene and *meso*-1,4-diacetoxycyclohexene with various nucleophiles was performed with an amphiphilic polystyrene-poly(ethylene glycol) (PS-PEG) resin-supported chiral imidazoindole phosphine-palladium complex in water as a single reaction medium under heterogeneous conditions to give the corresponding 1-acetoxy-4-substituted cycloalkenes with up to 99% ee.

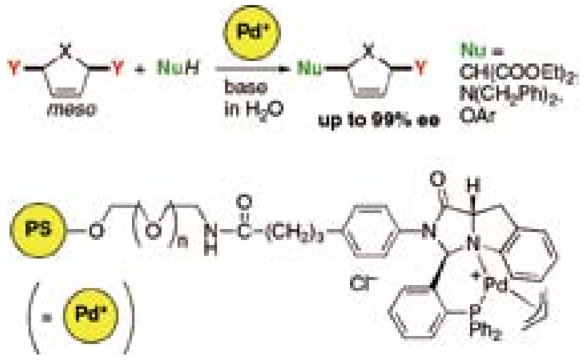

Scheme 2. Enantioselective Desymmetrization of *meso*-Cycloalkenyl Diacetate in Water with an Amphiphilic Resin-Supported Complex.

3. π-Allylic Sulfonylation in Water with Amphiphilic Resin-Supported Palladium-Phosphine Complexes[4)]

π-Allylic substitution of allyl esters with sodium arylsulfinate was performed with an amphiphilic polystyrene-poly(ethylene glycol) (PS-PEG) resin-supported phosphine-palladium complex in water as a single reaction medium under heterogeneous conditions to give allyl sulfones in good to high yields. Catalytic asymmetric allylic substitution of cycloalkenyl esters also took place in water using a PS-PEG resin-supported chiral imidazoindolephosphine-palladium complex to give cycloalkenyl sulfones with up to 81% ee.

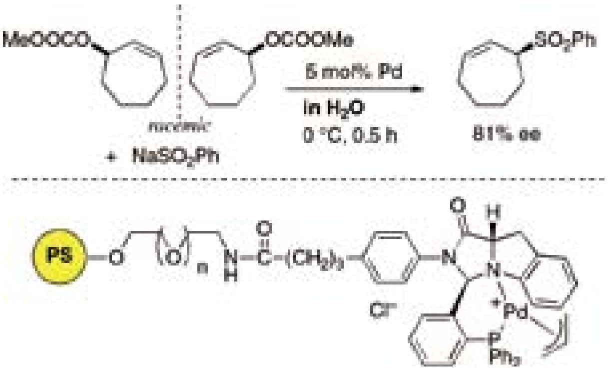

Scheme 3. Enantioselective Sulfonation of Cycloalkenyl Esters in Water with an Amphiphilic Resin-Supported Complex.

4. Highly Efficient Heterogeneous Aqueous Kharasch Reaction with an Amphiphilic Resin-Supported Ruthenium Catalyst[5)]

An amphiphilic polystyrene-polyethylene glycol (PS-PEG) resin-supported ruthenium complex was designed and prepared. The polymeric Ru complex was found to promote the transition metal-catalyzed atom transfer radical addition of halogenated compounds to olefins, the Kharasch reaction, in water under heterogeneous as well as AIBN-free conditions with a high level of atom-economy to meet green chemical requirements.

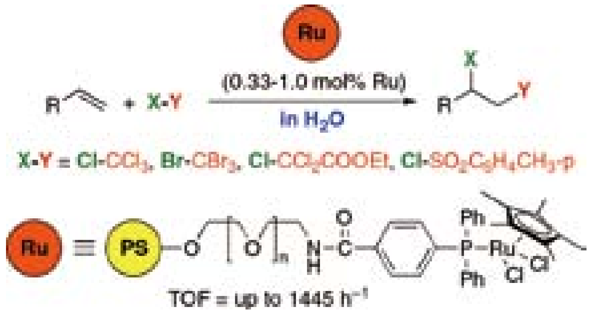

Scheme 4. Kharasch Reaction in Water with an Amphiphilic Resin-Supported Ruthenium Complex.

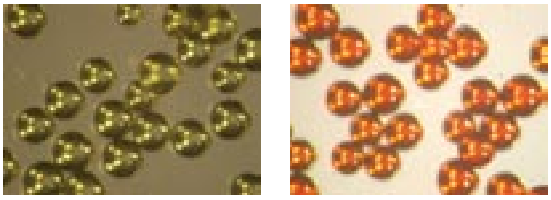

Figure 1. Microscopic Images of PS-PEG-NHCO-C_6H_4-PPh_2 (left) and PS-PEG-NHCO-C_6H_4-PPh_2-$RuCpCl_2$ (right).

References

1) Y. M. A. Yamada and Y. Uozumi, *Tetrahedron* **63**, 8492–8498 (2007).
2) Y. Uozumi, *Pure Appl. Chem.* **79**, 1481–1489 (2007).
3) Y. Uozumi, H. Takenaka and T. Suzuka, *Synlett* 1557–1561 (2008).
4) Y. Uozumi and T. Suzuka, *Synthesis* 1960–1964 (2008).
5) Y. Oe and Y. Uozumi, *Adv. Synth. Catal.* **350**, 1771–1775 (2008).

Award

YAMADA, Yoichi M. A.; The Commendation for Science and Technology by the Minister of Education, Culture, Sports, Science and Technology: The Young Scientists' Prize 2008.

---

* Present Address; RIKEN, Wako, Saitama 351-0198

† Present Address; Doshisha University, Kyotanabe, Kyoto 610-0321

Synthesis of Metal Complexes Aiming to Convert between Chemical Energy and Electrical One

Department of Life and Coordination-Complex Molecular Science
Division of Functional Coordination Chemistry

TANAKA, Koji	Professor
WADA, Tohru	Assistant Professor
OZAWA, Hironobu	IMS Fellow
KOSHIYAMA, Tamami	Post-Doctoral Fellow
FUKUSHIMA, Takashi	Post-Doctoral Fellow
TSUKAHARA, Yuhei	Graduate Student
YAMAGUCHI, Yumiko	Secretary
NAKAGAKI, Shizuka	Secretary

Metal ions involved in various metal proteins play key roles to generate metabolic energies through redox reactions of organic molecules. Metal complexes that have an ability to oxidize organic molecules at potentials more negative than reduction of dioxygen are feasible energy converter between chemical energy and electrical one. Some of high valent Ru=O complexes obtained by sequential proton and electron loss of the corresponding aqua-Ru complexes are proven to be active for the oxidation of organic molecules. However, the oxidation potentials of those aqua complexes to prepare high valent Ru=O ones are too positive to use as an energy transducer. We have succeeded smooth conversion from aqua to oxo ligands on Ru-dioxolene framework through proton coupled intramolecular electron transfer from the deprotonated form of the Ru–OH moiety to the dioxolene ligand (eq 1). The aqua-oxo conversion using the unique redox behavior of Ru–dioxolene frameworks allowed us to isolate an unprecedented metal-oxo radical complex.

$$[Ru^{II}(dbQ)(trpy)(OH_2)]^{2+} \underset{+H^+}{\overset{-H^+}{\rightleftharpoons}} [Ru^{II}(dbQ)(trpy)(OH^-)]^+$$

$$(dbQ = dibutylquinone) \quad \underset{+H^+}{\overset{-H^+}{\rightleftharpoons}} [Ru^{II}(dbSQ)(trpy)(O^{-\bullet})]^0 \qquad (1$$

In addition to elucidation of the reactivity of Ru-oxyl radical complexes as electrocatalysts toward the oxidation of organic molecules, we are also aiming to develop multi-electron reduction of small inorganic molecules such as CO_2, N_2, and H_2O under mild reactions conditions, which would be key reactions to construct a renewable society. The difficulty in reductive activation of those molecules is attributable to the undesirable formation of high energy intermediates that are produced during stepwise one-electron transfer to the reaction centers. Recently, we showed that a mononuclear $[Ru^{II}(pbn)(bpy)_2]^{2+}$ (bpy = 2,2'-bipyridine, pbn = 2-(2-pyridyl)benzo[b]-1,5-naphthyridine) ($[\mathbf{1}]^{2+}$) is smoothly converted to $[Ru(pbnH_2)(bpy)_2]^{2+}$ ($[\mathbf{1}HH]^{2+}$) by not only electrochemical but also photochemical reductions in the presence of proton (eq 2). Furthermore, the resultant $[Ru(pbnH_2)(bpy)_2]^{2+}$ works as a functional model as the nicotinamide adenine dinucleotide $NAD^+/NADH$ redox reaction that plays a key role in a reservoir/source of two electrons and one proton in various biological energy transfer systems.

(2

1. Photochemical and Radiolytic Production of an Organic Hydride Donor with a Ru^{II} Complex Containing an NAD$^+$ Model Ligand

The Ru-pbn complex with an $NAD^+/NADH$ model ligand, $[Ru(bpy)_2(pbn)]^{2+}$ ($[\mathbf{1}]^{2+}$), which acts as a catalyst in the electrochemical reduction of acetone to 2-propanol, similar to the enzymatic $NAD^+/NADH$. The complex $[\mathbf{1}]^{2+}$ undergoes the reversible $pbn^{-\bullet}/pbn$ redox reaction at –0.72, V versus SCE in CH_3CN, which shows pH dependent (59 mV/pH) between pH 2 and 11 in H_2O, indicating the occurrence of one-electron reduction coupled with a proton-transfer reaction. The excited state of $[\mathbf{1}]^{2+}$ was reductively quenched by an amine to produce the one-electron-reduced species in dry organic solvents. The one-electron-reduced species is a pbn ligand radical anion and is stable in CH_3CN. On the other hand, continuous photolysis ($\lambda > 300$ nm) of a CH_3CN/triethanolamine (TEOA) solution (4 :1, v/v) containing $[\mathbf{1}](PF_6)_2$ produced $[(\mathbf{1})HH]^{2+}$ with a quantum yield of 0.21 at l = (355±6) nm. Single crystals of $[(\mathbf{1})HH](PF_6)_2 \cdot 2CH_3CN$ is similar to that of $[\mathbf{1}]^{2+}$ except for the pbn and $pbnH_2$ ligands. Elongation of the C8–C10 and C8–C12 bonds of $[(\mathbf{1})HH]^{2+}$ (1.510(4) and 1.498(6)) compared with those of $[\mathbf{1}]^{2+}$ (1.376(10) and 1.399(9)) demonstrates the

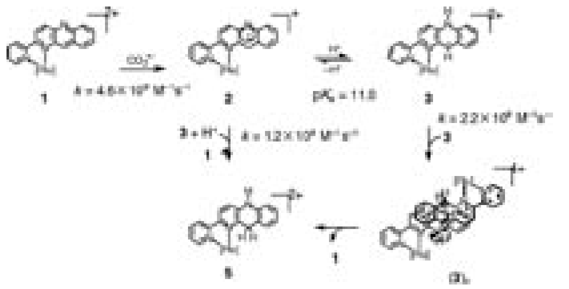

Scheme 1. The mechanism for photochemical two-electron reduction of $[\mathbf{1}]^{2+}$.

formation of the 1,4-dihydropyridine framework in the pbnHH ligand (eq 2). Reduction of $[\mathbf{1}]^{2+}$ by $CO_2^{-\bullet}$ is first order in the concentration of $[\mathbf{1}]^{2+}$ and the protonation is very fast in a pH range from 3 to 13. A bimolecular decay of the transient species $[(\mathbf{1})H]^{2+}$ reveals that the species reacts via disproportionation to form $[\mathbf{1}]^{2+}$ and $[(\mathbf{1})HH]^{2+}$. Thus, the photochemical reduction of $[\mathbf{1}]^{2+}$ produces $[(\mathbf{1})HH]^{2+}$ without accompanying undesirable the carbon-centered radical–radical coupling of $[\mathbf{1}]^{+}$ or $[H(\mathbf{1})]^{2+}$ radicals because of the steric interaction associated with the bulky $\{Ru(bpy)_2\}$ moiety. The photochemical two-electron reduction of $[\mathbf{1}]^{2+}$ is reasonably explained by Scheme 1. The initial step is one-electron reduction of $[\mathbf{1}]^{2+}$ by $CO_2^{-\bullet}$ affording (**2**), and the following rapid protonation of the nitrogen atom (**3**). The resultant neutral pbnH$^{\bullet}$ radical ligand (**3**) forms a π–π complex ((**3**)$_2$). The subsequent electron coupled proton transfer or hydrogen atom transfer from one neutral pbnH$^{\bullet}$ to another one in the π–π complex produces the equimolar amount of $[\mathbf{1}]^{2+}$ and $[\mathbf{1}HH]^{2+}$. The finding of the photochemical two-electron reduction through disproportionation affording an equimolar amount of the oxide and two-electron reduced forms (Scheme 1) opens a new era for the photochemical multi-electron reduction of metal complexes, since the repeat of the photochemical two-electron reduction of the pbn moiety allowed smooth photochemical four-electron reduction of an analogous $[Ru(bbnp)(trpy)]^{2+}$ (bbnp = 2,6-bis(benzo[b]-1,5- naphthyridin-6-yl)-4-*tert*-butylpyridine) under illumination of visible light in CH_3CN/TEOA by (eq 3).

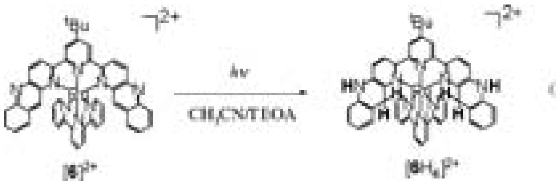

(3)

2. Water Oxidation by a Ruthenium Complex with Noninnocent Quinone Ligands: Possible Formation of an O–O Bond at a Low Oxidation State of the Metal

We have reported that a novel dinuclear Ru complex, $[Ru_2(OH)_2(3,6\text{-}Bu_2Q)_2(btpyan)](SbF_6)_2$ (3,6-Bu_2Q = 3,6-ditertbutyl-1,2-benzoquinone, btpyan = 1,8-bis-(2,2':6',2"-terpyrid4'-yl)anthracene), that contains redox active quinone ligands and has an excellent electrocatalytic activity for water oxidation (TON > 35000) when immobilized on an ITO electrode (*Inorg. Chem.* **40**, 329–337 (2001)). The novel features of the dinuclear and related mononuclear Ru species with quinone ligands, and comparison of their properties to those of the Ru analogues with the bpy ligand (bpy = 2,2'-bipyridine) replacing quinone, are discussed together with new theoretical and experimental results that show striking features for both the dinuclear and mononuclear species. The identity and oxidation state of key mononuclear species, including the oxyl radical, have been reassigned. Gas-phase theoretical calculations indicate that the Ru-dinuclear catalyst seems to maintain predominantly Ru(II) centers while the quinone ligands and water moiety are involved in redox reactions throughout the entire catalytic cycle for water oxidation. Theoretical study identifies $[Ru_2(O_2^-)(Q^{-1.5})_2(btpyan)]^0$ as a key intermediate and the most reduced catalyst species that is formed by removal of all four protons before four-electron oxidation takes place. The over all reaction mechanism for the four-electron oxidation of water catalyzed by the dinucler Ru complex is shown in Scheme 2.

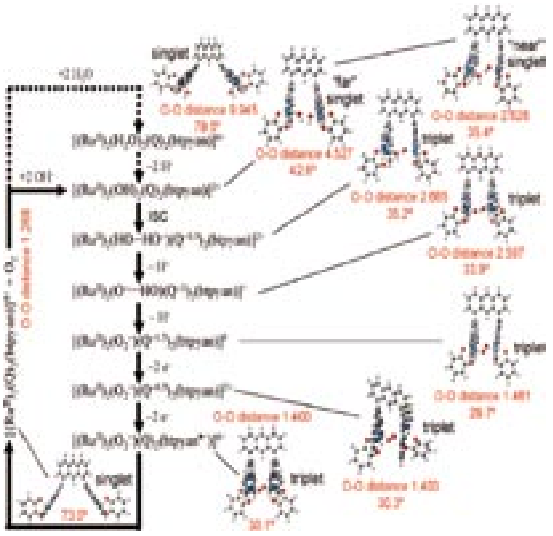

Scheme 2. The mechanism of eight-electron of water catalyzed by a Ru dinuclear complex.

References

1) (a) D. Polansky, D, Cabelli, J. Muckerman, E. Fujita, T. Koizumi, T. Fukushima, T. Wada and K. Tanaka, *Angew. Chem., Int. Ed.* **46**, 5728–5730 (2007). (b) H. Tannai, T. Koizumu and K. Tanaka, *Angew. Chem., Int. Ed.* **46**, 7112–7115 (2007).

2) (a) T. Koizumi and K. Tanaka, *Angew. Chem., Int. Ed.* **44**, 5891–5894 (2005). (b) J. Muckerman, D. Polansky, T. Wada, K. Tanaka and E. Fujita, *Inorg. Chem.* **47**, 3958–3968 (2008).

Synthesis and Reactions of Transition Metal Complexes Having Aryloxide-Based Ligands, Especially with Regard to Activation of Small Molecules

Department of Life and Coordination-Complex Molecular Science
Division of Functional Coordination Chemistry

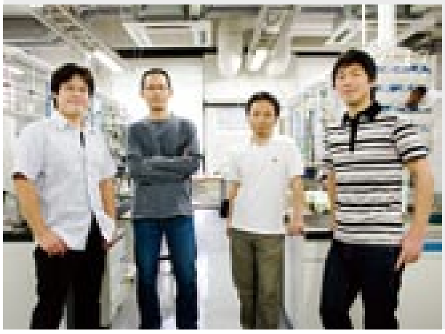

KAWAGUCHI, Hiroyuki	Associate Professor*
ISHIDA, Yutaka	Assistant Professor[†]
WATANABE, Takahito	IMS Fellow[†]
AKAGI, Fumio	Post-Doctoral Fellow[‡]

This project is focused on the design and synthesis of new ligands that are capable of supporting novel structural features and reactivity. Currently, we are investigating multidentate ligands based on aryloxide and thiolate. In addition, we set out to study metal complexes with sterically hindered aryloxide and arylthiolate ligands. Our recent efforts have been directed toward activation of small molecules.

Development of ligands that play important roles in coordination chemistry has been the subject of intense interest. The chemistry of metal aryloxide complexes has shown that aryloxide ligands can promote various important transformations at metal centers. Therefore, aryloxide ligands complement the well-studied cyclopentadienyl-based systems, with the major difference being the greater reactivity of the aryloxide complexes due to their relatively higher unsaturation and lower coordination numbers for a $(\mathrm{ArO})_n\mathrm{M}$ fragment. However, coordinatively unsaturated metal complexes undergo facile ligand redistribution reactions, which are occasionally a severe obstacle to synthetic efforts.

One of strategies for overcoming this problem is the use of covalently linked ancillary ligands, thereby limiting ligand mobility and leaving little possibility to reorganize the molecule. This feature might lead to the isolation and structural characterization of a number of metal complexes that are difficult to obtain with aryloxide monodentate ligands.

1. Diniobium Tetreahydride Complex Bearing a Tripodal Triaryloxide Ligand[1)]

We previously reported the synthesis of early transition metal hydride complexes supported by a linear triaryloxide ligand. As part of our studies of ancillary ligand effects, we recently began to study transition metal complexes with a tripodal triaryloxide ligand $[\mathbf{O}_3]^{3-}$. The $[\mathbf{O}_3]$ ligand provides a rigid and facial donor environment. Herein, we were interested in extending this chemistry to niobium.

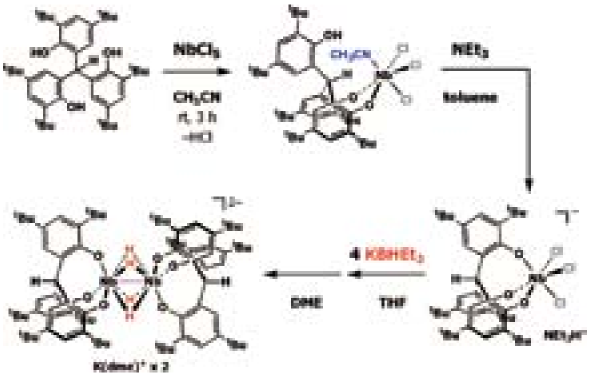

Figure 1. Synthesis of the hydride complex.

Treatment of NbCl$_5$ with the pro-ligand $\mathrm{H_3}[\mathbf{O}_3]$ in CH$_3$CN to give $\mathrm{H}[\mathbf{O}_3]\mathrm{NbCl_3(CH_3CN)}$ in 77% yield. The remaining hydroxy group in the nitrile adduct was deprotonated by NEt$_3$ in toluene at 80 °C, yielding $[\mathrm{NEt_3H}][(\mathbf{O}_3)\mathrm{NbCl_3}]$ as a red powder in 92%. An X-ray structure analysis of the trichloride complex reveals that the triaryloxide ligand coordinates to Nb facially.

Reaction of the trichloride complex with 4 equivalents of KBHEt$_3$ in toluene/THF followed by recrystallization from DME gave yellow crystals of $[\mathrm{K(dme)}]_2[\{(\mathbf{O}_3)\mathrm{Nb}\}_2(\mu\text{–H})_4]$ in 66% yield along with evolution of H$_2$. During the reaction, KBHEt$_3$ partially acts as a reductant, and the metal center is reduced from Nb(V) to Nb(IV). The deuterated analogue was quantitatively prepared by treatment of the hydride complex under D$_2$ gas for three days at room temperature and was characterized by NMR spectroscopy.

An X-ray crystal structure determination of the hydride complex reveals a dimeric structure with two $[(\mathbf{O}_3)\mathrm{Nb}]$ fragments bridged by four hydride ligands. The short Nb–Nb distance of 2.5690(5) Å indicates metal–metal bonding, thus accounting for the observed diamagnetism. The NMR spectra of the hydride complex are consistent with its solid-state structure if a fluxional process is invoked to explain the observed equivalence of the aryloxide groups on the NMR timescale at 25 °C. The bridging hydrides are observed as a broad signal at 6.29 ppm in the ^1H NMR spectrum. Upon cooling the sample, we did not detect any significant change in the hydride region.

2. Dinitrogen Activation by the Hydride Complex

Activation of molecular nitrogen by soluble metal complexes has attracted widespread attention from both fundamental and practical points of view. Dinitrogen cleavage by metal hydride complexes could be important in a catalytic system and is relevant to the Harber-Bosch process and a biological nitrogen-fixing system constituted by the metalloenzyme nitrogenase. Although late-transition-metal hydride complexes are often found to weakly bind dinitrogen with concomitant elimination of H_2, conversion of an early-transition-metal hydride to a dinitrogen complex is a rarely documented phenomenon.

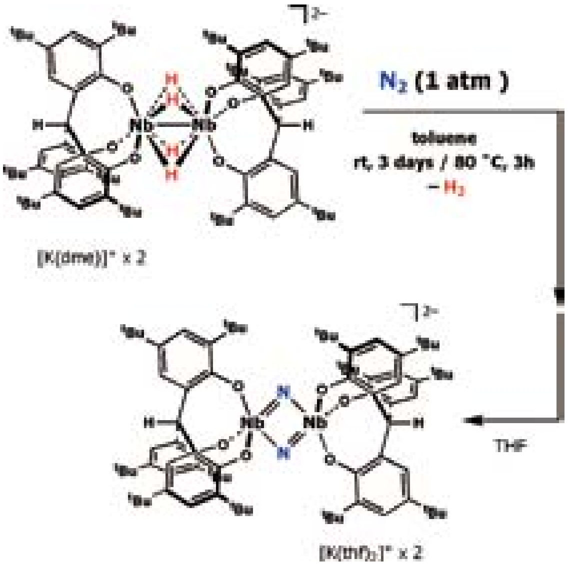

Figure 2. Reaction of the hydride complex with N_2.

The diniobium tetrahydride complex appears to be thermally stable in solution under argon, while exposure of its toluene solution to an atmosphere of N_2 at room temperature resulted in a gradual color change from maroon to yellow brown for 3 days. Recrystallization from THF/pentane gave $[K(thf)_2]_2[\{(\mathbf{O}_3)Nb\}_2(\mu\text{–}N)_2]$ as yellow crystals in 37% yield. The isotopically labeled complex was prepared analogously under $^{15}N_2$ and exhibits a single resonance at 311 ppm in the ^{15}N NMR spectrum. This result confirms that the origin of the nitride ligands is added N_2. In the ^1H NMR spectrum, the nitride complex possesses high symmetry in solution, as equivalent aryloxide groups are observed.

An X-ray crystal structure determination of the nitride complex has shown it to be dimeric, constructed around a planar Nb_2N_2 four-membered ring that resides on a pseudo-two-fold axis. Reduction of dinitrogen by the hydride complex results in cleavage of the N≡N bond, as evidenced by the N–N separation of 2.589(5) Å. Each niobium center displays five-coordinate, distorted trigonal-bipyramidal coordination.

The nucleophilic behavior of the nitride groups was observed in the reaction with methyl iodide. The nitride complex was treated with excess of methyl iodide at room temperature to afford $[K(thf)][\{(\mathbf{O}_3)Nb\}_2(\mu\text{-}N)(\mu\text{-}NMe)]$. When the reaction mixture was carried out at 60 °C for 5 days, the remaining nitride was methylated, giving a bis-imide complex $[\{(\mathbf{O}_3)Nb\}_2(\mu\text{-}NMe)_2]$.

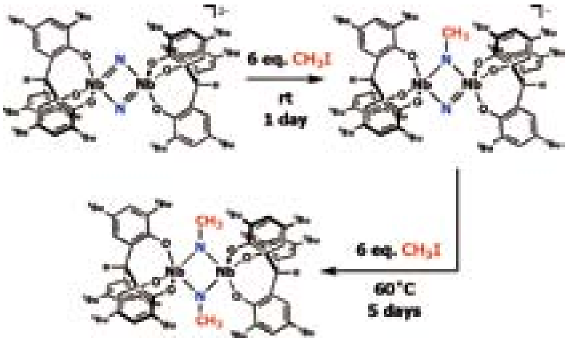

Figure 3. Reaction of the nitride complex with MeI.

Reduction of N_2 utilizing the hydride complex as described here is closely related to work by Fryzuk *et al.*, who used the tantalum(IV) hydride complex $[\{(\mathbf{NPN})Ta\}_2(\mu\text{-}H)_4]$ ([**NPN**] = $PhP(CH_2SiMe_2NPh)_2$). This complex was found to react with N_2 through partial loss of H_2 to give the dinitrogen complex $[\{(\mathbf{NPN})Ta\}_2(\mu\text{-}\eta^1\text{:}\eta^2\text{-}N_2)(\mu\text{-}H)_2]$, in which two hydride ligands remain coordinated. Subsequent treatment with boranes, silanes, and zirconium hydrides resulted in N_2 triple bond cleavage of the coordinated N_2 molecule. In our case, the cleavage proceeded spontaneously and did not require external reducing agent. This process corresponds to an overall six-electron reduction of N_2, in which two electrons are initially stored in a metal–metal bond, and four additional electrons are provided by H_2 elimination.

Reference

1) F. Akagi, T. Matsuo and Y. Ishida, *Angew. Chem., Int. Ed.* **46**, 8778–8781 (2007).

---

* Present Position; Professor, Department of Chemistry, Tokyo Institute of Technology, Ookayama, Meguro-ku, Tokyo 152-8551

† Present Adress; Department of Chemistry, Tokyo Institute of Technology, Ookayama, Meguro-ku, Tokyo 152-8551

‡ Present Adress; Department of Materials Science and Environmental Engineering, Tokyo University of Science, Yamaguchi, Sanyo-onodashi, Yamaguchi 756-0884

Visiting Professors

Visiting Professor

ITOH, Shinobu *(from Osaka University)*

Dioxygen Activation Mechanism by Copper Proteins and Their Models

The structure and reactivity of copper/active-oxygen complexes have attracted much interest during the past decades because of their potential relevance to biological systems and numerous copper-catalyzed oxidation reactions. In our laboratory, we have been studying the reactivity of several types of copper/active-oxygen species such as mononuclear and dinuclear copper(II)-peroxo and copper(III)-oxo complexes in order to evaluate the catalytic mechanism of copper oxygenases and to develop efficient oxidation catalysts for organic synthesis.

Visiting Associate Professor

HASEGAWA, Miki *(from Aoyama Gakuin University)*

Development of Lanthanide Complexes with Novel Optical Properties by the Coordination Chemistry

The 4f-electrons of the lanthanides, which are the key to developing functional molecules such as molecular magnets and emissive compounds, are shielded by the 5d and 6s orbitals. The interrelation of molecular design and functionality has not been established yet, because the electronic structure of f-elements is more complicated than that of d-block ions. Coordination chemistry is useful in this context. For instance, we succeeded in manipulating the ff-emission selectively by tuning the energy state of the ligand with some substituents. In addition, molecular arrangements on ultra-thin films have been used to induce polarized optical behavior. These approaches are based on our concepts to develop high-efficient optical materials under a scientific strategy. The ff-transitions of lanthanide complexes can be observed easily, but the underlying theory is not sufficient yet. We are ambitious to control the optical functionality of lanthanide ions with the help of coordination chemistry.

Visiting Associate Professor

TAKAHASHI, Satoshi *(from Osaka University)*

Dynamics of Protein Folding by Single Molecule and Ensemble Techniques

Protein is a linear macromolecule that has a unique property to fold to a specific three-dimensional structure from fully unfolded conformations. We are interested in the physical principles that connect the unfolded and the folded conformations of proteins. To detect fast kinetic processes involved in protein folding, we use rapid mixing device for the time resolved observation of average protein structures. To observe heterogeneity and dynamic fluctuations, we use single molecule observation systems. Based on the ensemble measurements on several proteins using small angle X-ray scattering and circular dichroism spectroscopy, we proposed “collapse and search” mechanism of protein folding. The recent application of single molecule fluorescence measurements clarified a relatively slow conformational dynamics in the unfolded state. We are hoping to obtain important information required for the protein structure prediction and design through the further examination of protein folding dynamics.

RESEARCH FACILITIES

The Institute includes five research facilities. This section describes their latest equipment and activities. For further information please refer to older IMS Annual Review issues (1978–2007).

UVSOR Facility

KOSUGI, Nobuhiro	Director
KATOH, Masahiro	Professor
SHIGEMASA, Eiji	Associate Professor
KIMURA, Shin-ichi	Associate Professor
HIKOSAKA, Yasumasa	Assistant Professor
ITO, Takahiro	Assistant Professor
MOCHIHASHI, Akira	Assistant Professor*
ADACHI, Masahiro	Assistant Professor
HORIGOME, Toshio	Technical Associate
NAKAMURA, Eiken	Technical Associate
YAMAZAKI, Jun-ichiro	Technical Associate
HASUMOTO, Masami	Technical Associate
SAKAI, Masahiro	Technical Associate
HAYASHI, Kenji	Technical Associate
KONDO, Naonori	Technical Associate
HAGIWARA, Hisayo	Secretary

Outline of UVSOR

The UVSOR accelerator complex consists of a 15 MeV injector linac, a 600 MeV booster synchrotron, and a 750 MeV storage ring. The magnet lattice of the storage ring is the so-called double-bend achromat. The double RF system is routinely operated for the user beam time, and the lifetime of the electron beam has been improved to around 6 hours at 200 mA. The storage ring is normally operated under multi-bunch mode with partial filling. The single bunch operation is also conducted about two weeks per year, which provides pulsed synchrotron radiation (SR) for time-resolved experiments. Initial beam currents stored under multi-bunch and single-bunch modes are 350 mA and 70 mA, respectively.

Eight bending magnets and three insertion devices are available for utilizing SR. The bending magnet with its radius of 2.2 m provides SR, whose critical energy is 425 eV. After completing the upgrade project, there are 14 beamlines available in total (13 operational, and 1 under construction) at UVSOR, which can be classified into two categories. 9 of them are the so-called “Open beamlines,” which are open to scientists of universities and research institutes belonging to the government, public organizations, private enterprises and those of foreign countries. The rest of the 5 beamlines are the so-called “In-house beamlines,” which are dedicated to the use of the research groups within IMS. We have 1 soft X-rays (SX) station equipped with a double-crystal monochromator, 8 EUV and SX stations (one of them is under construction) with a grazing incidence monochromator, 3 VUV stations with a normal incidence monochromator, 1 (far) infrared station equipped with FT interferometers, 1 station with a multi-layer monochromator.

Figure 1. Overview of the UVSOR storage ring room.

Collaborations at UVSOR

Variety of investigations related to molecular/material science is carried out at UVSOR by IMS researchers. In addition, many researchers outside IMS visit UVSOR to conduct their own research work. The number of visiting researchers per year tops about 800, whose affiliations extend to 60 different institutes. International collaboration is also pursued actively and the number of visiting foreign researchers reaches over 80, across 10 countries. UVSOR invites new/continuing proposals for research conducted at the open beamlines twice a year. The proposals from academic and public research organizations (charge-free) and from enterprises (charged) are acceptable. The fruit of the research activities using SR at UVSOR is published as a UVSOR ACTIVITY REPORT annually. The refereed publications per year count more than 60 since 1996. In recent five years, the number of beamlines has been reduced from 22 to 14. The upgrade project of the UVSOR storage ring, in which the creation of four new straight sections and the achievement of much smaller emittance (27 nm-rad) were planned in 2002–2003, has been accomplished on schedule. The upgraded storage ring is named UVSOR-II. The numbers of users and related publications have shown an upward tendency, since 2004.

Highlights of Users' Researches 2007

1) Infrared Reflection-Absorption Spectroscopy of Alq_3 Thin Film on Silver Surface Using Synchrotron Radiation

Y. Sakurai, S. Kimura, K. Seki *(UVSOR, Nagoya Univ.)*

Recently, organic semiconductors are attracting attention because of possible applications to electronic devices such as organic light emitting diodes (OLEDs). In OLEDs, tris(8-hydroxyquinoline) aluminum (Alq_3) is most widely used as the electron transport/light emitting material. Alq_3 has two possible geometrical isomers of meridional (C_1 symmetry) and facial (C_3 symmetry) forms. It is important to find whether facial isomer exists at the interface between the metal and the Alq_3 film or not.

Vibrational spectroscopy such as infrared (IR) spectroscopy is suitable technique for distinguishing these isomers. We examined whether the facial isomer exists at the interface between the Ag and the Alq_3 film or not by infrared reflection-absorption spectroscopy (IRAS) using a synchrotron radiation (SR) light source. Use of highly brilliant infrared synchrotron radiation (IRSR) source enables us to obtain IRAS spectra in the low wavenumber region, which cannot be covered by conventional IRAS system using globar light source because of its low brilliance.

Figure 2 indicates the thickness dependence of the IRAS spectra of an Alq_3 film deposited on an Ag surface. The observed IRAS spectra suggest that the Alq_3 film predominantly consists of meridional isomer including the first monolayer adsorbed on the Ag surface. In the spectrum of monolayer Alq_3, Al–N stretching mode slightly shifts to the lower wavenumber side than that of multilayer Alq_3, possibly due to the charge transfer between the Alq_3 and Ag surface.

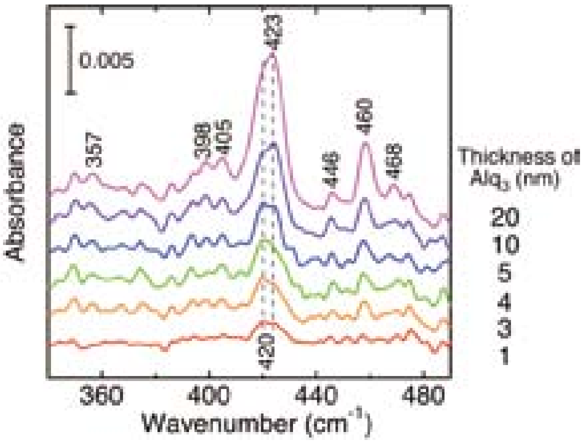

Figure 2. The thickness dependence of the IRAS spectra of an Alq_3 film on Ag surface.

2) Electronic Structure at Highly Ordered Organic/Metal Interfaces

H. Yamane, K. Kanai, K. Seki *(Nagoya Univ.)*

The electronic structure at the interface formed between an organic semiconductor film and a metal electrode plays a crucial role in the performance of electronic devices using organic semiconductors such as electroluminescent displays, field-effect transistors, and photovoltaic cells.

We have studied the electronic structure of well- ordered thin films of pentacene (Pn) molecules prepared on Cu(110) in the monolayer regime, by using angle-resolved UV photoemission spectroscopy. The Pn molecules on Cu(110) in the monolayer regime form a highly ordered film structure with planar adsorption geometry, where the molecular long axis is parallel to the $[1\bar{1}0]$ substrate direction.

Figure 3(a) and (b) shows the observed energy versus momentum $[E(\boldsymbol{k}_{\|})]$ relation for the flat-lying Pn monolayer film on Cu(110) along (a) $\phi = 0°$ (the $[1\bar{1}0]$ substrate direction) and (b) $\phi = 28°$. The selected raw ARUPS spectra of the valence levels and the secondary-electron cutoff are shown in Figure 3(c) and (d), respectively.

We found that the change in the work function upon the adsorption of the flat-lying Pn monolayer film is $\Delta = -0.9$ eV [Figure 3(d)] due to the formation of the interfacial dipole layer. We clearly observed the electronic structure characteristic of the interface with the following findings: (i) formation of the interface states with possible modification of the orbital symmetry and the energy position, and (ii) two-dimensional inter- molecular band dispersion of these interface states with the effective mass of the hole for the upper branch being 0.24 m_0 at 300 K.

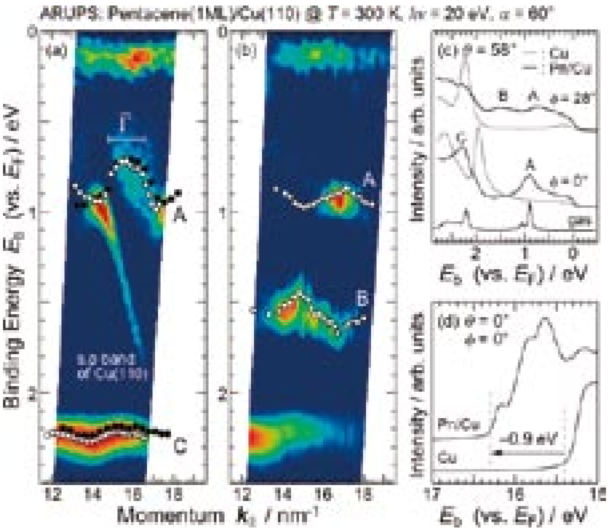

Figure 3. (a,b) $E(\boldsymbol{k}_{\|})$ relation for the highly ordered flat-lying Pn monolayer film on Cu(110) at ϕ = (a) 0° and (b) 28°. Open and filled circles indicate the position of the Pn-derived peaks measured at $h\nu$ = 20 and 30 eV, respectively. (c,d) Selected ARUPS spectra of the Pn monolayer film and the bare substrate for the regions of (c) valence levels and (d) secondary-electron cutoff.

---

* Present Address; JASRI

Research Center for Molecular Scale Nanoscience

YOKOYAMA, Toshihiko	Director, Professor
HIRAMOTO, Masahiro	Professor
NISHI, Nobuyuki	Professor
OKAMOTO, Hiromi	Professor
NAGAYAMA, Kuniaki	Professor (OIIB)
UOZUMI, Yasuhiro	Professor
NAGASE, Shigeru	Professor
OGAWA, Takuji	Professor
KATO, Koichi	Visiting Professor*
SUZUKI, Toshiyasu	Associate Professor
NAGATA, Toshi	Associate Professor
SAKURAI, Hidehiro	Associate Professor
NISHIMURA, Katsuyuki	Associate Professor
TANAKA, Shoji	Assistant Professor
TANAKA, Hirofumi	Assistant Professor
SAKAMOTO, Yoichi	Assistant Professor
NAGASAWA, Takayuki	Assistant Professor
HIGASHIBAYASHI, Shuhei	Assistant Professor
SASAKAWA, Hiroaki	Assistant Professor
NAKAO, Satoru	Post-Doctoral Fellow (NanoNet project)
SUGIHARA, Takahiro	Research Fellow†
NOTO, Madomi	Secretary
SUZUKI, Hiroko	Secretary
WATANABE, Yoko	Secretary
ITO, Yumi	Secretary (Nanonet project)
FUNAKI, Yumiko	Sectretary (Nanonet project)

Research Center for Molecular Scale Nanoscience was established in 2002 with the mission of undertaking comprehensive studies of “Molecular Scale Nanoscience.” The Center consists of one division staffed by full-time researchers (Division of Molecular Nanoscience), two divisions staffed by adjunctive researchers (Divisions of Instrumental Nanoscience and Structural Nanoscience), one division staffed by visiting researchers (Division of Advanced Molecular Science). Their mandates are

1) Fabrication of new nanostructures based on molecules
2) Systematic studies of unique chemical reactions
3) Systematic studies of physical properties of these nanostructures.

The Center administers offers public usage of the advanced ultrahigh magnetic field NMR (Nuclear Magnetic Resonance, 920 MHz) spectrometer not only for solution specimens but for solid samples. Since 2004 a number of collaborating researches with the 920 MHz NMR measurements have been examined. Figure shows the apparatus, together with a typical example of the NMR spectra, where one can easily find much better resolving power than that of a standard 500 MHz NMR spectrometer. (1) dynamic structures of biological macromolecules, (2) structure of bioactive natural products, (3) characterization of metal ion complexes and so forth. We will continuously call for the collaborating research applications using the 920MHz NMR spectrometer with a view to use the NMR of a wide scientific tolerance (*e.g.* structural biology, organic chemistry, catalyst chemistry, *etc*.).

Since 2005, Nanoforum has been organized, which supports small international/domestic meetings and seminars related to nanoscience. The Center also conducts the Nanotechnology Network Project of the Ministry of Education, Culture, Sports, Science and Technology (MEXT) as a core organization, and provides various kinds of nanotechnology public support programs to Japanese and foreign researchers. This project will be described in the other section in this book.

Figure 1. 920 MHz NMR spectrometer and an example measured using 920 and 500 MHz spectrometers. Much higher resolution in 920 MHz can be clearly seen.

---

* from Nagoya City University

† from JEOL Datum

Laser Research Center for Molecular Science

OHMORI, Kenji	Director, Professor
KATOH, Masahiro	Professor
OKAMOTO, Hiromi	Professor
OHSHIMA, Yasuhiro	Professor
MATSUMOTO, Yoshiyasu	Professor
TAIRA, Takunori	Associate Professor
HISHIKAWA, Akiyoshi	Associate Professor
ISHIZUKI, Hideki	Assistant Professor
WATANABE, Kazuya	Assistant Professor
UEDA, Tadashi	Technical Associate
CHIBA, Hisashi	Technical Associate
NAKAGAWA, Nobuyo	Secretary
MASUDA, Michiko	Secretary

The center aims to develop new experimental apparatus and methods to open groundbreaking research fields in molecular science, in collaboration with the Department of Photo-Molecular Science. Those new apparatus and methods will be served as key resources in advanced collaborations with the researchers from the community of molecular science. The main targets are (1) advanced photon sources covering wide energy ranges from terahertz to soft X-day regions; (2) novel quantum-control schemes based on intense and ultrafast lasers; and (3) high-resolution optical imaging and nanometric microscopy. The center also serves as the core of the joint research project “Extreme Photonics” between IMS and RIKEN.

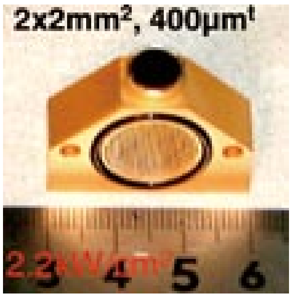

Figure 1. Microchip laser developed at the center.

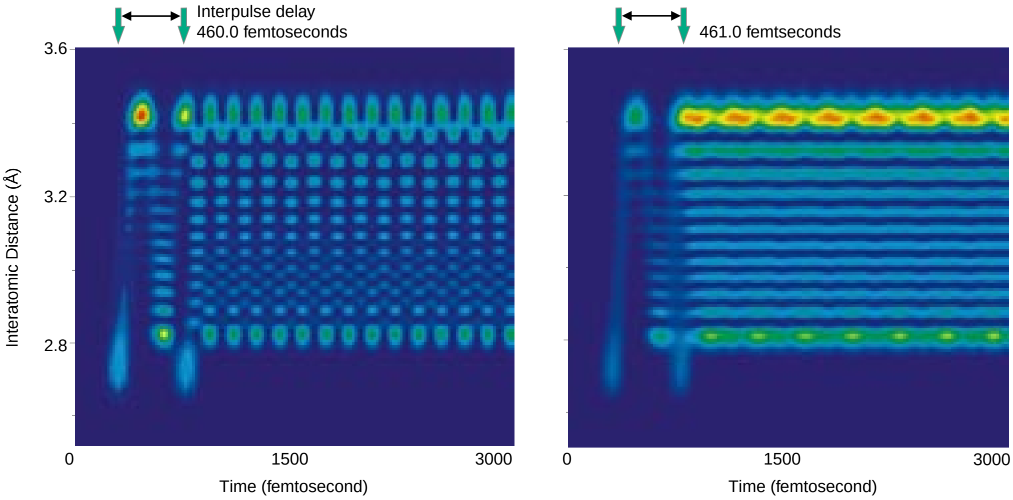

Figure 2. Theoretical simulation of quantum interferometric images generated in a single molecule with a pair of two laser pulses whose timing is controlled on the attosecond (10^{-18} sec) timescale.

Instrument Center

YAKUSHI, Kyuya	Director
YAMANAKA, Takaya	Technical Associate
TAKAYAMA, Takashi	Technical Associate
FUJIWARA, Motoyasu	Technical Associate
OKANO, Yoshinori	Technical Associate
MIZUKAWA, Tetsunori	Technical Associate
MAKITA, Seiji	Technical Associate
NAKANO, Michiko	Technical Associate
SAITO, Midori	Technical Associate
SAKAI, Yasuko	Secretary
OTA, Akiyo	Secretary

Instrument Center was organized in April of 2007 by integrating the general-purpose facilities of research center for molecular-scale nanoscience and laser research center for molecular science. The mission of Instrument Center is to support the in-house and external researchers in the field of molecular science, who are conducting their researches using general-purpose instruments such as ESR, x-ray diffractometer, fluorescence spectrometer, *etc*. The staffs of Instrument Center maintain the best condition of the machines, and provide consultation for how to use them. The main instruments are NMR (JEOL JNM-LA500, JEO JNM-LA400), mass spectrometer (Voyager DE-STR), powder x-ray diffractometer (Rigaku RINT-Ultima III), and circular dichroic spectrometer (JASCO JW-720WI) in Yamate campus and ESR (Bruker E680, E500, EMX Plus), SQUID magnetometer (Quantum Design MPMS-7, MPMS-XL7minTK), powder (MAC Science MXP3) and single-crystal (Rigaku Mercury CCD, RAXIS IV, 4176F07) diffractometer, dilution refrigerator (Oxford 400µ) with superconducting magnet (12 T), thermoanalysis system (TA TGA2950, DSC2920, SDT2960), fluorescence spectrophotometer (SPEX Fluorogll), UV-VIS-NIR (Hitachi U-3500) spectrophotometer, excimer+dye laser (LPX105i), Nd-YAG+OPO laser (GCR-250), and excimer laser (Complex 110F) in Myodaiji campus. Instrument Center provides liquid nitrogen and liquid helium using helium liquefiers. The staffs of Instrument Center provide consultation for how to treat liquid helium, and provide various parts necessary for low-temperature experiments. Instrument Center supports also the network sharing system of the chemistry-oriented instruments, which started in the April of 2007. In the fiscal year of 2007 (April 2007 to March 2008), Instrument Center accepted 27 applications from 27 institutions outside of IMS. The users mainly used SQUID (15), ESR (18), x-ray diffractometer (21), mass spectrometer (2), NMR (3), and Excimer-dye laser (2), where the numbers in parenthesis shows the number of use by external users.

Figure 1. High-Frequency/High-Field ESR Spectrometer (Bruker E680).

Figure 2. Matrix-Assisted Laser Desorption Ionization—Time of Flight Mass Spectrometer (Applied Biosystems Voyager DE-STR).

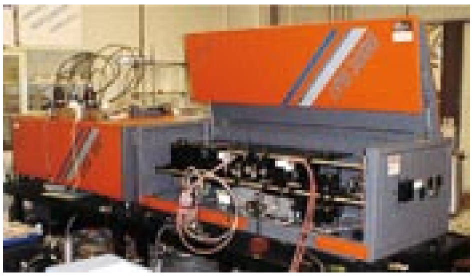

Figure 3. Excimer+dye laser (Lambda physics LPX 105i + LPD3002).

Equipment Development Center

URISU, Tsuneo	Director
MIZUTANI, Nobuo	Technical Associate
AOYAMA, Masaki	Technical Associate
YANO, Takayuki	Technical Associate
KONDOU, Takuhiko	Technical Associate
YOSHIDA, Hisashi	Technical Associate
UTCHIYAMA, Kouichi	Technical Associate
TOYODA, Tomonori	Technical Associate
NAGATA, Masaaki	Technical Associate
MIYASHITA, Harumi	Technical Fellow
TAKAMATSU, Yoshiteru	Technical Fellow
URANO, Hiroko	Secretary

Design and fabrication including the research and developments of the new instruments necessary for the molecular science are the mission of this center, which consists of the mechanical, electronics and glass work sections. We expanded our service to the outside researchers of universities and research institutes since 2005. The main aims of this new attempt are to contribute to the molecular science community and to improve the technology level of the center staffs.

The technical staff of the Equipment Development Center is engaged in planning, researching, designing and constructing high technology experimental instruments in collaboration with the scientific staff. And these experimental instruments are manufactured by incorporating with new technologies and new mechanical ideas. A part of our activity in the current fiscal year is described below.

Development of a Cell for a Gas-Phase Nuclear Magnetic Resonance Spectrometer

This project was proposed by Prof. Fuke (Department of Chemistry, Kobe University), who is developing a gas-phase NMR spectrometer. The apparatus was selected in System Development Program for Advanced Measurement and Analysis of JST (*Development of Systems and Technology for Advanced Measurement and Analysis*) in 2007, and it was adopted as the institution use of the latter period in 2007.

NMR spectroscopy is widely used for liquid and solid samples. The aim of the development is to extend the NMR application to the gaseous ions. The system consists of a FT ICR (ion cyclotron resonance) mass analyzer and a NMR spectrometer, and provides us NMR data of mass-selected ions. It is expected to be available with the gas phase molecular ions ($m/e < 2000$, $< 10^5$ /cm^3).

In this project, the NMR cell, which is mounted in 12T magnet, was designed and constructed. Since the magnetic bore (ϕ 155 mm × 2000 mm) is long and spatially limited, there are several difficult points for designing the cell. Figure 1 shows the schematic design of NMR cell. In order to trap slow-velocity ions in the NMR cell, the electrical noise aroused from RF magnetic fields must be efficiently suppressed. To overcome this problem, the electric wires were introduced through inside of the pipes which support the cell mechanically. A technical development was also required to mount a Cu mesh (95% transparency) on the NMR-cell electrodes. In addition to these, there are several technical problems, which we are now overcoming.

In this program, Mr. Horigome, who is the staff of UVSOR Facility, also cooperated to accomplish this joint development project. Because he has enough experience of making vacuum machinery.

We had several meetings with the researchers of Kobe University and discussed on the design of the cell. The NMR cell is going to be constructed in the latter period in 2008.

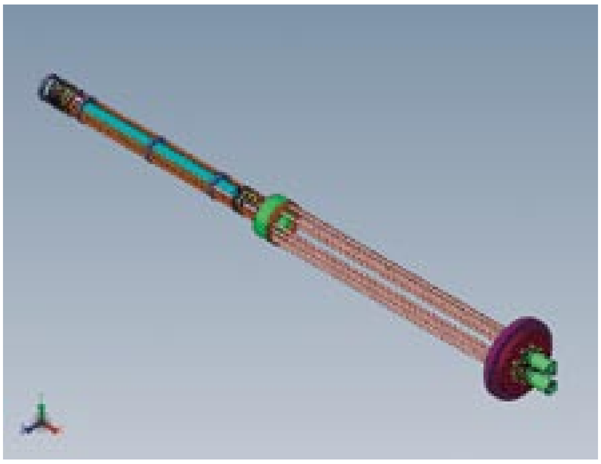

Figure 1. Schematic design of the NMR cell.

Fabrication of a Precision CNC Milling Machine

In recent years, micro fluidic channel is rapidly becoming important tools in wide science technology fields such as analytical chemistry and medical biology. The pattern of micro channels is usually fabricated by the photolithography. However, the photolithographic method requires complex chemical and mechanical processes and expensive photomasks. It is difficult to make a deep channel, and waste fluid processing an intractable problem. Due to these disadvantages of photolithographic method, importance of micromachining by cutting is becoming important. In relation to this, machine tool companies are selling various micro machinery tools. Moreover, needs for micromachining is also increasing in IMS. Based on these requirements, we started the developments of micromachining technology several years ago. However, since it is difficult to make precise microstructures by using old type machine due to large cutting errors, we decided to fabricate a precise CNC milling machine. As shown in Figure 2, this machine consists of a spindle, the xyz submicron stage and a substance microscope. We fixed the spindle to an auto collimator base which is used for coarse control. As shown in Figure 3, we made a mask for synchrotron radiation etching by using this machine. This mask has 25 through holes in a plate with 30 µm thickness. We thought it was difficult to make this by using our old type machine, and the importance of the new type of precise machinery has been demonstrated.

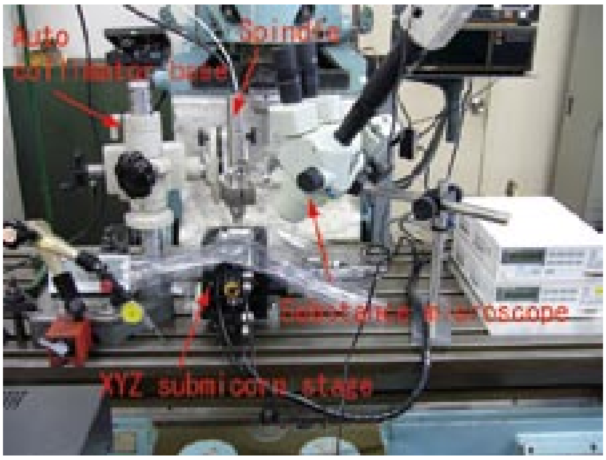

Figure 2. Newly developed Precision CNC milling machine.

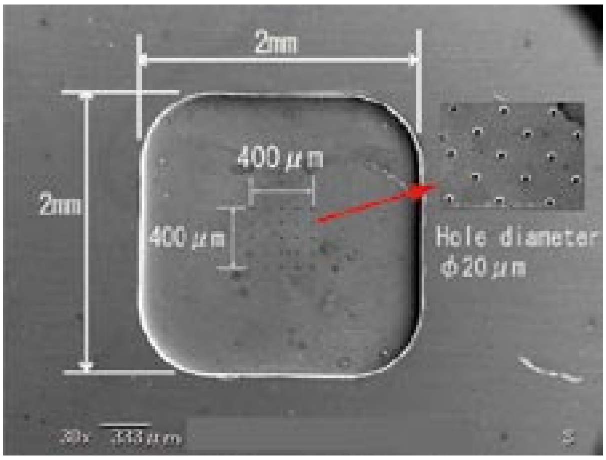

Figure 3. Mask for synchrotron radiation etching.

Research Center for Computational Science

HIRATA, Fumio	Director, Professor
SAITO, Shinji	Professor
EHARA, Masahiro	Professor
OONO, Hitoshi	Assistant Professor
ISHIDA, Tateki	Assistant Professor
KIM, Kang	Assistant Professor
MIZUTANI, Fumiyasu	Technical Associate
TESHIMA, Fumitsuna	Technical Associate
NAITO, Shigeki	Technical Associate
SAWA, Masataka	Technical Associate
IWAHASHI, Kensuke	Technical Associate
MATSUO, Jun-ichi	Technical Associate
NAGAYA, Takakazu	Technical Associate
TOYA, Akiko	Secretary
ISHIHARA, Mayumi	Secretary

Research Center for Computational Science, Okazaki Research Facilities, National Institutes of Natural Sciences, provides state-of-the-art computational resources and software to academic researchers in molecular science and related fields. The Center currently has over 600 users in 145 project groups from a wide range of molecular science, *i.e.* quantum chemistry, molecular simulation, chemical reaction dynamics and solid state physics. In order to meet a wide variety of users' demands, the computer systems consist of Fujitsu PRIMEQUEST, SGI Altix4700, and Hitachi SR-16000. These systems are linked to Internet through Science Information Network (SINET3).

The Center provides a number of state-of-the-art application programs, including Gaussian 03, GAMESS, Molpro, AMBER, NAMD, *etc*, which are installed to the computer systems and kept updated for immediate use of the users. The Center also maintains and offers the Quantum Chemistry Literature Database (QCLDB, http://qcldb2.ims.ac.jp/), which has been developed by the Quantum Chemistry Database Group in collaboration with staff members of the Center. The latest release, QCLDB II Release 2007, contains 97,718 data of quantum chemical studies. Detailed information on the hardware and software at the Center is available on the web site (http://ccinfo.ims.ac.jp/).

In addition to offering computer resources to molecular scientists, another vital aspect of the Center is to perform leading computational researches with massive computations. In 2003, the Center joined the National Research Grid Initiative (NAREGI) project, a three-year national project by National Institute of Informatics (NII) and IMS. This joint project aimed at developing grid computing system (NII) and thereby realizing extremely large-scale computational studies in the frontier of nanoscience (IMS). For these purposes, two supercomputer systems, Hitachi SR11000 and HA8000, were introduced to the Center in 2004, with combined performance exceeding 10 TFlops. In 2006, the NAREGI project was reformed to join a new national project Development and Application of Advanced High-Performance Supercomputer Project by RIKEN, where IMS plays an important role in the application of the PFlops-scale supercomputer to nanoscience. Further information on next-generation supercomputer project and computer systems at the Center is found on the web site (http://ims.ac.jp/nanogrid/).

Figure 1. Super-High-Performance Molecular Simulator.

Okazaki Institute for Integrative Bioscience

AONO, Shigetoshi	Professor
KUWAJIMA, Kunihiro	Professor
KATO, Koichi	Professor
FUJII, Hiroshi	Associate Professor
KURAHASHI, Takuya	Assistant Professor
YOSHIOKA, Shiro	Assistant Professor
MAKABE, Koki	Assistant Professor
YAMAGUCHI, Takumi	Assistant Professor
ISOGAI, Miho	Secretary
TANIZAWA, Misako	Secretary
TANAKA, Kei	Secretary

The main purpose of Okazaki Institute for Integrative Bioscience (OIIB) is to conduct interdisciplinary, molecular research on various biological phenomena such as signal transduction, differentiation and environmental response. OIIB, founded in April 2000, introduces cutting edge methodology from the physical and chemical disciplines to foster new trends in bioscience research. OIIB is a center shared by and benefited from all three institutes in Okazaki, thus encouraging innovative researches adequately in advance of academic and social demands. The research groups of three full professors and one associate professor who have the position in IMS join OIIB. The research activities of these groups are as follows.

Aono group is studying the bioinorganic chemistry of hemeproteins that show a novel function. They solved the structure and function relationships of the CO sensor protein CooA and O_2 sensor protein HemAT. They also reported the structure and function relationships of aldoxime dehydratase, which is a novel heme-containing dehydrase enzyme. Kato group is studying structure, dynamics, and interactions of biological macromolecules primarily using ultra-high field nuclear magnetic resonance (NMR) spectroscopy. In particular, they conducted studies aimed at elucidating the dynamic structures of glycoconjugates and proteins for integrative understanding of the mechanisms underlying their biological functions. Kuwajima group is studying mechanisms of *in vitro* protein folding and mechanisms of molecular chaperone function. Their goals are to elucidate the physical principles by which a protein organizes its specific native structure from the amino acid sequence. In this year, they studied the equilibrium and kinetics of canine milk lysozyme folding/unfolding by peptide and aromatic circular dichroism and tryptophan fluorescence spectroscopy. Fujii group is studying molecular mechanisms of metalloenzymes, which are a class of biologically important macromolecules having various functions such as oxygen transport, electron transfer, oxygenation, and signal transduction, with synthetic model complexes for the active site of the metalloenzymes. In this year, they studied molecular mechanisms of metalloenzymes relating to monooxygenation reactions and denitification processes.

OIIB is conducting the cooperation research program, “Frontiers of Membrane Protein Research,” with Institute for Protein Research, Osaka University from 2005. In this program, the following projects have being carried out to elucidate the role of membrane proteins in life: (i) the development of expression systems, purification methods, and chemical synthesis of membrane proteins, (ii) the development of new methods for analyzing the structure and function of membrane proteins. As a part of this cooperation program, International Symposium on Membrane Protein Research—Perspective in Structural Biology of Membrane Proteins and Biological Macromolecules was held in Osaka on March 22, 2008.

Safety Office

TANAKA, Koji	Director
TOMURA, Masaaki	Assistant Professor
TANAKA, Shoji	Assistant Professor
SUZUI, Mitsukazu	Technical Associate
YOSHIDA Hisashi	Technical Associate
NAGATA, Masaaki	Technical Associate
YAMANAKA, Takaya	Technical Associate
UEDA, Tadashi	Technical Associate
TAKAYAMA, Takashi	Technical Associate
HAYASHI, Kenji	Technical Associate
MAKITA, Seiji	Technical Associate
ONITAKE, Naoko	Secretary
TSURUTA, Yumiko	Secretary

The Safety Office was established in April 2004. The mission of the Office is to play a principal role in the institute to secure the safety and health of the staffs by achieving a comfortable workplace environment, and improvement of the working conditions. In concrete terms, it carries out planning, work instructions, fact-findings, and other services for safety and health in the institute. The Office is comprised of the following staffs: The Director of the Office, Safety-and-Health Administrators, Safety Office Personnel, Operational Chiefs, and other staff members appointed by the Director General. The Safety-and-Health Administrators patrol the laboratories in the institute once every week, and check whether the laboratory condition is kept sufficiently safe and comfortable to conduct researches. The Office also edits the safety manuals and gives safety training courses, for Japanese and foreign researchers.

SUPPORTING STAFF

Public Affairs Office

HIRATA, Fumio	Head
OHSHIMA, Yasuhiro	Vice-Head
HARADA, Miyuki	Technical Associate
NAKAMURA, Rie	Technical Fellow

Archives

YAKUSHI, Kyuya	Head
MINAMINO, Satoshi	Technical Associate
KIMURA, Katsumi	Professor Emeritus
SUZUKI, Satomi	Secretary

Technical Division

SUZUI, Mitsukazui	Head
OMARU, Tadakazu	Technical Fellow

Reception

OHHARA, Kyoko	Secretary
SUGIYAMA, Kayoko	Secretary
TSURUTA, Yumiko	Secretary
KAMO, Kyoko	Secretary
NOGAWA, Kyoko	Secretary

The commission of the Technical Division is mainly to provide support for maintaining and managing Research Centers and Facilities of IMS. Most of the members belong to these stations.

In addition, we also support Safety Office, Research groups, Public Affairs Office, Archives and Reception of the IMS.

The Research Centers and Facilities are;

(1) UVSOR Research Center: Operation and maintenance of the Synchrotron Radiation Facility and support of visiting researchers.

(2) Laser Research Center for Molecular Science: Maintenance of the laser devices and support of visiting researchers.

(3) Instrument Center: Maintenance and support of general-use research devices such as NMR, ESR, SQUID, MS, X-ray difractometers, dilution refrigerator and several kinds of spectrometers. The network system for efficient use of research equipments is also taken care for. Liquid nitrogen and liquid helium are also provided.

(4) Equipment Develop Center: R&D center consisting of mechanical engineering, electrical engineering and manufacturing of chemical glass tools.

(5) Research Center for Computational Science: Operation and maintenance of the computer resources including super computers and support of users outside IMS. In addition, Orion and IMS networks are maintained.

The annual meeting is regularly organized since 1975 for technical staff of research Institutes and Universities. Various technical problems related to research are discussed. The proceedings are published and stored in the computer server.

Special Research Projects

IMS has special research projects supported by national funds. Five projects in progress are:

(a) Next Generation Integrated Nanoscience Simulation Software
Development & Application of Advanced High-Performance Supercomputer Project
(b) Formation of Interdisciplinary and International Bases for Natural Sciences, NINS
"Development of New Computational Methods for Large-Scale Systems and Establishment of Advanced Simulation Center for Molecules and Materials"
(c) Extreme Photonics
(d) MEXT Nanotechnology Network
Nanotechnology Support Project in Central Japan: Synthesis, Nanoprocessing and Advanced Instrumental Analysis
(e) Inter-University Network for Efficient Utilization of Chemical Research Equipments

These five projects are being carried out with close collaboration between research divisions and facilities. Collaborations from outside also make important contributions. Research fellows join these projects.

(a) Next Generation Integrated Nanoscience Simulation Software Development & Application of Advanced High-Performance Supercomputer Project

A national project entitled, "Next Generation Integrated Nanoscience Simulation Software" was initiated on April 1, 2006 at Institute for Molecular Science (IMS). The project is a part of the "Development & Application of Advanced High-Performance Supercomputer Project" of MEXT, which aims to develop a next generation supercomputer and application software to meet the need in the computational science nation-wide.

The primary mission of our project is to resolve following three fundamental problems in the field of nanoscience, all of which are crucial to support society's future scientific and technological demands: (1) "Next Generation Energy" (*e.g.*, effective utilization of the solar energy), (2) "Next Generation Nano Biomolecules" (*e.g.*, scientific contributions toward overcoming obstinate diseases), and (3), "Next Generation Nano Information Function and Materials" (*e.g.*, molecular devices). In these fields, new computational methodologies and programs are to be developed to clarify the properties of nanoscale substances such as catalysts (enzymes), biomaterials, molecular devises, and so forth, by making the best use of the next generation supercomputer.

Among many application programs developed in the project, we have selected six programs, three from the molecular science and three from the solid state physics, as "core applications" in the nano-science, and concentrating our effort to tune those programs to the next generation machine. The programs in molecular science are concerned with the MD simulation, the quantum chemistry, and the statistical mechanics of liquids.

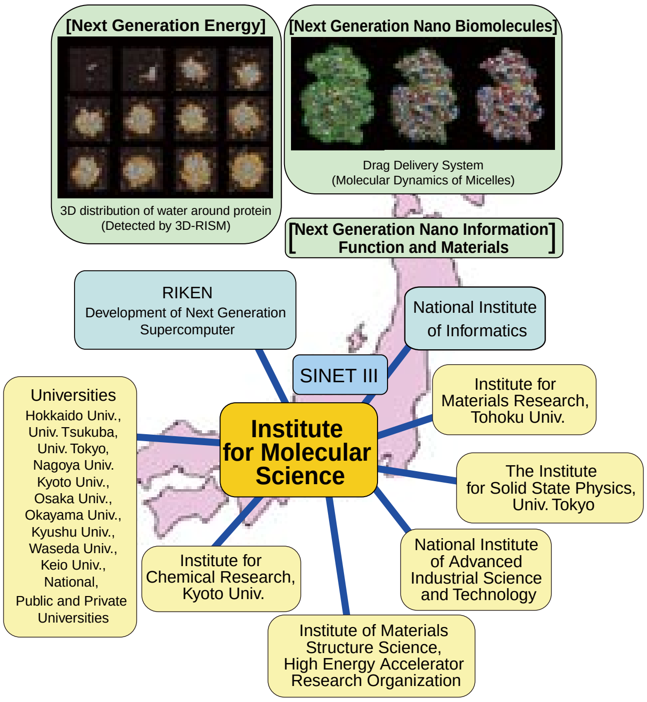

(b) Formation of Interdisciplinary and International Bases for Natural Sciences, NINS "Development of New Computational Methods for Large-Scale Systems and Establishment of Advanced Simulation Center for Molecules and Materials"

This project aims to establish a core computational science center for molecular and material systems and to develop advanced methodologies for large-scale calculations. We are trying to create a new interdisciplinary field by integrating the different views and methodologies in each field that belongs to a different hierarchy of natural sciences. Structures and dynamics of large-scale complex systems, such as nanomaterials and biological systems, are investigated with a variety of sophisticated computational methods based on theories of quantum and statistical mechanics, and so on. Seminars and workshops for the advanced calculations and for the development of human resources are also conducted by this project.

The project is organized by five institutes of the National Institutes of Natural Sciences, *i.e.* Institute for Molecular Science, National Astronomical Observatory of Japan, National Institute for Fusion Science, National Institute for Basic Biology, and National Institute for Physiological Sciences, and other universities and research institutes.

The followings are the research titles of groups participating from IMS:

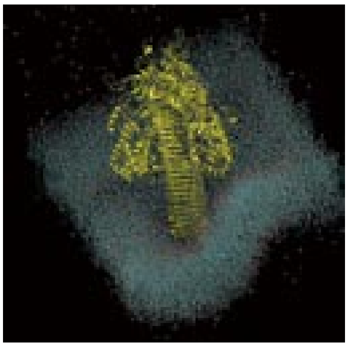

Massive molecular dynamics to simulate puncture of lipid bilayer by gp5.

EHARA, Masahiro	Theoretical Studies of Molecular Excited States and Chemical Reactions
HIRATA, Fumio	Theoretical Study of Molecular Recognition Based on the 3D-RISM Theory
NAGASE, Shigeru	Quantum Chemistry Calculations of Nanomolecules
NOBUSADA, Katsuyuki	Theoretical Calculations for Electron Dynamics Strongly Coupled to the Electromagnetic Field
SAITO, Shinji	Theoretical Studies of Condensed Phase Dynamics by Using Molecular Simulation
YONEMITSU, Kenji	Theory for Nonequilibrium Control of Collective Dynamics in Quantum-Classical Hybrid Many-Particle Systems
YANAI, Takeshi	Theory Development for Multireference Electronic Structures with ab initio Quantum Chemical Methods

(c) Extreme Photonics

Institute for Molecular Science has a long-standing tradition of promoting spectroscopy and dynamics of molecules and molecular assemblies. Accordingly, photo-molecular science is one of major disciplines in molecular science. This field is not confined in the traditional spectroscopy, but makes solid basis for other disciplines including nanoscience and bioscience, *etc*. Therefore, continuing developments in spectroscopy and microscopy are vital to enhance our abilities to elucidate more complex systems in time and spatial domains. In order to achieve full developments of photo-molecular science, we need to pursue three branches in developing: (1) new light source, (2) new spatio-temporally resolved spectroscopy, and (3) new methods to control atomic and molecular dynamics. Since 2005, we have started the program of "Extreme Photonics" in collaboration with the RIKEN institute. Currently 6 groups in IMS are involved in this program, and the specific research titles are as follows:

(1) Development of new light sources

TAIRA, Takunori	Micro Solid-State Photonics

(2) Development of new spatio-temporally resolved spectroscopy

OKAMOTO, Hiromi	Development of Extreme Time-Resolved Near-Field Spectroscopy
MATSUMOTO, Yoshiyasu	Development of Spatio-Temporally Resolved Spectroscopy for Surfaces and Interfaces

(3) Development of new methods to control atomic and molecular dynamics

OHMORI, Kenji	Development of Attosecond Coherent Control and Its Applications
HISHIKAWA, Akiyoshi	Reaction Imaging and Control with Extremely Short Laser Pulses
OHSHIMA, Yasuhiro	Quantum-State Manipulation of Molecular Motions by Intense Coherent Laser Pulses

(d) MEXT Nanotechnology Network Nanotechnology Support Project in Central Japan: Synthesis, Nanoprocessing and Advanced Instrumental Analysis

The Ministry of Education, Culture, Sports, Science and Technology (MEXT), Japan started the Nanotechnology Network Project in April 2007 in order to support Japanese nanotechnology researches not only for university and government researchers but also for private company researchers. IMS participates in this project as a core organization (project leader: YOKOYAMA, Toshihiko, Prof. & Director of Research Center for Molecular Scale Nanoscience) with Nagoya University (representative: BABA, Yoshinobu, Prof.), Nagoya Institute of Technology (representative: SUMIYAMA, Kenji, Prof.) and Toyota Technological Institute (representative: SAKAKI, Hiroyuki, Prof. & Vice President of TTI), and establishes a nanotechnology support center in central Japan area for these five years. We will support

1) Public usage of various advanced nanotechnology instruments such as ultrahigh magnetic field NMR (920 MHz), advanced transmission electron microscopes, and so forth
2) Design, synthesis and characterization of organic, inorganic and biological molecules and materials,
3) Semiconductor nanoprocessing using advanced facilities and technologies.

We will promote applications not only to each supporting element, but to combined usage of several supporting elements such as a nanobiotechnology field that is highly efficient in this joint project. In 2007 Oct.–2008 Spt., the number of accepted projects applied to IMS amounted 112 (the total number of days is 674).

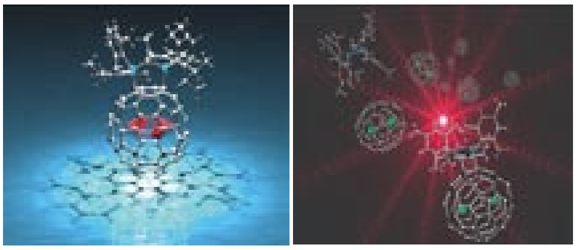

Example of the outstanding achievement obtained by the collaboration between the theoretical group (supported by Prof. Nagase) and the experimental user group (Prof. Akasaka *et al.* in University of Tsukuba). These pictures were published as the covers of *Chem. Comm.* of Jul. 24, 2007 and Feb. 7, 2008.

List of Supports in IMS

Person in Charge	Support Element
OKAMOTO, Hiromi	Space- and Time-Resolved Near-Field Microspectroscopy
YOKOYAMA, Toshihiko	Magneto-Optical Characterization of Surface Nanomagnetism
YOKOYAMA, Toshihiko	Electron Spectroscopy for Chemical Analysis
NISHI, Nobuyuki	Tunable Picosecond Raman Spectroscopy
HIRAMOTO, Masahiro	Fabrication and characterization of organic semiconductor devices
NISHI, Nobuyuki	300kV Transmission Analytical Electron Microscopy
YOKOYAMA, Toshihiko	Focus Ion Beam Processing & Field Emission Scanning Electron Microscopy
NAGAYAMA, Kuniaki	Phase Contrast Transmission Electron Microscopy for Nanobiological materials
YOKOYAMA, Toshihiko; KATO, Koichi	920 MHz NMR Spectrometer
OGAWA, Takuji	Preparation of Molecular Electronic Devices and Electric Conductivity Measurements
NAGASE, Shigeru	Quantum Chemical Calculation for Molecular Design
SUZUKI, Toshiyasu; NAGATA, Toshi; SAKURAI, Hidehiro	Synthesis & Design of Functional Organic Nanomaterials

(e) Inter-University Network for Efficient Utilization of Chemical Research Equipments

Academic and industrial activities in Chemistry in Japan have been world-leading over the past 30 years. Needless to say, it is highly important to improve the supporting environment for research and education in science and engineering. In particular, research equipments are advancing all the time to more intelligent and expensive ones, making measurement time shorter with higher reliability. It would be economic and efficient for the researchers and students of all national universities to share such equipments for performing high level research and education.

From 2007, we started the 5 year project “Functioning of Inter-University Network for Efficient Utilization of Chemical Research Equipments.” This network is operated through an internet machine-time reservation and charging system by the help of equipment managers and accounting sections in each university. All the universities are grouped into 12 regions and in each region the hub university organizes the regional committee for the operation of regional network system. There is no barrier for every user to access to any universities beyond his/her regional group.

Although the financial condition of the government is now extremely hard, the government decided to start this project in the end of 2006. In 2007, some starting budget was appropriated for preparing the new system and we started a trial network operation with 119 equipments offered by 55 universities and IMS. In 2008, the budget increased more than ten times and has been used for preparing a full-scale operation system of machine reservation/charging, and for repairing/upgrading of 19 instruments. In the end of August, the number of user registrants amounts to 4300 in 72 universities and IMS covering 1161 laboratories in Japan. From the fall of 2008, the registered equipment increases to 200. This may also increase the number of users and laboratories.

We believe that this innovative system can motivate and stimulate researchers and students to carry out new researches, and make chemistry research in Japan far more successful and active.

Okazaki Conference

The 67th Okazaki Conference
Molecular Science and Chemical Biology of Biomolecular Function

Organizers: Y. Mizutani (*Osaka Univ.*), S. Aono (*IMS, Okazaki Inst. Integ. Biosci.*), M. Fujii (*Tokyo Tech.*), K. Ishimori (*Hokkaido Univ.*), M. Saito (*Tohoku Univ.*), H. Sekiya (*Kyushu Univ.*), T. Tahara (*RIKEN*)

Invited Overseas Speakers: P. M. Champion (*Northeastern Univ.*), D. P. Giedroc (*Indiana Univ.*), M. T. Green (*Penn State Univ.*), B. H. Huynh (*Emory Univ.*), M. Lim (*Pusan National Univ.*), R. Walker (*Univ. Maryland*), R. Weinkauf (*Heinrich-Heine Univ. Düsseldorf*)

The 67th Okazaki Conference was held on Nov. 10–12, 2007 in Okazaki Conference Center, in which we had about 120 of attendees including 31 invited speakers and 53 poster presenters. The following five sessions were arranged for the invited talks in the conference: (1) Hydrogen bonding network and proton transfer, (2) Properties and dynamics of soft interface, (3) Protein structure and dynamics: spectroscopy and crystallography, (4) Design of active sites of proteins and model complexes, and (5) Biomolecular function: from molecules to cells.

Molecular science is an interdisciplinary research field between chemistry and physics, and a frontier of which is the research on the elucidation and regulation of molecular system in biological function. Chemical biology is also an interdisciplinary research field between chemistry and biology. Both research fields have the same goal to understand the biological function in molecular level. In this conference, the researchers in the field of molecular science and chemical biology discussed their recent results and exchanged views with one another.

Joint Study Programs

As one of the important functions of an inter-university research institute, IMS facilitates joint study programs for which funds are available to cover the costs of research expenses as well as the travel and accommodation expenses of individuals. Proposals from domestic scientists are reviewed and selected by an interuniversity committee.

(1) Special Projects

A. New Developments in Spin Science Using Pulsed and High-Frequency ESR

KATO, Tatsuhisa *(Josai Univ.)*
MIZOGUCHI, Kenji *(Tokyo Metropolitan Univ.)*
SAKAMOTO, Hirokazu *(Tokyo Metropolitan Univ.)*
NAKAMURA, Toshikazu *(IMS)*
FURUKAWA, Ko *(IMS)*

In order to develop advanced ESR (electron spin resonance) spectroscopy for materials science, we performed functional materials studies, both on isolated molecules and on molecular assemblies. The following two topics were investigated: 1) We determined the molecular structure of novel systems such as N@C_{60}/C_{60} nano-whisker and their spin interaction using ESR spectroscopy, and explored the functionality of the complicated molecule system. 2) We carried out an analysis of spin dynamics for functional molecular assemblies, including molecular conductors and magnetic materials. We searched for cooperative phenomena involved in intra-molecule freedom, and new functional physical-properties originating in molecular assemblies.

A-1 Characterization of N@C_{60}/C_{60} Nano-Whisker by ESR

Endohedral N@C_{60} exhibits the spin ground state ($^4S_{3/2}$) due to the atomic nitrogen, which is located in the center of the fullerene cage. Because of the high symmetry, the guest nitrogen is subjected to isotropic environment and keeps the spherical symmetry of the free atom. The conventional spin relaxation processes are missing for the highly symmetric N@C_{60}, so even small deviation from the ideal structure like modification by crystal field can apparently be detected via interaction with the quartet spin.

C_{60} nano-whisker (NW) containing N@C_{60} was prepared by the crystal growth at the interface between toluene and isopropyl alcohol solutions. Comparing the spectrum of powder N@C_{60}/C_{60}, NW exhibited more enhanced broadening of ESR lines. The enhanced broadening reflects that the local symmetry at the nitrogen site in NW becomes lower than in C_{60} powder. ESR spectrum of N@C_{60}/C_{60} NW would give a good indicator of the solvation in the crystal growth process.

A-2 Spin and Lattice Dynamics near the Spin-Peierls Transition in Alkali-TCNQ

The dynamical nature of the spin-Peierls transition in K-TCNQ and Rb-TCNQ has been unveiled with the frequency and the temperature dependences of ESR line width and resonance positions. The spin-Peierls transition is governed by the competition of the thermal excitation and the exchange energy gain of singlet dimer formation in the half-filled Mott insulators, such as K-TCNQ.

With approaching temperature to the spin-Peierls transition T_{SP}, the singlet dimer of TCNQ molecules could be thermally excited to the triplet dimer in the singlet ground state. ESR observes the so-called "Pake-doublet" signals caused by the dipolar interaction between two electrons in an excited triplet dimer. With further approach to T_{SP}, the triplet dimer dissociates to the two isolated spin solitons with spin 1/2, resulting in the doublet ESR signals with the reduced peak separation due to the increased spin-spin distances on the dynamical average.

Thus, the separation of the doublet signals rapidly decreases near T_{SP}, accompanied with the maximum of the ESR line width which is dominated by the spin-lattice relaxation rate due to quasi-1D diffusion of the spin solitons. Therefore, these analyses of the frequency and the temperature dependences could provide ample information on the spin and lattice dynamics, important for the understanding of the phase transitions.

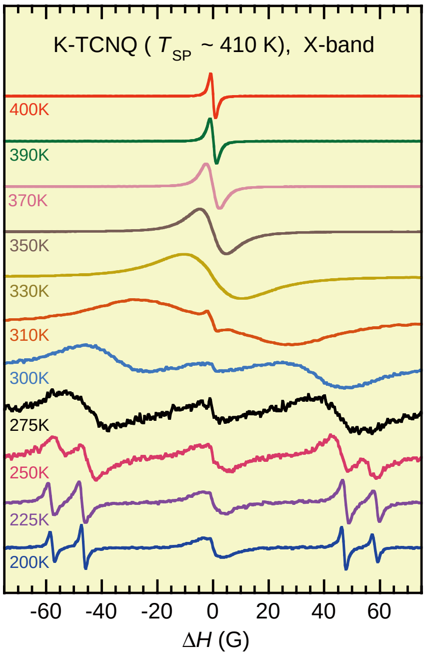

Figure 1. The temperature dependence of ESR spectra of K-TCNQ taken at X-band (~9.5 GHz). The center signals at $\Delta H = 0$ below 310 K might be originated by defects. Doublets correspond to the signal pairs around ±50 G or ±60 G.

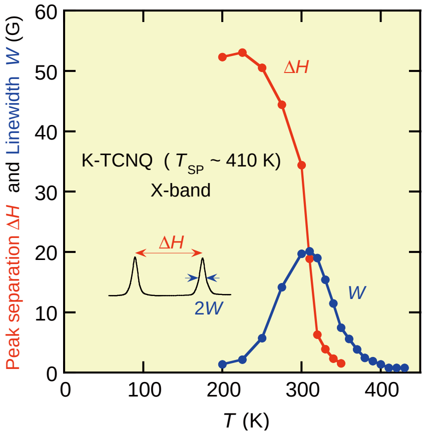

Figure 2. The temperature dependence of the peak separation for the outer doublet at ±60 G and the ESR linewidth. Note the steep disappearance of ΔH and the peak of ESR linewidth.

A-3 Spin-Dynamics Investigation by Pulsed-ESR for Phase Boundary between Spin-Peierls and Antiferromagnetic States in (TMTTF)$_2X$

(TMTTF)$_2$SbF$_6$ is considered to be located at the most negative pressure side in the generalized phase diagram of (TMTCF)$_2X$ at present. Observation of superconductivity in (TMTTF)$_2$AsF$_6$ (at 4.5 GPa) and (TMTTF)$_2$SbF$_6$ (6 GPa) under high pressure is also supporting this scenario. However, this model has produced a new unsolved problem: Another antiferromagnetic phase can be expected on the negative pressure side of the spin-Peierls phase according to ^{13}C NMR measurements for (TMTTF)$_2$SbF$_6$ under physical pressures. However, this phase diagram is based on the preconceived idea that a quantum one-dimensional spin-Peierls phase is sandwiched by two antiferromagnetic phases. In our knowledge, antiferromagnetic phases are stabilized with finite inter-chain interaction by applying pressure. It is also an open question whether the two antiferromagnetic phases (AF-I and AF-II) are of the same origin or not. To understand the P-T phase diagram of (TMTCF)$_2X$, we carried out pulsed-ESR measurements on (TMTTF)$_2$[(AsF$_6$)$_x$(SbF$_6$)$_{1-x}$].

While the ESR spin-lattice relaxation rate, ESR-T_1^{-1}, of (TMTTF)$_2$AsF$_6$ shows an anomalous but spin-gap behavior below the spin-Peierls phase transition temperature, T_{SP}, the ESR-T_1^{-1} behavior of (TMTTF)$_2$[(AsF$_6$)$_x$(SbF$_6$)$_{1-x}$] (x ~ 0.5) does not follow a conventional gap behavior suggesting that this salt is situated in the vicinity of the phase boundary between the spin-Peierls and antiferromagnetic phases.

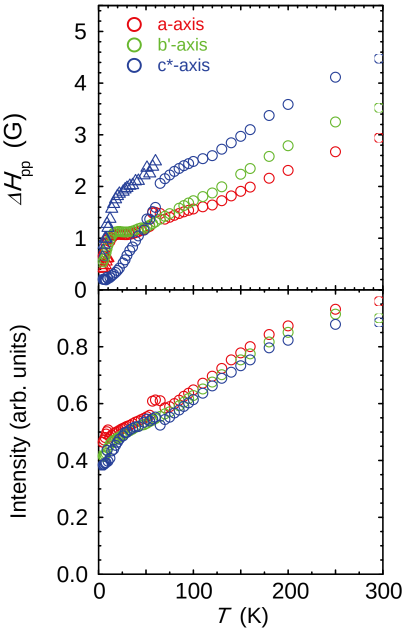

Figure 3. (left) Temperature dependence of the ESR linewidth, ΔH_{pp}, and integrated intensity (relative spin susceptibility) for (TMTTF)$_2$-[(AsF$_6$)$_x$(SbF$_6$)$_{1-x}$] (x ~ 0.5) determined by CW-ESR measurements.

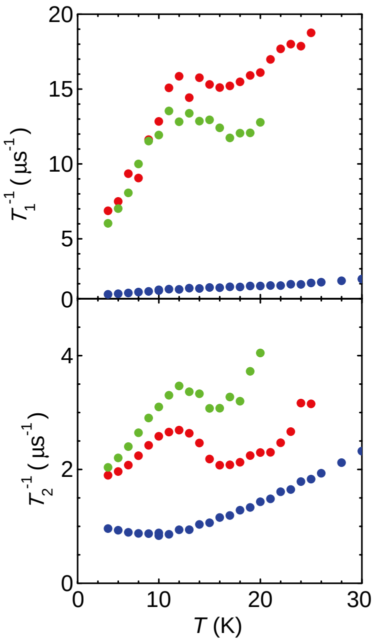

Figure 4. (right) Temperature dependence of the ESR spin-lattice relaxation rate, T_1^{-1}, and spin-spin relaxation rate, T_2^{-1}, for (TMTTF)$_2$-[(AsF$_6$)$_x$(SbF$_6$)$_{1-x}$] (x ~ 0.5) determined by pulsed-ESR measurements.

B. Construction of the Research Methodology for Biomolecular Sensing System

URISU, Tsuneo *(IMS)*
TERO, Ryugo *(IMS)*
TOMINAGA, Makoto *(OIIB)*
SHIGEMOTO, Ryuichi *(OIIB)*
MORIGAKI, Kennichi *(AIST)*
ISODA, Hiroko *(Univ. Tsukuba)*
YAWO, Hiromu *(Tohoku Univ.)*

Although more than 50% of genome drag discovery targets are the membrane proteins, there is no efficient biosensors necessary for screening. Patch clamp using a pipette is a well known and established technique for ion channel current measurements. However, it is not suitable for the screenings due to that it requires a high level of skills and the system scale down is difficult. In this work we are developing a new incubation type planer ion channel biosensor using Si substrates suitable for neural cell function analysis.

B-1 Development of Incubation Type Si-Based Planar Ion Channel Biosensor[1)]

A new planar-type ion channel biosensor with the function of cell culture has been fabricated using silicon on an insulator substrate as the sensor chip material. Coating of the sensor chip with fibronectin was essentially important for cell incubation on the chip (Figure 1a and 1b). Although the seal resistance (R_s) was quite low (~7 MΩ) compared with the pipette patch-clamp gigaohm seal, the whole-cell channel current of the transient receptor potential vanilloid type 1 (TRPV1) channel expressing HEK293 cells was successfully observed (Figure 1c), with a good signal-to-noise ratio, using capsaicin as a ligand molecule. The good agreement between calculated and measured values of R_s indicates that the model of the gap between cell and substrate surface and the assumed value of the cleft thickness, 75 nm, are good approximations.

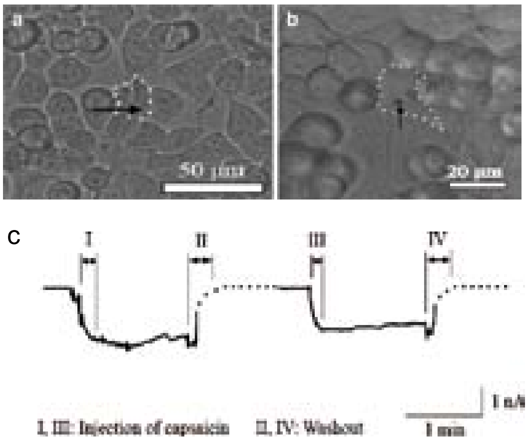

Figure 1. (a, b) Optical microscope images of HEK293 cells spreading on the pores of the planar-type ion channel biosensor. The seal resistance were (a) 6.3 MΩ, and (b) 8.4 MΩ (confluent cells). The arrows show the positions of the pores. The white dotted lines show the cells spreading on the pores. Round cells are sitting on the spreading cells. (c)Whole-cell current of TRPV1-transfected HEK-293 cell measured for the sample of (b) activated by repeated capsaicin (0.5 μmol l^{-1}) applications. Desensitization in the extracellular solution containing Ca^{2+} is observed. Holding voltage is −30 mV. Data are not shown for the dotted line region, where the signal is significantly disturbed by the noise induced by washout operations.

B-2 Development of Light Gated Ion channel Biosensor

The network function between neuronal cells has been investigated using an artificial signal input and output detection. In the investigation of the electrically excitable cells, photostimulation provides a versatile alternative to electrode stimulation. Channel of the excitable cell by the photo stimulation is especially useful in constructing the neural network analysis device. In the present work, we have expressed Chlamydomonas reinhardii channelrhodopsin 2 (ChR2) on the cell membrane of a kind of excitable cell C2C12, and measured the basic characteristics of the photo-response. ChR2 has a light absorbance peak at 460 nm and forms a non-selective cation channel, the gating of which is triggered by the photoisomerization of the all-trans retinal to 13-cis configuration. To investigate the photo-response characteristics of ChR2-expressed C2C12 cell, we have constructed the incubation type planer ion channel biosensor by putting a single C2C12 cell on the micropore of the Si substrate and successfully observed the light-gated whole cell channel current.

Reference

1) T. Urisu, T. Asano, Z. Zhang, H. Uno, R. Tero, H. Junkyu, I. Hiroko, Y. Arima, H. Iwata, K. Shibasaki and M. Tominaga, *Anal. Bioanal. Chem.*, published online, 2008.

(2) Research Symposia

(From Oct. 2007 to Sep. 2008)

Dates	Theme	Chair
Aug. 29–31, 2007	Self-Organization in the Material and Biological Systems: New Frontiers in Intergrated Research	**TOMINAGA, Masahide** **SAITO, Shinji**
Dec. 4– 5, 2007	New Development of Coordination Photochemistry by Fusing of Photofunctionality and High Reaction Selectivity	**SUZUKI, Takayoshi** **KAWAGUCHI, Hiroyuki**
Dec. 17–19, 2007	Advanced ESR Investigations for Noble Functionalities of Molecular Materials	**MIZOGUCHI, Kenji** **NAKAMURA, Toshikazu**
Mar. 10–11, 2008	Photosynthesis from Molecular Perspectives	**SUGIURA, Miwa** **NAGATA, Toshi**
Jun. 23, 2008	Preparatory Meeting for Molecular Science Summer School	**TAKEDA, Akihiro** **HISHIKAWA, Akiyoshi**
Jul. 18–19, 2008	Creation and Application of Functional Metal Complexes Based on Rational Design of Supporting Ligands —From Biological Systems to Catalysts and Devises—	**ITO, Shinobu** **AONO, Shigetoshi**

(3) Numbers of Joint Study Programs

Categories		Oct. 2007–Mar. 2008	Apr. 2008–Sep. 2008	Total
Special Projects		0	2	2
Research Symposia		3	2	5
Research Symposia for Young Researchers		–	1	1
Cooperative Research		47	46	93
Use of Facility	Instrument Center	28	25	53
	Equipment Development Center	6	4	10
Use of UVSOR Facility		77	70	147
Use of Facility Program of the Computer Center				146*

* from Apr. 2007 to Mar. 2008

Collaboration Programs

(a) IMS International Program

IMS has accepted many foreign scientists and hosted numerous international conferences since its establishment and is now universally recognized as an institute that is open to foreign countries. In 2004, IMS initiated a new program to further promote international collaborations. As a part of this new program, IMS faculty members can (1) nominate senior foreign scientists for short-term visits, (2) invite young scientists for long-term stays, and (3) undertake visits overseas to conduct international collaborations.

Leader	Title	Partner
OHMORI, Kenji	Quantum Control of Atoms and Molecules with Amplitude- and Phase-Shaped Optical Pulses	France: Prof. GIRARD, Bertrand and group members U.S.A.: Prof. LEVIS, Robert J. and group members
JIANG, Donglin	Studies on Molecular Design and Self-Assembly of Light-Harvesting Antennae	China: Prof. WANG, Changchun and group members
URISU, Tsuneo	Construction of Neural Cell Molecular Signal Transmission System and Development of Molecular Science New Field	China: Prof. WANG, Chang-Shun Mr. HE
KIMURA, Shin-ichi	Optical and Photoelectrical Studies on the Local to Itinerant Electronic Structure of Strongly Correlated Electron Systems	Korea: Prof. KWON, Yong-Seung Dr. IM, Hojun Dr. KIM, Hyeong-do and their group members
KOSUGI, Nobuhiro	Resonant Soft X-Ray Spectroscopic Study at UVSOR BL3U	Germany: Prof. RUEHL, Eckart Dr. WINTER, Bernd and their group members Sweden: Prof. PETTERSSON, Lars G. M. Prof. GEL'MUKANOV, Faris and their group members France: Dr. MIRON, Catalin and group members U.S.A.: Dr. GUO, Jinghua and group members
TANAKA, Koji	Photochemical Water Oxidation and Multi-Electron Reduction of Carbon Dioxide	U.S.A.: Dr. MUCKERMAN, James T. Dr. FUJITA, Etsuko and their group members
KATOH, Masahiro	Beam Dynamics in Free Electron Laser	France: Dr. COUPRIE, Marie Emmanuelle Dr. BIELAWSKI, Serge and their group members
TAIRA, Takunori	Q-Switched Nd-Microchip Lasers with COB Doubler	France: Prof. AKA, Gerard Philippe Dr. MORTIER, Michel and their group members

SHIGEMASA, Eiji	Deexcitation Dynamics of Core Excited Molecules Studied by Electron Spectroscopy	France: Dr. SIMON, Marc and group members U.K.: Prof. ELAND, John H. D.
OKAMOTO, Hiromi	Near-Field Spectroscopy of Plasmon-Induced Enhanced Electric Fields in Metal Nanoparticle Systems	Korea: Prof. JEONG, Dea Hong and group members

(b) Asian Core Program "Frontiers of Material, Photo- and Theoretical Molecular Sciences"

Asian Core Program is a multilateral international collaboration program carried our by JSPS (Japan Society for the Promotion of Science). It is designed to create world-class research hubs in selected fields within the Asian region, while fostering the next generation of leading researchers. The program is based on a principle of equal partnership among core institutions in Japan and other Asian countries, so that each institution is expected to secure its own matching fund. Institute for Molecular Science has launched a collaboration project "material, photo- and theoretical molecular sciences" (2006–2011) within the framework of this Asian Core Program with three key institutes in east Asian countries: Institute of Chemistry, Chinese Academy of Science (China); The College of Natural Science, Korea Advanced Institute of Science and Technology (Korea); and Institute of Atomic and Molecular Sciences, Academia Sinica (Taiwan). At present, eight joint researches are in progress, and seven joint seminars are planned within JFY 2008.

Professor Keiji Morokuma's Scientific Achievement

Emeritus Professor Keiji Morokuma was awarded the Imperial and Japan Academy Prizes of 2008 for his outstanding scientific achievements in understanding the structure, function, and reactivity of molecules by theoretical and computational approaches. The award is in recognition of the fact that theoretical and computational chemistry can make major contributions in the progress of molecular science, Professor Morokuma being the outstanding pioneer. The award ceremony was held at Tokyo on June 9 in the presence of both the Emperor and Empress. The Imperial Prize is the most authoritative in the prizes of the Japan Academy, and the winner is selected from among recipients for that year's Japan Academy Prize. Professor Morokuma's research work has been very highly rated also in experimental chemistry. Professor Morokuma has made great contribution to the nurturing of talented researchers. It is not too much to say that Professor Morokuma has affected directly (or indirectly) almost all Japanese researchers who are at present active at the forefront of electronic state theory. He is a world leader in theoretical and computational chemistry and won other honors including International Academy of Quantum Molecular Science (IAQMS) Award in 1978, Chemical Society Award from the Chemical Society of Japan in 1992, Schrödinger Medal from the World Association of Theoretical Organic Chemists (WATOC) in 1993, and Fukui Medal from Asia-Pacific Association of Theoretical & Computational Chemists (APATCC) in 2005. He also acted as president for IAQMS during six years since 2000 and contributed to the development in molecular theory and computation at an international level, which leads to the spread to various experimental research fields. We do hope that Professor Morokuma continues to do active research work as an international top leader in theoretical and computational molecular science.

Mr. Yoshida's Technical Achievements

Mr. Hisashi Yoshida, the chief of the electronics section of Equipment Development Center, has received The CSJ Award for Technical Achievement in 2007. The Chemical Society of Japan (CSJ) awards every year a person who has contributed to the development or improvement of experimental techniques in chemistry or chemical engineering. Mr. Yoshida is recognized for his contribution to "Development of Advanced Measurement and Control Apparatuses for Molecular Science." His main achievements awarded are "Multi-dimensional coincidence measuring instrument for electron Compton scattering experiments," "Computer-controlled liquid helium transfer system," "Multichannel spectrophotometry data acquisition system by using image sensor," "Fast rising HV pulse generator for TOF mass spectrum analyzer," *etc*. He developed many equipments necessary for molecular science experiments through the cooperation with scientists who need the instruments, and attained a great contribution to the molecular science.

LIST OF VISITING FOREIGN SCHOLARS

Visitors from abroad are always welcome at IMS and they have always played an important role in the research activities of the Institute. The foreign scientists who visited IMS during the past year (September 2007–August 2008) are listed below.

(1) MONKASHO (Ministry of Education, Culture, Sports, Science and Technoogy, Japan) or JSPS (Japan Society for the Promotion of Science) Invited Fellow

Dr. Yarasi Soujanya	Indian Inst. of Chem. Tech.	India	Jul. ’08–Aug. ’08

(2) IMS Visiting Professor or Associate Professor from Abroad (period of stay from 3 to 12 months)

Prof. Jang Joonkyung	Pusan Natl. Univ.	Korea	Jul. ’08–Aug. ’08

(3) JSPS Post-Doctoral or Ronpaku Fellow

Dr. Guo Jia	Fudan Univ.	China	Oct. ’07–Sep. ’09
Dr. Chen Penglei	Inst. of Chem. Chinese Acad. of Sci.	China	Jun. ’08

(4) IMS Visiting Scientist

Prof. Guelmoukhanov Faris	Royal Inst. of Tech.	Sweden	Oct. ’07
Dr. Watson Mark Adrian	Univ. Tokyo	Japan	Oct. ’07
Mr. Subramaniam Chandramauli	Indian Inst. of Tech. Madras	India	Oct. ’07–Nov. ’07
Mr. Choi Hyeonho	Seoul Natl. Univ.	Korea	Oct. ’07–Apr. ’08
Mr. Kim Sull	KAIST	Korea	Oct. ’07–Apr. ’08
Prof. Salikhov Kev M.	Kazan Phys.-Tech. Inst. of the Russian Acad. of Sci.	Russia	Nov. ’07
Prof. Lu Jing	Peking Univ.	China	Dec. ’07
Ms. Zhou Jing	Peking Univ.	China	Dec. ’07
Prof. Petrosky Yamakoshi Tomio	Univ. of Texas Austin	U.S.A.	Jan. ’08–Feb. ’08
Prof. Wang Changshun	Shanghai Jia Tong Univ.	China	Jan. ’08–Feb. ’08
Prof. Chintalagiri Mohan Rao	Centre for Cellular and Molecular Bio.	India	Jan. ’08
Dr. Watson Mark Adrian	Univ. Tokyo	Japan	Jan. ’08
Prof. Sastry G.Narahari	Indian Inst. of Chem. Tech.	India	Jan. ’08
Prof. Wu Yao-Ting	Natl. Cheng Kung Univ.	China	Jan. ’08–Feb. ’08
Prof. Sorokin Evgeni	Photonics Inst. TU Vienna	Austria	Jan. ’08–Feb. ’08
Prof. Sorokina Irina	Norwegian Univ. of Sci. and Tech.	Norway	Jan. ’08–Feb. ’08
Dr. Pavel Nicolaie	Natl. Inst. for Laser Plasma and Radiation Phys.	Rumania	Jan. ’08–Feb. ’08
Dr. Dascalu Traian	Natl. Inst. for Laser Plasma and Radiation Phys.	Rumania	Jan. ’08–Feb. ’08
Prof. Aka Gerard	Ecole Natl. Suprieure de Chimie de Paris/Univ. Pierre & Marie Curie	France	Jan. ’08–Feb. ’08
Dr. Georges Patrick	Inst. of Optique	France	Jan. ’08–Feb. ’08
Mr. Krankel Christian	Univ. of Hamburg	Germany	Jan. ’08–Feb. ’08
Mr. Richter Andre	Univ. of Hamburg	Germany	Jan. ’08–Feb. ’08
Ms. Fredrich-Thornton Susanne	Univ. of Hamburg	Germany	Jan. ’08–Feb. ’08
Ms. Teisset Catherine	Univ. Muenchen/Maz-Planck-Inst. of Quantum Optics	Germany	Feb. ’08
Dr. Watson Mark Adrian	Univ. Tokyo	Japan	Feb. ’08
Dr. Smith Stanley	Temple Univ.	U.S.A.	Mar. ’08
Mr. Brady John	Temple Univ.	U.S.A.	Mar. ’08
Dr. Watson Mark Adrian	Univ. Tokyo	Japan	Mar. ’08
Dr. Kim Yong Hoon	Inst. for Molecular Sci.	Japan	Mar. ’08–Mar. ’10
Dr. Watson Mark Adrian	Univ. Tokyo	Japan	Apr. ’08
Dr. Peng Daoling	Univ. Tokyo	Japan	Apr. ’08
Prof. Aka Gerard	Ecole Natl. Suprieure de Chimie de Paris/Univ. Pierre & Marie Curie	France	Apr. ’08
Prof. Loiseau Pascal	Ecole Natl. Suprieure de Chimie de Paris/Univ. Pierre & Marie Curie	France	Apr. ’08
Mr. Kim Sull	KAIST	Korea	May ’08–Jun. ’08
Dr. Schmidt Mike	Iowa State Univ.	U.S.A.	Jun. ’08
Mr. Kim Seong Yong	Seoul Natl. Univ.	Korea	Jul. ’08
Prof. Jeong Dae Hong	Seoul Natl. Univ.	Korea	Jul. ’08
Mr. Pfutzner Steffen	Dresden Univ. of Tech. Inst. for Applied Photophys.	Germany	Jul. ’08
Prof. Kwon Yong Seung	Sungkyunkwan Univ.	Korea	Jul. ’08–Aug. ’08
Prof. Oh Hyunjin	Masan College	Korea	Jul. ’08–Aug. ’08
Prof. Han Woong Yeom	Yonsei Univ.	Korea	Jul. ’08
Ms. Lee Kyeng Eun	Sungkyunkwan Univ.	Korea	Jul. ’08

Dr. Wang Lu	Peking Univ.	China	Aug. ’08–Mar. ’09
Prof. Eland John Hugh David	Sungkyunkwan Univ.	Korea	Aug. ’08–Sep. ’08
Prof. Mao Yanli	Henan Univ.	China	Aug. ’08
Prof. Wang Chagshun	Shanghai Jiao Tong Univ.	China	Aug. ’08–Sep. ’08
Dr. Yildiz Fikret	Max-Planck-Inst. für Mikrostruktur Phys.	Germany	Aug. ’08–Sep. ’08
Mr. He Ting-Chao	Shanghai Jiao Tong Univ.	China	Aug. ’08–Feb. ’09
Dr. Ibrahim Heide	Inst. für Experimentalphysik	U.S.A.	Aug. ’08–Nov. ’08

(5) Visitor to IMS

Prof. Pal Tarasankar	Indian Inst. of Tech.	India	Sep. ’07
Mr. Westerstom Alexander	Stockholm Univ.	Sweden	Sep. ’07–Dec. ’07
Prof. Ivo Nezbeda	Organization J. E. Purkinje Univ.	Czech	Nov. ’07
Prof. Myroslav Holovko	Inst. for Condensed Matter Phys. Natl. Acad. of Sci. of Ukraine	Ukraine	Nov. ’07–Dec. ’07
Ms. Teisset Catherine	Ludwig-Maximilians-Univ. Muenchen	Germany	Nov. ’07
Prof. Hellingwerf Klaas Jan	Univ. of Amsterdam	Holland	Dec. ’07
Prof. Fejer Martin	Stanford Univ.	U.S.A.	Jan. ’08–Feb. ’08
Prof. Lupei Voicu	Inst. of Atomic Phys. Bucharest	Rumania	Jan. ’08–Feb. ’08
Prof. Huber Guenter	Univ. of Hamburg	Germany	Jan. ’08–Feb. ’08
Dr. Petermann Klaus	Univ. of Hamburg	Germany	Jan. ’08–Feb. ’08
Mr. Metzger Thomas	Max-Planck-Inst. of Quantum Optics	Germany	Feb. ’08
Prof. Vodopyanov Konstantin	Stanford Univ.	U.S.A.	Feb. ’08
Prof. Wittrock Ulrich	Muenster Univ. of Appllied Sci.	Germany	Feb. ’08
Prof. Kubecek Vaclav	Czech Tech. Univ.	Czech	Feb. ’08
Prof. Shakhnovich Eugene	Harvard Univ.	U.S.A.	Feb. ’08
Prof. Rovira Angulo Concepcio	Inst. de Ciencia de Materials de Barcelona (CSIC)	Spain	Mar. ’08
Prof. Veciana Jaume	Inst. de Ciencia de Materials de Barcelona (CSIC)	Spain	Mar. ’08
Prof. Miller William	Univ. of California, Berkeley	U.S.A.	Mar. ’08
Prof. Sheldon Roger A.	Delft Univ. of Tech.	Holland	Apr. ’08
Prof. Braams Bastiaan J.	Emory Univ.	U.S.A.	Apr. ’08
Ms. Teisset Catherine	Ludwig-Maximilians-Univ. Muenchen	Germany	Apr. ’08
Prof. Field Robert W.	Massachusetts Inst. of Tech.	U.S.A.	May ’08
Prof. Orr Brian	Macquarie Univ.	Australia	Jul. ’08
Prof. Batail Patrick	Univ. of Angers, CNRS	France	Jul. ’08
Dr. Zhang Bin	Inst. of Chem. Chinese Acad. of Sci.	China	Jul. ’08
Prof. Brooks James S.	Florida State Univ.	U.S.A.	Jul. ’08
Prof. Kang Woun	Ewha Womans Univ.	Korea	Jul. ’08
Prof. Swietlik Roman	Inst. of Molecular Phys. Polish Acad. of Sci.	Poland	Jul. ’08
Prof. Bourbonnais Claude	Univ. of Sherbrooke	Canada	Jul. ’08
Prof. Jochen Wosnitza	Forshungszentrum Dresden Rossendorf	Germany	Jul. ’08
Prof. Pierre Monceau	Inst. Neel CNRS	France	Jul. ’08
Dr. John Schulueter	Argonne Natl. Lab.	U.S.A.	Jul. ’08
Prof. Bandrauk Andre	Univ. of Sherbrooke	Canada	Aug. ’08
Prof. Dugourd Philippe	Univ. Lyon 1	France	Aug. ’08
Prof. Manz Jorn	Freie Univ. Berlin	Germany	Aug. ’08
Prof. Mou Chung-Yuan	Natl. Taiwan Univ.	Taiwan	Aug. ’08
Dr. Musaev Jamal	Emory Univ.	U.S.A.	Aug. ’08
Prof. Mooijen Marcel	Univ. of Waterloo	Canada	Aug. ’08
Prof. Power Philip	Univ. of California, Davis	Ireland	Aug. ’08
Prof. Pyykko Pekka	Univ. of Helsinki	Finland	Aug. ’08
Prof. Thompson Ward	Univ. of Kansas	U.S.A.	Aug. ’08
Prof. Ziegler Tom	Univ. of Calgary	Canada	Aug. ’08
Prof. Cina Jeffrey A.	Univ. of Oregon	U.S.A.	Aug. ’08–Sep. ’08

Scientists who would like to visit IMS under programs (1) and (2) are invited to make contact with IMS staff in their relevant field.

Theoretical and Computational Molecular Science

D. WANG, J. LU, L. LAI, M. NI, W. N. MEI, G. LI, S. NAGASE, Y. MAEDA, T. AKASAKA, Z. GAO and Y. ZHOU, “Effects of Hole Doping on Selectivity of Naphthalene towards Single-Wall Carbon Nanotubes,” *Comput. Mater. Sci.* **40**, 354–358 (2007).

B. WANG, S. NAGASE, J. ZHAO and G. WANG, “The Stability and Electronic Structure of Single-Walled ZnO Nanotubes by Density Functional Theory,” *Nanotechnology* **18**, 345706 (6 pages) (2007).

J. LU, L. LAI, G. LUO, J. ZHOU, R. QIN, D. WANG, L. WANG, W. N. MEI, G. LI, Z. GAO, S. NAGASE, Y. MAEDA, T. AKASAKA and D. YU, “Why Semiconducting Single-Wall Carbon Nanotubes Are Separated from their Metallic Counterparts?” *Small* **3**, 1566–1576 (2007).

M. SAITO, S. IMAIZUMI, T. TAJIMA, K. ISHIMURA and S. NAGASE, “Synthesis and Structure of Pentaorganostannate Having Five Carbon Substituents,” *J. Am. Chem. Soc.* **129**, 10974–10975 (2007).

Y. MAEDA, M. HASHIMOTO, T. HASEGAWA, M. KANDA, T. TSUCHIYA, T. WAKAHARA, T. AKASAKA, Y. MIYAUCHI, Y. MARUYAMA, J. LU and S. NAGASE, “Extraction of Metallic Nanotubes of Zeolite-Supported Single-Walled Carbon Nanotubes Synthesized from Alcohol,” *NANO* **2**, 221–226 (2007).

Z. SLANINA, F. UHLIK, S. -L. LEE, L. ADAMOWICZ and S. NAGASE, “Computations of Production Yields for $Ba@C_{74}$ and $Yb@C_{74}$,” *Mol. Sim.* **33**, 563–568 (2007).

Z. ZHOU and S. NAGASE, “Coaxial Nanocables of AlN Nanowire Core and Carbon/BN Nanotube Shell,” *J. Phys. Chem. C* **111**, 18533–18537 (2007).

E. RIVARD, R. C. FISCHER, R. WOLF, Y. PENG, W. A. MERRILL, N. D. SCHLEY, Z. XHU, L. PU, J. C. FETTINGER, S. J. TEAT, I. NOWIK, R. H. HERBER, N. TAKAGI, S. NAGASE and P. P. POWER, “Isomeric Forms of Heavier Main Group Hydrides: Experimental and Theoretical Studies of the $[Sn(Ar)H]_2$ (Ar = Terphenyl) System,” *J. Am. Chem. Soc.* **129**, 16197–16208 (2007).

T. TSUCHIYA, R. KUMASHIRO, K. TANIGAKI, Y. MATSUNAGA, M. O. ISHITUKA, T. WAKAHARA, Y. MAEDA, Y. TAKANO, M. AOYAGI, T. AkASAKA, M. T. H. LIU, T. KATO, K. SUENAGA, J. S. JEONG, S. IIJIMA, F. KIMURA, T. KIMURA and S. NAGASE, “Nanorods of Endohedral Metallofullerene Derivative,” *J. Am. Chem. Soc.* **130**, 450–451 (2008).

B. GAO, H. NIKAWA, T. NAKAHODO, T. TSUCHIYA, Y. MAEDA, T. AKASAKA, H. SAWA, Z. SLANINA, N. MIZOROGI and S. NAGASE, “Addition of Adamantylidene to $La_2@C_{78}$: Isolation and Single-Crystal X-Ray Structural Determination of the Monoadducts,” *J. Am. Chem. Soc.* **130**, 983–989 (2008).

M. YAMADA, C. SOMEYA, T. WAKAHARA, T. TSUCHIYA, Y. MAEDA, T. AKASAKA, K. YOZA, E. HORN, M. T. H. LIU, N. MIZOROGI and S. NAGASE, “Metal Atoms Collinear with the Spiro Carbon of 6,6-Open Adducts, $M_2@C_{80}$ (Ad) (M = La and Ce, Ad = Adamantylidene),” *J. Am. Chem. Soc.* **130**, 1171–1176 (2008).

M. YAMADA, T. WAKAHARA, T. TSUCHIYA, Y. MAEDA, M. KAKO, T. AKASAKA, K. YOZA, E. HORN, N. MIZOROGI and S. NAGASE, “Location of the Metal Atoms in $Ce_2@C_{78}$ and Its Bis-Silylated Derivative,” *Chem. Commun.* 558–560 (2008).

T. NAKAHODO, M. OKADA, H. MORITA, T. YOSHIMURA, M. O. ISHITSUKA, T. TSUCHIYA, Y. MAEDA, H. FUJIHARA, T. AKASAKA, X. GAO and S. NAGASE, “[2+1] Cycloaddition of Nitrene onto C_{60} Revisited: Interconversion between an Aziridinofullerene and an Azafulleroid,” *Angew. Chem., Int. Ed.* **47**, 1298–1300 (2008).

T. AKASAKA, T. KONO, Y. MATSUNAGA, T. WAKAHARA, T. NAKAHODO, M. O. ISHITSUKA, Y. MAEDA, T. TSUCHIYA, T. KATO, M. T. H. LIU, N. MIZOROGI, Z. SLANINA and S. NAGASE, “Isolation and Characterization of Carbene Derivatives of $La@C_{82}$ (C_s), ” *J. Phys. Chem. A* **112**, 1294–1297 (2008).

A. D. KULKARNI, S. R. GADRE and S. NAGASE, “Quantum Chemical and Electrostatic Studies of Anionic Water Clusters, $(H_2O)_n^-$,” *THEOCHEM* **851**, 213–219 (2008).

T. NAKAHODO, K. TAKAHASHI, M. O. ISHITSUKA, T. TSUCHIYA, Y. MAEDA, H. FUJIHARA, S. NAGASE and T. AKASAKA, “Synthesis of Selenyfullerene with Selenium-Containig Dibenzo[b,g]cyclooctane Moiety,” *Tetrahedoron Lett.* **49**, 2302–2305 (2008).

B. WANG, X. WANG, G. CHEN, S. NAGASE and J. ZHAO, “Cage and Tube Structures of Medium-Sized Zinc Oxide Clusters $(ZnO)_n$ (n = 24, 28, 36, and 48),” *J. Chem. Phys.* **128**, 144710 (6 pages) (2008).

K. ISHIMURA and S. NAGASE, “A New Algorithm of Two-Electron Repulsion Integral Calculations: A Combination of Pople-Hehre and McMurchie-Davidson Methods,” *Theor. Chem. Acc.* **120**, 185–189 (2008).

T. ASADA, S. NAGASE, K. NISHIMOTO and S. KOSEKI, “Molecular Dynamics Simulation Study on Stabilities and Reactivities of NADH Cytochrome B5 Reductase,” *J. Phys. Chem. B* **112**, 5718–5727 (2008).

Z. SLANINA, F. UHLIK, S-. L. LEE, L. ADAMOWICZ and S. NAGASE, “Computational Screening of Metallofullerenes for Nanoscience: $Sr@C_{74}$,” *Mol. Sim.* **34**, 17–21 (2008).

N. TOKITOH, K. WAKITA, T. MATSUMOTO, T. SASAMORI, R. OKAZAKI, N. TAKAGI, M. KIMURA and S. NAGASE, “The Chemistry of Stable Silabenzenes,” *J. Chin. Chem. Soc.* **55**, 487–507 (2008).

X. LU, H. NIKAWA, T. NAKAHODO, T. TSUCHIYA, M. O. ISHITSUKA, Y. MAEDA, T. AKASAKA, M. TOKI, H. SAWA, Z. SLANINA, N. MIZOROGI and S. NAGASE, “Chemical Understanding of a Non-IPR Metallofullerene: Stabilization of Encaged Metals on Fused-Pentagon Bonds in $La_2@C_{72}$,” *J. Am. Chem. Soc.* **130**, 9129–9136 (2008).

X. GAO, Z. ZHOU, Y. ZHAO, S. NAGASE, S. B. ZHANG and Z. CHEN, “Comparative Study of Carbon and BN Nanographenes: Ground Electronic States and Energy Gap Engineering,” *J. Phys. Chem. C* **112**, 12677–12682 (2008).

M. YAMADA, T. WAKAHARA, T. TSUCHIYA, Y. MAEDA, T. AKASAKA, N. MIZOROGI and S. NAGASE, “Spectroscopic and Theoretical Study of Endohedral Metallofullerene having Non-IPR Fullerene Cage: $Ce_2@C_{72}$,” *J. Phys. Chem. A* **112**, 7627–7631 (2008).

T. YASUIKE and K. NOBUSADA, “Quasi-Diabatic Decoupling of Born-Oppenheimer Potential Energy Curves for Adsorbate-Metal Surface Systems,” *Chem. Phys. Lett.* **457**, 241–245 (2008).

K. SHIRATORI and K. NOBUSADA, "Finite-Temperature Density Functional Calculation with Polarizable Continuum Model in Electrochemical Environment," *Chem. Phys. Lett.* **451**, 158–162 (2008).
T. YASUIKE and K. NOBUSADA, "Open-Boundary Cluster Model for Calculation of Adsorbate-Surface Electronic States," *Phys. Rev. B* **76**, 235401 (12 pages) (2007).
K. NOBUSADA and T. IWASA, "Oligomeric Gold Clusters with Vertex-Sharing Bi- and Triicosahedral Structures," *J. Phys. Chem. C* **111**, 14279–14282 (2007).

T. YANAI and G. K-L. CHAN, "A Canonical Transformation Theory from Extended Normal Ordering," *J. Chem. Phys.* **127**, 104107 (14 pages) (2007).
D. GHOSH, J. HACHMANN, T. YANAI and G. K-L. CHAN, "Orbital Optimization in Density Matrix Renormalization Group, with Applications to Polyenes and β-Carotene," *J. Chem. Phys.* **128**, 144117 (14 pages) (2008).
H. SEKINO, Y. MAEDA, T. YANAI and R. J. HARRISON, "Basis Set Limit Hartree-Fock and Density Functional Theory Response Property Evaluation by Multiresolution Multiwavelet Basis," *J. Chem. Phys.* **129**, 034111 (6 pages) (2008).

Y. YONETANI, Y. MARUYAMA, F. HIRATA and H. KONO, "Comparison of DNA Hydration Patterns Obtained Using Two Distinct Computational Methods, Molecular Dynamics (MD) Simulation and Three-Dimensional Reference Interaction Site Model (3D-RISM) Theory," *J. Chem. Phys.* **128**, 185102 (9 pages) (2008).
N. YOSHIDA, T. ISHIDA and F. HIRATA, "Theoretical Study of Temperature and Solvent Dependence of the Free Energy Surface of the Intramolecular Electron Transfer Based on the RISM-SCF Theory; Application to 1,3-Dinitrobenzene Radical Anion in Acetonitrile and Methanol," *J. Phys. Chem. B* **112**, 433–440 (2008).
S. PHONPHANPHANEE, N. YOSHIDA and F. HIRATA, "On the Proton Exclusion of Aquaporins: A Statistical Mechanics Study," *J. Am. Chem. Soc. (Communications)* **130**, 1540–1541 (2008).
R. ISHIZUKA, S. -H. CHONG and F. HIRATA, "An Intergral Equation Theory for Inhomogeneous Molecular Fluids: The Reference Interaction Site Model Approach," *J. Chem. Phys.* **128**, 34504–34513 (2008).
T. MIYATA and F. HIRATA, "Combination of Molecular Dynamics Method and 3d-RISM Theory for Conformational Sampling of Large Flexible Molecules in Solution," *J. Comput. Chem.* **29**, 871–882 (2008).
T. MIYATA, "Reference Interaction Site Model Study on the Anomeric Equilibrium of D-Glucose in Aqueous Solution," *Cond. Matt. Phys.* **10**, 433–439 (2007).
N. YOSHIDA, "Analytical Free Energy Gradient for the Molecular Ornstein-Zernike Self-Consistent-Field Method," *Cond. Matt. Phys.* **10**, 363–372 (2007).
Y. MARUYAMA, M. MATSUGAMI and Y. IKUTA, "Probing Cations Recognized by a Crown Ether with the 3D-RISM Theory. II. 18-Crown-6 Ether," *Cond. Matt. Phys.* **10**, 315–322 (2007).
S. PHONPHANPHANEE, N. YOSHIDA and F. HIRATA, "A Statistical Mechanics Study on Equilibrium Water Distribution in Aquaporin," *Chem. Phys. Lett.* **449**, 196–201 (2007).
T. IMAI, R. HIRAOKA, T. SETO, A. KOVALENKO and F. HIRATA, "Three-Dimensional Distribution Function Theory for the Prediction of Protein-Ligand Binding Sites and Affinities: Application to the Binding of Noble Gases to Hen Egg-White Lysozyme in Aqueous Solution," *J. Phys. Chem. B* **111**, 11585–11591 (2007).

K. YONEMITSU, N. MAESHIMA and T. HASEGAWA, "Suppression of Rectification at Metal-Mott-Insulator Interfaces,'' *Phys. Rev. B* **76**, 235118 (6 pages) (2007).
Y. TANAKA and K. YONEMITSU, "Charge Order with Structural Distortion in Organic Conductors: Comparison between θ-$(ET)_2RbZn(SCN)_4$ and α-$(ET)_2I_3$,'' *J. Phys. Soc. Jpn.* **77**, 034708 (9 pages) (2008).
N. MAESHIMA and K. YONEMITSU, "Polaronic States with Spin-Charge-Coupled Excitation in a One-Dimensional Dimerized Mott Insulator K-TCNQ,'' *J. Phys. Soc. Jpn.* **77**, 074713 (6 pages) (2008).
K. YONEMITSU and K. NASU, "Theory of Photoinduced Phase Transitions in Itinerant Electron Systems,'' *Phys. Rep.* **465**, 1–60 (2008).
K. ONDA, S. OGIHARA, K. YONEMITSU, N. MAESHIMA, T. ISHIKAWA, Y. OKIMOTO, X. -F. SHAO, Y. NAKANO, H. YAMOCHI, G. SAITO and S. KOSHIHARA, "Photoinduced Change in the Charge Ordering Pattern in the Quarter-Filled Organic Conductor $(EDO\text{-}TTF)_2PF_6$ with Strong Electron-Phonon Interaction,'' *Phys. Rev. Lett.* **101**, 067403 (4 pages) (2008).

N. YOSHII and S. OKAZAKI, "A Molecular Dynamics Study of Structure and Dynamics of Surfactant Molecules in SDS Spherical Micelle," *Cond. Matt. Phys.* **10**, 573–578 (2007).
S. KAJIMOTO, N. YOSHII, J. HOBLEY, H. FUKUMURA and S. OKAZAKI, "Electrostatic Potential Gap at the Interface between Triethylamine and Water Phases Studied by Molecular Dynamics Simulation," *Chem. Phys. Lett.* **448**, 70–74 (2007).
A. YAMADA and S. OKAZAKI, "Quantum Equation of Motion for Chemical Reaction Systems on an Adiabatic Double-Well Potential Surface in Solution Based on the Framework of Mixed Quantum-Classical Molecular Dynamics," *J. Chem. Phys.* **128**, 044507 (8 pages) (2008).

T. YAGASAKI and S. SAITO, "Ultrafast Intermolecular Dynamics of Liquid Water: A Theoretical Study on Two-Dimensional Infrared Spectroscopy," *J. Chem. Phys.* **128**, 154521 (7 pages) (2008).

T. MIYAMAE, A. MORITA and Y. OUCHI, "First Acid Dissociation at an Aqueous H_2SO_4 Interface with Sum Frequency Generation Spectroscopy," *Phys. Chem. Chem. Phys.* **10**, 2010–2013 (2008).
A. MORITA and B. C. GARETT, "Molecular Theory of Mass Transfer Kinetics and Dynamics at Gas/Water Interface," *Flu. Dyn. Res*. **40**, 459–473 (2008).

N. YOSHIDA, T. ISHIDA and F. HIRATA, "Theoretical Study of Temperature and Solvent Dependence of the Free-Energy Surface of the Intramolecular Electron-Transfer Based on the RISM-SCF Theory: Application to the 1,3-Dinitrobenzene Radical Anion in Acetonitrile and Methanol," *J. Phys. Chem. B* **112**, 433–440 (2008).

T. ISHIDA, "Optimal Charge and Charge Response Determination through Conformational Space: Global Fitting Scheme for Representative Charge and Charge Response Kernel," *J. Phys. Chem. A* **112**, 7035–7046 (2008).

T. ISHIDA and P. J. ROSSKY, "Consequences of Strong Coupling between Solvation and Electronic Structure in the Excited State of a Betaine Dye," *J. Phys. Chem. B* **112**, 11353–11360 (2008).

M. NISHINO, K. BOUKHEDDADEN, Y. KONISHI and S. MIYASHITA, "Simple Two-Dimensional Model for the Elastic Origin of Cooperativity among Spin States of Spin-Crossover Complexes," *Phys. Rev. Lett.* **98**, 247203 (4 pages) (2007).

Photo-Molecular Science

M. K. HOSSAIN, T. SHIMADA, M. KITAJIMA, K. IMURA and H. OKAMOTO, "Raman and Near-Field Spectroscopic Study on Localized Surface Plasmon Excitation from the 2D Nanostructure of Gold Nanoparticles," *J. Microsc.* **229**, 327–330 (2008).

K. IMURA and H. OKAMOTO, "Ultrafast Photoinduced Changes of Eigenfunctions of Localized Plasmon Modes in Gold Nanorods," *Phys. Rev. B* **77**, 041401(R) (2008).

T. SHIMADA, K. IMURA, M. K. HOSSAIN, H. OKAMOTO and M. KITAJIMA, "Near-Field Study on Correlation of Localized Electric Field and Nanostructures in Monolayer Assembly of Gold Nanoparticles," *J. Phys. Chem. C* **112**, 4033–4035 (2008).

M. K. HOSSAIN, T. SHIMADA, M. KITAJIMA, K. IMURA and H. OKAMOTO, "Near-Field Raman Imaging and Electromagnetic Field Confinement in the Self-Assembled Monolayer Array of Gold Nanoparticles," *Langmuir* **24**, 9241–9244 (2008).

H. HASEGAWA and Y. OHSHIMA, "Nonadiabatic Rotational Excitation of Benzene by Nonresonant Intense Femtosecond Laser Fields," *Chem. Phys. Lett.* **454**, 148–152 (2008).

H. HASEGAWA and Y. OHSHIMA, "Quantum State Reconstruction of a Rotational Wave Packet Created by a Nonresonant Intense Femtosecond Laser Field," *Phys. Rev. Lett.* **101**, 053002 (4 pages) (2008).

K. OHMORI, "Development of Ultrahigh-Precision Coherent Control and Its Applications," *Proc. Jpn. Acad., Ser. B* **84**, 167–175 (2008).

B. WINTER, E. F. AZIZ, N. OTTOSSON, M. FAUBEL, N. KOSUGI and I. V. HERTEL, "Electron Dynamics in Charge-Transfer-to-Solvent States of Aqueous Chroride Revealed by Cl^- 2p Resonant Auger-Electron Spectroscopy," *J. Am. Chem. Soc.* **130**, 7130–7138 (2008).

M. YAMAZAKI, J. ADACHI, Y. KIMURA, A. YAGISHITA, M. STENER, P. DECLEVA, N. KOSUGI, H. IWAYAMA, K. NAGAYA and M. YAO, "Decay Channel Dependence of the Photoelectron Angular Distributions in Core-Level Ionization of Ne Dimers," *Phys. Rev. Lett.* **101**, 043004 (4 pages) (2008).

A. LINDGREN, N. KOSUGI, M. GISSELBRECHT, A. KIVIMÄKI, F. BURMEISTER, A. NAVES de BRITO and S. L. SORENSEN, "Core Localization and σ^* Delocalization in the O 1s Core-Excited Sulfur Dioxide Molecule," *J. Chem. Phys.* **128**, 114311 (10 pages) (2008).

M. NAGASAKA, H. KONDOH, K. AMEMIYA, T. OHTA and Y. IWASAWA, "Proton Transfer in a Two-Dimensional Hydrogen-Bonding Network: Water and Hydroxyl on a Pt(111) Surface," *Phys. Rev. Lett.* **100**, 106101 (4 pages) (2008).

B. YANG, Y. Y. LI, L. X. WEI, C. Q. HUANG, J. WANG, Z. Y. TIAN, R. YANG, L. S. SHENG, Y. W. ZHANG and F. QI, "An Experimental Study of the Premixed Benzene/Oxygen/Argon Flame with Tunable Synchrotron Photoionization," *Proc. Combust. Inst.* **31**, 555–563 (2007).

B. P. KAFLE, H. KATAYANAGI, MD. S. I. PRODHAN, H. YAGI, C. HUANG and K. MITSUKE, "Absolute Total Photoionization Cross Section of C_{60} in the Range of 25–120eV: Revisited," *J. Phys. Soc. Jpn.* **77**, 014302 (5 pages) (2008).

H. KATAYANAGI, B. P. KAFLE, J. KOU, T. MORI, K. MITSUKE, Y. TAKABAYASHI, E. KUWAHARA and Y. KUBOZONO, "The 4d → 4f Dipole Resonance of the Pr Atom in an Endohedral Metallofullerene, Pr@C_{82}," *J. Quant. Spectrosc. Radiat. Transfer* **109**, 1590–1598 (2008).

M. HASHIMOTO, T. YOSHIDA, H. YAGI, M. TAKIZAWA, A. FUJIMORI, M. KUBOTA, K ONO, K. TANAKA, D. H. LU, Z. -X. SHEN, S. ONO and Y. ANDO, "Doping Evolution of the Electronic Structure in the Single-Layer Cuprate $Bi_2Sr_{2-x}La_xCuO_{6+\delta}$: Comparison with Other Single-Layer Cuprates," *Phys. Rev. B* **77**, 094516 (9 pages) (2008).

A. MATSUDA, E. J. TAKAHASHI and A. HISHIKAWA, "Dalitz-Plot Analysis of Coulomb Exploding O_3 in Ultrashort Intense Laser Fields," *J. Chem. Phys.* **127**, 114318 (6 pages) (2007).

A. HISHIKAWA, A. MATSUDA, M. FUSHITANI and E. J. TAKAHASHI, "Visualizing Recurrently Migrating Hydrogen by Few-Cycle Intense Laser Pulses," *J. Phys.: Conf. Series* **88**, 012056 (6 pages) (2007).

A. HISHIKAWA, A. MATSUDA, M. FUSHITANI and E. J. TAKAHASHI, "Visualizing Recurrently Migrating Hydrogen in Acetylene Dication by Intense Ultrashort Laser Pulses," *Phys. Rev. Lett.* **99**, 258302 (4 pages) (2007).

A. HISHIKAWA, A. MATSUDA, E. J. TAKAHASHI and M. FUSHITANI, "Acetylene-Vinylidene Isomerization in Ultrashort Intense Laser Fields Studied by Triple-Ion Coincidence Momentum Imaging," *J. Chem. Phys.* **128**, 084302 (5 pages) (2008).

M. LABAT, C. BRUNI, G. LAMBERT, M. HOSAKA, M. SHIMADA, M. KATOH, A. MOCHIHASHI, T. TAKASHIMA, T. HARA and M. E. COUPRIE, "Local Heating Induced by Coherent Harmonic Generation on Electron Beam Dynamics in Storage Ring," *Europhys. Lett.* **81**, 34004 (2008).

M. SHIMADA, M. KATOH, S. KIMURA, A. MOCHIHASHI, M. HOSAKA, Y. TAKASHIMA, T. HARA and T. TAKAHASHI, "Intense Terahertz Synchrotron Radiation by Laser Bunch Slicing at UVSOR-II Electron Storage Ring," *Jpn. J. Appl. Phys.* **46**, 7939–7944 (2007).

S. BIELAWSKI, C. EVAIN, T. HARA, M. HOSAKA, M. KATOH, S. KIMURA, A. MOCHIHASHI, M. SHIMADA, C. SZWAJ, T. TAKAHASHI and Y. TAKASHIMA, "Tunable Narrowband Terahertz Emission from Mastered Laser–Electron Beam Interaction," *Nat. Phys.* **4**, 390–393 (2008).

M. LABAT, G. LAMBERT, M. E. COUPRIE, M. SHIMADA, M. KATOH, M. HOSAKA, Y. TAKASHIMA, T. HARA and A. MOCHIHASHI, "Coherent Harmonic Generation Experiments on UVSOR-II Storage Ring," *Nucl. Instrum. Methods Phys. Res., Sect. A* **593**, 1–5 (2008).

K. E. LEE, C. I. LEE, H. J. OH, H. J. IM, T. PARK, S. KIMURA and Y. S. KWON, "Optical Evidence for a Change in the Heavy Electron Fermi Surface at a Magnetic Quantum Critical Point of CeNi$_{1-x}$Co$_x$Ge$_2$," *J. Phys.: Condens. Matter* **20**, 285202 (5 pages) (2008).

H. J. IM, T. ITO, H. -D. KIM, S. KIMURA, K. E. LEE, J. B. HONG, Y. S. KWON, A. YASUI and H. YAMAGAMI, "Direct Observation of Dispersive Kondo Resonance Peaks in a Heavy-Fermion System," *Phys. Rev. Lett.* **100**, 176402 (4 pages) (2008).

S. KIMURA, H. OKAMURA, T. NANBA and H. KIMURA, "Preface," *Infrared Phys. Tech.* **51**, 361–362 (2008).

T. YAJI, Y. YAMAMOTO, T. OHTA and S. KIMURA, "A New Beamline for Infrared Microscopy in the SR Center of Ritsumeikan University," *Infrared Phys. Tech.* **51**, 397–399 (2008).

Y. Y. SONG, K. E. LEE, J. B. HONG, H. J. IM, S. KIMURA and Y. S. KWON, "Dramatic Change of Optical Properties at a Quantum Critical Point in the Heavy Fermion System CeNi$_{1-x}$Co$_x$Ge$_2$," *Infrared Phys. Tech.* **51**, 485–487 (2008).

C. I. LEE, K. E. LEE, Y. Y. SONG, H. J. IM, S. KIMURA and Y. S. KWON, "Hybridization Gap-Open in CeIn$_3$," *Infrared Phys. Tech.* **51**, 488–490 (2008).

G. FUNABASHI, H. FUJIWARA, A. SEKIYAMA, M. HASUMOTO, T. ITO, S. KIMURA, P. BALTZER and S. SUGA, "Ultrahigh-Resolution Vacuum Ultraviolet Light Source System for Extremely Low Energy Photoelectron Spectroscopy," *Jpn. J. Appl. Phys.* **47**, 2265–2269 (2008).

S. KIMURA, T. MIZUNO, K. MATSUBAYASHI, K. IMURA, H. S. SUZUKI and N. K. SATO, "Infrared Study on the Electronic Structure of SmS in the Black Phase," *Physica B* **403**, 805–807 (2008).

H. MIYAZAKI, T. ITO, S. OTA, M. KATO, S. YAGI, K. SODA, H. J. IM and S. KIMURA, "Angle-Resolved Photoemission Study on the Ferromagnetic Ordering of EuO Thin Films," *Physica B* **403**, 917–918 (2008).

J. SICHELSCHMIDT, S. KIMURA, C. KRELLNER, C. GEIBEL and F. STEGLICH, "Optical Properties of YbRh$_2$Si$_2$ and YbIr$_2$Si$_2$: A Comparison," *Physica B* **403**, 775–777 (2008).

Y. HIKOSAKA, Y. VELKOV, E. SHIGEMASA, T. KANEYASU, Y. TAMENORI, J. LIU and F. GEL'MUKHANOV, "X-Ray Absorption Measured in the Resonant Auger Scattering Mode," *Phys. Rev. Lett.* **101**, 073001 (4 pages) (2008).

T. KANEYASU, Y. HIKOSAKA, E. SHIGEMASA, P. LABLANQUIE, F. PENENT and K. ITO, "Auger Decays of 1s Shake-up and Shake-off States in N$_2$ Molecules," *J. Phys. B* **41**, 135101 (6 pages) (2008).

Y. HIKOSAKA, P. LABLANQUIE, E. SHIGEMASA, T. AOTO and K. ITO, "Sub-Natural Linewidth Spectroscopy on Core-Valence Doubly Ionized States of OCS," *J. Phys. B* **41**, 025103 (4 pages) (2008).

T. KANEYASU, Y. HIKOSAKA, E. SHIGEMASA, F. PENENT, P. LABLANQUIE, T. AOTO and K. ITO, "Autoionization of the Ne$^+$ Rydberg States Formed via Valence Photoemission," *J. Phys. B* **40**, 4047–4060 (2007).

Y. HIKOSAKA, P. LABLANQUIE, F. PENENT, T. KANEYASU, E. SHIGEMASA, J. H. D. ELAND, T. AOTO and K. ITO, "Single, Double, and Triple Auger Decay of the Xe 4p Core-Hole States," *Phys. Rev. A* **76**, 032708 (6 pages) (2007).

T. KANEYASU, Y. HIKOSAKA, E. SHIGEMASA, F. PENENT, P. LABLANQUIE, T. AOTO and K. ITO, "State-Selective Cross Sections of Multiple Photoionization in Ne," *Phys. Rev. A* **76**, 012717 (7 pages) (2007).

J. SAIKAWA, M. FUJII, H. ISHIZUKI and T. TAIRA, "High-Energy, Narrow-Bandwidth Periodically Poled Mg-Doped LiNbO$_3$ Optical Parametric Oscillator with a Volume Bragg Grating," *Opt. Lett.* **32**, 2996–2998 (2007).

Y. PETIT, B. BOULANGER, P. SEGONDS and T. TAIRA, "Angular Quasi-Phase-Matching," *Phys. Rev. A* **76**, 063817 (7 pages) (2007).

R. BHUSHAN, H. YOSHIDA, K. TSUBAKIMOTO, H. FUJITA, M. NAKATSUKA, N. MIYANAGA, Y. IZAWA, H. ISHIZUKI and T. TAIRA, "Generation of High Efficiency 2μm Laser Pulse from a Periodically Poled 5 mol% MgO-Doped LiNbO$_3$ Optical Parametric Oscillator," *Appl. Phys. Express* **1**, 022007 (3 pages) (2008).

R. BHUSHAN, H. YOSHIDA, K. TSUBAKIMOTO, H. FUJITA, M. NAKATSUKA, N. MIYANAGA, Y. IZAWA, H. ISHIZUKI and T. TAIRA, "High Efficiency and High Energy Parametric Wavelength Conversion Using a Large Aperture Periodically Poled MgO:LiNbO$_3$," *Opt. Commun.* **281**, 3902–3905 (2008).

J. SAIKAWA, M. MIYAZAKI, M. FUJII, H. ISHIZUKI and T. TAIRA, "High-Energy, Broadly Tunable, Narrow-Bandwidth Mid-Infrared Optical Parametric System Pumped by Quasi-Phase-Matched Devices," *Opt. Lett.* **33**, 1699–1701 (2008).

M. FUYUKI, K. WATANABE, D. INO, H. PETEK and Y. MATSUMOTO, "Electron-Phonon Coupling at an Atomically Defined Interface: Na Quantum Well on Cu(111)," *Phys. Rev. B* **76**, 115427 (5 pages) (2007).

Y. TAMENORI, K. OKADA, K. TABAYASHI, T. GEJO and K. HONMA, "Specific Fragmentation of [(CH$_3$)$_2$CO]Ar$_n$ Heteroclusters Induced by the Ar L$_{23}$- and O K-Shell Excitation," *Chem. Phys. Lett.* **462**, 40–44 (2008).

Materials Molecular Science

M. INAMO, C. OKABE, T. NAKABAYASHI, N. NISHI and M. HOSHINO, “Femtosecond Time-Resolved Photo-Absorption Studies on the Excitation Dynamics of Chromium(III) Porphyrin Complexes in Solution,” *Chem. Phys. Lett.* **445**, 167–172 (2007).

J. NISHIJO, O. OISHI, K. JUDAI and N. NISHI, “Facile and Mass-Producible Fabrication of One-Dimensional Ag Nanoparticle Arrays,” *Chem. Mater.* **19**, 4627–4629 (2007).

K. INOUE, K. OHASHI, T. IINO, K. JUDAI, N. NISHI and H. SEKIYA, “Infrared Spectroscopy of $Cu^+(H_2O)_n$ and $Ag^+(H_2O)_n$: Coordination and Solvation of Noble-Metal Ions,” *J. Chem. Phys.* **126**, 194302 (2007).

K. JUDAI, S. NUMAO, A. FURUYA, J. NISHIJO and N. NISHI, “Increased Electric Conductance through Physisorbed Oxygen on Copper Nanocables Sheathed in Carbon,” *J. Am. Chem. Soc.* **130**, 1142–1143 (2008).

B. -H. BOO, S. -J. KIM, M. -H. LEE and N. NISHI, “Molecular Structures and Energies of Low-Lying Li_xSi_x (x = 1–4) Clusters: Comparison with Li_xC_x (x = 1, 2, 4) Clusters,” *Chem. Phys. Lett.* **453**, 150–154 (2008).

K. YAMAMOTO, S. IWAI, S. BOYKO, A. KASHIWAZAKI, F. HIRAMATSU, C. OKABE, N. NISHI and K. YAKUSHI, “Strong Optical Nonlinearity and Its Ultrafast Response Associated with Electron Ferroelectricity in an Organic Conductor,” *J. Phys. Soc. Jpn.* **77**, 074709 (6 pages) (2008).

T. NAKAGAWA, Y. TAKAGI, Y. MATSUMOTO and T. YOKOYAMA, “Enhancements of Spin and Orbital Magnetic Moments of Submonolayer Co on Cu(001) Studied by X-Ray Magnetic Circular Dichroism Using a Superconducting Magnet and a Liquid He Cryostat,” *Jpn. J. Appl. Phys.* **47**, 2132–2136 (2008).

D. MATSUMURA, T. NAKAGAWA, H. WATANABE, H. ABE, K. AMEMIYA, T. OHTA and T. YOKOYAMA, “Magnetization Process of Co/Pd(111) Thin Films: Chemisorption-Induced Spin Reorientation Transition,” *Surf. Sci.* **602**, 1999–2003 (2008).

Y. NEGISHI, N. K. CHAKI, Y. SHICHIBU, R. L. WHETTEN and T. TSUKUDA, “Origin of Magic Stability of Thiolated Gold Clusters: A Case Study on $Au_{25}(SC_6H_{13})_{18}$,” *J. Am. Chem. Soc.* **129**, 11322–11323 (2007).

S. KANAOKA, N. YAGI, Y. FUKUYAMA, S. AOSHIMA, H. TSUNOYAMA, T. TSUKUDA and H. SAKURAI, “Thermosensitive Gold Nanoclusters Stabilized by Well-Defined Vinyl Ester Star Polymers: Reusable and Durable Catalysts for Aerobic Alcohol Oxidation,” *J. Am. Chem. Soc.* **129**, 12060–12061 (2007).

T. MATSUMOTO, P. NICKUT, T. SAWADA, H. TSUNOYAMA, K. WATANABE, T. TSUKUDA, K. AL-SHAMERY and Y. MATSUMOTO, “Deposition and Fabrication of Alkanethiolate Gold Nanocluster Film on TiO_2 (110) and the Effects of Plasma Etching,” *Surf. Sci.* **601**, 5121–5126 (2007).

T. MATSUMOTO, P. NICKUT, H. TSUNOYAMA, K. WATANABE, T. TSUKUDA, K. AL-SHAMERY and Y. MATSUMOTO, “Thermal and Photochemical Reactivity of Oxygen Atoms on Gold Nanocluster Surfaces,” *Surf. Sci.* **601**, 5226–5231 (2007).

Y. MURASE, T. KITAGAWA, M. IMAMURA, A. TANAKA, H. YASUDA, Y. NEGISHI, T. TSUKUDA, S. UEDA, Y. YAMASHITA, H. YOSHIKAWA and K. KOBAYASHI, “Electronic Structure of Dendrimer-Au Hybrid Nanoparticle: Hard X-Ray Photoemission Study,” *Trans. Mater. Res. Soc. Jpn.* **33**, 169–172 (2008).

N. K. CHAKI, Y. NEGISHI, H. TSUNOYAMA, Y. SHICHIBU and T. TSUKUDA, “Ubiquitous 8 and 29 kDa Gold:alkanethiolate Cluster Compounds: Mass-Spectrometric Determination of Molecular Formulas and Structural Implications,” *J. Am. Chem. Soc.* **130**, 8608–8610 (2008).

E. S. SHIBU, M. A. HABEEB MUHAMMED, T. TUSKUDA and T. PRADEEP, “Ligand Exchange of $Au_{25}SG_{18}$ Leading to Functionalized Gold Clusters: Spectroscopy, Kinetics and Luminescence,” *J. Phys. Chem. C* **112**, 12168–12176 (2008).

M. URUICHI, Y. YUE, K. YAKUSHI and T. MOCHIDA, “Two-Phase Coexistence in the Monovalent-to-Divalent Phase Transition in Dineopentylbiferrocene-Fluorotetracyanoquinodimethane, (npBifc-($F_1TCNQ)_3$), Charge-Transfer Salt,” *J. Phys. Soc. Jpn.* **76**, 124707 (6 pages) (2007).

M. TANAKA, K. YAMAMOTO, M. URUICHI, T. YAMAMOTO, K. YAKUSHI, S. KIMURA and H. MORI, “Charge-Ordering Phase Transition in β-(DMBEDT-TTF)$_2$PF$_6$ Neighboring on a Superconducting State,” *J. Phys. Soc. Jpn.* **77**, 024714 (8 pages) (2008).

S. IWAI, K. YAMAMOTO, F. HIRAMATSU, H. NAKAYA, Y. KAWAKAMI and K. YAKUSHI, “Hydrostatic Pressure Effect on Photoinduced Insulator-to-Metal Transition in Layered Organic Salt α-(BEDT-TTF)$_2$I$_3$,” *Phys. Rev. B* **77**, 125131 (5 pages) (2008).

T. YAMAMOTO, H. M. YAMAMOTO, R. KATO, M. URUICHI, K. YAKUSHI, H. AKUTSU, A. SATO-AKUTSU, A. KAWAMOTO, S. S. TURNER and P. DAY, “Inhomogeneous Site-Charges at the Boundary between the Insulating, Superconducting, and Metallic Phases of β”-Type ET Molecular Charge-Transfer Salts, (ET = bisethylene-dithiatetrathiafulvalene),” *Phys. Rev. B* **77**, 205120 (14 pages) (2008).

H. NAKAYA, F. HIRAMATSU, Y. KAWAKAMI, S. IWAI, K. YAMAMOTO and K. YAKUSHI, “30 fs Infrared Spectroscopy of Photo-Induced Phase Transition in 1/4 Filling Organic Salt,” *J. Lumin.* **128**, 1065–1068 (2008).

K. YAMAMOTO, S. IWAI, S. BOYKO, A. KASHIWAZAKI, F. HIRAMATSU, C. OKABE, N. NISHI and K. YAKUSHI, “Strong Optical Nonlinearlity and Its Ultrafast Response Associated with Electron Ferroelectricity in an Organic Conductor,” *J. Phys. Soc. Jpn.* **77**, 074709 (6 pages) (2008).

M. URUICHI, C. NAKANO, M. TANAKA, K. YAKUSHI, T. KAIHATSU and J. YAMADA, “Infrared and Raman Spectroscopic Study of BDA-TTP [1,5-bis(1,3-dithian-2-ylidene)-1,3,4,6-tetrathiapentalene] and Its Charge-Transfer Salts,” *Solid State Commun.* **47**, 484–489 (2008).

K. SATO, R. RAHIMI, N. MORI, S. NISHIDA, K. TOYOTA, D. SHIOMI, Y. MORITA, A. UEDA, S. SUZUKI, K. FURUKAWA, T. NAKAMURA, M. KITAGAWA, K. NAKASUJI, M. NAKAHARA, H. HARA, P. CARL, P. HOFER and T. TAKUI, “Implementation of Molecular Spin Quantum Computing by Pulsed ENDOR Technique: Direct Observation of Quantum Entanglement and Spinor,” *Physica E* **40**, 363–366 (2007).

T. KAKIUCHI, Y. WAKABAYASHI, H. SAWA, T. TAKAHASHI and T. NAKAMURA, “Charge Ordering in α-(BEDT-TTF)$_2$I$_3$ by Synchrotron X-Ray Diffraction,” *J. Phys. Soc. Jpn.* **76**, 113702 (4 pages) (2007).

LIST OF PUBLICATIONS

K. MAEDA, T. HARA, K. FURUKAWA and T. NAKAMURA, "Multi-Frequency ESR Studies on Low-Dimensional Antiferromagnets, ζ-(BEDT-TTF)$_2$PF$_6$(THF) and γ-(BEDT-TTF)$_2$PF$_6$," *Bull. Chem. Soc. Jpn.* **81**, 84–90 (2008).

H. M. YAMAMOTO, Y. KOSAKA, R. MAEDA, J. YAMAURA, A. NAKAO, T. NAKAMURA and R. KATO, "Supramolecular Insulating Networks Sheathing Conducting Nanowires Based on Organic Radical Cations," *ACS Nano* **2**, 143–155 (2008).

M. ITOI, C. ARAKI, M. HEDO, Y. UWATOKO and T. NAKAMURA, "Anomalously Wide Superconducting Phase of One-Dimensional Organic Conductor (TMTTF)$_2$SbF$_6$," *J. Phys. Soc. Jpn.* **77**, 023701 (4 pages) (2008) [Editors' Choice].

T. HARA, K. FURUKAWA, T. NAKAMURA, Y. YAMAMOTO, A. KOSAKA, W. JIN, T. FUKUSHIMA and T. AIDA, "Possible One-Dimensional Helical Conductor: Hexa-*peri*-hexabenzocoronene Nanotube," *J. Phys. Soc. Jpn.* (OPEN SELECT) **77**, 034710 (6 pages) (2008).

R. CHIBA, K. HIRAKI, T. TAKAHASHI, H. M. YAMAMOTO and T. NAKAMURA, "Charge Disproportionation and Dynamics in θ-(BEDT-TTF)$_2$CsZn(SCN)$_4$," *Phys. Rev. B* **77**, 115113 (10 pages) (2008).

A. XIA, J. HU, C. WANG and D. JIANG, "Synthesis of Magnetic Microspheres with Controllable Structure via Polymerization-Triggered Self-Positioning of Nanocrystals," *Small* **3**, 1811–1817 (2007).

D. YANG, G. GUO, J. HU, C. WANG and D. JIANG, "Hydrothermal Treatment to Prepare Hydroxyl Group Modified Multi-Walled Carbon Nanotubes," *J. Mater. Chem.* **18**, 350–354 (2008).

A. HINDERHOFER, U. HEINEMEYER, A. GERLACH, S. KOWARIK, R. M. J. JACOBS, Y. SAKAMOTO, T. SUZUKI and F. SCHREIBER, "Optical Properties of Pentacene and Perfluoropentacene Thin Films," *J. Chem. Phys.* **127**, 194705 (6 pages) (2007).

K. OHKUBO, Y. SAKAMOTO, T. SUZUKI, T. TSUZUKI, D. KUMAKI and S. TOKITO, "Synthesis, Structure, and Transport Property of Perfluorinated Oligofluorenes," *Chem. Eur. J.* **14**, 4472–4474 (2008).

N. KOCH, A. GERLACH, S. DUHM, H. GLOWATZKI, G. HEIMEL, A. VOLLMER, Y. SAKAMOTO, T. SUZUKI, J. ZEGENHAGEN, J. P. RABE and F. SCHREIBER, "Adsorption-Induced Intramolecular Dipole: Correlating Molecular Conformation and Interface Electronic Structure," *J. Am. Chem. Soc.* **130**, 7300–7304 (2008).

I. SALZMANN, S. DUHM, G. HEIMEL, J. P. RABE, N. KOCH, M. OEHZELT, Y. SAKAMOTO and T. SUZUKI, "Structural Order in Perfluoropentacene Thin Films and Heterostructures with Pentacene," *Langmuir* **24**, 7294–7298 (2008).

S. KANAOKA, N. YAGI, Y. FUKUYAMA, S. AOSHIMA, H. TSUNOYAMA, T. TSUKUDA and H. SAKURAI, "Thermosensitive Gold Nanoclusters Stabilized by Well-Defined Vinyl Ether Star Polymers: Reusable and Durable Catalysts for Aerobic Alcohol Oxidation," *J. Am. Chem. Soc.* **129**, 12060–12061 (2007).

R. C. S. WONG, M. -L. OOI, H. SAKURAI and S. -W. NG, "Tris[2-(deuteriomethylsulfanyl)phenyl]phosphinedeuteriochloroform 0.125-solvate," *Acta Crystallogr., Sect. E: Struct. Rep. Online* **64**, o898 (2008).

S. HIGASHIBAYASHI and H. SAKURAI, "Asymmetric Synthesis of a Chiral Buckybowl, Trimethylsumanene," *J. Am. Chem. Soc.* **130**, 8592–8593 (2008).

R. YAMADA, H. KUMAZAWA, T. NOUTOSHI, S. TANAKA and H. TADA, "Electrical Conductance of Oligothiophene Molecular Wires," *Nano Lett.* **8**, 1237–1240 (2008).

F. NISHIYAMA, K. OGAWA, S. TANAKA and T. YOKOYAMA, "Direct Conformational Analysis of a 10 nm Long Oligothiophene Wire," *J. Phys. Chem. B* **112**, 5272–5275 (2008).

K. ONO, H. TOTANI, T. HIEI, A. YOSHINO, K. SAITO, K. EGUCHI, M. TOMURA, J. NISHIDA and Y. YAMASHITA, "Photooxidation and Reproduction of Pentacene Derivatives Substituted by Aromatic Groups," *Tetrahedron* **63**, 9699–9704 (2007).

M. TOMURA, K. ONO, M. KAIDEN, K. TSUKAMOTO and K. SAITO, "2*H*,10*H*-1,4-Dioxepino[5',6':4,5]thieno[3,2-*e*][1,4]dioxepine-5,7(3*H*,9*H*)-dione," *Acta Crystallogr., Sect. E: Struct. Rep. Online* **63**, o4568–o4569 (2007).

K. ONO, M. TOMURA and K. SAITO, "9,9-Bis(4-methoxyphenyl)-9*H*-cyclopenta[2,1-*b*:3,4-*b*']dipyridine," *Acta Crystallogr., Sect. E: Struct. Rep. Online* **63**, o4612–o4612 (2007).

M. TOMURA, "(*E*)-2-(2,6-Dichlorophenyl)-2-(phenylimino)acetamide," *Acta Crystallogr., Sect. E: Struct. Rep. Online* **64**, o170–o171 (2008).

M. TOMURA, H. YAMAGUCHI, K. ONO, M. KAIDEN and K. SAITO, "6,11-Dihydroxynaphthacene-5,12-dione," *Acta Crystallogr., Sect. E: Struct. Rep. Online* **64**, o172–o173 (2008).

K. ONO, M. TOMURA and K. SAITO, "Diethyl 2,3-Dihydrothieno[3,4-*b*]-1,4-dioxine-5,7-dicarboxylate," *Acta Crystallogr., Sect. E: Struct. Rep. Online* **64**, o468–o468 (2008).

M. TOMURA and Y. YAMASHITA, "3,8-Bis(4-chlorophenyl)-4,7-dimethyltricyclo[4.2.2.0^{2,5}]deca-3,7-diene," *Acta Crystallogr., Sect. E: Struct. Rep. Online* **64**, o545–o545 (2008).

M. TOMURA and Y. YAMASHITA, "Crystal Structure of 4-Cyanopyridinium Hydrogen Chloranilate," *Anal. Sci.* **24**, x31–x32 (2008).

M. KUJIME, C. IZUMI, M. TOMURA, M. HADA and H. FUJII, "Effect of a Tridentate Ligand on the Structure, Electronic Structure, and Reactivity of the Copper(I) Nitrite Complex: Role of the Conserved Three-Histidine Ligand Environment of the Type-2 Copper Site in Copper-Containing Nitrite Reductases," *J. Am. Chem. Soc.* **130**, 6088–6098 (2008).

K. ONO, K. TSUKAMOTO, M. TOMURA and K. SAITO, "1,4-Bis[(2,6-dimethoxyphenyl)ethynyl]benzene," *Acta Crystallogr., Sect. E: Struct. Rep. Online* **64**, o1069–o1069 (2008).

M. R. MOHAMADI, N. KAJI, M. TOKESHI and Y. BABA, "Dynamic Cross-Linking Effect of Mg^{2+} to Enhances Sieving Properties of Low-Viscosity Poly (vinylpyrrolidone) Solutions for Microchip Electrophoresis of Proteins," *Anal. Chem.* **80**, 312–318 (2008).

H. OKADA, N. KAJI, M. TOKESHI and Y. BABA, "Poly(methylmethacrylate) Microchip Electrophoresis of Proteins Using Linear-Poly(acrylamide) Solution as Separation Matrix," *Anal. Sci.* **24**, 321–325 (2008).

L. MAHMOUDIAN, N. KAJI, M. TOKESHI, M. NILSSON and Y. BABA, "Rolling Circle Amplification and Circle-to-Circle Amplification of a Specific Gene Integrated with Electrophoretic Analysis on a Single Chip," *Anal. Chem.* **80**, 2483–2490 (2008).
L. MAHMOUDIAN, J. MELIN, M. R. MOHAMADI, K. YAMADA, M. OHTA, N. KAJI, M. TOKESHI, M. NILSSON and Y. BABA, "Microchip Electrophoresis for Specific Gene Detection of the Pathogenic Bacteria V. Cholerae by Circle-to-Circle Amplification," *Anal. Sci.* **24**, 327–332, (Hot Article) (2008).
D. ONOSHIMA, N. KAJI, M. TOKESHI and Y. BABA, "Nuclease Tolerant FRET Probe Based on DNA-Quantum Dot Conjugation," *Anal. Sci.* **24**, 181–183, (Hot Article) (2008).

Y. KONDO, H. YOSHIKAWA, K. AWAGA, M. MURAYAMA, T. MORI, K. SUNADA, S. BANDOW and S. IIJIMA, "Preparation, Photocatalytic Activities, and Dye-Sensitized Solar-Cellperformance of Submicron-Scale TiO_2 Hollow Spheres," *Langmuir* **24**, 547–550 (2008).
T. FUJIMOTO, R. SUIZU, H. YOSHIKAWA and K. AWAGA, "Molecular, Crystal, and Thin-Film Structures of Octathio[8]circulene: Release of Anti-Aromatic Molecular Distortion and Lamellar Structure of Self-Assembling Thin Films," *Chem. Eur. J.* **14**, 6053–6056 (2008).
K. AWAGA, Y. UMEZONO, W. FUJITA, H. YOSHIKAWA, H. -B. CUI, H. KOBAYASHI, S. STANILAND and N. ROBERTSON, "Diverse Magnetic and Electrical Properties of Molecular Solids Containing the Thiazyl Radical BDTA," *Inorg. Chim. Acta* **361**, 3761–3770 (2008).

Life and Coordination-Complex Molecular Science

S. F. EL-MASHTOLY, Y. GU, H. YOSHIMURA, S. YOSHIOKA, S. AONO and T. KITAGAWA, "Protein Conformation Changes of HemAT-Bs upon Ligand Binding Probed by Ultraviolet Resonance Raman Spectroscopy," *J. Biol. Chem.* **283**, 6942–6949 (2008).
M. NISHIMURA, H. YOSHIMURA, K. OZAWA, S. YOSHIOKA, M. KUBO, T. KITAGAWA and S. AONO, "Hydrogen Bonding Interaction on the Heme-Bound Ligand in the Heme-Based O_2 Sensor Protein," *J. Porphyrins Phthalocyanines* **12**, 142–148 (2008).

T. INOBE, K. TAKAHASHI, K. MAKI, S. ENOKI, K. KAMAGATA, A. KADOOKA, M. ARAI and K. KUWAJIMA, "Asymmetry of the GroEL-GroES Complex under Physiological Conditions as Revealed by Small-Angle X-Ray Scattering," *Biophys. J.* **94**, 1392–1402 (2008).
K. KUWAJIMA, "Structure, Stability and Dynamics of Authentic and Recombinant α-Lactalbumin," *Milk Science* (in Japanese) **56**, 119–122 (2008).

Y. YAMAGUCHI, T. HIRAO, E. SAKATA, Y. KAMIYA, E. KURIMOTO, Y. YOSHIDA, T. SUZUKI, K. TANAKA and K. KATO, "Fbs1 Protects the Malfolded Glycoproteins from the Attack of Peptide:*N*-Glycanase," *Biochem. Biophys. Res. Commun.* **362**, 712–716 (2007).
H. SASAKAWA, E. SAKATA, Y. YAMAGUCHI, M. MASUDA, T. MORI, E. KURIMOTO, T. IGUCHI, S. HISANAGA, T. IWATSUBO, M. HASEGAWA and K. KATO, "Ultra-High Field NMR Studies of Antibody Binding and Site-Specific Phosphorylation of α-Synuclein," *Biochem. Biophys. Res. Commun.* **363**, 795–799 (2007).
E. KURIMOTO, M. SUZUKI, E. AMEMIYA, Y. YAMAGUCHI, S. NIRASAWA, N. SHIMBA, N. XU, T. KASHIWAGI, M. KAWAI, E. SUZUKI and K. KATO, "Curculin Exhibits Sweet-Tasting and Taste-Modifying Activities through Its Distinct Molecular Surfaces," *J. Biol. Chem.* **282**, 33252–33256 (2007).
Y. KAMIYA, D. KAMIYA, K. YAMAMOTO, B. NYFELER, H. -P. HAURI and K. KATO, "Molecular Basis of Sugar Recognition by the Human L-Type Lectins ERGIC-53, VIPL and VIP36," *J. Biol. Chem.* **283**, 1857–1861 (2008).
H. YAGI, M. NAKAGAWA, N. TAKAHASHI, S. KONDO, M. MATSUBARA and K. KATO, "Neural Complex-Specific Expression of Xylosyl *N*-Glycan in *Ciona Intestinalis*," *Glycobiology* **18**, 145–151 (2008).
B. NYFELER, Y. KAMIYA, F. BOEHLEN, K. YAMAMOTO, K. KATO, P. DE MOERLOOSE, H. -P. HAURI and M. NEERMAN-ARBEZ, "Deletion of 3 Residues from the C-Terminus of MCFD2 Affects Binding to ERGIC-53 and Causes Combined Factor V and Factor VIII Deficiency," *Blood* **111**, 1299–1301 (2008).
E. KURIMOTO, Y. NISHI, Y. YAMAGUCHI, T. ZAKO, R. IIZUKA, N. IDE, M. YOHDA and K. KATO, "Dynamics of Group II Chaperonin and Prefoldin Probed by ^{13}C NMR Spectroscopy," *Proteins: Struct., Funct., Bioinf.* **70**, 1257–1263 (2008).
H. YASHIRODA, T. MIZUSHIMA, K. OKAMOTO, T. KAMEYAMA, H. HAYASHI, T. KISHIMOTO, S. NIWA, M. KASAHARA, E. KURIMOTO, E. SAKATA, K. TAKAGI, A. SUZUKI, Y. HIRANO, S. MURATA, K. KATO, T. YAMANE and K. TANAKA, "Crystal Structure of a Chaperone Complex that Contributes to the Assembly of Yeast 20S Proteasomes," *Nat. Struct. Mol. Biol.* **15**, 228–236 (2008).
H. YAGI, N. YASUKAWA, S. -Y. YU, C. -T. GUO, N. TAKAHASHI, T. TAKAHASHI, W. BUKAWA, T. SUZUKI, K. -H. KHOO, Y. SUZUKI and K. KATO, "The Expression of Sialylated High-Antennary *N*-Glycans in Edible Bird's Nest," *Carbohydr. Res.* **343**, 1373–1377 (2008).
H. YAGI, K. YAMADA, E. OHNO, M. UTSUMI, Y. YAMAGUCHI, E. KURIMOTO, N. TAKAHASHI, S. OKA, T. KAWASAKI and K. KATO, "Development and Application of High Performance Liquid Chromatography Map of Glucuronyl *N*-Glycans," *Open Glycoscience* **1**, 8–18 (2008).
S. MIYAKAWA, Y. NOMURA, T. SAKAMOTO, Y. YAMAGUCHI, K. KATO, S. YAMAZAKI and Y. NAKAMURA, "Structural and Molecular Basis for Hyperspecificity of RNA Aptamer to Human Immunoglobulin G," *RNA* **14**, 1154–1163 (2008).
Y. HIRANO, T. KANEKO, K. OKAMOTO, M. BAI, H. YASHIRODA, K. FURUYAMA, K. KATO, K. TANAKA and S. MURATA, "Dissecting β-Ring Assembly Pathway of the Mammalian 20S Proteasome," *EMBO J.* **27**, 2204–2213 (2008).

M. KUJIME, C. IZUMI, T. TOMURA, M. HADA and H. FUJII, "Effect of a Tridentate Ligand on the Structure, Electronic Structure, and Reactivity of the Copper(I) Nitrite Complex: Role of the Conserved Three-Histidine Ligand Environment of the Type-2 Copper Site in Copper-Containing Nitrite Reductases," *J. Am. Chem. Soc.* **130**, 6088–6098 (2008).

T. KURAHASHI, A. KIKUCHI, T. TOSHA, Y. SHIRO, T. KITAGAWA and H. FUJII, "Transient Intermediates from Mn(salen) with Sterically-Hindered Mesityl Groups: Interconversion between Mn(IV)-Phenolate and Mn(III)-Phenoxyl Radical as an Origin for Unique Reactivity," *Inorg. Chem.* **47**, 1674–1686 (2008).

T. KURAHASHI and H. FUJII, "Chiral Distortion in $Mn^{IV}(salen)(N_3)_2$ from Jacobsen's Catalyst as a Conformation Model for Enantioselective Reactions," *Inorg. Chem.* **47**, 7556–7567 (2008).

T. URISU, T. ASANO, Z. ZHANG, H. UNO, R. TERO, H. JUNKYU, I. HIROKO, Y. ARIMA, H. IWATA, K. SHIBASAKI and M. TOMINAGA, "Incubation Type Si-Based Planar Ion Channel Biosensor," *Anal. Bioanal. Chem.* **391**, 2703–2709 (2008).

Z. L. ZHANG, T. ASANO, H. UNO, R. TERO, M. SUZUI, S. NAKAO, T. KAITO, K. SHIBASAKI, M. TOMINAGA, Y. UTSUMI, Y. L. GAO and T. URISU, "Fabrication of Si-Based Planar Type Patch Clamp Biosensor Using Silicon on Insulator Substrate," *Thin Solid Films* **516**, 2813–2815 (2008).

Y. MAO, R. TERO, Y. IMAI, T. HOSHINO and T. URISU, "The Morphology of $GM1_x/SM_{0.6-x}/Chol_{0.4}$ Planar Bilayers Supported on SiO_2 Surfaces," *Chem. Phys. Lett.* **460**, 289–294 (2008).

R. TERO, T. UJIHARA and T. URISU, "Effect of Solid Surface Properties on the Formation Process and Structure of Supported Planar Bilayer Membrane," *Hyomen* (in Japanese) **46**, 287–299 (2008).

R. TERO, T. UJIHARA and T. URISU, "Supported Lipid Bilayers Membranes on SiO_2 and TiO_2: Substrate Effects on Membrane Formation and Shape Transformation," *Proc. SPIE* **6769**, 67690J (12 pages) (2007).

R. AOKI, T. ARAKAWA, N. MISAWA, R. TERO, T. URISU, A. TAKEUCHI and T. OGINO, "Immobilization of Protein Molecules on Step-Controlled Sapphire Surfaces," *Surf. Sci.* **601**, 4915–4921 (2007).

A. KANNO, Y. YAMANAKA, H. HIRANO, Y. UMEZAWA and T. OZAWA, "Cyclic Luciferase for Real-Time Sensing of Caspase-3 Activities in Living Mammals," *Angew. Chem., Int. Ed.* **46**, 7595–7599 (2007).

M. TAKEUCHI and T. OZAWA, "Methods for Imaging and Analyses of Intracellular Organelles Using Fluorescent and Luminescent Proteins," *Anal. Sci.* **23**, 25–29 (2007).

T. OZAWA and Y. UMEZAWA, "Identification of Proteins Targeted into the Endoplasmic Reticulum by cDNA Library Screening," *Methods Mol. Biol.* **390**, 269–280 (2007).

T. OZAWA and Y. UMEZAWA, "A Genetic Method to Identify Mitochondrial Proteins in Living Mammalian Cells," *Methods Mol. Biol.* **390**, 119–130 (2007).

Y. M. A. YAMADA and Y. UOZUMI, "Development of a Convoluted Polymeric Nanopalladium Catalyst: α-Alkylation of Ketones and Ring-Opening Alkylation of Cyclic 1,3-Diketones with Primary Alcohols," *Tetrahedron* **63**, 8492–8498 (2007).

Y. UOZUMI, "Asymmetric Allylic Substitution of Cycloalkenyl Esters in Water with an Amphiphilic Resin-Supported Chiral Palladium Complex," *Pure Appl. Chem.* **79**, 1481–1489 (2007).

Y. UOZUMI, H. TAKENAKA and T. SUZUKA, "Allylic Substitution of *meso*-1,4-Diacetoxycycloalkenes in Water with an Amphiphilic Resin-Supported Chiral Palladium Complex," *Synlett* 1557–1561 (2008).

Y. UOZUMI and T. SUZUKA, "π-Allylic Sulfonylation in Water with Amphiphilic Resin-Supported Palladium-Phosphine Complexes," *Synthesis* 1960–1964 (2008).

Y. OE and Y. UOZUMI, "Highly Efficient Heterogeneous Aqueous Kharasch Reaction with an Amphiphilic Resin-Supported Ruthenium Catalyst," *Adv. Synth. Catal.* **350**, 1771–1775 (2008).

H. TANNAI, T. KOIZUMI, T. WADA and K. TANAKA, "Electrochemical and Photochemical Behavior of a Ruthenium(II) Complex Bearing Two Redox Sites as a Model for the NAD^+/NADH Redox Couple," *Angew. Chem., Int. Ed.* **46**, 7112–7115 (2007).

Y. MIYAZATO, T. WADA, J. MUCKERMAN, E. FUJITA and K. TANAKA, "Generation of Ru(II)–Semiquinone–Anilino Radical through Deprotonation of Ru(III)–Semiquinone–Anilido Complex," *Angew. Chem., Int. Ed.* **46**, 5728–5730 (2007).

D. POLANSKY, D. CABELLI, J. MUCKERMAN, E. FUJITA, T. KOIZUMI, T. FUKUSHIMA, T. WADA and K. TANAKA, "Photochemical and Radiolytic Production of an Organic Hydride Donor with a Ru^{II} Complex Containing an NAD^+ Model Ligand," *Angew. Chem., Int. Ed.* **46**, 4169–4172 (2007).

H. OHTSU, S. TAKAISHI, K. IMAMURA, A. ISHII, K. TANAKA, M. HASEGAWA and M. YAMASHITA, "Remarkable Functions of Long-Chain Alkyl Groups in Halogen-Bridged Nickel(III) Nanowire Complexes," *Eur. J. Inorg. Chem.* **46**, 4425–4428 (2007).

M. YAMASHITA, H. FURUTACHI, T. TOSHA, S. FUJINAMI, W. SAITO, Y. MAEDA, K. TAKAHASHI, K. TANAKA, T. KITAGAWA and M. SUZUKI, "Regioselective Arene Hydroxylation Mediated by a (μ-peroxo)diiron(III) Complex: A Functional Model for Toluene Monooxygenase," *J. Am. Chem. Soc.* **129**, 2–3 (2007).

J. MUCKERMAN, D. POLANSKY, T. WADA, K. TANAKA and E. FUJITA, "Water Oxidation by a Ruthenium Complex with Non-Innocent Quinone Ligands: Possible Formation of an O–O Bond at a Low Oxidation State of the Metal," *Inorg. Chem.* **47**, 1787–1802 (2008).

D. POLANSKY, D. CABELLI, J. MUCKERMAN, T. FUKUSHIMA, K. TANAKA and E. FUJITA, "Mechanism of Hydride Donor Generation Using a Ru(II) Complex Containing an NAD^+ Model Ligand: Pulse and Steady-State Radiolysis Studies," *Inorg. Chem.* **47**, 3958–3968 (2008).

F. AKAGI, T. MATSUO and H. KAWAGUCHI, "Dinitrogen Cleavage by a Diniobium Tetrahydride Complex: Formation of a Nitride and Its Conversion into Imide Species," *Angew. Chem., Int. Ed.* **46**, 8778–8781 (2007).

T. MATSUO and H. KAWAGUCHI, "Anisole-Diphenoxide Ligands and Their Zirconium Dichloride and Dialkyl Complexes," *Inorg. Chem.* **46**, 8426–8434 (2007).

Y. SHIBUYA, K. NABARI, M. KONDO, S. YASUE, K. MAEDA, F. UCHIDA and H. KAWAGUCHI, "The Copper(II) Complex with Two Didentate Schiff Base Ligands. The Unique Rearrangment that Proceeds under Alcohol Vapor in the Solid State to Construct Noninclusion Structure," *Chem. Lett.* **37**, 78–79 (2008).

A. KUNISHITA, J. TERAOKA, J. D. SCANLON, T. MATSUMOTO, M. SUZUKI, C. J. CRAMER and S. ITOH, "Aromatic Hydroxylation Reactivity of a Mononuclear Cu(II)-Alkylperoxo Complex," *J. Am. Chem. Soc.* **129**, 7248–7249 (2007).

T. NAGATAKI and S. ITOH, "Catalytic Alkane Hydroxylation Reaction with Nickel(II) Complexes Supported by Di- and Triphenol Ligands," *Chem. Lett.* **36**, 748–749 (2007).

M. INOSAKO, C. SHIMOKAWA, H. SUGIMOTO, N. KIHARA, T. TAKATA and S. ITOH, "Reaction of Copper(II) Complexes and Na_2S_2. An Alternative Method for the Preparation of Dicopper(II)-Disulfido Complexes," *Chem. Lett.* **36**, 1306–1307 (2007).

Y. NAKAIKE, N. TABA, S. ITOH, Y. TOBE, N. NISHIWAKI and M. ARIGA, "Nucleophilic Substitution Accompanying Carbon–Carbon Bond Cleavage Assisted by a Nitro Group," *Bull. Chem. Soc. Jpn.* **80**, 2413–2417 (2007).

H. SUGIMOTO, H. TANO, R. TAJIMA, H. MIYAKE, H. TSUKUBE, H. OHI and S. ITOH, "In-Situ Generation of Oxo-Sulfido Bis(dithiolene) Tungsten(VI) Complexes: Active Site Models for the Aldehyde Ferredoxin Oxidoreductase Family of Tungsten Enzymes," *Inorg. Chem.* **46**, 8460–8462 (2007).

A. KUNISHITA, H. ISHIMARU, S. NAKASHIMA, T. OGURA and S. ITOH, "Reactivity of Mononuclear Alkylperoxo Copper(II) Complex. O–O Bond Cleavage and C–H Bond Activation," *J. Am. Chem. Soc.* **130**, 4244–4245 (2008).

D. MAITI, A. A. N. SARJEANT, S. ITOH and K. D. KARLIN, "Suggestion of an Organometallic Intermediate in an Intramolecular Dechlorination Reaction Involving Copper(I) and a $ArCH_2Cl$ Moiety," *J. Am. Chem. Soc.* **130**, 5644–5645 (2008).

K. SUZUKI, C. SHIMOKAWA, C. MORIOKA and S. ITOH, "Monooxygenase Activity of *Octopus vulgaris* Hemocyanin," *Biochemistry* **47**, 7108–7115 (2008).

T. HIRAYAMA, M. TAKI, Y. KASHIWAGI, M. NAKAMOTO, A. KUNISHITA, S. ITOH and Y. YAMAMOTO, "Colorimetric Response to Mercury-Induced Abstraction of Triethylene Glycol Ligand from Gold Nanoparticle Surface," *Dalton Trans.* 4705–4707 (2008).

H. TANO, R. TAJIMA, H. MIYAKE, S. ITOH and H. SUGIMOTO, "Selenido-Bis(dithiolene) M(IV) Complexes (M = Mo and W) Potentially Related to the Nicotinic Acid Hydeosylase Reaction Center: Redox Aspects in Electrochemistry and Oxygen Atom Transfer from Me_3NO to M(IV) Centers," *Inorg. Chem.* **47**, 7465–7467 (2008).

LIST OF REVIEW ARTICLES AND TEXTBOOKS

Theoretical and Computational Molecular Science

Z. SLANINA, K. KOBAYASHI and S. NAGASE, "Isomeric Fullerenes and Endofullerenes: Stability Computations on Promising Nanoscience Agents, " in *Handbook on Theoretical and Computational Nanotechnology*, M. Rieth and W. Schommers, Eds., American Scientific Publishers; Los Angeles, **Vol. 8**, pp. 457–505 (2007).
Y. MAEDA, T. HASEGAWA, T. AKASAKA and S. NAGASE, "Development in Separation Methods of Metallic Single-Walled Carbon Nanotubes," *Chemical Engineering* (in Japanese) **53**, 35–41 (2008).

K. YONEMITSU, "Theory of Photoinduced Phase Transitions: Coherent Oscillations and Transient States,'' *The Review of Laser Engineering* (in Japanese) **36**, 343–348 (2008).

Photo-Molecular Science

K. IMURA and H. OKAMOTO, "Imaging of Plasmon Wavefunctions in Noble Metal Nanoparticles by Near-Field Optical Microscopy," *J. Surf. Sci. Soc. Jpn.* (in Japanese) **29**, 336–343 (2008).
K. IMURA and H. OKAMOTO, "Development of Novel Near-Field Microscpectroscopy and Imaging of Local Excitations and Wavefunctions of Nanomaterials," *Bull. Chem. Soc. Jpn.* **81**, 659–675 (2008).
H. OKAMOTO and K. IMURA, "Near-Field Optical Imaging of Nanoscale Optical Fields and Plasmon Waves," *Jpn. J. Appl. Phys.* **47**, 6055–6062 (2008).

A. HISHIKAWA, "Attosecond Dynamics," *Parity* (in Japanese), Maruzen, **Vol. 23**, No. 01, pp.13–15 (2008).

T. TAIRA, "Palm Top Optical Synthesizers—State of the Art of Micros Solid-State Photonics—," in *World of Opto-Science—from quantum to bio*— (in Japanese), NINS Symposium 2, Kubapro; Tokyo, pp. 35–66 (2007).
T. TAIRA and Y. SATO, "Thermal Conductivity Model of Optical Materials," in *SPIE Defense & Security 2008*, 6952-13 (2008).
T. TAIRA, "Giant Micro Photonics," *The Review of Laser Engineering* (in Japanese), The Laser Society of Japan, **36**, p. 109 (2008).
T. TAIRA and Y. SATO, "A General Model of a Thermal Conductivity for Optical Materials," *Proc. of SPIE* **6952**, pp. 69520E-1–10 (2008).

Materials Molecular Science

T. YOKOYAMA, T. NAKAGAWA and Y. TAKAGI, "Magnetic Circular Dichroism for Surface and Thin Film Magnetism: Measurement Techniques and Surface Chemical Applications," *Int. Rev. Phys. Chem.* **27**, 449–505 (2008).

H. TSUNOYAMA and T. TSUKUDA, "Size Selective Synthesis and Catalytic Activity of Polymer-Stabilized Gold Clusters Dispersed in Water," *The Bulletin of the Society of Nano Science and Technology* (in Japanese) **6**, 61–66 (2008).

K. FURUKAWA and T. NAKAMURA, "W-Band ESR Investigations of Electronic Properties in Molecular Based Solids," *Journal of the Japan Society of Infrared Science and Technology* (in Japanese) **16**, 40–44 (2007).
T. NAKAMURA and K. FURUKAWA, "The Molecular Solid from a Viewpoint of Photo-Induced Phase Transition and Related Phenomena," *The Review of Laser Engineering* (in Japanese) **36**, 339–342 (2008).
C. ARAKI, Y. UWATOKO, M. ITOI, M. HEDO and T. NAKAMURA, "Observation of Unusual Pressure-Induced Superconductivity in 1-D Organic Conductor $(TMTTF)_2SbF_6$," *Kotai Butsuri* (in Japanese) **43**, 409–418 (2008).

M. HIRAMOTO, "Organic Solar Cells," *Oyo Butsuri* (in Japanese) **77**, 539–544 (2008).
M. HIRAMOTO, "Efficient Organic Thin-Film Solar Cells Incorporating Highly Purified Organic Semiconductors," *Kino Zairyo* (in Japanese) **28**, 25–32 (2008).

H. SAKURAI, "A Novel Carbon Compound Connects Inorganic and Organic Chemistry," *Kagaku to Kyoiku* (in Japanese) **55**, 606–609 (2007).

Y. BABA, "Preventive Medicine Based on Nanobioimaging and Nanobiomeasurement," in *Research Trends in Nanomedicine*, Ohm Publishers, 2–12 (2008).
N. KAJI, M. TOKESHI and Y. BABA, "Single Molecule Measurements with a Single Quantum Dot," *Chemical Record* **7**, 295–304 (2007).

Life and Coordination-Complex Molecular Science

S. AONO, “Regulation of Biological Functions by Gas Molecules Acting as a Molecular Switch,” *Kagaku* (in Japanese) **62**, 68–69 (2007).
S. AONO, “Metal-Containing Sensor Proteins Sensing Diatomic Gas Molecules,” *Dalton Trans.* 3137–3146 (2008).

K. KATO and Y. KAMIYA, “Structural Views of Glycoprotein-Fate Determination in Cells,” *Glycobiology* **17**, 1031–1044 (2007).
E. SAKATA and K. KATO, “The Activating Mechanism of the Cullin-Based E3 Ligases by Neddylation,” *Jikken Igaku* (in Japanese) **26**, 207–213 (2008).
K. KATO, H. SASAKAWA, Y. KAMIYA, M. UTSUMI, M. NAKANO, N. TAKAHASHI and Y. YAMAGUCHI, “920 MHz Ultra-High Field NMR Approaches to Structural Glycobiology,” *Biochim. Biophys. Acta—General Subjects* **1780**, 619–625 (2008).
E. KURIMOTO, E. AMEMIYA and K. KATO, “Structural Biology of Curculin, a Taste-Modifying Protein,” *Foods & Food Ingredients J. Jpn.* **213**, 645–652 (2008).

T. URISU, Ed., *Nanomedicine: Medical Application of Nanotechnology* (in Japanese), Ohmsha; Tokyo (2008).

C. WEI, M. YAMOTO, W. WEI, Z. ZHAO, K. TSUMOTO, T. YOSHIMURA, T. OZAWA and Y. J. CHEN, “Genetic Nanomedicine and Tissue Engineering,” *Med. Clin. North Am.* **91**, 889–898 (2007).

S. ITOH and S. FUKUZUMI, “Monooxygenase Activity of Type-3 Copper Proteins,” *Acc. Chem. Res.* **40**, 592–600 (2007).

INDEX

to “Research Activities”

MAPS AND DIRECTIONS

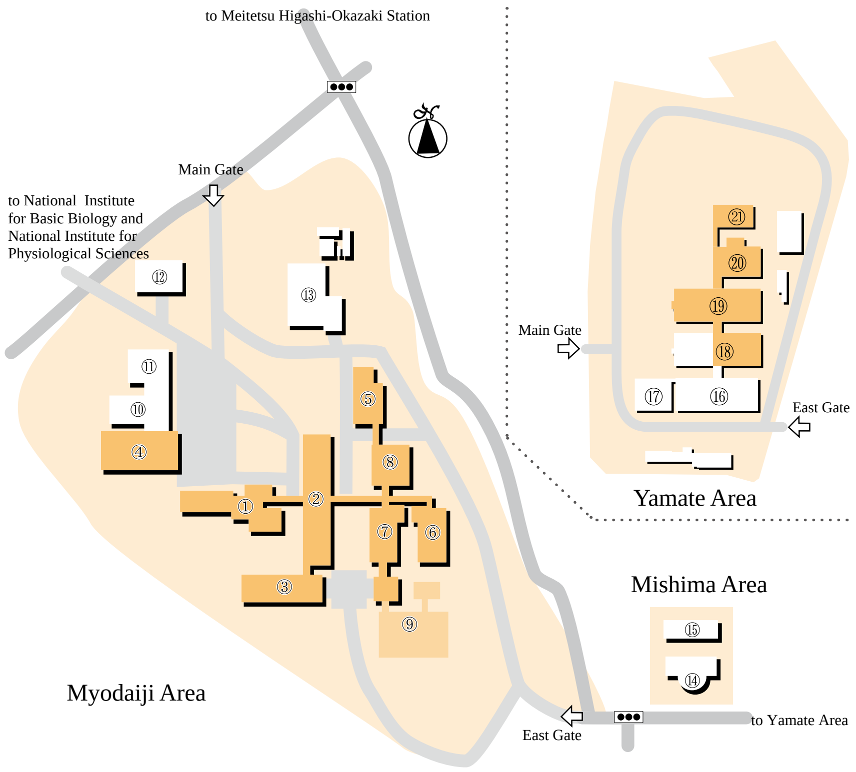

1. Research Office Building
2. Main Laboratory Building
3. South Laboratory Building
4. Research Center for Computational Science
5. Low-Temperature Facilities Building
6. Instrument Center
7. Laser Research Center for Molecular Science
8. Equipment Development Center
9. UVSOR Facility
10. Central Administration
11. Library
12. Faculty Club
13. Power Station
14. Okazaki Conference Center
15. Mishima Lodge
16. Yamate Bldg. 1A
17. Yamate Bldg. 1B
18. Yamate Bldg. 2
19. Yamate Bldg. 3
20. Yamate Bldg. 4
21. Yamate Bldg. 5

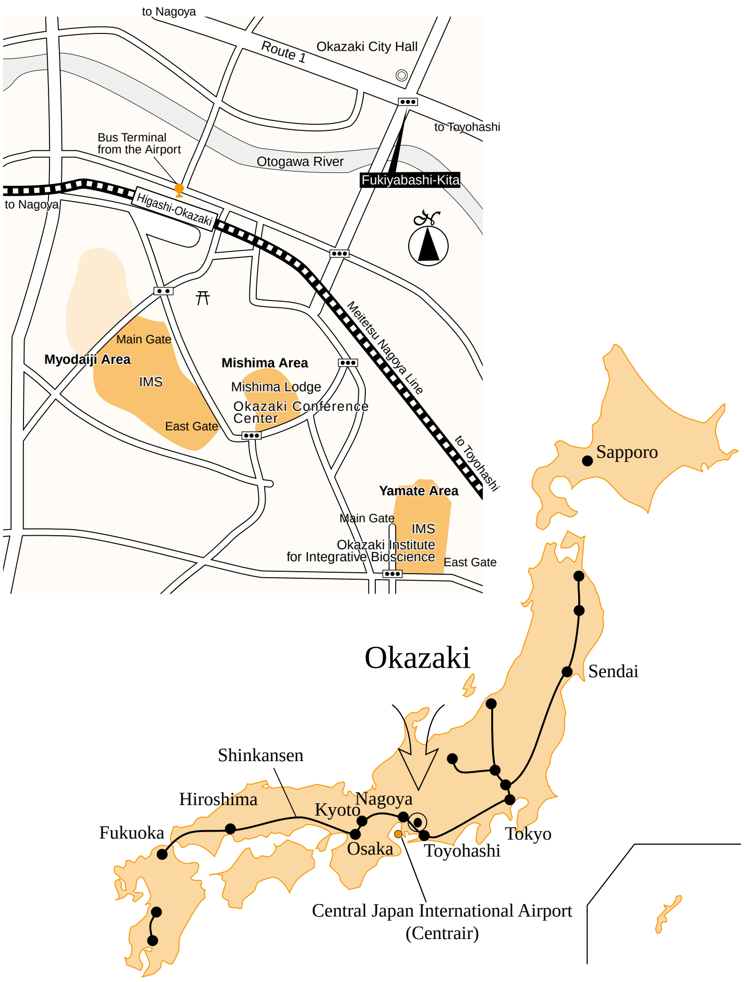

From Tokyo

At Toyohashi Station, catch the Meitetsu train and get off at Higashi-Okazaki Station (approx. 20 min from Toyohashi to Higashi-Okazaki). Turn left at the ticket gate and walk south for approx. 7 min.

From Osaka

At Meitetsu Nagoya Station, catch the Meitetsu train and get off at Higashi-Okazaki Station (approx. 30 min from Meitetsu Nagoya to Higashi-Okazaki). Turn left at the ticket gate and walk south for approx. 7 min.

From Central Japan International Airport (Centrair)

By Train

Catch the Meitetsu train at Central Japan International Airport Station and get off at Higashi-Okazaki Station (approx. 65 min form the Central Japan International Airport Station to Higashi-Okazaki). Turn left at the ticket gate and walk south for approx. 7 min.

By Bus

Catch the Meitetsu bus at Central Japan International Airport and get off at Higashi-Okazaki Bus Station (approx. 65 min from the Airport to Higashi-Okazaki). You are on the north side of the Meitetsu Higashi-Okazaki Station. Go through the passage connecting the south side of the Higashi-Okazaki Station and further walk south for approx. 7 min.

By Car

Take the Okazaki Exit on the Tomei Highway. Approx. 1.5 km toward Nagoya, turn left at the Fukiyabashi-Kita turnoff (approx. 10 min from Okazaki Exit).

NATIONAL INSTITUTES OF NATURAL SCIENCES

Institute for Molecular Science

Myodaiji Area: 38 Nishigo-Naka, Myodaiji, Okazaki 444-8585, Japan